The University of Leeds

School of Medicine

Faculty of Medicine and Health

Leeds Institute of Cardiovascular and Metabolic Medicine

Insulin-like growth factor binding protein-2 and its role in angiogenesis

Pooja Trusha Mehool Shah

September 2018

Thesis submitted to The University of Leeds in accordance with the requirements for the Degree of Doctor of Philosophy

Intellectual Property and Publication Statements

Acknowledgements

Firstly, I would like to sincerely thank my main supervisor Dr Stephen Wheatcroft for his continuous guidance, knowledge and support that has inspired me to completion of my PhD. I am also extremely grateful to my co-supervisor Dr Kirti Kain for her dedication and guidance to motivate me through my PhD. I would especially like to thank my second co-supervisor, Dr Hema Viswambharan for all the support and advice you have given me since I came to you as a placement student.

This project would be nothing without the lessons I was taught by Dr Paul Cordell. Thank you for being extremely patient with me during all of the mutagenesis work and helping me achieve the bulk of my PhD. I would like to thank Dr Nadira Yuldasheva for all her help with the animal work carried out in this project. Thank you very much to Miss Jess Smith; I have been so lucky to have the pleasure to work with someone as kind and helpful as you.

I would like to thank Dr Natalie Haywood, Dr Alex Bruns and Dr Thomas Slater for their continuous laboratory advice and helping me optimise all my experimental work. I would like to acknowledge Melanie Reay and Andrew Horner for their help in the animal house and Sally Boxall for her help using the bio-imaging facilities. I would also like to thank Dr Kerrie Smith for all her support through my PhD.

The support provided by all the members in Professor Mark Kearney's group since my placement at LICAMM has made my PhD experience unforgettable and helped through every step with their laboratory and research knowledge.

I would like to specially thank Professor David Bates and Dr Andrew Benest for inviting me to The University of Nottingham to carry out my permeability studies. It was a pleasure to work with you both.

I am so grateful for all the support provided by my greatest friends, Saba Ullah, Marium Anwar, Anneesa Sarwar, Courtney Williams, Eleanor Cawthorne, Elizabeth Taylor, Julie Mawson, Carla Asquith, Nathan Asquith, Katarina Miteva and Katie Musalowski. I would not have been able to complete this PhD without your motivation and inspiration during my lowest points.

I would sincerely like to thank my amazing grandparents, parents, Masi and Masa, my sister, Shriya and my fiancée, Dr Arpan Patel from the bottom of my heart for their unbelievable and irreplaceable encouragement. Unfortunately, both my grandads,

Nana and Bapuji passed away during my PhD but I hope my Ba (grandma), late Nani (grandma), late Nana and late Bapuji are proud of my achievements.

Finally, none of this work would have been possible without funding provided by the University of Leeds 110 Anniversary Research Scholarship, British Heart Foundation, European Research Council, The Biochemical Society and Leeds Institute of Cardiovascular and Metabolic Medicine. This funding has covered all my maintenance, laboratory supplies and attendance and presentations at conferences throughout my PhD.

Abstract

Therapeutic angiogenesis is currently under investigation to restore tissue perfusion in peripheral arterial disease (PAD). However, clinical trials have proved to be disappointing in stimulating the development of functional blood vessels and reducing adverse events.

Insulin-like growth factor binding protein-2 (IGFBP-2) has demonstrated potential in pro-angiogenic activity but the molecular mechanisms remain unestablished. Structurally, IGFBP-2 possesses domains which can interact with insulin-like growth factor (IGF), receptor protein tyrosine phosphatase-β, glycosaminoglycans, integrins and can potentially translocate into the nucleus to activate cellular and pathological processes.

In this project, we used two IGFBP-2 over-expressing mouse models, namely a global and an endothelial specific model, to determine whether increasing IGFBP-2 can increase perfusion in an experimental model of ischemia *in vivo.* The angiogenic potential of IGFBP-2 was investigated in an array of *in vitro* angiogenic signalling and functionality studies in vascular endothelial cells. Recombinant IGFBP-2 was generated, in which site-directed mutagenesis was employed to disrupt the integrin binding site (RGD), IGF binding site, or the heparin binding domain-1/nuclear localisation signal. These mutants were used to determine the primary mechanism IGFBP-2 may use to exert *in vitro* angiogenic effects.

Upregulation of IGFBP-2 in ischemic muscles was confirmed in wild-type mice following hind limb ischemia surgery. IGFBP-2 over-expression significantly enhanced perfusion at early stages of recovery. *In vitro* angiogenic signalling and functional assays demonstrated IGFBP-2 increased phosphorylation of Akt and ERK/MAPK, as well as enhancing endothelial cell adhesion, wound closure and tube formation. Site-directed mutagenesis identified the RGD domain to be critical in IGFBP-2-stimulated *in vitro* angiogenic activity. In contrast to VEGF, exposure of IGFBP-2 to endothelial cells did not affect endothelial monolayer permeability. In conclusion, IGFBP-2, via its RGD domain displays promising potential as a new therapeutic angiogenic treatment.

Contents page

List of figures

List of tables

Abbreviations

AAS	Antibiotic-antimyotic Solution
ALS	Acid Labile Subunit
Akt	Protein Kinase B
ATP	Adenosine Triphosphate
AUC	Area Under the Curve
BMI	Body Mass Index
BSA	Bovine Serum Albumin
CAG	Chicken β-Actin
CHD	Coronary Heart Disease
CLI	Critical Limb Ischemia
CMV	Cytomegalovirus
CVD	Cardiovascular Disease
DMEM	Dulbecco's Modified Eagle Media
DMSO	Dimethylsulfoxide
EGF	Epidermal Growth Factor
ELISA	Enzyme-linked Immunosorbent Assay
eNOS	Endothelial Nitric Oxide Synthase
EPC	Endothelial Progenitor Cells
ERK	Extracellular signal-related kinase
FA	Focal Adhesions
FAK	Focal Adhesion Kinase
FBS	Fetal Bovine Serum
FGF	Fibroblast Growth Factor
FitC	Fluorescein-5-isotheiocyanate
GLUT4	Glucose Transporter Type 4
GSK-3β	Glycogen Synthase Kinase 3β
HBD	Heparin Binding Domain
HBSS	Hanks' Balanced Salt Solution
Het	Heterozygous
HGF	Hepatocyte Growth Factor
HIF-1	Hypoxia inducible factor-1

hIGFBP-2	Human Insulin-like Growth Factor Binding Protein-2
HF	High-Fidelity
HLI	Hindlimb Ischemia
Hom	Homozygous
HSaVECs	Human Saphenous Vein Endothelial Cells
HUVECs	Human Umbilical Vein Endothelial Cells
IGF	Insulin-like Growth Factor
IGF-R	Insulin-like Growth Factor Receptor
IGFBP	Insulin-like Growth Factor Binding Protein
IGFBP-2	Insulin-like Growth Factor Binding Protein-2
IHD	Ischemic Heart Disease
ILK	Integrin-linked kinase
JNK	c-Jun N-terminal Kinase
kDa	Kilodaltons
KO	Knock-out
LB	Lysogeny Broth
LDL	Low-Density Lipoproteins
MAPK	Mitogen-activated Protein Kinase
MCS	Multiple Cloning Site
mIGFBP-2	Mouse Insulin-like Growth Factor Binding Protein-2
MW	Molecular Weight
NFkβ	Nuclear factor kappa β
NO	Nitric Oxide
PAD	Peripheral Arterial Disease
PAPP-A	Pregnancy-Associated Plasma Protein-A
PBS	Dulbecco's Phosphate Buffered Saline
PBLEC	PBS (pH 6.8) with the addition of 1M $MgCl_2$, 1M $CaCl_2$, 1M $MnCl_2$, 10% Triton X-100
PCR	Polymerase Chain Reaction
PECs	Pulmonary Endothelial Cells
PI3K	Phosphatidylinositol 3-Kinase

pM-secSUMOstar vector or pM-SUMOstar vector	Mammalian Small Ubiquitin-like Modifier Secretory Vector
PTEN	Phosphatase and Tensin Homolog
RGD	Arginine, Glycine-Aspartic Acid
RPTPβ	Receptor Protein Tyrosine Phosphatase-β
RT	Room Temperature
SEM	Standard Error of the Mean
SF	Serum-free
SUMO	Small Ubiquitin-like Modifier
TBST	Tris Buffered Saline Tween 20
TG	Transgenic
TNF-α	Tumour Necrosis Factor-α
VSMCs	Vascular Smooth Muscle Cells
VEGF	Vascular Endothelial Growth Factor
VEGF-R	Vascular Endothelial Growth Factor Receptor
VehiHom	Homozygous over-expression of endothelial-specific hIGFBP-2 in mice
VE-PTP	Vascular Endothelial Protein Tyrosine Phosphatase
WT	Wild-type

Chapter 1 – Introduction

1.1 Introduction

Cardiovascular disease (CVD) is currently and predicted to continue to be the principal cause of worldwide morbidity and mortality, accounting for approximately a third of all recorded deaths (Roth et al., 2017). Peripheral arterial disease (PAD), along with coronary heart disease (CHD), stroke and aortic diseases are the four main types of CVD for which there are currently no definite cures. There are pharmacological endovascular and surgical treatments available to improve symptoms and to help prevent further damage from the restriction of blood supply to the limbs in PAD. However, the increasing prevalence of diabetes and an ageing population has led to an increased number of patients with diffuse disease refractory to revascularisation, causing critical limb ischemia, often with amputation as the only solution. Therefore, the need for new treatments to improve tissue perfusion in CVD and in patients with PAD in particular, is more pressing than ever.

Therapeutic angiogenesis has recently evolved as a potential treatment for limb ischemia (Makarevich & Parfyonova, 2017). This involves exploiting angiogenesis by an injection of growth factors or other pro-angiogenic factors to stimulate the formation of new blood vessels from pre-existing vessels, if successful, this leads to restoration of oxygenated blood supply to the lower limb via the newly formed network, preventing the need for amputation (Figure 1.1). Current clinical trials of this treatment have included the use of a potent angiogenesis inducer, vascular endothelial growth factor (VEGF). However, in these trials VEGF-therapy produced weak and unstable blood vessels which caused leakage of blood (Deveza et al., 2012).

Insulin-like growth factor binding protein-2 (IGFBP-2) has recently been identified by our laboratory as a possible acute angiogenesis treatment option. The association of IGFBP-2 with angiogenesis was first reported in some cancers, as tumour growth positively correlated with the upregulation of IGFBP-2 expression (Adamo et al., 1992; Kanety et al., 1993). In recent years, further exploration of IGFBP-2 has distinguished its role as a significant enhancer of cell migration, proliferation, differentiation, survival and invasion across many cell types, via interactions through

certain of its structural domains with cell surface receptors (Han et al., 2014; Wang et al., 2017a, 2017c).

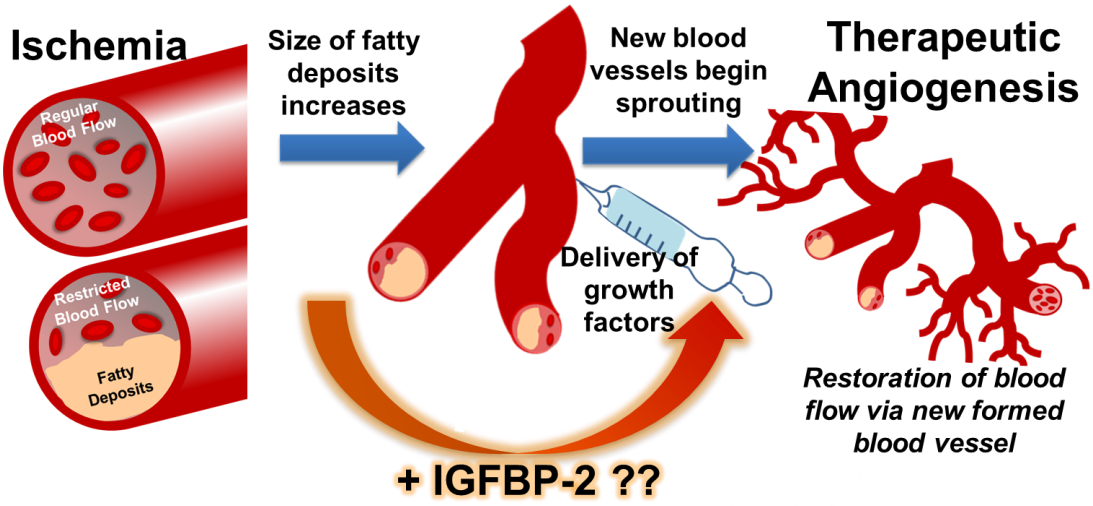

Figure 1.1 Schematic displaying delivery of growth factors can stimulate angiogenic growth from a pre-existing vessel in an ischemic setting
This figure displays the development of an atheroma, narrowing the blood vessel and restricting the blood supply. The obstructed blood supply finds an alternate route to reduce blood pressure and the delivery of pro-angiogenic growth factors promotes formation of new smaller blood vessels to help handle the increase in blood flow and direct it to the ischemic site.

Integrins, glycosaminoglycans, receptor protein tyrosine phosphatase-β (RPTPβ) and nuclear transport importins, in addition to insulin-growth factors (IGF) are examples of the multiple molecules to which IGFBP-2 can bind via its structural domains.

IGFBP-2 displays other properties that make it stand out as a potential option for therapeutic angiogenesis. IGFBP-2 can exert a protective nature against the onset of metabolic diseases. It has been shown to protect against obesity and insulin resistance by preventing the proliferation and differentiation of pre-adipocytes following high fat feeding in murine models (Carter et al., 2014; Wheatcroft et al., 2007). This suggests IGFBP-2 has the ability to promote or suppress angiogenic effects by preventing or enhancing activity via its interactions. This ensures it can modulate healthy angiogenesis, ensuring the vessels formed can withstand the forces of shear stress (Fletcher et al., 2013).

Although associations between IGFBP-2 and angiogenesis have been demonstrated, no evidence of IGFBP-2 directly inducing vessel formation has been shown in vascular endothelial cells. The aim of this thesis is to investigate the

angiogenic potential of IGFBP-2 as a clinical therapeutic strategy in critical limb ischemia.

Firstly, to address this aim, global and endothelial specific over-expressing human IGFBP-2 (hIGFBP-2) mice were studied to investigate a potential favourable action of IGFBP-2 in enhancing recovery from hind limb ischemia *in vivo*. Next, the effect of IGFBP-2 on endothelial cell *in vitro* angiogenic signalling pathways were interrogated leading on to its role in influencing angiogenic mechanisms via *in vitro* angiogenic assays. To determine the predominant interaction and mechanism that stimulates IGFBP-2 activity, binding-sites of the protein were mutated to inhibit interaction with their receptors. The effects of these mutations were interrogated by replicating *in vitro* angiogenic signalling and assay studies in vascular endothelial cells. We then examined the influence of IGFBP-2 on permeability of the endothelial monolayer, recognising the importance of excluding an adverse effect on vascular permeability for any new angiogenic agent. Findings from the final studies determined which IGFBP-2 domain we could exploit as an angiogenic therapeutic target, to promote formation of healthy and viable vessels that could rescue a critically ischemic limb.

1.2 Cardiovascular disease

CVD is mostly characterised by luminal narrowing of blood vessels which restricts blood flow to a tissue or organ. This results in ischemia which contributes to tissue damage and if prolonged, can lead to necrosis due to restriction of an oxygenated blood supply. The narrowing is due to atherosclerosis; the pathological process which is characterised by an accumulation of inflammatory material and lipids, primarily cholesterol-rich particles and other lipids such as low-density lipoproteins (LDL). The development of atherosclerotic plaques often follows damage to the endothelial layer, compromising its ability to act as a protective barrier between circulating plasma and the vessel wall (George & Johnson, 2010). Expansion of the atherosclerotic plaque is driven by endothelial cells attracting monocytes to the accumulating lesion. As monocytes differentiate into macrophages, they engulf more LDL which stimulates further differentiation of macrophages into foam cells. Foam cells secrete chemokines which attract more monocytes to the lesion and activation of this feedback loop eventually causes plaque expansion and vessel remodelling leading to luminal compromise (Figure 1.2) (Bentzon et al., 2014).

Following reduction of oxygenated blood flow to the tissues, hypoxic and inflammatory signalling pathways become activated due to the inhibition of oxygen-sensing prolylhydroxylase enzymes which require oxygen to function (Eltzschig &

Carmeliet, 2011). Hypoxia-inducible factor-1 (HIF-1) and nuclear factor-κB (NFκB) are activated via signalling cascades, which in turn interact with hypoxia response elements, inducing the transcription of angiogenic growth factors such as vascular endothelial growth factor (VEGF), epidermal growth factor (EGF), fibroblast growth factor (FGF) and platelet derived growth factor (PDGF) (Ramakrishnan et al., 2014). A subunit of HIF-1, HIF-1α has also been reported to stimulate the transcription of IGFBP-2 (Das et al., 2013). Growth factors including VEGF, FGF and PDGF begin to stimulate angiogenesis in an attempt to restore blood flow to the ischemic limb or tissue in CVD. However, whether IGFBP-2 promotes angiogenesis in the context of tissue ischemia remains unclear and has only been established in the context of tumour expansion (Lin et al., 2015).

Cardiovascular risk factors promote the development of atherosclerosis and significantly increase the risk of a CVD event. The major risk factors include diabetes mellitus, hypertension, high cholesterol levels and smoking: which can all be modulated via lifestyle changes to prevent a CVD event (Canto & Iskandrian, 2003). However, genetic factors have also been shown to contribute to offspring having a higher risk of developing CVD if their parents are sufferers of CVD (Lloyd-Jones et al., 2004).

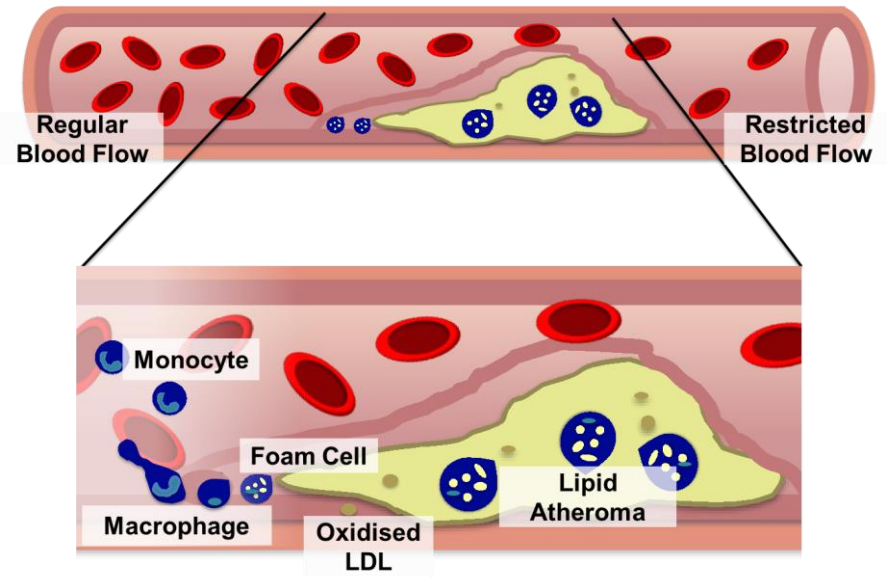

Figure 1.2 Schematic diagram of atheroma formation
The mechanism of atheroma formation, attracting more monocytes and their differentiation into macrophages and then foam cells, continuously contributing to the expansion of the lesion. This leads to a restriction of the blood supply through the vessel and contributes to contributing factors of CVD, such as hypertension.

1.2.1 Peripheral arterial disease

PAD is increasingly affecting morbidity and mortality across the worldwide population, affecting approximately 200 million people by 2010 (Sampson et al., 2014). This value continues to rise as CVD continues to grow as the majority cause of worldwide deaths.

Atherosclerosis is the main contributor to PAD, by narrowing the lumen of lower limb arteries via atheroma formation and thereby reducing perfusion of the lower limbs. There are many burdens associated with PAD such as atypical leg pain, leg weakness, claudication and ulcers which compromise quality of life and if left untreated can progress to critical limb ischemia (CLI) (Morley et al., 2018). Necrosis, ganagrene, non-healing wounds and pain in a resting state are the symptoms which characterise CLI (American Academy of Family Physicians. & Santilli, 1999). Up to 40% of CLI patients are unable to undergo revascularisation treatments or revascularisation attempts have failed, leaving major amputation as the only solution (Novo et al., 2004). Although CLI itself may not be the cause of death, the risk of CHD events significantly increases, with 25% of PAD patients also suffering from CHD, giving patients approximately a 2-year life expectancy (Sigvant et al., 2007; Soga et al., 2014).

Increasing prevalence of diabetes and increasing population age in the last few decades have resulted in an increase in the number of individuals with PAD who reach the stage of CLI. Patients are treated with two different aims: firstly, to decrease the risk of a cardiovascular event; and secondly to rescue perfusion of the limb. Treatments for CVD will be discussed in more depth in Section 1.2.2 of this chapter. Non-pharmalogical approaches such as exercise, significantly reduce pain levels at rest and when walking, however there is no definite evidence to confirm the reduction in pain is due to reperfusion to the limb (Olin & Sealove, 2010). Pharmacological oral treatment provided as secondary prevention is used to help improve blood flow to the lower limbs, as well as prevent CVD events. Studies with ACE inhibitors and antiplatelet therapies have demonstrated a 22-23% reduction in PAD-associated CVD events (Antithrombotic Trialists' Collaboration, 2002; Heart Outcomes Prevention Evaluation Study Investigators et al., 2000). Although combined therapy including antiplatelet drugs, thienopyridines, aspirin and warfarin have proved successful in other CVD, the combination of anti-platelet drugs and warfarin offered no positive effect compared to anti-platelet drugs alone and increased the risk of death by bleeding on patients with PAD (Warfarin Antiplatelet Vascular Evaluation Trial Investigators et al., 2007).

Unfortunately, these treatments sometimes fail to sufficiently optimise perfusion of the ischemic limb via the existing vessel network, resulting in CLI and leaving amputation as the only option. New treatments are urgently needed to restore perfusion. Recently, a new approach by promoting the formation of a new blood vessel network to restore limb perfusion has been pre-clinically investigated (Iyer & Annex, 2017). New blood vessel development arises through three complex and highly regulated distinct processes, depending on the pathophysiological context and life-stage. These processes are categorised as angiogenesis, vasculogensis and arteriogenesis and will be discussed in more detail in Section 1.3.

1.2.2 Cardiovascular disease treatments

By assessing risk factors, we can identify individuals who may be at a high risk of CVD events. Primary prevention involves preventing the onset of CVD in those who are at risk by influencing lifestyle change or initiating risk-lowering medication. Drugs currently in clinical use are usually offered in combination to reduce risk of thrombosis, lower cholesterol levels and lower blood pressure (Wirtz et al., 2016). Secondary prevention is the prevention of recurrent CVD in patients who have previously suffered from a CVD event and also involves lifestyle and pharmacological approaches.

The final mode of treatment available is interventional or surgical procedures, which involve revascularisation to deprived organs. Revascularisation can be broadly classified as percutaneous interventions (involving angioplasty and stent implantation) and surgical procedures in which narrowed or occluded arteries are ‘bypassed’ by native or artificial consults. Angioplasty and stents are commonly used to recanalise or dilate the lumen of obstructed vessels in the peripheral, coronary or cerebral circulations (Al-Lamee et al., 2016). These procedures are effective and widely used, but in minority of individuals are associated with restenosis, thrombosis or neo-atherosclerosis. Angioplasty offers treatment using a balloon to widen the vessel. Early elastic recoil can limit long-term success but can be prevented by deployment of a metallic stent (Livingston & Lynm, 2012). The occurrence of stent restenosis, due to excessive smooth muscle cell proliferation and intimal hyperplasia, has become less of a clinical problem since the evolution of drug-eluting stents, which elute drugs to prevent excessive proliferation of vascular smooth muscle cells (VSMC) (Htay & Liu, 2005). However, drug-eluting stent restenosis remains a clinically challenging problem in some individuals.

Surgical revascularisation can be applied to the peripheral, coronary or cerebral circulations. Typically, this involves suturing a native artery or vein, or an artificial conduit, to 'bypass' the diseased segment of artery. The choice of percutaneous or surgical revascularisation is decided based on the extent and severity of the arterial disease, and the patient's co-morbidities and overall fitness for surgery.

In the majority of patients with CVD, symptom control and satisfactory tissue perfusion can be achieved through a combination of risk-factor modification, pharmacological therapy and revascularisation. However, there remains a group of patients who have ongoing symptoms and tissue ischemia despite conventional management. These patients may have severe diffuse arterial disease which is anatomically unsuitable for percutaneous or surgical revascularisation or may have developed restenosis or progressive native arterial disease despite previous successful revascularisation (Lozano et al., 2015). Such patients (sometimes termed 'no-option' patients) comprise up to 40% of the total number of individuals with CVD (Teraa et al., 2016; Ylä-Herttuala & Baker, 2017). In these individuals, current approaches usually focus on symptom control, but quality of life and prognosis are often poor. In the setting of PAD, critical limb ischaemia in patients unsuitable for (further) revascularisation may require amputation of the affected limb. It is these clinical scenarios in which novel therapies, such as those investigated in this thesis, are likely to be most appropriate. As mentioned previously in relation to PAD, an approach to improve tissue perfusion is to facilitate the development of new blood vessels via angiogenesis processes.

1.3 Angiogenesis, vasculogenesis and arteriogenesis

Angiogenesis is the process characterised by the formation of a new vascular network from pre-existing blood vessels, carefully regulated by the balance of pro-angiogenic and anti-angiogenic growth factors. Growth factor expression is elevated in response to activation of hypoxic and inflammatory signalling cascades during ischemia to induce revascularisation via activation of cellular angiogenic mechanisms such as migration and proliferation. The definition of angiogenesis differs from vasculogenesis; which specifically refers to the process of *de novo* blood vessel formation, stimulated by migration and differentiation of endothelial precursor or stem cells (angioblasts), rather than by hypoxia in embryonic growth (Vailhé et al., 2001). Although vasculogenesis is typically restricted to embryonic development, it has recently been reported that endothelial progenitor cells may stimulate post-natal neovascularisation (Balaji et al., 2013; Ribatti et al., 2001).

Arteriogenesis does not involve the growth of new vessels, but instead involves the expansion and growth of pre-existing collateral vessels, resulting in lumen area expansion via endothelial remodelling mechanisms (Rizzi et al., 2017). This process is triggered by enhanced mechanical forces influenced by fluid shear stress as a result of an occlusion preventing normal perfusion (Heil et al., 2006). (Figure 1.3).

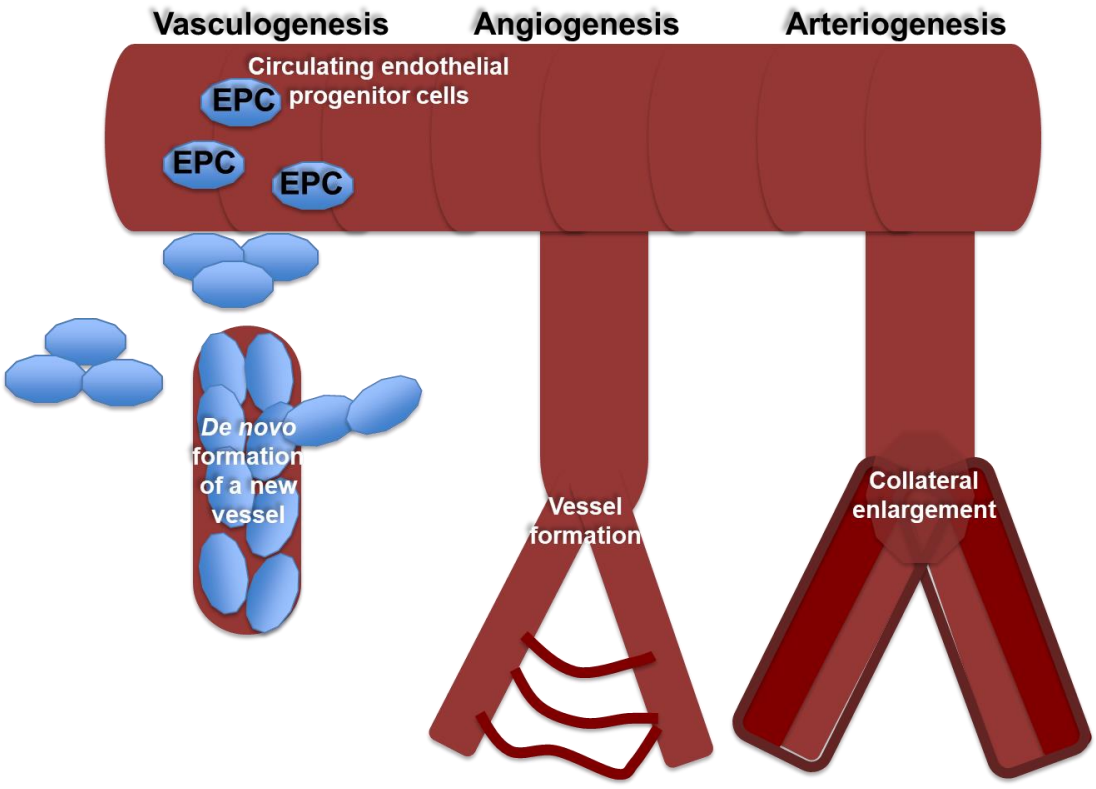

Figure 1.3 Diagram highlighting different angiogenic mechanisms; vasculogenesis, angiogenesis and arteriogenesis
Visual demonstrating the difference between these three types of vessel formation. Vasculogenesis is driven by endothelial progenitor cells. Angiogenesis is the formation of new vessels from pre-existing vessels. Arteriogenesis is the enlargement of the collateral vessels to restore perfusion.

Angiogenesis may be sub-dived into several types, including 'developmental' and 'pathological'. Developmental angiogenesis is a highly regulated process required for vascularisation during early development of an organism and in physiological growth and repair (wound healing). Dysregulation of pro-angiogenic growth factors can cause the onset of pathological angiogenesis, which has been implicated in several disease states including cancer, diabetic retinopathy and psoriasis. Pathological angiogenesis is driven by rapid uncontrolled formation of new vascular networks and progression of this can be difficult to halt (Chung & Ferrara, 2011).

Modulation of the expression of pro-angiogenic growth factors on a transcriptional level determines angiogenic activity. This modulation has been exploited as a possible therapeutic to promote vessel growth and development via angiogenesis and arteriogenesis across CVDs but has shown particular promise as a treatment for PAD.

1.3.1 Pro-angiogenic growth factors and signalling pathways

Upregulation of HIF-1α during ischemia enhances the transcription of cytokines, including tumour necrosis factor (TNF-α) and pro-angiogenic growth factors, which in turn activate angiogenic signalling cascades to induce an angiogenic response. In this section, the molecular actions of the pro-angiogenic factors which are activated to induce vessel growth are summarised.

TNF-α is a well-established cytokine secreted in response to an inflammatory response with its main role in angiogenesis being to influence cells ability to secrete pro-angiogenic growth factors such as VEGF and PDGF. A small insult with TNF-α promotes endothelial tip cell formation via upregulation of pro-angiogenic factors during the initial sprouting stage of angiogenesis, however continuous expression of TNF-α delays the angiogenic effect by blocking VEGF Receptor-2 (VEGFR-2) (Giraudo et al., 1998; Sainson & Harris, 2008).

VEGF is the most potent and well-established pro-angiogenic factors across metabolic diseases and cancer, as well as in the maintenance of regular homeostasis. There are 5 members to the human VEGF family, however VEGF-A has been implicated to induce the most pronounced angiogenic response in comparison to its other isoforms. It exerts its activity via binding to its tyrosine kinase receptor, VEGFR-2 with high affinity. (Ferrara et al., 2003).

VEGF-A as well as FGF-1 and FGF-2, which belong to a family of 18 members are well known to enhance cell survival, migration and proliferation via activation of key cell growth and development signalling cascades such as focal adhesion kinase (FAK), protein kinase B (Akt) and mitogen-activated protein kinase (MAPK) (Goetz et al., 2014; Johnson & Wilgus, 2014). These pathways will be discussed in more detail towards the end of this section.

Each of these growth factors cross talk with one another or their receptors, directly affecting expression levels. VEGF, as well FGF-1 and FGF-2 independently as well as coordinating with each other are important for vessel formation *in vivo*, as co-stimulation with VEGF-A and FGF-2 significantly increased the formation of a neo

vessel network (Kano et al., 2005). FGF may modulate the effects of VEGF as disruption of FGF signalling reduced VEGFR-2 expression.

VEGF-A has been demonstrated to exert its angiogenic properties through its heparin binding domain. Expression of a truncated VEGF variant in murine models led to poor survival past early childhood (Carmeliet et al., 1996; Ferrara et al., 1996). However, VEGF-A over-expression has also been associated with increasing permeability of the endothelial layer in vessels walls, resulting in vascular leakage and mortality in mice (Lee et al., 2000).

PDGF, EGF and angiopoietins are also crucial growth factors in angiogenesis by regulating cell recruitment, differentiation and survival. Recently it has emerged that FGF-2 stimulates PDGF signalling to induce pericyte proliferation and recruitment, supporting previous literature highlighting that FGF and PDGF both induce migration of osteoblasts via ERK signalling (Hosaka et al., 2018; Kim et al., 2007). The IGF axis is also well known for is potent activation of the Akt pathway, promoting cell migration and proliferation, and mediating vessel remodelling activity (Franklin et al., 2003; Lopez-Lopez et al., 2004).

The majority of pro-angiogenic growth factors activate Akt and ERK/MAPK signalling cascades. Akt signalling is mediated by the growth factor's ability to interact with cell surface tyrosine kinase receptors such as RPTPβ which regulates the inhibition of phosphatase and tensin homolog (PTEN) phosphorylation, resulting in downstream activation of Akt via phosphatidylinositol 3-kinase (PI3K). During angiogenesis, Akt activation can lead to further enhanced expression of VEGF and angiopoietins, creating a feedback loop for continuous activation of angiogenic mechanisms. Mutations of PTEN, as well as Akt itself have been identified in cancers, contributing to continuous and enhanced activation of the Akt pathway (Dillon & Miller, 2014; Yi & Lauring, 2016).

MAPK is activated in response to inflammation and induces the expression of genes involved in cell proliferation, migration and differentiation (Srinivasan et al., 2009). There are three characterised MAPK families which lead the signal from the cell membrane to the nucleus; extracellular signal-regulated kinase (ERK) which is the classical MAPK pathway, c-Jun N-terminal kinase (JNK) and p38 kinase. In angiogenesis, most growth factors stimulate this pathway by the phosphorylation and translocation of ERK1 and ERK2 which is activated by small GTP binding proteins, MEK1 and MEK2 (Santarpia et al., 2012).

The cross talk between pro-angiogenic factors and their action of Akt and MAPK signalling pathways has been extensively researched. Therefore, using the activation

mechanisms, we can modulate activity to achieve sufficient vessel growth via angiogenesis to restore perfusion to ischemic limbs.

1.3.2 Collateral vessels

Collateral circulation is an alternate vessel network consisting of small capillary like vessels which supply blood flow to an ischemic tissue, bypassing an occluded area in a artery or arteriole (Meier et al., 2013). Collateral vessels pre-exist in the vasculature in a non-perfused state. Their expansion is induced by an arteriogenic response initiated by elevated mechanical forces of fluid shear stress caused by the occlusion of blood flow in the main vessel and increased perfusion pressure of the collateral vessels. The opening and widening of collaterals take place following the remodelling of the endothelial layer driven by migration and proliferation in response to endothelial nitric oxide synthase (eNOS) expression. Monocyte recruitment and their differentiation into macrophages stimulate secretion of the inflammatory cytokine, TNF-α and VEGF expression, which upregulates growth factor expression of PDGF, and FGF (Clauss et al., 1990). Shear stress also induces endothelial cells to directly stimulate expression of PDGF and FGF (Patrick, Jr. & McIntire, 1995).

Arteriogenesis stimulating the opening of collateral vessels drives blood flow to the ischemic tissues by maturing collateral arterioles into larger and stable arteries which can hold larger volumes of blood to compensate for the restriction in perfusion (van Royen et al., 2001).

1.3.3 Therapeutic angiogenesis

As discussed previously in Section 1.2.2, angiogenesis can be exploited to promote the formation of new blood vessels in order to restore perfusion to ischemic tissues when revascularisation treatments are unsuitable for CVD patients. Therapeutic angiogenesis has been investigated in pre-clinical and clinical studies over the last two decades as an alternative therapy to amputation; however, progress of this treatment option has been fairly limited.

Angiogenesis to improve tissue perfusion can be promoted by local or systemic delivery of pro-angiogenic factors, via gene, cell or protein therapy. Gene therapy involves the transport of genes which encode angiogenic growth factors to the host genome via viral or non-viral vectors. Cell therapy relies on the delivery of selected cells (e.g. endothelial progenitor cells) involved in vessel formation to ischemic tissues. (Shimamura et al., 2013). However, both methods are not specific or controlled enough to be successful as therapeutic options. They rely on the

uncontrolled release of angiogenic growth factors from cells and therefore the circulating concentrations and duration of release of growth factors can vary from person to person.

Protein delivery could eliminate the problems associated with gene and cell therapy as it involves a systemic or local injection of pro-angiogenic growth factors to the ischemic tissues. As protein therapy does not rely on hosts, the concentration of pro-angiogenic growth factors and administration times can be controlled to achieve the desired result. However, systemic protein injections have resulted in poor delivery due to mechanisms which modulate clearance of growth factors as they are transported to the ischemic site (Chu & Wang, 2012).

There are several pro-angiogenic factors which have shown promise as angiogenic therapeutic agents in early phase-clinical studies. Plasmid human (ph) $VEGF_{165}$ was administered to a CLI patient with occluding vessels and gangrene by using an angioplasty balloon, directly transferring the VEGF plasmid DNA onto the popliteal artery in the lower limb. There was a significant increase in collateral vessels after 4 weeks, which remained at 12 weeks, restoring perfusion by up to 80%. It was reported that the patient developed peripheral edema in the legs, caused by the hyperpermeability activity of VEGF, resulting in swelling of the lower limbs and claimed to be restored via separate treatment. The treated leg had to be amputated 5 months after treatment as gene therapy was inefficient to rescue the limb from gangrene, however the leakage of fluid could have possibly contributed to further problems in the limb. (Isner et al., 1996). Nevertheless, this study provided hope that direct delivery of growth factors could be exploited and optimised to successfully restore perfusion.

Clinical trials on improving recovery from PAD in the last 20 years have been attempted using a variety of growth factor and growth factor combinations. Table 1.1 summarises the growth factors and cells used in the last 10 years which resulted in improvement to PAD, as well as delivery mode and study findings from patients suffering from CLI (Iyer & Annex, 2017). Therapeutic angiogenesis via bone marrow mononuclear cells has shown promising effects in clinical trials, reaching to phase III trials, as well as in enhancing endothelial tube formation *in vitro* and restoration of perfusion in ischemic skeletal muscle *in vivo* studies (Zhao et al., 2008).

Author/Trial	Treatment	Delivery	Findings
Madaric et al., 2017; Phase II	Bone marrow mononuclear cells	Intramuscular, cell therapy	Improvement in oxidative stress and limb salvage
Liotta et al., 2018; Phase II and III	Bone marrow mononuclear cells and Endothelial Progenitor Cells	Intramuscular, cell therapy	Improved muscle perfusion, rest pain, pain-free walking distance, wound healing and ankle-brachial index
Deev et al., 2018; Phase II and III	p-CMV-VEGF165	Intramuscular, gene therapy	Improved target limb recovery. Improved pain-free walking distance. Increased ankle brachial index but this decreased after 5 years.
Gorenoi et al., 2017; Review of 20 growth factor trials	FGF, HGF and VEGF	Gene therapy	No difference in amputation rates or improvement in walking ability but may reduce the rate of amputation

Table 1.1 Recent advances in clinically trialled therapeutic angiogenic treatments for CLI
This table summarises the recent developments made in phase II and III clinical trial treatments to improve recovery from critical limb ischemia. Many of the trials recently investigated are cell therapy techniques, predominantly with the use of bone marrow-derived mononuclear cells. This data was extracted from a variety of published data referenced in the table.

Although VEGF previously had shown poor side effects following treatment, recent interrogation by a Russian group has confirmed the therapeutic effect stimulated by VEGF gene therapy can last for 5 years (Deev et al., 2018). However, the problems associated with failure of therapeutic angiogenic treatment lies with the method of delivery. Cell therapy has thus far proved the most effective as a therapeutic angiogenic treatment via bone marrow-derived mononuclear cells. Treatment with this stem cell therapy has also displayed beneficial effects to nitric oxide levels by reducing expression levels of its inhibitor, asymmetric dimethylarginine (Madaric et al., 2017). Bone marrow-derived allogenic mesenchymal stromal cell therapy is also due to be trailed for no-option critical limb ischemia patients as an early hypothesis

suggests the vasculoregenerative characteristics of these cells can regulate revascularisation to the limbs (Wijnand et al., 2018).

Gene therapy has failed to improve recovery from CLI significantly over a pro-longed period (Deev et al., 2018). Although protein therapy has theoretical benefits over gene therapy, attempts to improve myocardial perfusion in patients with coronary artery disease via protein delivery failed, possibly due to protein half-life being shortened in the ischemic environment (Simons et al., 2002; Simons & Ware, 2003). Failure of FGF and hepatocyte growth factor (HGF) to improve CLI may be due to the administration method used and protein half-life. Another explanation may be the growth factors do not independently activate angiogenesis to a sufficient level to restore blood supply. It is clear VEGF can induce vessel formation; however, the negative side effects can cause further damage (Ylä-Herttuala & Baker, 2017) and this has to be modulated via the method of delivery. Therefore, there is potential for a protein that is able to modulate activity in ischemia to prevent negative effects, as well as enhance recovery effects from CLI to be used as a therapeutic angiogenic agent.

1.4 Vascular permeability

An endothelial cell monolayer lines the inner most layer of the vessel wall, maintaining a physical barrier ensuring large molecules do not enter the blood stream from the tissue (Stevens et al., 2000). A strong endothelial monolayer and stable communication between neighbouring endothelial cells is required for a healthy blood vessel.

Cell-cell and cell-extracellular matrix junctions determine cell permeability and communication. There are three main types of junctions, adherens (anchoring), gap (communication between cells) and tight junctions (sealing of adjacent cells). Cadherins are calcium-dependent cell adhesion molecules which regulate the formation of adheren junctions between cells. Vascular endothelial (VE)-cadherin marks the junctions between endothelial cells. It is specifically recognised for its role in mediating the organisation of the endothelial layer, the permeability and stabilisation of the endothelial barrier via phosphorylation of its tyrosine residue, Tyr685 (Gavard, 2014; Sidibé & Imhof, 2014).

The endothelial dysfunction which drives atherosclerosis results in an imbalance of vasodilators and constrictors, specifically a reduction in nitric oxide (NO) bioavailability (Gimbrone & García-Cardeña, 2016). Nitric oxide is a key regulator of

the endothelial barrier by modulating vasodilation and the influx of small molecules such as water, ions and nutrients into circulation. In the absence of NO, the endothelial permeability decreases due to wall stiffening caused by calcification from atherosclerosis, disabling movement of molecules between the barrier. Conversely, during the formation of new blood vessels, the use of VEGF in clinical trials as a therapeutic agent led to hyperpermeability of the endothelial layer and caused leakage between the blood and vessel wall. VEGF disrupts VE-cadherin by pulling cell-cell junctions apart, resulting in a weak endothelial barrier (Hoang et al., 2011). Although, In order to induce angiogenesis, signals from VEGF have to increase permeability to enable large sized plasma proteins to pass through the barrier to form a foundation scaffold for migrating endothelial cells (Senger et al., 1996). Therefore, vascular permeability induced by VEGF needs to be highly regulated. It is essential that new vessels formed by delivery of growth factors by therapeutic angiogenesis can withstand strong forces of shear stress, hydrostatic and fluid pressure as well as mediate the influx and outflow of small molecules by maintaining endothelial barrier permeability.

1.5 Insulin-like growth factor axis

The insulin-like growth factor (IGF) family makes a significant contribution to reproduction, repair, survival, metabolism and apoptotic pathways. This family consists of two growth hormones, named IGF-I and IGF-II, their respective receptors, IGF-IR and IGF-2R and binding proteins which regulate the activity of the IGF growth factors. In recent years, it has become clear that several components of the axis are implicated in vascular pathophysiology and more specifically in angiogenesis. In this section, the importance of each of the components of the IGF-axis and how they function in order to activate downstream signalling cascades is discussed.

1.5.1 Insulin-like growth factors

IGF-I and –II are evolutionally highly conserved growth factors, which are important in driving growth in-utero and post-natally until adolescence. Growth hormone is responsible for IGF secretion from hepatocytes as well as their endocrine functions. The majority of plasma IGF-I circulates bound to an IGF binding protein, which modulates its biological activity and bioavailability. IGF-I regulates many different cellular and physiological processes. IGF-I has been identified as a key molecule involved in regulating growth and survival mechanisms in many different cell types,

including endothelial cells, smooth muscle cells, endothelial progenitor cells and pericytes, which make it a key player in angiogenesis (Bagley et al., 2005; Okura et al., 2001; Shigematsu et al., 1999). It is mainly known to function through the angiogenic signalling pathways mentioned earlier in this chapter, Akt and ERK (Choi et al., 2008; Schiaffino & Mammucari, 2011). IGF-I also plays a significant role in metabolic homeostasis by reducing high glucose levels via IGF-I dependent activation of the PI3/Akt pathway, activating glycogen synthase activity (Muhič et al., 2015).

IGF-I expression fluctuates in different diseased states, suggesting it plays different roles upon different stimuli. For example, obese, type 2 diabetic and insulin-resistant states affect the normal functionality of IGF-I, also resulting in a reduction in its expression (Aguirre et al., 2016; Imrie et al., 2009; Martha et al., 2008).

IGF-II expression is upregulated during embryonic development and levels drop post-natally, coupled by an increase in IGF-I levels (Kadakia & Josefson, 2016; Switkowski et al., 2017). Although IGF-II shares significant structural homology with IGF-I, post-natally, IGF-II has been shown to function differently to IGF-I. IGF-II has displayed potential in mediating cell migration in hepatocellular cancer and bone marrow cells however clear signalling mechanisms which activate these effects remain unestablished (Fiedler et al., 2006; Nussbaum et al., 2008). Single nucleotide polymorphisms of IGF-II have been shown to be associated with increased bodyweight in adult males and increase body mass index (BMI), therefore suggesting IGF-II may play a protective role against obesity (Gaunt et al., 2001).

The pleiotropic effects of IGFs, specifically IGF-I and their involvement in growth and metabolism means it is unlikely they could be exploited as potential therapeutics.

1.5.2 Insulin-like growth factor receptors

IGF signalling is mediated via interactions of IGFs with their cognate transmembrane tyrosine kinase receptors, IGF-IR and IGF-IIR. IGF receptors are made up of two α and two β subunits, sharing high structural homology with the insulin receptor (IR) which also has the same structural conformation. Both IGFs can interact with IGF-IR with high affinity, however only IGF-II can bind to the IGF-IIR but the binding of IGF-II to the IGF-IIR fails to activate intracellular signalling pathways due to the lack of an intracellular tyrosine kinase domain (Tian et al., 2016).

IGF-I shares structural homology to insulin, and between the receptors, IGF-I can also bind to IR, blocking insulin-stimulated intracellular signalling and increasing insulin resistance (Boucher et al., 2010). The IGF-IR has been widely investigated by

Professor Mark Kearney's group in our laboratory in the context of metabolic diseases. One set of α and β subunits from IGF-IR and one set from the IR are able to bind together to form a hybrid receptor. Insulin can still bind to this hybrid; however, it has a greater affinity for IGF-I, preventing insulin from carrying out its actions, resulting in a decrease in insulin sensitivity (Abbas et al., 2011). Mice over-expressing IGF-1R endothelial cells display enhanced cell migration. These mice also reduced NO bioavailability, however increased endothelial regeneration following arterial injury surgery (Imrie et al., 2012). Therefore, the manipulation of IGF-IR and the hybrids could be used to promote IGF-I stimulated angiogenic cell mechanisms to promote vessel growth and repair.

1.5.3 Insulin-like growth factor binding proteins

Insulin-like growth factor binding proteins (IGFBPs) are a family of six circulating proteins which bind IGFs with high affinity. IGFBPs are approximately 50% structurally homologous, with conserved disulphide bonds between cysteine molecules in the N and C terminals with molecular weights ranging between 22-36kDa.

Their primary function is to modulate the bioactivity of IGF by stimulating or suppressing IGF activity (Figure 1.3). Approximately 90% of all IGFs in the system circulate bound to an IGFBP, although the number of IGF/IGFBP complexes is reliant on the circulating concentrations and half-life of IGFBPs (Twigg & Baxter, 1998). IGFBPs have the ability to increase IGF half-life from its unbound form at 5 mins in serum to between 90 min and 2 hours if complexed with IGFBP-1 or -2 and up to 16 hours with IGFBP-3 or -5 (Clemmons, 2012).

The presence of an 80kDa glycosylated acid-labile subunit (ALS) attached to IGFBP-3 and -5 stabilises the tertiary complex formed with IGF-I. This enables the whole complex with a molecular weight (MW) of 130kDa to circulate in its bound form for pro-longed periods of time, however due to its large size the complex is unable to cross the endothelium. IGFBP-3 is the most abundant of the IGFBP family in circulation; therefore, there are significantly more IGFBP-3/IGF complexes in serum. IGFBP-2 is the second most abundant circulating protein; however, IGFBP-2/IGF complexes have a extremely short half-life and are rarely found circulating in its complex form compared to IGFBP-3, due to the absence of the ALS.

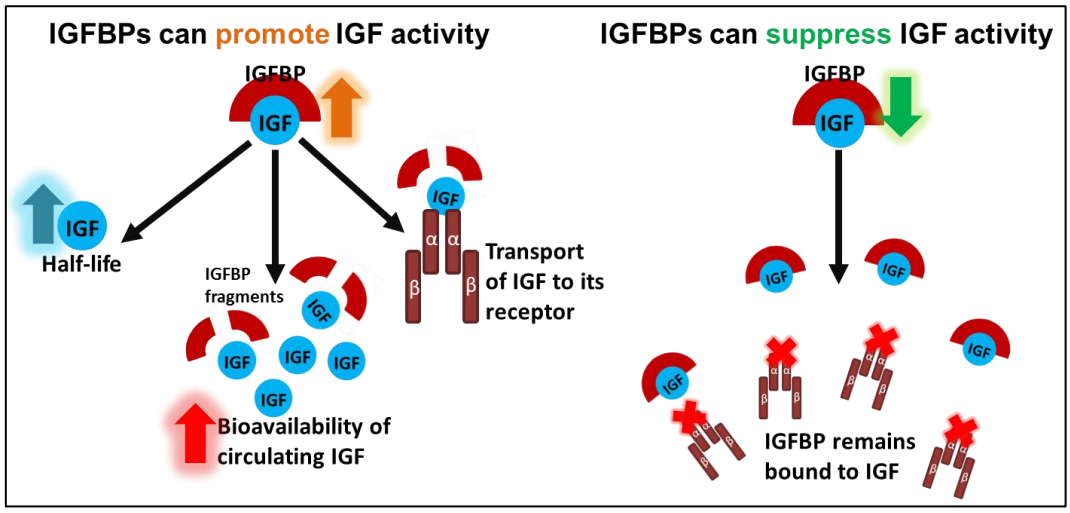

Figure 1.4 IGFBPs regulation of IGF bioavailability and activity
IGFBPs promote IGF activity by increasing IGF half-life, increasing the bioavailability of IGF in the circulation and directly transporting IGF to its receptor. However, IGFBPs can also suppress activity by remaining bound to the IGF and preventing its interaction with its IGF-IR or IGF-IIR.

The variable central region of IGFBPs provides flexibility to form a pocket to bind IGF molecules via the conserved IGF binding sites located on both the N- and C-terminus. Several publications highlight that mutation of one of the IGF binding sites eliminates all IGF binding ability, confirming the method of sequestering free IGF molecules and maintaining the complex via binding to both domains (Perks et al., 2002; Shen et al., 2012).

IGFBP-1, 3 and 5 are able to undergo phosphorylation which enhances their affinity for IGF, via phosphorylation sites located in the central variable region (Coverley & Baxter, 1997; Gupta, 2015; Mishra & Murphy, 2003). IGFBP-3, -and -4 are the only IGFBPs which undergo N-linked glycosylation. This linkage is vital for structural stability in order to bind IGF in IGFBP-4; however, IGFBP-3 displays the same affinity for IGF in its glycosylated and non-glycosylated form. Glycosylation has also been highlighted to interfere with interactions between glycosylated IGFBPs and cell surfaces. Glycosylated IGFBP-3 displayed restricted cell membrane interactions compared to its non-glycosylated form, due to changes in the folding of the protein (Firth & Baxter, 1999). IGFBP-5 and 6 have established O-glycosylated sites, with glycosylation affecting the activity of these proteins in different ways. IGFBP-5 has an increased affinity for heparin in its glycosylated form, suggesting the glycosylation interferes with ECM interactions (Forbes et al., 2012; Graham et al., 2007). Alternatively, to IGFBP-5, glycosylated IGFBP-6 displays a lack of interactions via its heparin binding domain, compared to its non-glycosylated state. Glycosylated

IGFBP-6 increases its half-life by reducing proteolytic activity and in turn increasing the sequestering time period of IGF molecules. (Marinaro et al., 2000). This confirms each IGFBP is unique in its function, with variable factors influencing their final effects.

The non-homologous areas account for interactions independent of IGF binding. IGFBP-I and IGFBP-2 are the only binding proteins with the ability to interact with integrins via their Arginine-Glycine-Aspartic Acid (RGD) domain, located on the C terminus of the protein (Brandt et al., 2015). Most of the IGFBPs have heparin binding potential excluding IGFBP-1 and -4 (Boes et al., 2002; Fowlkes et al., 1997). All heparin binding domains share a similar motif of BBBXXB within the C terminal or the central linker domain of the protein. In the central linker domains of all IGFBP-s, as well as crossing into the C terminus of IGFBP-1, 2, 4 and 6, thyroglobulin type 1 domain (Forbes et al., 2012). The role of this domain is to initiate proteolytic degradation of the protein, enabling the release of IGF molecules to continue with their designated activity. IGFBP-2, 3 and 5 possess a nuclear localisation signal in the variable regions enabling translocation of the complete protein via the importin β nuclear transport factor. It has been hypothesised that these IGFBPs activate nuclear secreted factors, such as VEGF (Planque, 2006).

IGFBP-2 is of particular interest to us because it is the only binding protein that can bind to variety of cell surface tyrosine kinase receptors as it has an integrin recognition site, heparin binding potential, nuclear entry potential, as well as IGF binding capability. All of these domains in other proteins are known to activate angiogenic-like signalling pathways and therefore we aim to identify if these can be exploited for therapeutic potential in IGFBP-2.

1.5.4 IGFBPs in disease

IGFBPs have been implicated in several pathophysiological processes and diseases. A brief overview of the role of IGFBPs in clinical/physiological context is provided in this section, followed by a more in-depth discussion of the actions of IGFBP-2 in Section 1.8.

IGFBP-1 and IGFBP-2 have shown strong associations with insulin sensitivity. Expression of IGFBP-1 is blunted by insulin, however it acts as a biomarker for type 1 diabetes due to its upregulated levels (Kabir et al., 2010). IGFBP-1 has been shown to enhance insulin sensitivity, which is hypothesised to function through the IGFBP-1's RGD domain (Haywood et al., 2017). IGFBP-1 expression levels in VSMCs are elevated by activation of an inflammatory response. Interleukin or TNFα stimulated

secretion of IGFBP-1 in response to inflammation has shown to increase cell proliferation via IGF and IGF independent mechanisms (Wang et al., 2012). Low circulating IGFBP-1 and -2 levels have been associated with diabetes and CVD (Heald et al., 2006; Rajwani et al., 2012). Decreased IGFBP-2 levels have been associated with enhanced levels of lipoprotein in the plasma and therefore may prove to be a biomarker of the onset of atherosclerosis (Carter et al., 2014). Contrastingly, IGFBP-4 along with IGFBP-5 expression has been shown to promote the pathogenesis of atherosclerosis, due to upregulation of the binding proteins in atheroma plaques (Conover et al., 2010; Zheng et al., 1998). Pregnancy-Associated Plasma Protein-A (PAPP-A) is the protein responsible for the cleavage of IGFBP-4 and -5 to release bound IGF molecules. Transgenic mouse model over-expressing PAPP-A promoted the development of atherosclerotic regions, suggesting atherosclerosis development is stimulated by IGF-I delivery by IGFBP-4, or even possibly IGFBP-5 (Harrington et al., 2007). IGFBP-6 expression is mediated by hypoxia in vascular endothelial cells but has been shown to inhibit IGF-stimulated angiogenesis in sarcoma development (Zhang et al., 2012).

The role of IGFBP-3 in metabolic diseases is relatively unestablished as the majority of its research refers to its role within cancer (Hoeflich et al., 2018). With more than 90% of all circulating IGFs bound to IGFBP-3, it exerts suppressive effects on cancer angiogenesis, across prostate and lung cancer (Mehta et al., 2011; Wang et al., 2017b). Many cancer types, such as colorectal, breast, gastric and prostate cancer, have shown a positive correlation between tumour angiogenesis and the upregulation of IGFBPs. Expression of IGFBP-3 elevated levels have shown an association with increasing levels of epidermal growth factor receptor in triple-negative breast cancer tumours, suggesting they coordinate their bioactivity to promote tumour growth and survival (Marzec et al., 2015). IGFBP-2 is the only other binding protein which has demonstrated a positive correlation with tumour growth in breast, collateral, prostate and pancreatic (Liu et al., 2017; Yau et al., 2015a). IGFBP-1 and -5 are well known for their tumour suppressive abilities by inhibiting cancer cell invasion and migration (Dai et al., 2014; Sureshbabu et al., 2012). IGFBP-4's role in cancer development remains relatively unclear as it displays multiple effects according to the cancer type and stage of tumour growth, however, IGFBP-4 has the potential to exert tumour suppressor activity by supressing the growth and survival of colon and prostate cancer cells (Damon et al., 1998). However, in a different colon cell line, upregulation of IGFBP-4 correlated with cell differentiation (Corkins et al., 2002).

This summary highlights that all IGFBPs can induce IGF-independent-mediated effects in diseased states. With many disease variables affecting the fluctuation of IGFBP expression levels, it is difficult to distinguish clear mechanisms by which IGFBPs exert their effects.

1.5.5 IGFBP-related proteins

In addition to the 6 members of the IGFBP family, in the recent decades, further IGFBP related proteins have been discovered, namely IGFBP-rP1-9. These proteins share homology with the N-terminal end from IGFBPs-1-6 but display structural differences beyond this region, resulting in a lower binding affinity for IGF-I (Kim et al., 1997). IGFBP-rP1, also referred to as Mac25 or IGFBP-7 has been gaining much interest in the recent years as it also displays insulin binding capabilities, as well as IGF, through the conserved cysteines in the N terminal region (Akaogi et al., 1996). Research highlights the multiple metabolic roles IGFBP-rP1 may have, however mechanisms are not clearly established. The other related IGFBP-rPs have not surfaced to play significant roles in the modulation of IGF or IGF-independent interactions with metabolism and therefore are rarely the focus of research.

1.6 Insulin-like growth factor binding protein-2

IGFBP-2 has been reported to have roles in regulating metabolic activity, as well as pathophysiological processes in a range of diseased states and cell types. However, very few articles have attempted to identify the mechanisms IGFBP-2 functions through to exert its cellular effects due to its complex interactions with multiple cell surface tyrosine kinase receptors and possibly nuclear entry (Figure 1.5).

IGFBP-2 is a 36kDa protein and is the second most abundant circulating binding protein that can increase the half-life of IGFs. However, IGFBP-2 also exerts several IGF-independent effects via its RGD domain, HBD1 and HBD2 sites and its nuclear localisation signal. The majority of these IGF-independent interactions have been demonstrated to drive cell migration and proliferation, as well as to suppress tumour growth in a variety of cancer and non-cancer cell types including glioma, prostate cancer cells, VSMCs, osteoblasts and adipocytes. However, extremely limited research has been carried out to investigate the actions of IGFBP-2 on vascular endothelial cells.

1.6.1 Insulin-like growth factor binding

IGFBP-2, similar to all IGFBPs, is able to increase the half-life of IGFs and it can transport IGFs directly to the IGF receptors, in turn enhancing IGF dependent mechanisms. The half-life of IGF in the circulation is only extended to a short period of between 90 min and 2 hours by IGFBP-2, due to the absence of the ALS in the complex formed (Clemmons, 2012). The central variable and flexible region of IGFBPs enables IGFBP-2 to mould around IGF-I and –II molecules to 'sequester' them. The capturing process enables IGFBP-2 to control the activity of IGF by release via proteolysis of IGFBP-2 or by remaining in its bound form, in turn inhibiting binding to the IGF-IR. IGFBP-2 also requires both IGF binding domains to remain completely functional for successful IGF regulation (Demambro et al., 2012).

This study by Demambro et al., (2012) highlighted a functional IGF binding domain is essential to mediate the differentiation of osteoclasts via activation of the Akt signalling pathway, which is not stimulated through PTEN dephosphorylation. However, IGF/IGFBP-2 interactions are less pronounced compared to IGFBP-2's IGF independent stimulated effects, therefore there is limited research on the activity of the IGF binding potential of IGFBP-2.

1.6.2 Receptor Protein Tyrosine Phosphatase-β interactions

IGFBP-2 HBD1, which is present in the central variable region interacts with the tyrosine kinase receptor RPTPβ, located on the cell surface and induces intracellular Akt signalling cascades in certain cells, e.g. vascular smooth muscle cells and osteoclasts. The mechanism by which IGFBP-2 stimulates RPTPβ is by mediating the dephosphorylation of PTEN, activating downstream targets PIP_3, PDK, and eventually leading to Akt. This IGFBP-2 interaction has been demonstrated to play a critical role in many cellular and pathological processes.

HBD1, although to a lesser extent than HB2 in the C terminal protects against obesity be supressing preadipocyte differentiation into adipocytes, suggesting some of this activity may be due to RPTPβ (Xi et al., 2013). This initial observation of the inhibition of preadipocyte differentiation was reported by (Wheatcroft et al., 2007), however a global over-expressing hIGFBP-2 mouse model was used for this study and specific signalling via one of IGFBP-2 structural domains was not studied.

In vitro over-expression of RPTPβ inhibited osteoclast differentiation in the absence of IGFBP-2 as inactive RPTPβ is unable to modulate the dephosphorylation of PTEN. PTEN in its phosphorylated form prevents the activation of downstream targets leading to Akt, hence preventing Akt mediated differentiation. However, with the

addition of IGFBP-2, osteoclast differentiation was rescued confirming this differentiation is stimulated by IGFBP-2 HBD1. (Xi et al., 2014).

In pancreatic cancer, the suggested mechanism for the nuclear translocation and phosphorylation of NF-κB was through HBD1/ RPTPβ- activated Akt signalling. Cells from this malignancy upregulated levels of IGFBP-2 and this was associated with tumour growth. Pancreatic carcinoma cells failed to induce the activation of NF-κB signalling in response to elevated PTEN levels, confirming this activity was stimulated by IGFBP-2/ RPTPβ interactions to stimulate Akt phosphorylation (Gao et al., 2016). The importance of IGFBP-2/ RPTPβ's interaction was supported further by the following study. Mice over-expressing a hIGFBP-2 mutant with a non-functional HBD1 site, displayed a phenotype with reduced neuronal markers affecting the overall function of the brain (Schindler et al., 2017). Anxiety-like characteristics were eliminated by 80 weeks of age, suggesting IGFBP-2 activated RPTPβ plays a significant role in early brain development.

From these findings, we can assume IGFBP-2-activation of RPTPβ is critical to cell differentiation and activation of certain signalling pathways, indirectly stimulated by Akt. Abolishment of IGFBP's ability to act with the tyrosine kinase receptor via its HBD1 domain resulted in complete loss of activity, suggesting there aren't any mechanisms stimulated by IGFBP-2 that can compensate for the loss of Akt activation.

1.6.3 Nuclear transport

IGFBP-2 has been reported to enter the nucleus and participate in transcriptional regulation, although the evidence for this is weak. The main mechanism reported is nuclear importins are able to translocate IGFBP-2 into the nucleus where it activates VEGF and mediates its transport to its receptor, VEGFR2, activating VEGF signalling pathways (Azar et al., 2011, 2014). This was hypothesised to be the driving force for the enhancement of *in vitro* endothelial cell tube formation by IGFBP-2 (Das et al., 2013). There is some controversy over the nuclear localisation of IGFBP-2 reported in neuroblastoma cancer cells as cell membranes were permeabilised prior to experimental exposure to IGFBP-2 (Azar et al., 2014). It is unclear whether IGFBP-2 in the extracellular space can cross the cell membrane in a physiological setting.

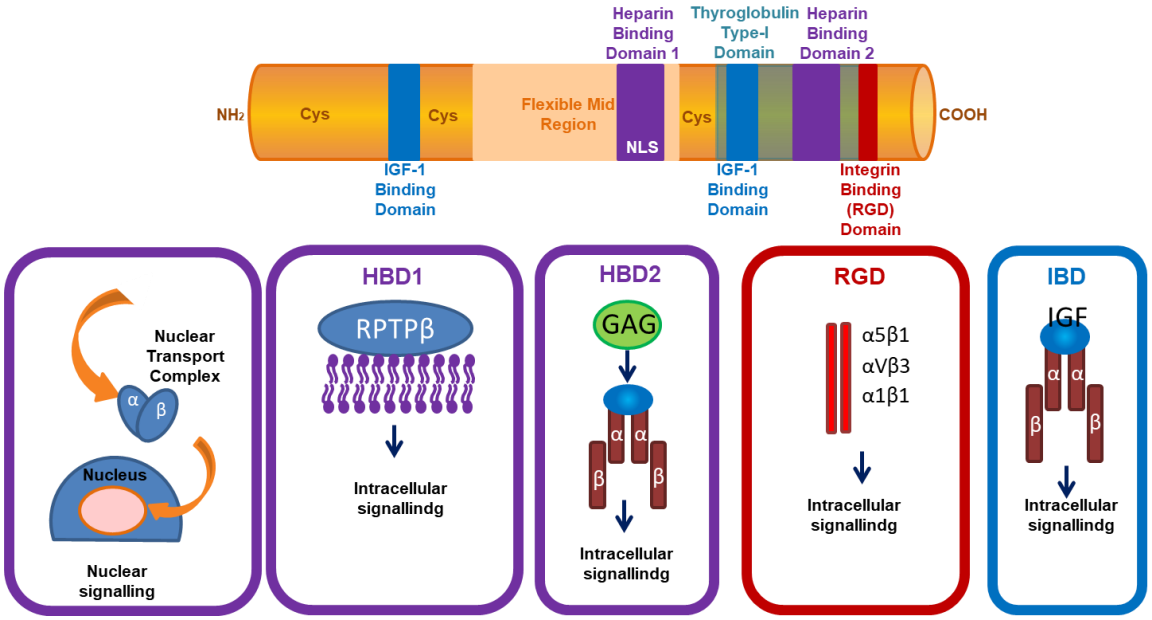

Figure 1.5 Potential Interaction of IGFBP-2
This diagram displays all the possible interactions IGFBP-2 has been associated with in literature to drive intracellular and nuclear signalling. This image has been adapted using findings from the publications discussed in this section (1.6).

1.6.4 Glycosaminoglycan interactions

IGFBP-2 mediated glycosaminoglycan interactions are thought to be mediated predominantly via HBD2 while HBD1 mediates RPTPβ activation. Interaction via this HBD2 domain is relatively unestablished. Differentiation of pre-adipocytes is inhibited more potently by HBD2 than HBD1, as confirmed by mutation of the heparin binding domain sites (Xi et al., 2013). Arai et al., (1996) found that heparin binding capability of IGFBP-2 is only initiated once IGFs have bound to the binding protein, inducing a conformational structural change, and exposing the HBD.

These interactions may not be as potent as the interactions between IGFBP-2 and RPTPβ and therefore effects of this interaction may not be as pronounced. More research needs to take place to understand the role of how glycosaminoglycan functions with IGFBP-2 and what signalling pathways it specifically activates.

1.6.5 Integrin interactions

IGFBP-2 has been shown to interact with integrins via its RGD domain which modulates cell proliferation and migration mechanisms via activation of MAPK signalling pathways. As mentioned briefly in Section 1.5.1, IGF-I activates PI3K/Akt to induce cellular glucose uptake. However, IGFBP-2-modulated glucose uptake

appears to be stimulated by its RGD domain, via an upregulation of FAK and integrin-linked kinase (ILK), increasing levels of insulin mediated glucose transporter type 4 (GLUT4) (Reyer et al., 2015).

Glioma cell proliferation, invasion and migration are driven by the interaction of IGFBP-2 with β1 integrin subunit causing the activation of ERK/MAPK signalling cascades, confirmed by the knocking down of β1 which resulted in the loss of ERK activity (Han et al., 2014). IGFBP-2/α5 interactions have demonstrated a significant role in glioma cell mobility by increasing the number of focal adhesions. Mutant RGD domain failed to present focal adhesion and lamellipodia-like morphology, which promote migration of cells, however this was rescued with the addition of functional IGFBP-2 and α5 (Wang et al., 2006). Angiogenic mechanisms in melanoma have been suggested to be stimulated by IGFBP-2 via its interaction with αVβ3 (Das et al., 2013). However, this IGFBP-2/integrin interaction was previously described to modulate IGF activity. Breast cancer cells which upregulated αVβ3, when stimulated with IGFBP-2, IGFBP-2/αVβ3 interaction in-directly suppressed IGF-I mediated migration responses (Pereira et al., 2004).

Nevertheless, published literature demonstrates IGFBP-2 predominantly exerts its cellular activities via the interactions between the RGD domain and the integrins α1β1, α5β1 and αVβ3. The majority of these interactions have only been investigated in cancer cell lines and the exerted effects may vary between different cell types.

1.6.6 Insulin-like growth factor binding protein-2 in disease

IGFBP-2 has been implicated in playing a role in several diseased states. This section will bring together the published research on the role of IGFBP-2 within diseases to help us notice if certain mechanisms are cell type-dependent or disease-dependent. This will help us understand how IGFBP-2 may function in vascular endothelial cells and how it may mediate recovery in response to ischemia.

Metabolic diseases such as obesity and diabetes influence the concentration levels of IGFBP-2 in circulation. In obesity, IGFBP-2 concentrations are down-regulated compared to normal circulating levels (Hedbacker et al., 2010). IGFBP-2 was reported to prevent pre-adipocyte differentiation and proliferation, protecting against the onset of obesity in high fat fed mice and insulin resistance compared to WT littermates (Wheatcroft et al., 2007). This has been supported by findings confirming IGFBP-2 inhibits development of human visceral adipocytes by reducing expression of key lipogenic markers. This activity is thought to be mediated by IGFBP-2's HBD, as stimulation with mutant HBD resulted in reduction of lipid abundance, and

therefore restored activation of lipogenesis via FAK and Akt signalling (Yau et al., 2014). Insulin sensitivity in obese children has been associated with reduced IGFBP-2 circulating levels which matches the low IGFBP-2 levels associated with type 2 diabetes (Frystyk et al., 1999; Yau et al., 2018).

The majority of IGFBP-2 research is carried out in cancer cell lines, as in most of them IGFBP-2 expression is upregulated and this correlates with tumour growth. IGFBP-2 has recently been shown to promote cell invasion, proliferation and migration of glioma cells and breast cancer cells via activation of ERK/JNK mediated MAPK and de-phosphorylated PTEN activation of Akt (Foulstone et al., 2013; Han et al., 2014).

Contrastingly to reports of IGFBP-2 being upregulated to tumour progression in glioma, IGFBP-2 levels are found to be downgraded in a high-grade glioma. These reduced levels were shown to be due to p16, which is usually deleted in cancers. p16 is well known to down-regulate IGFBP-2 levels but does not halt glioma progression (Moore et al., 2009). Fluctuation of IGFBP-2 concentrations in relation to cancer stage was also investigated using prostate cancer cells, with IGFBP-2 being elevated in affected patients' plasma (Cohen et al., 1994). Studies with breast cancer cells confirmed IGFBP-2 drives growth and survival, and when IGFBP-2 is silenced, this effect is lost. Some studies suggest IGFBP-2 stimulated growth and survival of cancer cells is via integrin, or reduction in PTEN expression causing inactivation of Akt stimulated pathways (Pereira et al., 2004).

There are few data implicating IGFBP-2 in CVD and the studies that have been carried out are conflicting. High concentrations of IGFBP-2 were associated with dysfunctional left ventricular ejection fraction (Berry et al., 2015). De Kort et al., (2010) identified reduced levels of IGFBP-2 are a marker of increased risk of cardiovascular disease in young adults who were born small for gestational age.

IGFBP-2 demonstrates roles as a protector, an activator and a suppressor of different cell processes depending on its stimulus in diseased states. By identifying the mechanism that IGFBP-2 drives through endothelial cells to promote angiogenic-like characteristics, we could exploit and optimise that particular mechanism with additional stimuli to achieve our desired result.

1.7 Summary

IGFBP-2 remains an understudied binding protein which is known to function through its multiple domains to induce intracellular mechanisms via IGF-I, integrin, RPTPβ,

glycosaminoglycans interactions or nuclear entry. However, IGFBP-2 has shown promise with its effects in obesity and cancer, that it has the potential to regulate angiogenic-like mechanisms in endothelial cells. With growth factors failing in clinical trials for treatments for PAD, IGFBP-2 currently promotes functional changes in non-endothelial cell types by which it can promote and suppress their activity, dependent on external stimuli. These mechanisms could potentially be exploited in order to increase new healthy blood vessel growth in the setting of ischemia.

Chapter 2 - Hypothesis and aims

2.1 Hypothesis

IGFBP-2 can promote the formation of new, healthy blood vessels in ischaemia and provide a potential novel treatment for ischemic cardiovascular diseases.

2.2 Aim

To investigate the mechanisms by which IGFBP-2 promotes angiogenesis *in vitro* and interrogate the potential for IGFBP-2 to promote recovery from ischaemia *in vivo.*

2.3 Objectives

- Investigate if increasing IGFBP-2 concentration promotes recovery from hindlimb ischaemia *in vivo*.
- Determine if local expression of IGFBP-2 is upregulated in ischaemia and acts as a driver of angiogenesis.
- Identify which angiogenic signalling pathways are targeted by IGFBP-2.
- Interrogate whether angiogenic functionality of endothelial cells is upregulated by IGFBP-2.
- Create individual mutation of the IGF binding, RGD site and HBD/NLS via site-directed mutagenesis to identify which structural domain of IGFBP-2 is critical to stimulate angiogenic responses.
- Investigate whether IGFBP-2 modulates permeability of the endothelial monolayer.

2.4 Significance and impact

As described in the introduction, IGFBP-2 has been established to contribute significantly to cellular responses in metabolism, growth, diabetes and cancer which implies it could be potentially be exploited for therapeutic angiogenesis. However, the role of IGFBP-2 within ischemic cardiovascular diseases is unknown. The angiogenic potential of IGFBP-2 within ischemia has also not been fully investigated. By identifying the underlying mechanisms by which IGFBP-2 regulates angiogenesis, we may be able to propose IGFBP-2 as an additional therapeutic strategy for ischemic diseases. The development of IGFBP-2 as a therapeutic angiogenic agent

would add to current treatment options available, potentially resulting in a decrease in morbidity and mortality in patients with ischaemic disorders.

2.5 Ethical implications

The use of murine models was approved and all procedures were performed according to the guidelines set out in the project licences (40/3523, 70/8115, P144DDOD6) and awarded personal licence (I6AF7B00B), which have been approved by Home Office UK regulation – Animals (Scientific Procedures) Act 1986. Annual usage reports were submitted to the Home Office UK summarising the severity of all experimental procedures undertaken. All experiments were carried in designated rooms within the University of Leeds – Animal Facility or Leeds Institute of Cardiovascular and Metabolic Medicine.

2.6 Safeguarding of data

All data generated were stored according the safeguarding regulations outlined by the University of Leeds. The policy covers the confidentiality and the storage of all data on university-approved computers and networks.

Chapter 3 – General methods

3.1 Cell culture

All cell centrifugation steps were carried out at 300xg for 5 mins.

In order to count cells, trypan blue (Life Technologies, 1520061) and a cell counting chamber (Hawksley, AC100) were used to count the cells and were then split to achieve a cell density of $1x10^6$ (in a T75 flask), $3x10^5$ (in a T25 flask) or $1x10^4$ (per well of a 6-well plate (Sarstedt, 83.3920.300).

Cells were passaged by washing the cell monolayer with Dulbecco's phosphate buffered saline (PBS), pH 7.4, followed by addition of trypsin (Life Technologies, 25200072). Trypsin activity was deactivated with Dulbecco's Modified Eagle Media (DMEM), containing 10% Fetal Bovine Serum (FBS) and 1% antibiotic-antimyotic solution (AAS).

All cells were incubated at 37ºC with 5% CO_2 in a humidified incubator, unless stated otherwise.

3.1.1 Human Umbilical Vein Endothelial Cells

Pooled Human Umbilical Vein Endothelial Cells (HUVECs) (Promocell, C-12208) were either cultured in Promocell Endothelial Growth Media 2 (Promocell, C-22011), with supplement mix (Promocell, c-39216) and 1% AAS (Invitrogen, 15240) or M199 endothelial growth media (Sigma-Aldrich, M4530), supplemented with 20% FBS (BioSern, FB 1001/500), 2% 1M hepes (Sigma-Aldrich, 83264), 2% sodium pyruvate (Sigma-Aldrich, S8636), 0.5% endothelial cell growth supplement (Sigma-Aldrich, E2759), 0.5% heparin sodium (1000Units/ml) (LEO Laboratories) and 1% AAS.

3.2 Cell lysis

Cells were washed twice with ice-cold PBS pH 7.4. Cell extraction buffer (Invitrogen FNN0011) (with 0.002% protease (Sigma, P8340) and 0.002% phosphatase (Sigma, P0044) cocktail inhibitors) was used to lyse cells. Lysates were purified by centrifugation at 13,000 rpm, 4ºC for 15 mins and the supernatant was collected.

3.3 Immunoblotting

A Bicinchoninic acid (BCA) protein assay kit (Pierce 23225) was used to determine the total protein concentration of cell lysates. Samples were mixed with LDS sample

buffer and sample reducing agent. Samples were heated for 5 mins at 95ºC, before being loaded into wells of a 4-12% Bis-Tris gel (NuPAGE NP0335), with a MW marker (Biorad 161-0385). Gel was submerged in diluted MES SDS running buffer (20x) (NuPAGE NP002) and run at 180V for 1 hour.

Solution	Contents
Transfer buffer	0.48M tris base (Fisher Scientific, BP152), 0.39M glycine (Fisher Scientific, BP381-1) and 0.1% Sodium dodecyl sulphate (SDS) (Sigma, 05030)
Tris-buffered-saline (TBST) pH 7.2 (10x Stock Solution)	1.7M NaCl, 190mM Tris HCl (Fisher Scientific, BP153), 27mM KCl (Fisher Scientific, P/4280/60) and 0.1% tween 20 (Sigma, P9416)

Table 3.1 Transfer and TBST wash buffer recipe

The components and concentrations used to make transfer buffer for the transfer of the gel to the membrane and a 10x stock solution of TBST buffer to wash the membranes ready for blocking with the antibody. The 10x TBST stock as diluted to a 1x solution for experiments.

Polyvinylidene difluoride membranes (Millipore) were activated with methanol and sandwiched with the gel. Transfer buffer (Table 3.1) was diluted with methanol (Fisher Scientific, M/4056/17) and distilled water (dH_2O). The transfer was run at 100V for 45 mins.

Transferred membranes were blocked in 5% BSA (made up with TBST (table 2)) and then incubated in primary antibodies (Table 3.2) for 16-20 hours at 4ºC on an orbital shaker. All wash stages were performed with TBST at room temperature (RT). The membrane was submerged in secondary polyclonal antibodies (Table 3.3) for 1 hour at RT. Anti-western-C marker (Biorad 161-0385) was incubated with the membrane for 10 mins followed by final washing steps.

Immobilon Western Chemiluminescent HRP Substrate (Millipore, WBKLS0500) was pipetted over the blot. Imaging software, SynGENE and the SynGENE GBOX were used to capture an image of the membrane.

All membranes were stripped using 2% glycine stripping buffer (0.2M glycine, 0.1% SDS, pH2.5).

Antibody	Company	Molecular Weight (kDa)	Species	Dilution	Diluting agent
Phospho-eNOS	Cell Signalling	140	Rabbit	1/1000	All antibodies were diluted in 5% BSA (Made up with TBST) (except *)
eNOS	Cell Signalling	140	Rabbit	1/1000	
Phospho-FAK	Cell Signalling	125	Rabbit	1/1000	
FAK	Cell Signalling	125	Rabbit	1/1000	
Hsp90	Santa Cruz	90	Mouse	1/20000	
Phospho-Akt (Ser473)	Cell Signalling	60	Rabbit	1/1000	
Anti-Akt	BD Biosciences	60	Mouse	1/1000	
Phospho-PTEN	Cell Signalling	54	Rabbit	1/1000	
Phospho GSK3β	Cell Signalling	46	Rabbit	1/1000	
p-MAPK	Cell Signalling	42-44	Rabbit	1/1000	
*MAPK	Cell Signalling	42-44	Mouse	1/1000	*5% Milk (Sigma, 70166) in TBST
β-Actin	Santa Cruz	42	Mouse	1/3000	5% BSA in TBST
IGFBP-2	Santa Cruz	36	Goat	1/1000	

Table 3.2 Primary antibodies for immunoblotting

List of all the antibodies used in the immunoblotting experiments carried out throughout this thesis. The table consists of the company which the antibody was sourced from, the expected molecular weight and diluting agent used for signalling studies.

Antibody	Dilution
Donkey anti-mouse	Prepared to a 1:5000 dilution in 5% milk powder with TBST
Donkey anti-rabbit	
Donkey anti-goat	

Table 3.3 Secondary polyclonal antibodies

List of secondary antibodies sourced from Jackson ImmunoResearch Laboratories and the dilution used to help visualise the primary antibody on the membrane.

3.4 Biotinylated IGF-I ligand blotting

LDS sample buffer and lysis buffer were added to varying concentrations of commercially sourced recombinant IGFBP-2. Reducing agent was not added and the samples were not heated prior to being loaded on a 4-12% Bis-Tris gel with the molecular weight marker. The gel was run, and the transfer was carried out using the same conditions as the immunoblotting process in 2.3.4. Membranes were blocked in 5% BSA/TBST (as mentioned in Section 2.3.4) for 1 hour at room temperature. Biotinylated IGF-1, produced by Dr Paul Cordell was made to a 1:1000 dilution using 5% BSA/TBST and incubated with the membrane for 2 hours at room temperature. The membrane was washed 3x10 min with TBST. Streptavidin was diluted 1:5000 in 5% BSA/TBST and incubated with the membrane for 1 hour. The membrane was washed 2x10 min before being imaged in the same manner as stated in Chapter 3.3. Membranes were stripped and probed for IGFBP-2 using the immunoblotting method

Chapter 4 - Investigating the effect of over-expression of IGFBP-2 on recovery from hind limb ischemia *in vivo*

4.1 Background

There has been fairly limited research regarding IGFBP-2s involvement in angiogenesis. IGFBP-2 has been associated to promote many angiogenic-like characteristics such as invasion, migration, proliferation and survival (Foulstone et al., 2013; Han et al., 2014; Liu et al., 2017). In addition, due to the complexity of IGFBP-2s structure and multiple interactions, there is much uncertainty regarding the predominant mechanism responsible for these actions. The majority of research on IGFBP-2s potential in enhancing angiogenic-like characteristics has been carried out on cancer cells, and has not been investigated in a cardiovascular context (Azar et al., 2011; Patil et al., 2016). Many publications have reported IGFBP-2s protective mechanisms against the onset of obesity and therefore it is plausible these protective characteristics may be exerted upon an ischemic insult (Wheatcroft et al., 2007; Yau et al., 2015b).

In order to determine whether IGFBP-2 does play a role within ischemia-induced angiogenesis and whether this role can be exploited for therapeutic potential, it is necessary to identify the specific mechanisms through which it functions. As this has not previously been researched at an *in vitro* or *in vivo* level, the starting point of this project is to identify if IGFBP-2 plays a vascular angiogenic type role to aid recovery from ischemia in a mouse model. This would give us the validation to investigate the mechanisms activated further for the use of IGFBP-2 on a translational medicine level. As our main aim is to use IGFBP-2 as a potential therapeutic for PAD, we will be using an *in vivo* representative surgical model, hind limb ischemia (HLI) (Niiyama et al., 2009). Observing how over-expression of IGFBP-2 on a global and endothelial-specific level can help to restore perfusion to the lower limbs that have been starved of a blood supply, will enable us to determine if IGFBP-2 does play a role in angiogenesis.

.

4.1.1 IGFBP-2 *in vivo* models

Currently, the only IGFBP-2 *in vivo* animal models used to develop IGFBP-2 research are global mIGFBP-2 knock out (KO) and global hIGFBP-2 over-expression mice.

Initial characterisation of the KO IGFBP-2 mouse highlighted IGFBP-1, -3 and -4 levels were elevated in response to the absence of IGFBP-2 (Wood et al., 2000). This suggests there is a particular requirement for IGFBP-2 in regular homeostasis as the family of IGFBPs attempt to compensate for the loss of activity. The communication mechanisms between IGFBP-2 and the family of IGFBPs are relatively unestablished, however limited publications have highlighted IGFBP-2 and -3 function in combination to modulate IGF-I actions (Alkharobi et al., 2016). The KO IGFBP-2 model is mainly known for its gender-specific differences in bone development, with male mice demonstrating reduced proliferation of osteoblasts and osteoclasts compared to their female counterparts. They also identified the absence of IGFBP-2 caused a significant increase in PTEN levels compared to global over-expressing IGFBP-2 mice, confirming IGFBP-2 can regulate Akt signalling via modulation of PTEN. (DeMambro et al., 2008).

The first global hIGFBP-2 over-expressing murine line was produced and characterised by Hoeflich et al., (1999). This mouse model displayed a reduced carcass weight in globally over-expressing hIGFBP-2 transgenic mice compared to WT littermates. Further research carried out by Wheatcroft et al., (2007) on a global over-expressing hIGFBP-2 mouse line identified its protective nature, preventing the onset of obesity and insulin resistance following a high fat diet. IGFBP-2 directly prevented fat development by suppressing the proliferation and differentiation of adipocytes, resulting in protection against weight gain. Thus, again highlighting IGFBP-2 is able to exert protective properties to restore regular health, specifically in regard to cardiovascular disease.

4.1.2 Recovery from hind limb ischemia

HLI surgery is a commonly used *in vivo* angiogenesis experimental procedure, in which the blood flow to the lower leg is disrupted, resulting in an immediate inflammatory response. As there is no evidence of IGFBP-2 driving an angiogenic response or vessel growth directly, it is very difficult to hypothesise the effect IGFBP-2 over-expression may have on recovery. However, IGFBP-2 has been reported to be essential to embryonic vascular development in vertebrates (Wood et al., 2005).

Arteriogenesis, as discussed in Chapter 1, is the first mechanism to be activated in response to a restriction in blood supply. A build-up of shear stress from the blood flow attempts to relieve the pressure by causing the enlargement of vessels or collateral artery formation (Duvall et al., 2004). Collateral vessel circulation is an alternative network of smaller sized vessels which can compensate for a blockage in artery in order to relieve the blood pressure and transport the blood to its end location (Figure 4.1).

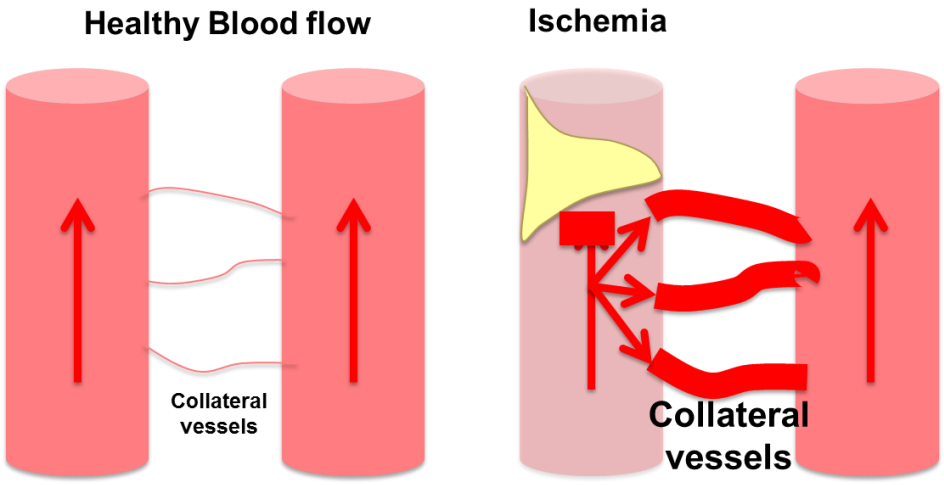

Figure 4.1 Arteriogenesis mechanism
Small capillary sized collateral vessels remain closed between healthy blood vessels. Blockage in the artery onsets arteriogenesis and causes the expansion of collateral vessels into larger sized arterioles to restore perfusion via the alternative artery. Adapted from Iwasawa et al., (2016).

Gene profiling following ligation of the penile artery in rats resulted in an ateriogenic recovery response; however IGFBP-2 was not involved as expression levels remained unchanged from before and after ligation (Lin et al., 2001)

As arteriogenesis is induced by shear stress and not hypoxia, it is the initial mode of recovery following HLI, before an inflammatory response is signalled. In contrast, angiogenesis is induced by hypoxia and drives the formation of small capillaries (Shireman, 2007). Therefore, angiogenesis would begin to occur later on in the recovery process. IGFBP-2 has been reported to regulate HIF-1α expression in neuroblastoma tumour metastasis and later findings have confirmed the interaction between IGFBP-2 and HIF-1α are critical for the growth of glioblastoma cells (Azar et al., 2011; Lin et al., 2015). Activation of VEGF, a potent inducer of angiogenesis, is modulated by IGFBP-2 to induce an angiogenic-type response in HUVECS *in vitro* (Das et al., 2013). This suggests IGFBP-2 begins to induce a response before

angiogenesis has begun, as it may be responsible for expression of the angiogenesis induction factor, HIF-1α and VEGF in ischemia. It is important to note that IGFBP-2 is upregulated in ischemic brain, probably as a result of hypoxia (Fletcher et al., 2013). Therefore, there is evidence that it might be playing a role in driving recovery from ischemia. Fletcher et al., (2013) also suggested a proposed mechanism that IGFBP-2 may transport IGF-I directly to the ischemic site and upregulate IGF-I pathways to rescue the blood flow as confirmed by an upregulation of IGF-I, correlating with upregulation of IGFBP-2 72 hours after stroke.

Therefore IGFBP-2 levels may also be elevated in response to PAD. To determine if IGFBP-2 drives arteriogenesis and/or angiogenesis mechanisms, we need to identify how long it takes IGFBP-2 to induce a response to the ischemic environment and how it functions in order to restore perfusion.

4.1.3 Summary

Although IGFBP-2 has never previously been known to directly promote angiogenesis, its upregulation has been positively correlated with tumour growth, via enhancement of mechanisms such as invasion, migration and proliferation. IGFBP-2 global KO and over-expressing mouse models have highlighted its role in mediating cell proliferation and differentiation *in vivo*, as well as displaying a protective nature in compromised health states.

Therefore IGFBP-2 has the potential to enhance the restoration of perfusion following HLI. The endothelial-specific over-expression of IGFBP-2 model will confirm if IGFBP-2 mediates endothelial cell migration and proliferation to drive an arteriogenic and angiogenic recovery response.

4.2 Experimental objectives

We aim to identify if IGFBP-2 plays an angiogenic reparative and a protective role in the context of PAD using *in vivo* murine models. This is important because we need to prove IGFBP-2s ability as a potential therapeutic angiogenic acute treatment in a clinical setting. Using *in vivo* models will also clarify IGFBP-2 does not cause the same negative angiogenic outcome caused by VEGF and functions through a VEGF-independent mechanism. Therefore, these findings would provide a foundation and reasoning to investigate IGFBP-2s role in angiogenesis further. The research in this chapter was carried out using the objectives listed:

- Investigate the local expression of IGFBP-2, in relation to VEGF in ischemic limbs in wild-type mice.
- Investigate the effects of the global over-expression of hIGFBP-2 and the endothelial-specific over-expression of hIGFBP-2 on perfusion recovery responses following the use of a PAD *in vivo* model, HLI.

4.3 Materials and Methods

4.3.1 Generation of gene modified mice

Global over-expressing hIGFBP-2 model

Dr Paul Crossey (Kings College London) produced this globally over-expressing hIGFBP-2 transgenic (TG) mouse model (Wheatcroft et al., 2007). The mice were purchased from The Jackson Laboratory where they had been banked after generation (stock number 008222).

The complete IGFBP-2 transgene, at a total MW of 39kb was extracted from a human cosmid clone Pronuclear microinjection was used to deliver the gene into FVB/N embryos. These transgenic mice were generated via backcrossing and continuously bred with C57BL/6J mice for a minimum of 9 generations. The C57BL/6J mice have been recommended as the non-carrier control/wild-type (WT) for hIGFBP-2 mice due to it sharing a 94% background with them. The line of mice globally overexpressing human IGFBP-2 has been maintained at the University of Leeds Animal Unit.

Endothelial-specific over-expressing hIGFBP-2 model

The flox hIGFBP-2 mouse was produced by Genoway in 2017. A Rosa26 approach was used to create the knock-in of hIGFBP-2. Genoway 'knocked' in a targeting vector containing hIGFBP-2, promoter and STOP cassette into the mouse's own Rosa26 locus. The Conditional hIGFBP-2 over-expression is driven by the Chicken β-Actin (CAG) promoter. However, there is a STOP casette in between the promoter and the protein therefore expression only takes place once the STOP casette has been excised. LoxP sites are placed either side of the STOP casette which can be catalysed by Cre recombinase, removing the STOP cassette, stimulating hIGFBP-2 over-expression (Figure 4.2).

An inducible VE-Cadherin Cre-recombinase mouse was a kind gift provided by Dr Ralf Adams. This mouse is inducible due to the estrogen receptor present after the cre-recombinase cassette. This receptor is only activated once stimulated by tamoxifen injections. In its inactive state, cre-recombinase is not expressed. Due to the VE-Cadherin, cre-recombinase is only expressed in endothelial cells once induced by tamoxifen. This recombinase mouse was bred with the floxed mouse generated by Genoway, resulting in a TG positive pup with both mouse genotypes (Figure 4.3).

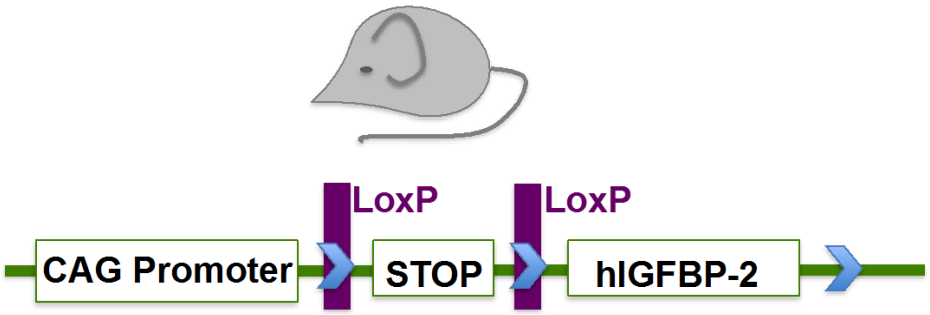

Figure 4.2 A schematic outline for the generation of the hIGFBP-2 flox mouse
The sequence within the hIGFBP-2 flox mouse has a CAG promoter, with a STOP cassette surrounded by two LoxP sites, with the hIGFBP-2 gene following after, in the distal position.

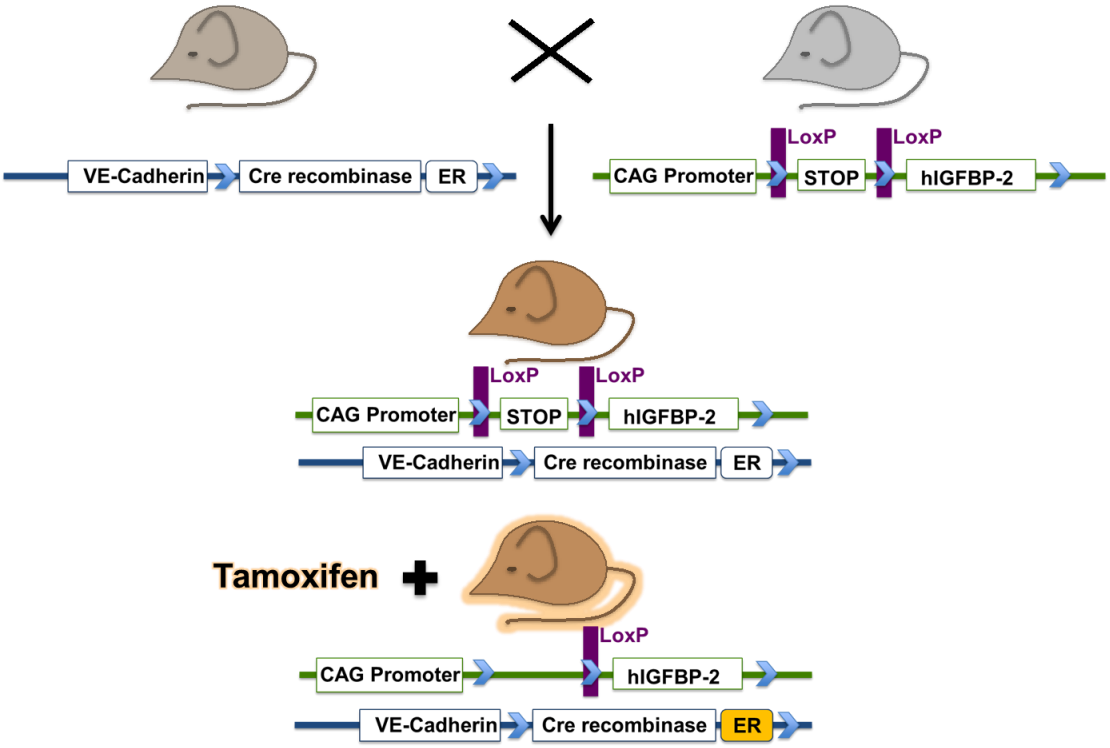

Figure 4.3 Inducible endothelial-specific over-expression hIGFBP-2 mouse
Inducible VE-cad cre-recombinase mouse was crossed with the hIGFBP-2 flox mouse to generate a mouse flanked with loxp sites around a STOP cassette preventing hIGFBP-2 and cre recombinase which is controlled by the estrogen receptor. Once induced by tamoxifen, the estrogen receptor drives cre-recombinase expression in endothelial cells, resulting in excision of the STOP cassette and over-expression of hIGFBP-2, driven by the CAG promoter

4.3.2 Tamoxifen injections

Mice were kept in a tamoxifen only room for safety reasons. Tamoxifen (Sigma-Aldrich,85266) was diluted into solution using corn oil (Sigma-Aldrich, C8267) to 10mg/ml. 100µl of this solution was injected intraperitoneally on alternate sides for 5 consecutive days. Injected mice were left for 7 further days in the tamoxifen only room to ensure tamoxifen would not be toxic to other colleagues.

4.3.3 Genotyping

To confirm over-expression of human IGFBP-2 in both mouse models compared to the wild-type littermates, DNA was extracted from ear notches. A HOTSHOT method was used to extract the DNA (Truett et al., 2000). The notches were incubated in an alkaline lysis solution (25mM NaOH, 0.2mM EDTA pH 12.0) and heated at 95ºC for 20 min. Neutralisation reagent (40mM Tris-HCL pH5) was added. Samples were stored short term at 4ºC or long term -20ºC. Genotypes were confirmed using polymerase chain reaction (PCR) as referred to in Section 4.3.3.1.

End products were run on a 1.5% agarose gel prepared with agarose (Sigma, A9539) and TAE buffer (40mM Tris Base (Fisher Scientific, BP152), 20mM Acetic Acid (Sigma, 506007), 1mM of 0.5M EDTA (Sigma, E9884)). Ethidium bromide (Sigma, E1510) was added to the gel before set. The gel was submerged in TAE buffer; PCR products were loaded with a 100bp MW ladder (New England Biolabs, N0467S) and run for 1 hour at 100V. The gel was imaged using SynGENE GBOX.

From mid-2017, all mice ear notches, including ear notches collected from the, hIGFBP-2 TG line, VE-hIGFBP-2 heterozygous and homozygous line were sent to an external genotyping service, TransnetYX.

4.3.3.1 Primer and PCR cycle data for the TG hIGFBP-2 line

PCR for the TG hIGFBP-2 mouse was carried out using the primers in the table 4.1.

Primer 5' Label	Sequence 5' → 3'
BP-2 Forward	CCT GTG CAG CAG CTT CTC GCT GAG
BP-2 Reverse	CCC AGG CTG GCA CCA TGC TCA CCT G
BP-2 Control Forward	CAA ATG TTG CTT GTC TGG TG
BP-2 Control Reverse	GTC AGT CGA GTG CAC AGT TT

Table 4.1 TG hIGFBP-2 genotyping primers

Primer sequences which amplify the TG hIGFBP-2 global over-expressing gene during genotyping PCR.

Each reaction was made up of 12.5µl Bio mix red PCR Mastermix (Bioline BIO25006), 0.5µl 10µM each primer, 1µl DNA and 9.5µl DNA/RNA free H_2O. The PCR cycle used is listed in table 4.2.

PCR Stage	Number of Cycles	Time	Temperature
Initial Denaturation	1	5 min	95°C
Denaturation	35x	1 min	95°C
Annealing		1 min	65°C
Extension		1 min	72°C
Final Extension	1	10 min	72°C
End	1	∞	4°C

Table 4.2 TG hIGFBP-2 genotyping protocol

PCR cycle used to amplify DNA products in order to determine the genotype of the TG hIGFBP-2 gene or the WT littermate**.**

4.3.3.2 Primer sequences for the VE-hIGFBP-2 heterozygous and homozygous mice lines

PCR for the VE-hIGFBP-2 heterozygous and homozygous mice were carried out by TransnetYX using primers in the table 4.3:

Primer	Primer Sequence 5' to 3'	PCR product size	
		Wild-type allele	**Inducible Knock-in allele**
182053creWHE1	CTCCCAAAGTCGCTCTGAGTTGTTATCA	778 bp	245 bp + 7378 bp*
182054creWHE1	CGATTTGTGGTGTATGTAACTAATCTGTCTGG		
0034-KIn-ROSAGX6044	GCAGTGAGAAGAGTACCACCATGAGTCC		

Table 4.3 VehiHom genotyping primers

Primer sequences which amplify the Cre and Flox inducible region during genotyping PCR.

4.3.4 Animal husbandry and breeding

Cages were housed in the animal unit within the University of Leeds. Temperature, humidity and light conditions were controlled at 21ºC and humidity at 55%, with 12 hour light cycles. All mice were fed a standard chow diet and provided drinking water. Breeding cages were assembled using 1 male and 2 female mice at approximately 7 weeks of age, consisting of TG and WT phenotypes to establish hIGFBP-2 colonies. C57/BL6 females were also mated with TG males. Breeding cages were re-established when reproduction rates were slow, birth of small sized litters or if the parental mice were becoming too old (8 months of age).

Offspring were weaned 3 weeks after birth and housed in cages to a maximum of 6 pups per cage and according to the sex of siblings. Cages consisting of mice above 6 weeks of age only housed a maximum of 5 mice per cage. An ear notching system was used to label the mice in each cage. Female mice were culled under the schedule 1 act at weaning unless females were required to replenish breeding cages.

4.3.5 Culling of mice

Mice were culled by two methods: the use of a CO_2 chamber or by cardiac puncture. 100% CO_2 is released into the chamber with the mice for 6mins at a flow rate of approximately 20% per min. The release was repeated to ensure death. Mice were placed under anaesthetic using Isoflurane (IsoFLo) and cardiac puncture was used to obtain a terminal blood flow. Dislocation of the neck was carried out after both methods to confirm death.

4.3.6 Weight measurements

Mice were weighed on a weekly basis and before and after tamoxifen injections, using standard weighing scales. Weight measurements were collected in grams.

4.3.7 General Anaesthesia

All mice were individually placed in an anaesthetic chamber. A constant flow of oxygen was maintained at 2L/min. Isoflurane was directed to the chamber, putting mice into an unconscious state after 2/3mins. Mice were then moved onto the nose cone, where the unconscious mouse was secured in place onto a heated surgical table set at 37ºC. The isoflurane rate was also reduced to 2.5-3%, with the oxygen flow maintained. A scavenger system was present to remove all toxic components from the isoflurane system to be removed from the environment. If mice were to be recovered following surgery, mice were removed to an environment free from isoflurane and placed on a heated surface, set at 37ºC. Mice typically recover from the anaesthetic within 5mins.

4.3.8 Hind limb ischaemia

Mice (8/9 weeks of age) were shaved below the abdomen on the front side in preparation for surgery on the following day. Surgery was carried out on a heated surface at 37ºC by Dr Nadira Yuldasheva. Lubrithal eye gel (Dechra) was applied to the eyes to prevent them drying out or contracting conjunctivitis during surgery before securing the mouse in place. Buprenorphine, an analgesic drug was injected via intraperitoneal injection and skin was washed with 3% Hydrogen Peroxide. Microscope (Ziess, OPM 1-FC) was used between x7.2 and x30 magnification (dependent on the view required) to create a small incision in the left hind limb area. The fat was removed in order to expose the femoral artery, vein and nerve. After separation of the femoral artery from the vein and nerve, sutures (using 8.0 vicryl suture) were placed at the proximal and distal ends of the artery, leaving a space of approximately 1mm between the sutured ends of the femoral artery, disrupting the arterial blood supply. The 1mm section of artery between the sutures was cut out. Isotonic saline solution (0.9% NaCl) was used to prevent tissues from drying out. The incision was closed using 8.0 vicryl suture and continuous stitching. Post-surgery saline solution was injected intraperitoneally to ensure the mice did not suffer from dehydration and leg exercises were carried out to help restore regular leg movement.

Mice were placed in a cage on a 37ºC surface until expected mobility and awareness was observed.

4.3.8.1 Laser Doppler imaging and analysis

Mice were anaesthetized using 5% isoflurane in oxygen. This was reduced to 1.8% as the mouse was placed on the stage. Double sided tape was used to stick feet in a position which can enable laser Doppler imaging. The calibrated Moor Instruments (Axminster, Devon) laser imager was started and took images from the toes to the abdomen, highlighting areas of blood flow in warm colours such as red. Reduced blood flow results in colder colours such as blue. Mice were left to recover from the anaesthetic on a heated table.

Analysis was carried out using MoorLDI V6 to measure blood flow changes. Using the polygon tool, an outline was drawn around the foot and leg up, just past the knee (Figure 4.3). The statistics tool is able to calculate the blood flow within the leg from the flux image in a numeric form. The left leg (ischemic) is normalised against the right leg (non-operated) to account for any variables that affect each mouse.

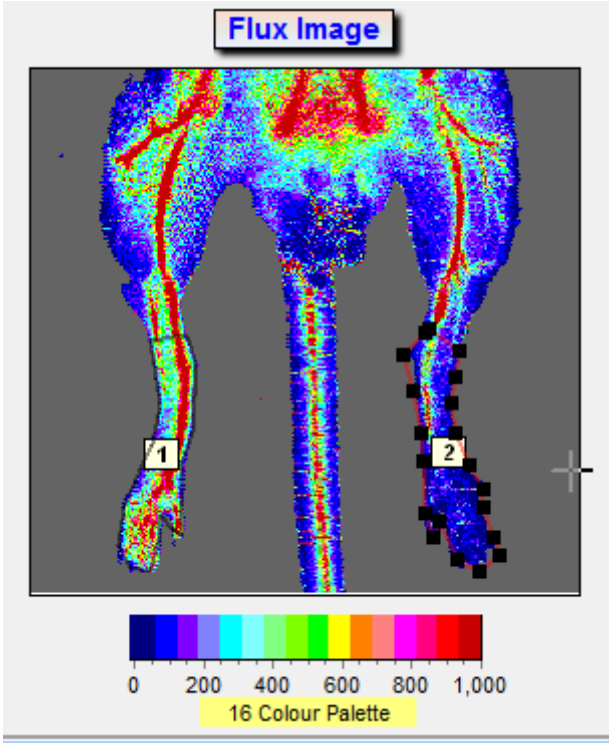

Figure 4.4 Example of the Laser Doppler analysis tool
An outline is drawn around the leg from just above the knee of both the non-operated (1) and ischemic (2) legs. The Moor Instruments Analysis Tool was then used to calculate the blood flow in that area.

4.3.9 Muscle Harvest

Mice were placed under general anaesthesia following 24 hours after HLI. Cardiac puncture was used obtain a terminal blood sample. Surgical tools were used to collect the Gastrocnemius, Soleus and Tibialis muscles from both legs. Muscles for PCR were immediately incubated into liquid nitrogen and later stored at -80 ºC for long term storage.

4.3.10 Cell culture

All cells were lysed in exactly the same manner as stated in Chapter 3.2. Lysates were used for immunoblotting (materials and methods can be found in Chapter 3.3).

4.3.10.1 Primary isolation of Pulmonary Endothelial Cells (PECs)

Lungs from wild-type (WT) and transgenic (TG) globally over-expressing IGFBP-2 mice were broken up using scalpel blades and collagenase, prepared in Hanks Balanced Salt Solution (HBSS). The collagenase and lung mixture was incubated at 37ºC for 45 mins. The precipitate was broken up further using a cannula and strippette, in order to ensure a single cell suspension. The mixture was then put through a 40mm sieve, following a wash with 5% BSA in PBS pH 7.4.

Collagenase solution was removed by centrifugation and pellet was washed with the BSA/PBS wash. Following another centrifugation at 1200rpm for 5 mins, the pellet was suspended in a small volume of BSA/PBS wash and incubated with CD146 (LSEC) microbeads (Miltenyi Biotec, 130-092-007) for 20 mins at 4ºC. The incubated mixture was centrifuged at 4000rpm for 5 mins. BSA/PBS wash was dropped through the MS column attached to the MACs magnet separator. The pellet containing the beads and sample was resuspended in BSA/PBS wash and put through a sieve, leading the washed MS column. Once the sample had entered into the column, 5 washes of BSA/PBS followed. The column was removed of the magnet and BSA/PBS wash was added to flush out all the contents in the column.

For all cells purified with a second column, the output is incubated with fresh LSEC beads again and put through the column again. Washes were carried out in the same manner.

Samples were centrifuged at 4000rpm for 5 mins and the pellet was resuspended in ECGM MV2 media (Promocell, C-22221), supplemented with supplement mix (Promocell, C-39226), 10% FBS and 1% AAS. Cells were plated onto 0.1% gelatin coated plates. After 1.5hour incubation at 37ºC and 5% CO_2, cells were washed with

PBS and fresh media was added. This was repeated the following day. Half media changes were carried out every other day.

4.3.11 IGFBP-2 ELISA

Blood was collected from a vein in the leg of the murine model and spun for 6000xg for 10mins at room temperature. The top plasma layer was collected into another tube. Plasma was diluted 1:200 using buffer A provided in IGFBP-2 ELISA kit (Abcam, ab215082). The remaining protocol was carried out according to the IGFBP-2 ELISA handout in the kit. The concentration of IGFBP-2 was determined in ng/ml using the standard curve calculated.

4.3.12 Real-time PCR

Below are the steps which need to be taken to obtain cDNA from tissue samples to use in real-time PCR to test for expression of species-specific genes.

4.3.12.1 RNA Extraction

Tri reagent and ball bearings were added to muscle samples and degraded by mechanical force using a tissue lyser. Samples were centrifuged at 15,000xg for 10 mins. Supernatant was transferred into a new eppendorf. Phenol chloroform was added, and samples were centrifuged at 15,000xg for 15 mins. The top layer which contains the RNA was pipetted into a fresh tube and isopropanol was added to each sample. The tubes were centrifuged at 15,000xg for 10 mins. Supernatant was discarded, and the pellet was washed with 70% ethanol. The wash step was repeated before samples were left to air dry. Pellets were then resuspended in DNA/RNA free H_2O. The RNA was validated using a Nanodrop to determine the 260/230nm ratio and 260/280nm ratio. Only RNA samples which had a 260/230nm value over 2 and a 260/280nm value of approximately 2 were used, as these values signified nucleic acid and RNA purity.

4.3.12.2 DNAse I Treatment

In order to remove contamination of DNA from the RNA extraction, a master mix of DNase I buffer and DNase I was made from a DNA removal kit (Invitrogen, AM1906). This was pipetted into each RNA sample and incubated at 37ºC for 1 hour. DNase inactivation reagent was added and incubated at room temperature for 5 mins. Samples were spun at 10,000xg for 1 min. RNA was transferred into a fresh tube. RNA concentration was determined using a Nanodrop. 260/230nm and 260/280nm

ratios were also used to validate the purity of the sample, as described in Section 4.3.12.1.

4.3.12.3 Reverse transcription

A high-capacity RNA to cDNA kit (Invitrogen, 4388950) was used for this conversion. RNA was diluted to a weaker concentration with DNA/RNA free H_2O, so that 2ng of RNA is present in a maximum volume of 9µl. 10µl of 2x RT Buffer mix, 1µl of 20x RT Enzyme mix and up to 9µl of RNA sample, made up to a total reaction volume of 20µl with DNA/RNA free H_2O. The cycle in table 4.4 was used for reverse transcription.

Step	Temperature (ºC)	Time (min)
1	37	60
2	95	5
3	4	∞

Table 4.4 Reverse transcription cycle

This table reports the steps which make up the reverse transcription cycle, highlighting the incubation times at certain temperatures in order to obtain cDNA.

4.3.12.4 Real-time PCR reaction

Primers were sourced from Bio-rad (Table 4.5) and their optimised protocol was used to produce the reaction mixture. mGAPDH was used as the housekeeping gene for all reactions.

Primer	Catalogue
hIGFBP-2	qHsaCED0043615
mIGFBP-2	qMmuCID0006519
mVEGF-A	qMmuCED0040260
mGAPDH	qMmuCED0027497

Table 4.5 Real-time Bio-rad primers

Bio-rad primers used for real-time PCR, in order to observe changes in gene expression with hIGFBPP-2, mIGFBP-2, mVEGF-A and mGAPDH and their catalogue numbers.

cDNA was dissolved to a useable concentration using DNA/RNA free H_2O. Per reaction in a 96 well plate, 1µl PrimePCR Assay (primer), 10µl Bio-Rad SYBR Green

Supermix, 1-4µl cDNA (equivalent to 200ng) was added. Variable volumes of nuclease-free water are added to make a total volume of 20µl. All samples were run in duplicate. The real-time cycle was performed using a thermal cycler, using the following cycle (Table 4.6).

PCR Stage	Number of Cycles	Time	Temperature
Polymerase Activation and Initial Denaturation	1	30 sec	95°C
Denaturation	35x	10 sec	98°C
Annealing/Extension		30 sec	60°C
Metal-Curve Analysis	1	5 sec	95°C

Table 4.6 Real-time PCR cycle
The different stages, including the cycle times and temperature which make up the entire real-time PCR cycle.

The raw cycle threshold (Ct) values were collected and the mGAPDH was subtracted from the gene of interest Ct values providing a difference value (ΔCt). The following formula was used to calculate the relative quantification (RQ), representing the total expression of a gene: $\mathbf{RQ = 2^{-\Delta Ct} x\ 100}$.

4.3.13 Ethical Implications

All experimental procedures were performed under the UK Home Office regulations as approved in the project licence (403523/P144DDOD6) and personal licence (I6AF7B00B). Mice were checked and weighed on a weekly basis to ensure a healthy status. Any mice with weights lower than 80% of the weights of their fellow siblings, due to unknown reasons were culled and not used for experimental procedures. Mice displaying irregular phenotypes were also removed from experiments.

4.3.14 Data analysis

MoorLDI V6 was used to carry out analysis following HLI. GeneTools was used to perform densitometry analysis of the bands on each western blot. Unpaired t-tests were used to test for significance. Error bars represent SEM.

4.4 Results

4.4.1 Effect of global over-expression of hIGFBP-2 on recovery in perfusion following HLI

Although this global over-expressing transgenic (TG) mouse model has been characterised previously in our laboratory, it is important to confirm the genetic modification is present to a significant level (Wheatcroft et al., 2007).

DNA extracted from mouse ear notches confirmed WT and global over-expression hIGFBP-2 (TG) genotypes (Figure 4.5 A). Results from the hIGFBP-2 ELISA kit confirmed significant over-expression of hIGFBP-2 in plasma from the TG mice compared to WT mice (Figure 4.5 B). There was no difference in weight between WT and TG mice. However, female TG mice were significantly smaller than male TG mice (Figure 4.5 C). Laser Doppler imaging visualised the improvement in perfusion after HLI surgery on a weekly basis for 28 days (Figure 4.6 A). The blood flow from ischemic limb compared against non-ischemic limb was significantly enhanced at day 7 in the TG mice compared to the WT mice (Figure 4.6 B). However, there was not an overall difference in perfusion to the ischemic limb between the TG and WT mice after 28 days of recovery (Figure 4.6 C)

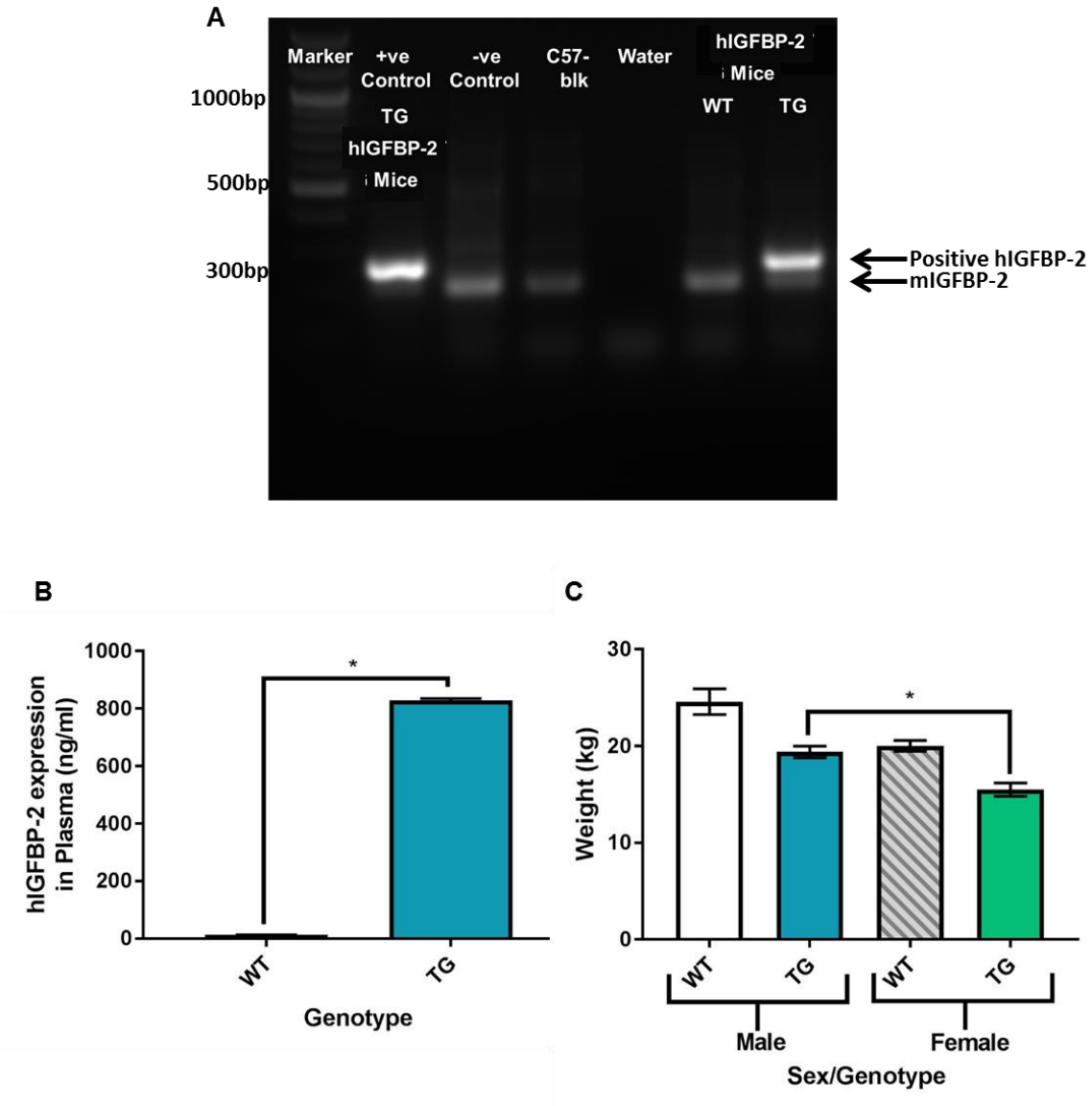

Figure 4.5 Characterisation of hIGFBP-2 TG mice
(A) Agarose gel (1.5%) stained with ethidium bromide has 5µl of DNA (2µg) loaded following RT-PCR extracted from ear notches in the mice with hIGFBP-2 forward and reverse primers, which amplify the hIGFBP-2 gene. Lane 1: Molecular weight (MW) marker; Lane 2: Positive control, TG hIGFBP-2 confirmed mouse (MW = 300bp); Lane 3: Negative control, non-TG hIGFBP-2 mouse line; Lane 4: C57blk mouse control; Lane 5: Water; Lane 6: WT hIGFBP-2 mouse; Lane 7 TG hIGFBP-2 mouse (MW = 300bp). The lighter band in the non-positive samples at a MW = 290bp represents mIGFBP-2.
(B) Plasma collected from blood taken from the leg of a mouse was run on an hIGFBP-2 ELISA kit. Final hIGFBP-2 concentrations in the samples were calculated in ng/ml. Error bars show SEM (*=p<0.02, n= WT=7, TG=7). **(C)** Mice, WT and TG from male and female litters were weighed (in kg) at 8 weeks of age. Error bars show SEM (*=p<0.05, n= Male WT=5, Male TG=4, Female WT=4. Female TG=4).

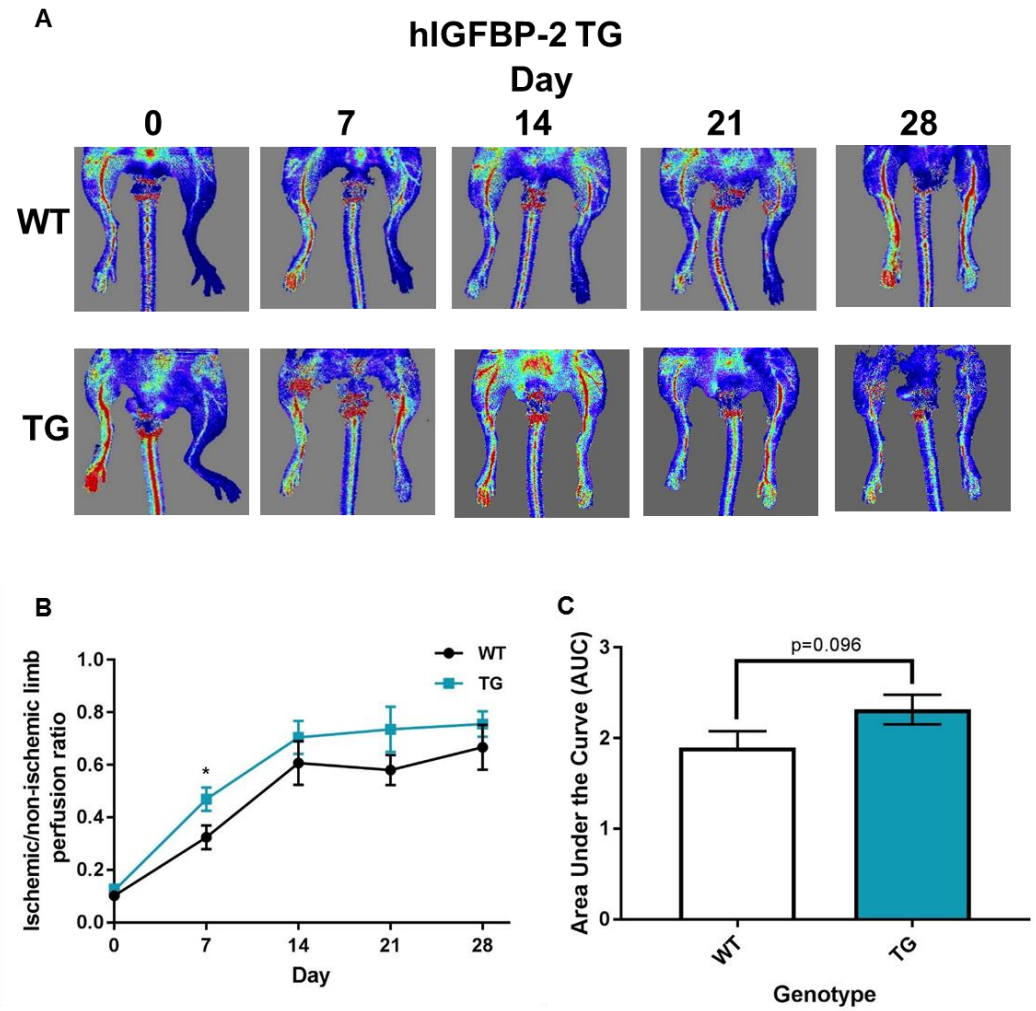

Figure 4.6 hIGFBP-2 causes a significant enhancement in perfusion following HLI at day 7

(A) Representative images of Laser Doppler imaging carried out on mice on a weekly basis following HLI surgery in WT and TG mice from 7-28 weeks. **(B)** Perfusion in the ischemic and non-operated legs was measured using Laser Doppler imaging and Moor Instruments Review tool. After taking account of the area of the leg measured, ischemic perfusion values were normalised against the non-operated (non-ischemic) perfusion values, providing a ratio displayed in the graph. Error bars show SEM (*=p<0.04, n= WT-13, TG=14). **(C)** Area under both curves, WT and TG was calculated from Figure 4.6B using Prism GraphPad. The AUC values are displayed in this graph. (p=0.096, n= WT-13, TG=14). Error bars show SEM

4.4.2 Signalling in PECs over-expressing hIGFBP-2

A common problem that occurs with PEC isolations is obtaining a mixed population of fibroblasts and endothelial cells. Fibroblasts as the modulator of endothelial cell proliferation and therefore have a more pronounced proliferative and invasive nature which is able to over-populate an endothelial cell culture (Eckermann et al., 2011). A positive correlation between IGFBP-2 levels and fibroblast differentiation has already been established resulting in high expression levels of mIGFBP-2 (Park et al., 2015). The antibody used to identify presence of IGFBP-2 in cell lysates is unable to distinguish between mouse and human IGFBP-2 therefore, mixed population of fibroblasts and PECs abolished over-expression of IGFBP-2 in TG compared to WT. However, second column purification resulting in pure endothelial cells displayed a significant enhancement in IGFBP-2 expression in TG PECs compared to WT (Figure 4.7). Over-expression of hIGFBP-2 in TG endothelial cells before ischemia did not enhance Akt or eNOS phosphorylation, compared to total levels (Figure 4.8).

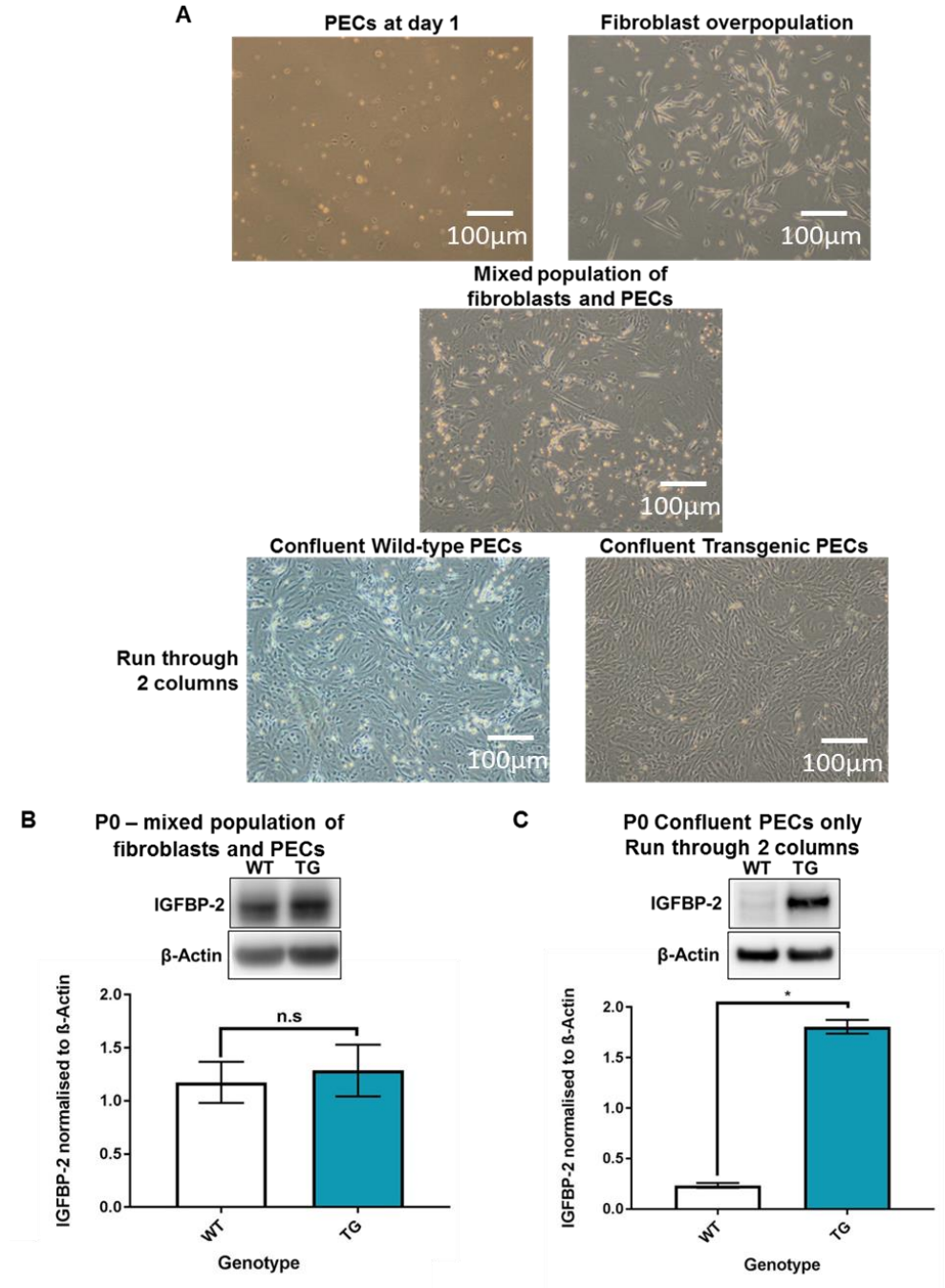

Figure 4.7 PECs confirm TG genotype

(A) Representative images taken using an optical microscope at a 40x magnification (scale 100µm) display mixed cultures of fibroblasts and endothelial cells before and following a 2nd separator column. **(B)** 40µg protein from WT and TG PEC lysates, pre-2nd column run, was loaded onto the western blot, probing for goat polyclonal anti-IGFBP-2 (MW=36kDa) and, the loading control, murine monoclonal anti-β-Actin (43kDa). Blots were stripped and reimaged to confirm no presence of attached primary antibodies between probing for IGFBP-2 and β-Actin. Densitometry was measured using Genetools and IGFBP-2 levels were normalised against the loading control. Error bars show SEM (n= WT=3, TG=3). **(C)** 40µg protein from WT and TG PEC lysates, post-2nd column run, was loaded onto the western blot, probing for goat polyclonal anti-IGFBP-2 (MW=36kDa) and, the loading control, murine monoclonal anti-β-Actin (43kDa). Blots were stripped and reimaged to confirm no presence of attached primary antibodies between probing for IGFBP-2 and β-Actin. Densitometry was measured using Genetools and IGFBP-2 levels were normalised against the loading control. (*=p<0.001, n= WT=3, TG=3). Error bars show SEM.

Figure 4.8 hIGFBP-2 over-expression in PECs does not phosphorylate Akt or eNOS

Representative images of immunoblots which were carried out using 40µg protein from WT and TG PEC lysates, post-2nd column run. Blots were imaged after being stripped to check no substrate or antibody remained bound between probing with different antibodies. **(A)** Probed for rabbit polyclonal anti-phospho Akt (MW=60kDa) and murine polyclonal anti-Akt (MW=60kDa) and, the loading control, murine monoclonal anti-β-Actin (43kDa). Lane 1 consists of WT PEC lysates, lane 2 contains TG PEC lysates. (n= WT=3, TG=3). **(B)** Probed for rabbit polyclonal anti-phospho eNOS (MW=140kDa) and rabbit polyclonal anti-eNOS (MW=140kDa) and, the loading control, murine monoclonal anti-β-Actin (43kDa). Lane 1 consists of WT PEC lysates, lane 2 contains TG PEC lysates. (n= WT=3, TG=3).

4.4.3 mVEGF levels after HLI

Laser Doppler images 24 hours after surgery confirm restriction of blood flow to the lower leg (Figure 4.9 A). Images were taken of the harvested muscles, the gastrocnemius, soleus and tibialis (Figure 4.9 B).

Real-time PCR of hIGFBP-2 in WT and TG muscles confirmed hIGFBP-2 was only present in the TG soleus muscle (Figure 4.10 A). mIGFBP-2 levels increased in the TG soleus following ischemia compared to non-operated (Figure 4.10 B). hIGFBP-2 levels were significantly elevated in TG ischemic soleus and tibialis compared to their non-operated control (Figure 4.10 C).

mIGFBP-2 levels were elevated in ischemic gastrocnemius, soleus and tibialis muscles in WT mice (Figure 4.11 A). mVEGF levels did not correlate with upregulated levels following ischemia in the WT or TG mice muscles (Figure 4.11 B & C).

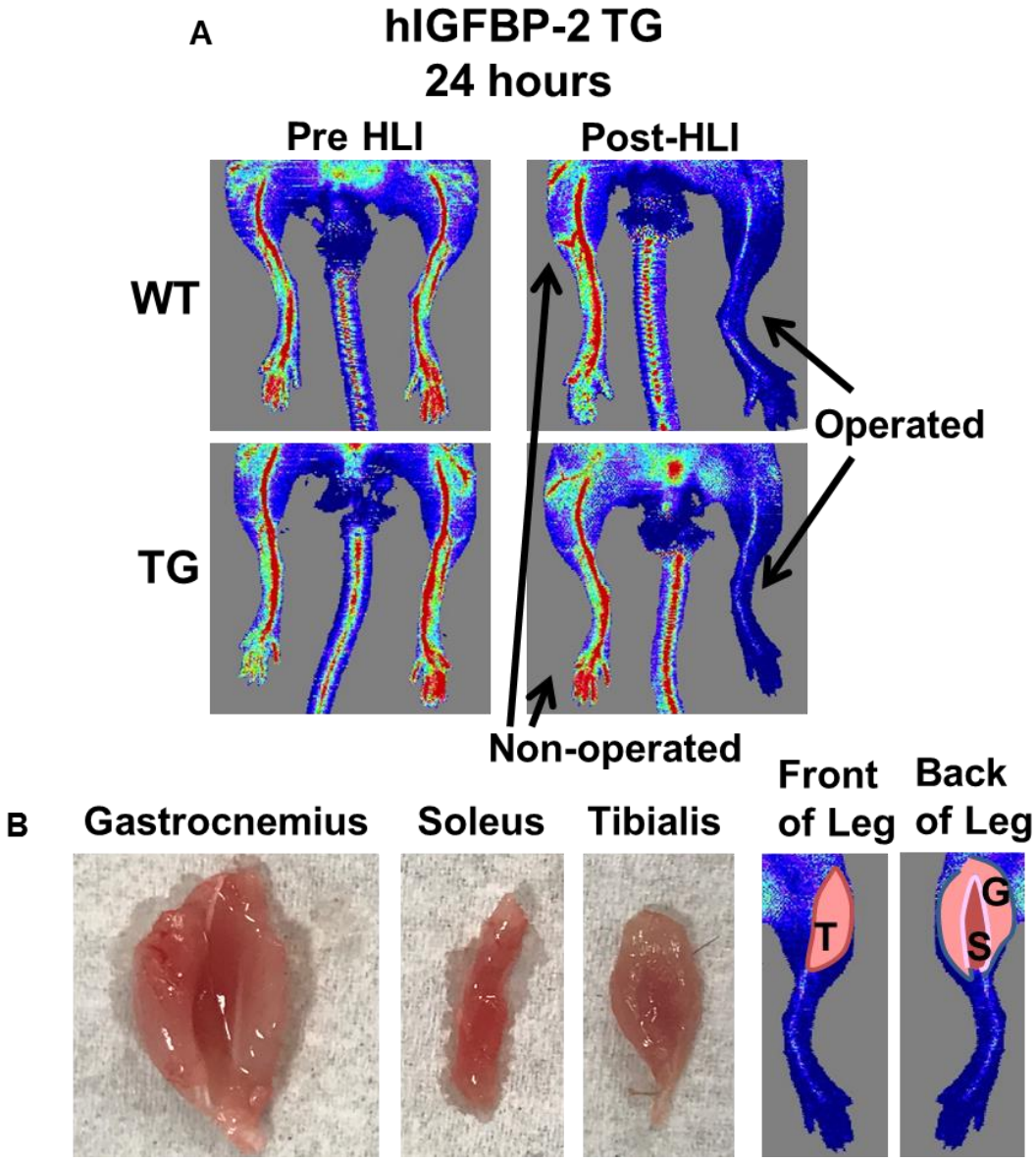

Figure 4.9 Muscles harvested 24 hours after HLI surgery
(A) Laser Doppler images captured loss of blood flow to the leg from before surgery to after 24 hours after HLI surgery. The surgery was only carried out on the left leg of each mouse as highlighted by the arrows. The right leg remained a non-operated control. **(B)** Images of the gastrocnemius, soleus and tibialis muscles were captured after harvest. The final images on this panel show the positioning of the tibialis, which is the muscle on the lower limb on the front side of the leg, and the gastrocnemius, which is located on the back of the leg. The soleus sits in the middle of the gastrocnemius muscle on the back side of the leg.

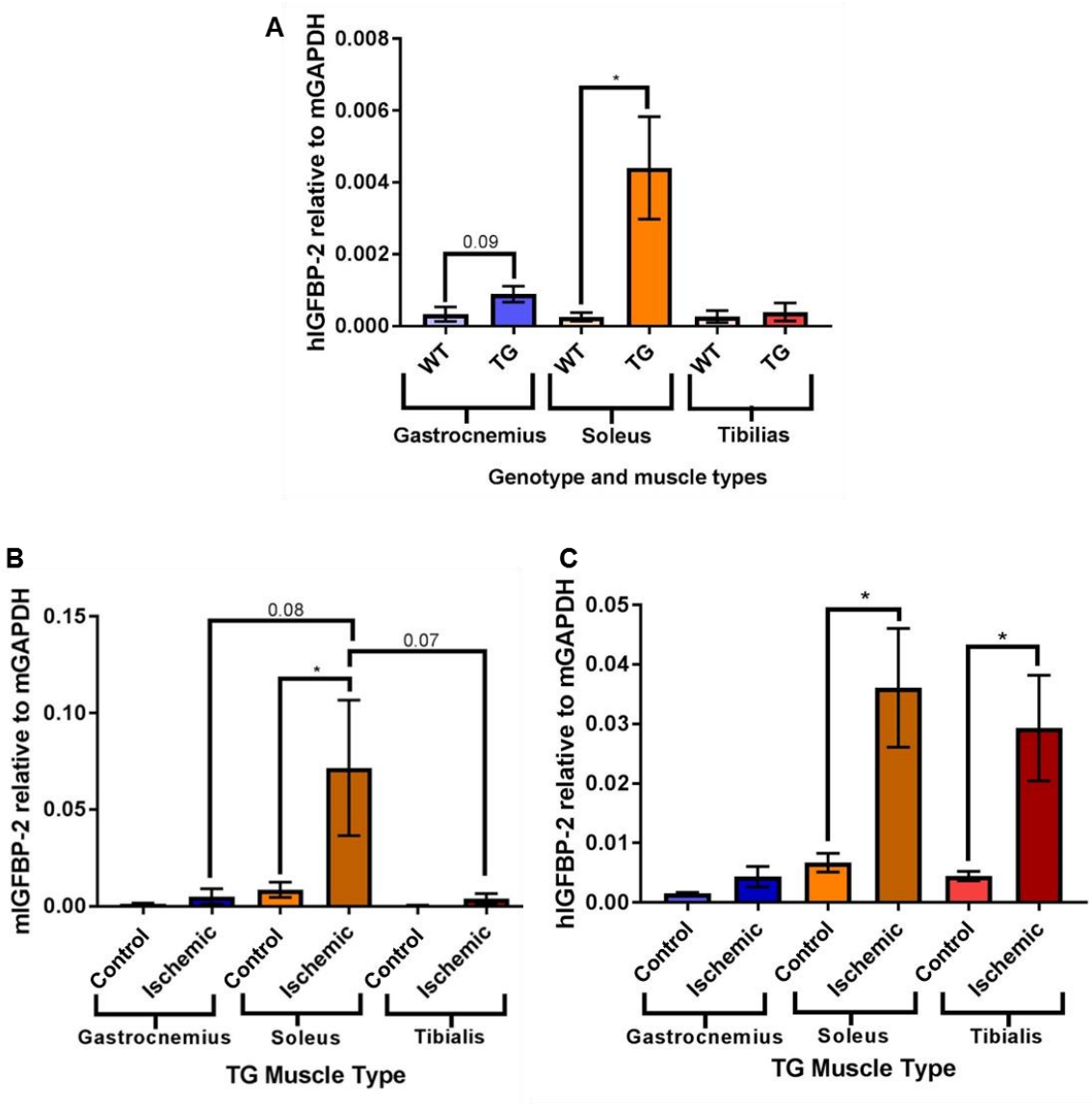

Figure 4.10 IGFBP-2 is located in specific muscles following HLI in TG mice
Real-time PCR was used to determine human and mouse IGFBP-2 levels, normalised to murine GAPDH across 3 different muscle types, gastrocnemius, soleus and tibialis, by genotype and by ischemic vs non-ischemic limbs. The controls were non-operated limbs from the relative operated mouse. **(A)** hIGFBP-2 levels were tested in gastrocnemius, soleus and tibialis muscles, which were harvested from WT and TG mice from the operated limb. hIGFBP-2 levels were normalised to murine GAPDH levels. (*=p<0.01, gastrocnemius WT vs TG p=0.09, n=7 for each condition). Error bars show SEM. **(B)** mIGFBP-2 levels were tested in gastrocnemius, soleus and tibialis muscles which were harvested from TG mice from the non-operated (control) and operated (ischemic) limbs. mIGFBP-2 levels were normalised to murine GAPDH levels. (*=p<0.01, gastrocnemius ischemic (operated) vs soleus ischemic (operated) p=0.08, soleus ischemic (operated) vs tibialis ischemic (operated) p=0.07, n-10 for each non-operated condition, n=7 for each ischemic condition). **(C)** hIGFBP-2 levels were tested in gastrocnemius, soleus and tibialis muscles which were harvested from TG mice from the non-operated (control) and operated (ischemic) limbs. hIGFBP-2 levels were normalised to murine GAPDH levels. (*=p<0.02, n=10 for each condition). Error bars show SEM.

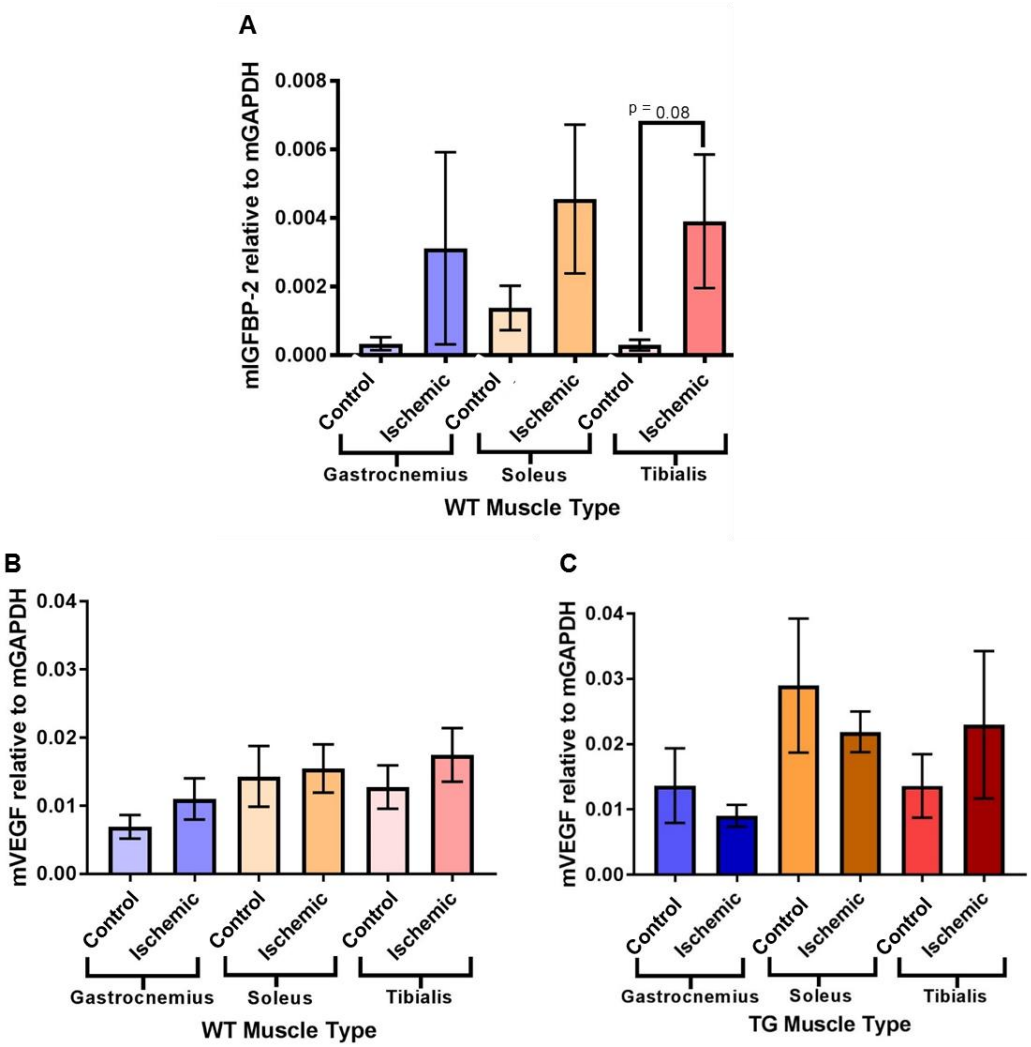

Figure 4.11 mIGFBP-2 up-regulation in response to ischemia does not correlate with VEGF-A expression

Real-time PCR was used to determine the levels of murine IGFBP-2 and murine VEGF-A, normalised to mouse GAPDH in WT and TG, non-operated and ischemic muscles, gastrocnemius, soleus and tibialis. The controls were non-operated limbs from the relative operated mouse. **(A)** mIGFBP-2 levels were tested in gastrocnemius, soleus and tibialis muscles, which were harvested from WT mice from the control (non-operated) and ischemic (operated) limb. mIGFBP-2 levels were normalised to murine GAPDH levels. (Tibialis control vs ischemic p=0.08, n=7 for each condition). Error bars show SEM. **(B)** mVEGF-A levels were tested in gastrocnemius, soleus and tibialis muscles, which were harvested from WT mice from the control (non-operated) and ischemic (operated) limb. mVEGF-A levels were normalised to murine GAPDH levels. (Gastrocnemius n=7, soleus n=3, tibialis n=5). **(C)** mVEGF-A levels were tested in gastrocnemius, soleus and tibialis muscles, which were harvested from TG mice from the control (non-operated) and ischemic (operated) limb. mVEGF-A levels were normalised to murine GAPDH levels. (Gastrocnemius n=6, soleus n=3, tibialis n=6). Error bars show SEM.

4.4.4 Effect of endothelial-specific expression of hIGFBP-2 on recovery in perfusion following HLI

The induction of hIGFBP-2 expression in the inducible models of the endothelial-specific hIGFBP-2 over-expressing homozygous mouse (VehiHom) colony after tamoxifen injections was confirmed by immunoblotting probing for IGFBP-2 in cultured PECs from WT and VehiHom TG mice (Figure 4.12 A). The generation of this mouse was described in Section 4.3.1. Upregulation of hIGFBP-2 was confirmed in plasma from VehiHom mice using a hIGFBP-2 ELISA (Figure 4.12 B).

There was no significant different in weight between WT and VehiHom mice in males (Figure 4.13 A) or in females (Figure 4.13 B). Tamoxifen injections did not cause any difference to weight in WT or VehiHom mice (Figure 4.13 C). Laser Doppler analysis after HLI surgery confirmed a significant enhancement in perfusion at day 14 in VehiHom mice compared to WT mice, however there was no overall difference in perfusion recovery over 28 days between both genotypes (Figure 4.14). Both the TG global over-expressing mouse and VehiHom mouse increased perfusion to a similar point at day 28 of recovery after HLI surgery (Figure 4.15).

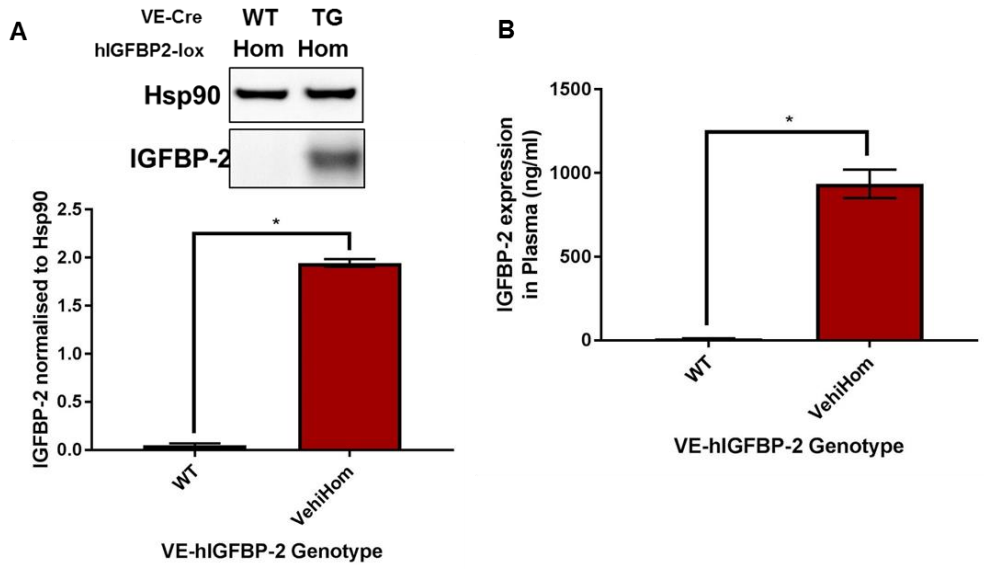

Figure 4.12 hIGFBP-2 is over-expressed in VehiHom TG mice following tamoxifen injections

(A) Representative images of immunoblots which were carried out using 40µg protein from WT and VEhiHom homozygous PEC lysates. Blots were cut at 60kDa to probe for goat polyclonal anti-IGFBP-2 (MW=36kDa) and murine monoclonal Hsp90 (MW=90kDa). Lane 1 consists of VE-Cre hIGFBP-2 lox WT homozygous and lane 2 consists of the VehiHom mouse. Densitometry measured using Genetools compared IGFBP-2 levels normalised to Hs90 levels. (*=p<0.001, WT n=6, VehiHom n=6). Error bars show SEM. **(B)** Plasma collected after tamoxifen injections from WT and VehiHom mice were tested for IGFBP-2 expression levels, using a hIGFBP-2 ELISA kit. (*=p<0.001, WT n=6, VehiHom n=6). Error bars show SEM.

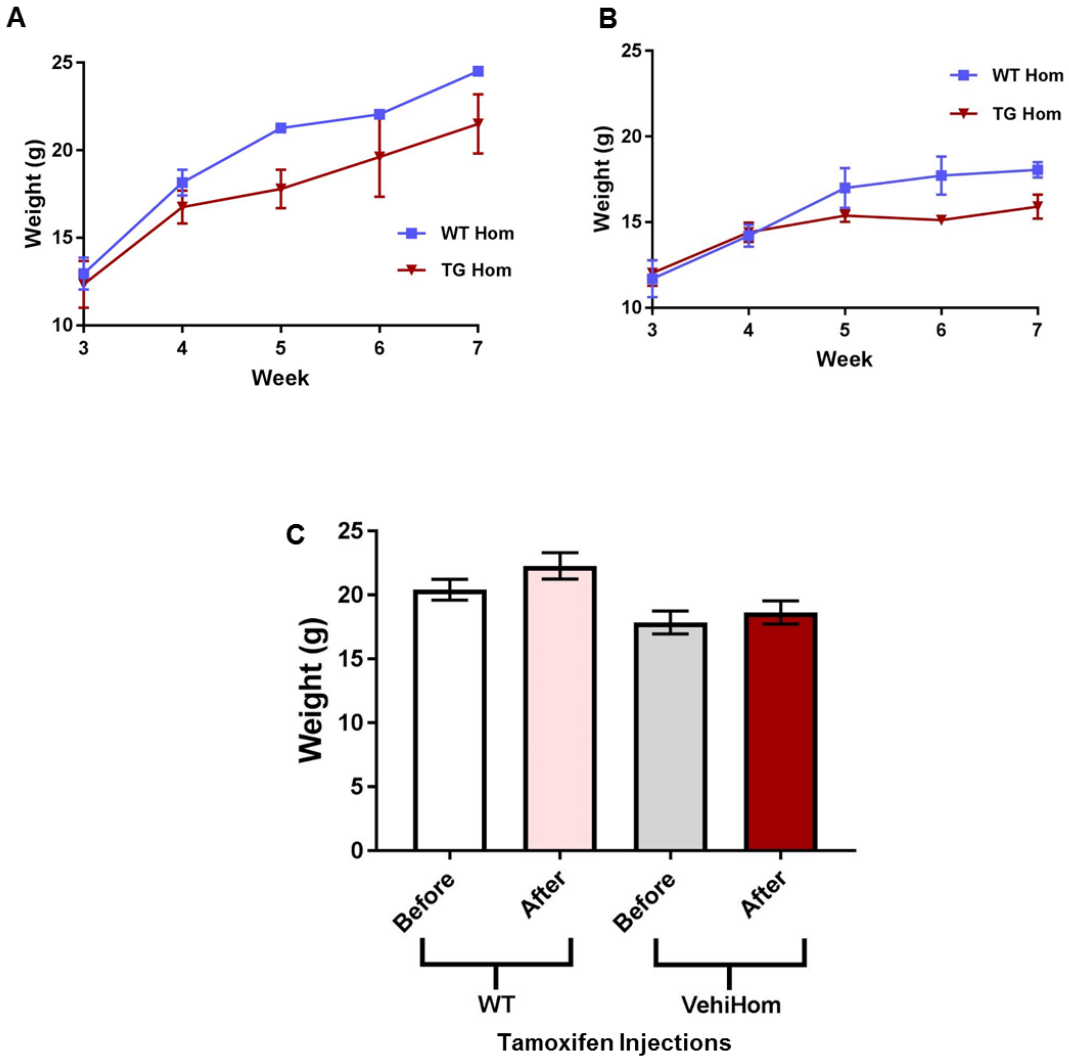

Figure 4.13 Endothelial-specific hIGFBP-2 over-expression or tamoxifen injections do not affect weight

The mouse weight was measured on a weekly basis after being weaned at 3 weeks up until 7 weeks of age. **(A)** Graphical representation of the weight of male mice. Mice were randomly selected for weighing. One mouse was chosen per litter from the WT and TG (VehiHom) mice (n=3). Error bars show SEM. **(B)** Female mice were randomly selected from individual litters and weighed on a weekly basis from weaning age (3 weeks) (n=3). Error bars show SEM. **(C)** WT and VehiHOM mice were weighed before and after 5 days of receiving tamoxifen injections (n=9). Error bars show SEM.

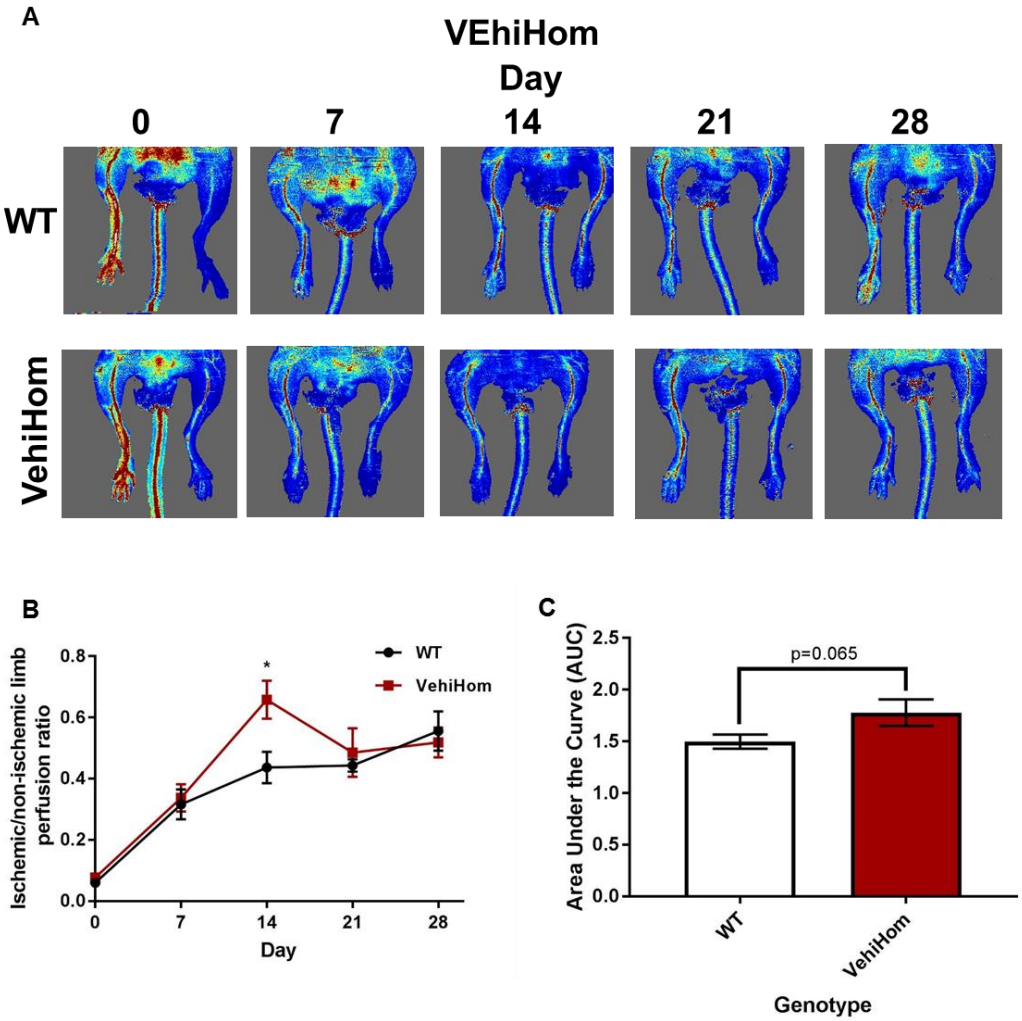

Figure 4.14 Perfusion in response to HLI was significantly enhanced in VehiHom mice at day 14

(A) Representative images taken from Laser Doppler imaging showing the change in perfusion over 28 days in WT and VehiHom mice. **(B)** Analysis using the Moor Instruments Review tool provided a value representing the blood flow, normalised to leg area. Perfusion values of ischemic (operated) limbs were compared against non-ischemic (non-operated) limbs (*=p<0.02, WT n=9, VehiHom n=8). Error bars represent SEM. **(C)** The area under the curve from Figure 4.14 B was calculated for WT and VehiHom mice (WT AUC vs VehiHom AUC p=0.065, WT n= 9, TG n=8). Error bars show SEM.

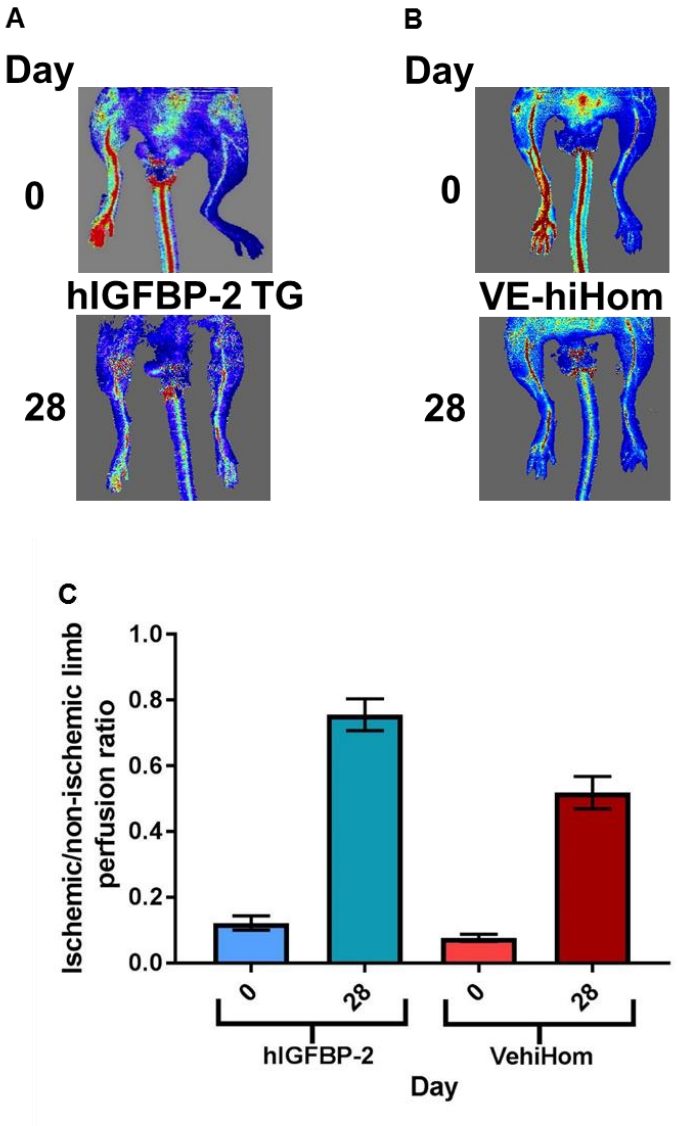

Figure 4.15 Comparative outcome between global and endothelial-specific hIGFBP-2 over-expressing mouse models
(A) Representative images of Laser Doppler imaging carried out on TG global hIGFBP-2 over-expressing mice on day 0, immediately following HLI surgery and day 28 after recovery. **(B)** Representative images of Laser Doppler imaging carried on VehiHom mice, after HLI surgery on the left leg and after 28 days of recovery. **(C)** HLI surgery was carried out on hIGFBP-2 globally over-expressing mice and VehiHom endothelial-specific over-expressing hIGFBP-2 mice at day 0. Occlusion of blood flow in the left leg, measured by Laser Doppler imaging, was compared to the non-operated (non-ischemic) limb. Recovery was measured at day 28 by comparing the restoration of blood flow to the operated limb vs the non-operated limb. Graphical representation of final recovery achieved at day 28 from day 0 in hIGFBP-2 over-expressing mice and VehiHom mice (hIGFBP-2 n=14, VehiHom n=10). Error bars show SEM.

4.5 Discussion

4.5.1 Global over-expression of hIGFBP-2 displays potential playing a role in the recovery from HLI

As there is currently ambiguity regarding IGFBP-2s specific role in angiogenesis, it was important we were able to see potential on an *in vivo* level before committing effort to try and find a mechanism to support all the characteristics exerted by IGFBP-2 in published literature. This *in vivo* model proved over-expression of hIGFBP-2 on a global scale did not cause any detrimental effects to overall health and especially did not drive tumour development in these mice as confirmed following the full harvest of organs.

Before beginning any surgical procedures on these mice, no differences in body weight between the TG and WT models were observed, suggesting good health. All mice matched the expected weight for their age point. It was significantly clear male mice were larger in size than female mice; however, this is a common phenomenon in mammals. For ease of surgery, male mice were used due to their larger size.

After comparing ischemic to non-ischemic limbs to measure to progress of perfusion after HLI surgery, a significant enhancement in recovery was observed at day 7 in the TG mice in comparison to its WT littermates. This early difference suggests IGFBP-2 may play a role in remodelling of the pre-existing vasculature via arteriogenesis, rather than angiogenesis (Shireman, 2007). Forces provided by shear stress from the blood flow will initiate collaterals to open up to aim to restore the blood flow, however for arteriogenesis to take place, the endothelial layer still needs to reform to enable the opening up effect. IGFBP-2 has been referenced to promote proliferation and migration of a range of cell types, including glioma, vascular smooth muscle and neural stem cells (Deng et al., 2017; Han et al., 2014; Shen et al., 2015). Although these mechanisms have not been established in endothelial cells, it is plausible to hypothesise IGFBP-2 may mediate arteriogenesis activity via enhancing proliferation and migration of the endothelial cells in the inner layer of the vessel.

The theory that IGFBP-2 induces arteriogenesis rather than angiogenesis is supported even further; TG mice fail to display a significant difference in overall recovery of perfusion in comparison to the WT mice at day 28. The over-expression of hIGFBP-2 seems to drive an immediate effect in enhancing recovery at an earlier rate and returns back to the normal WT recovery level. Angiogenesis, involving the formation of new blood vessels is a process that will take much longer than a week as it requires the upregulation of many growth factors and the recruitment and

communication between many cells, which make up the vessel wall (Limbourg et al., 2009). It is an extremely regulated process to ensure the blood flow is restored to the right location. One possible reason for why we may not see an increased effect in the TG mice post day 14 is due to the upregulation of growth factors such as VEGF, PDGF, FGF which have been secreted due to inflammatory signals. These growth factors may silence the effects of IGFBP-2, as they are extremely potent angiogenic promoters. Also, as we see the graph plateau, it suggests the recovery has reached its maximal point, and therefore even if we continued adding further IGFBP-2, we may not see an effect.

Therefore IGFBP-2 influencing arteriogenesis, rather than angiogenesis is a more positive outlook in regard to recovery from PAD than our original hypothesis. It is essential IGFBP-2 does not cause a significantly enhanced angiogenic response, as with VEGF it led to the formation of unstable blood vessels. We want IGFBP-2 to enhance the recovery immediately at a faster rate to the maximum level matching the normal end recovery outcome (to the WT level). Superficially enhanced or further vessel growth may result in formation of an unstable network and in turn display the negative side effects which have been associated with VEGF (Reardon et al., 2011).

4.5.2 PECs over-expressing IGFBP-2 fail to activate the Akt/eNOS pathway

PECs were isolated from the mice, which did not undergo HLI surgery, to confirm the gene modification of over-expression of IGFBP-2 in the TG model compared to the WT. The protocol had to be optimised to ensure we obtained a pure sample. Contamination by fibroblasts elevated total mIGFBP-2 levels in WT samples to a matching level with the TG sample containing both m and hIGFBP-2. IGFBP-2 has been reported to promote proliferation and differentiation of fibroblasts explaining the increased expression of IGFBP-2 (Brandt et al., 2015; Park et al., 2015). Once cultured cells displayed a more endothelial-like phenotype, after comparing cell images with previous images of positively stained endothelial cells, IGFBP-2 over-expression was confirmed in the TG mouse compared to the WT. Contrastingly to published research, into *in vitro* signalling changes observed by western blotting showed IGFBP-2 over-expression had no effect on Akt phosphorylation or activation of the downstream target eNOS (Mehrian-Shai et al., 2007; Xi et al., 2016). However, it is unknown if IGFBP-2 only functions in a compromised environment, it may explain why we do not observe any signalling changes before the induction of ischemia.

4.5.3 hIGFBP-2 and mIGFBP-2 in the TG model is located to the specific muscles

Although previous characterisation of the TG over-expression model highlighted IGFBP-2 over-expression in the muscle, only skeletal muscle has been interrogated (Hoeflich et al., 1999). We have identified that hIGFBP-2 global over-expression is modulated according to muscle type, pre-surgery, with the soleus displaying a 5-fold enhancement in hIGFBP-2 levels compared to the gastrocnemius and tibialis muscle. A possible explanation for why the soleus retains a larger abundance of hIGFBP-2 is that the soleus is the inner most muscle and is surrounded by a larger capillary network than the gastrocnemius and the tibialis are. Supporting this, mIGFBP-2 levels are elevated in the TG model in response to ischemia but the majority of the mIGFBP-2 is directed to the soleus over the other two muscles. Non-operated and ischemic muscle types were interrogated for hIGFBP-2 levels again to observe if ischemia affected the increased concentration of hIGFBP-2 in the soleus. Interestingly, the levels of hIGFBP-2 in the ischemic soleus had increased just less than 10-fold compared to non-operated limbs, but there was also a significant increase in hIGFBP-2 levels in the tibialis ischemic limb compared to its non-operated control. It has been reported that necrosis as a result of a poor/restricted blood supply to the limb effects the lower muscle groups, the gastrocnemius, soleus and tibialis in particular (Shireman, 2007). However, when observing the muscle types independently of each other, the tibialis and soleus muscle were the most affected, whereas the effect of necrosis to the gastrocnemius was variable (Shireman & Quinones, 2005). IGFBP-2 is well known for its role as a protector in regards to metabolic syndromes (Carter et al., 2014; Wheatcroft et al., 2007). Therefore, it may be possible hIGFBP-2 is drawn to a location where it is required to act as a protector to prevent further muscle damage as a result of femoral ligation.

4.5.4 mIGFBP-2 expression is elevated due to ischemia but does not correlate with mVEGF expression

We have found evidence that suggests IGFBP-2 expression is mediated by ischemia in a model of PAD. Although not significant due to high variability, there is an evident trend that 24 hours after the induction of ischemia, mIGFBP-2 expression is elevated in comparison to non-operated muscles in WT mice. This trend was seen across all lower limb muscle types. This supports the idea that IGFBP-2 does play an immediate role and is immediately required to possibly drive arteriogenesis to rescue perfusion.

The high variability displayed could be a result of the mice already having a collateral vessel network in place, which can compensate for the sudden restriction in blood flow. The already present collateral vessel network may suppress the full activity or requirement for IGFBP-2 to help rescue perfusion to the ischemic limb.

It is also important to note the upregulation of mIGFBP-2 or hIGFBP-2 in ischemic limbs did not correlate with mVEGF-A expression in WT or TG mice, contradicting findings from Das et al., (2013), that IGFBP-2 promotes the activation of VEGF. Interestingly, mVEGF-A expression in the ischemic muscle types remained the same as non-operated muscles. However, this may be because hypoxia, as an inflammatory marker drives the activation of VEGF (Krock et al., 2011; Ramakrishnan et al., 2014). 24 hours may not be enough time to induce an inflammatory response large enough to induce VEGF expression. VEGF is also known as a more potent regulator of angiogenesis, rather than arteriogenesis specifically, suggesting VEGF may start functioning later on in the recovery process (Hoeben et al., 2004). Additionally, collateral vessel growth via arteriogenesis does not require VEGF as a stimulus, therefore suggesting VEGF was not upregulated following ischemia as there may already be a collateral network in place.

4.5.5 Endothelial-specific over-expression of hIGFBP-2 plays a role in recovery from HLI

VehiHom mice were shown to over-express IGFBP-2 in cultured PECs and in plasma using a hIGFBP-2 ELISA. There was no difference in weight gain over time between the VehiHom and WT littermates and weight was not affected after 5 days of tamoxifen injections. There were no obvious differences in phenotype between the genotypes and deemed in a healthy state to undergo surgery.

Findings from the endothelial-specific hIGFBP-2 over-expressing mouse support the theory that IGFBP-2 is directly involved in mediating arteriogenesis endothelial remodelling as an enhancement in recovery was observed at an early stage of the recovery process. Comparison of the ischemic limb to the non-ischemic limb displayed a significant enhancement in rescue of perfusion at day 14 in the VehiHom in comparison to the WT mice after HLI surgery. The path of recovery mimics what is observed with the global TG over-expresser of hIGFBP-2, in that recovery after 21 days begins to plateux, therefore reaching its maximum recovery point. This suggests perfusion is restored predominantly through arteriogenesis (in the first 14 days), rather than angigogenesis, however, to support this claim, we would have to study the changes to the collateral network in the mice.

A sudden drop from the increase at day 14 to day 21 is observed. A possible explanation may be that inflammatory signals may be released to promote rapid expression of angiogenic growth factors such as VEGF, elevating perfusion rates to a significant level at day 14. VEGF is well established to drive uncontrollable vessel growth, resulting in a burst of perfusion. At day 21, the delivery of growth factors may have been achieved causing a suppression of the enhancement to a regular level.

However, IGFBP-2 has been referenced to exert apoptotic effects in human teratocarcinoma cells by blocking IGF-II survival (Granérus et al., 2001) It can also mediate the effects of IGF-I-stimulated survival signalling pathways via modulation of tumour suppressors such as p53 (Grimberg et al., 2006). It may be possible that IGFBP-2 senses the increase in perfusion at day 21 and modulate the angiogenic effects that are being exerted by endogenous growth factors instead of promoting them further.

Although we are trying to identify IGFBP-2 as a promoter of angiogenesis, if IGFBP-2 is able to regulate its effects, it may display more potential as a therapeutic than VEGF, which results in uncontrollable enhancement of growth and signalling pathways.

4.5.6 Study Limitations

It is important to note both TG models express more than double the concentration of IGFBP-2 present in humans and therefore are enhanced to a super-physiological level in the mice. Although all characteristics have displayed only minor differences in phenotype between the gene modified and WT mice, it is difficult to establish if the over-expression could be having adverse effects in the experimental procedures we are using. However, *In vitro* proliferation experiments carried out by other researchers have displayed no difference in activity using 1000ng/ml IGFBP-2 compared to 500ng/ml (Uzoh et al., 2011).

Another limitation observed regarding the use of IGFBPs is that IGFBP-1 and IGFBP-3 function at an enhanced ability when promoting a recovery response in a pro-inflammatory induced state (Aziz et al., 2018; Jiang et al., 2014). Therefore, we may observe a more pronounced effect with IGFBP-2 if induced at a later time point after HLI surgery, at a point where backup collateral vessels have failed to restore blood flow and necrosis has begun to take place. In a clinical setting, we believe IGFBP-2 would be the last source of treatment before amputation is the only solution. As we have inducible hIGFBP-2 over-expressing endothelial-specific models in place, we could test the theory of waiting until the post-operative limb begins to show signs of

necrosis, remaining within the guidelines of severity set out by the Home Office before inducing IGFBP-2 expression. An inducible global over-expressing hIGFBP-2 could also be used in this instance. This will determine if IGFBP-2 contributes to the formation of a new collateral vessel network from the pre-existing vessels, as the pre-existing collaterals will have failed to compensate the loss of perfusion.

The largest limitation of this study is that due to time constraints we were unable to quantify blood vessel density by histology, angiography or microCT. Therefore, we cannot confirm that angiogenesis, arteriogenesis or any type of new blood vessel formation occurred. However, as a segment of the femoral artery was cut, it is unlikely the increase in blood flow may purely be due to vasodilation, suggesting angiogenesis of some form must also take place. We did plan on carrying out immunohistochemistry to investigate the vascularity of the peripheral muscles using endothelial markers (e.g. CD31 to detect capillaries) and assess angiogenesis and adductor muscle using smooth muscle markers (e.g. smooth muscle actin to detect arteries and arterioles) to assess arteriogenesis. However, unfortunately due to time constraints, we were not able to complete these planned experiments.

4.6 Concluding remarks

For the first time we have highlighted IGFBP-2 levels are elevated 24 hours after ischemia in the lower mice limbs, representing a murine model of PAD. The enhancement in IGFBP-2 does not increase VEGF expression levels, suggesting IGFBP-2 exerts in actions in an ischemic setting independent of VEGF. PECs over-expressing hIGFBP-2 fail to show a difference in Akt or eNOS phosphorylation. We have also shown over-expression of IGFBP-2 on a global and endothelial-specific level plays a role in enhancing perfusion at early stages of recovery following HLI. Using published information regarding recovery after HLI, we believe IGFBP-2 drives arteriogenesis activity immediately; however, its role as a pro-angiogenic agent still remains unestablished. The enhanced recovery plateaus to a normal level, corresponding to the WT suggesting over-expression of IGFBP-2 does not drive uncontrollable vessel formation.

To identify if IGFBP-2 drives arteriogenesis or angiogenesis of new collateral formation, we could stain the collateral vessels and use a 3D CT imaging system to display differences in recovery of perfusion at different time points. For clinical relevance, HLI should be carried out on mouse models, which result in necrosis rather than complete recovery and induce IGFBP-2 expression to observe its rescuing properties.

Chapter 5 - Effects of IGFBP-2 on pro-angiogenic signalling in endothelial cells

5.1 Background

Findings from Chapter 4 confirmed IGFBP-2 does play a role in recovering perfusion following an ischemic insult at day 7 in the recovery process. We also showed IGFBP-2 is slightly elevated 24 hours after induction of ischemia in WT mice. The only mechanism investigated in vascular endothelial cells suggested that IGFBP-2 stimulated activation of VEGF signalling is responsible for enhancement in *in vitro* angiogenic responses (Das et al., 2013). However, we were unable to replicate any correlation between elevated IGFBP-2 levels and VEGF levels in response to ischemia. Therefore, we can deduce IGFBP-2 may be exerting angiogenic-like characteristics through other angiogenic signalling pathways. In order to understand how IGFBP-2 may be exerting the angiogenic-like activity we have seen in the previous chapter, we need to investigate the angiogenic signalling cascades activated by IGFBP-2.

IGFBP-2 has been associated to promote its angiogenic-like characteristics, such as migration and proliferation through a variety of signalling mechanisms, which differ between different cell types used for *in vitro* experiments. A summary of these published findings is discussed in Section 5.1.1. However, as endothelial cells are at the forefront of the initial angiogenesis stages, it is important we understand how IGFBP-2 may mediate their survival, migration and proliferation.

5.1.1 IGFBP-2 and angiogenic signalling

The Akt/PI3K is the most common signalling cascades which determine cell viability, motility and regular homeostasis (Karar & Maity, 2011). It is well established activation of IGF-I signalling also results in elevation of Akt phosphorylation (Assefa et al., 2017). IGFBP-2-stimulated Akt is also mediated via interaction between the HBD and RPTPβ, modulating the de-phosphorylation of PTEN, an upstream target of Akt activation. De-phosphorylation of PTEN results in an open conformation with an exposed and active phosphatase domain which rapidly enhances the degradation

of PTEN, causing an upregulation of Akt phosphorylation (Ross & Gericke, 2009). Knock-out models of IGFBP-2 resulted in down-regulation of Akt phosphorylation in mouse embryo fibroblasts, while PTEN tyrosine phosphorylation increased (Mehrian-Shai et al., 2007). Therefore IGFBP-2 is possibly regulating Akt signalling cascades via HBD interactions.

In an esophageal adenocarcinoma cell line, activation of the MAPK pathway, as well as Akt was shown to modulate the IGFBP-2 stimulated cell proliferation, migration and invasion (Myers et al., 2015). The association of elevated IGFBP-2 levels and increased MAPK signalling has been reported in the growth and survival of many cancer cell lines such as epithelial carcinoma and glioma cells (Yoshino et al., 2006). Recent advances have suggested the MAPK-induced migration is dependent on IGFBP-2 integrin interactions with β1 or α5 subunits by enhancing ERK and JNK activation (Han et al., 2014; Mendes et al., 2010; Wang et al., 2017c). IGFBP-2s interaction with the tumour suppressor, p53 is responsible for inhibiting IGF-induced ERK activation. Low levels of IGFBP-2 also promote cell growth by suppressing p53's ability to down-regulate IGF-I stimulated-activation of ERK/MAPK signalling pathway. (Grimberg et al., 2006)

Via the cell adhesion modulators, β-catenin and integrin, IGFBP-2 mediates the inactivation of GSK3β by modulating Akt and FAK signalling. IGFBP-2-stimulated Akt suppresses GSK3β's ability to degrade β-catenin, which in turn prohibits the Wnt signalling pathway to regulate cell migration and death (Atkins et al., 2012). Stabilisation of β-catenin is necessary for Wnt signalling. Cell surface integrin actions stimulated by IGFBP-2 also mediate the activation of GSK3β via FAK phosphorylation. However, IGFBP-2 stimulated-FAK functions in a contrasting manner by enhancing phosphorylation of GSK3β, driving stabilisation of β-catenin and activation of Wnt signalling (Patil et al., 2016).

Therefore, the cross-talk between IGFBP-2 binding domains determines the activation of the Akt, MAPK and FAK signalling pathways. All these pathways are well known to drive angiogenic responses, suggesting IGFBP-2 may directly influence angiogenesis via one or more of its interactions (Figure 5.1).

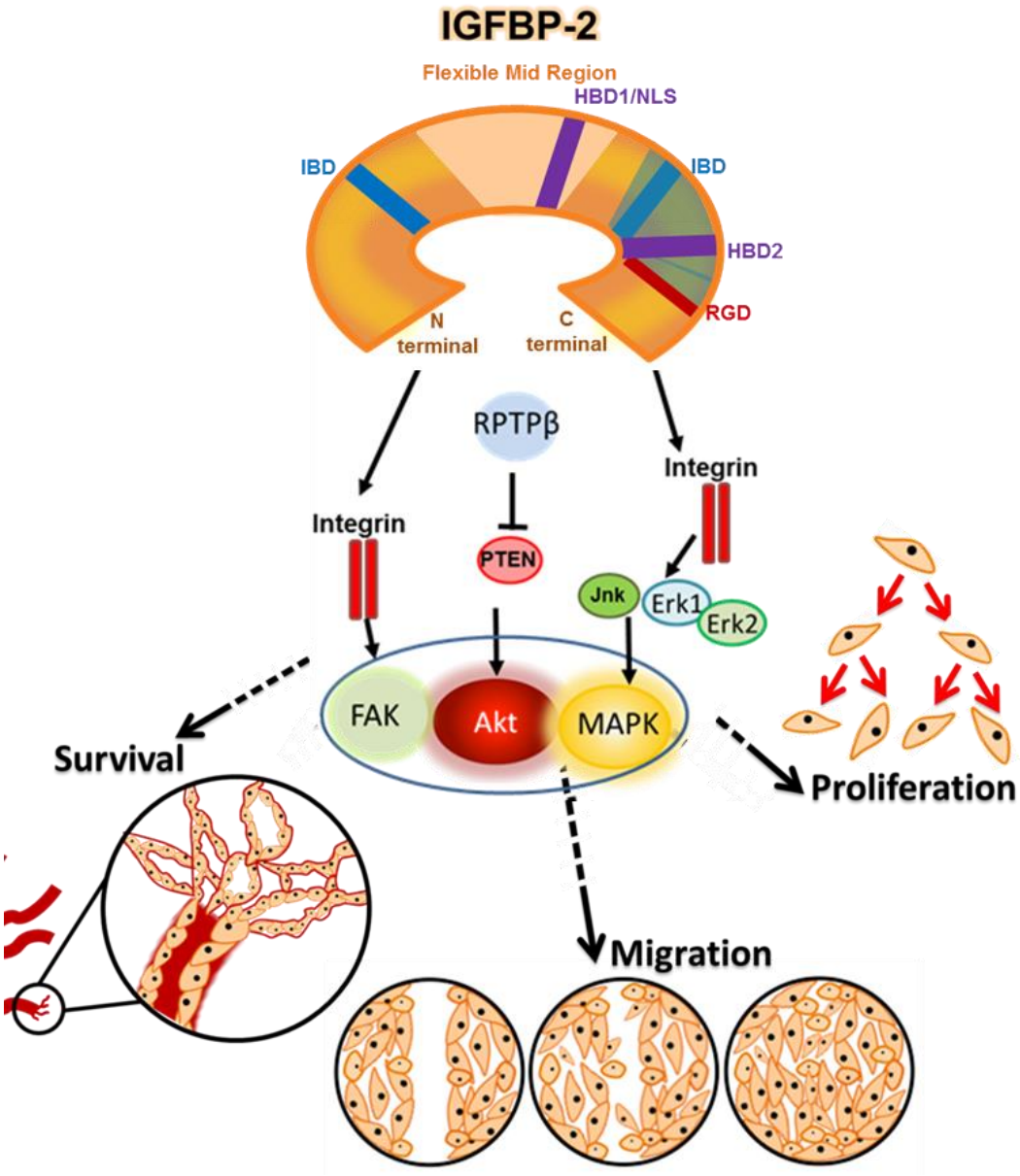

Figure 5.1 Proposed mechanisms of IGFBP-2 IGF-independent activation of angiogenic signalling pathways
Published articles have shown how IGFBP-2 IGF-independently can activate FAK, Akt and MAPK to stimulate characteristics such as survival, migration and proliferation in non-endothelial cell types. This schematic highlights which signalling molecules can be responsible for IGFBP-2 angiogenic-like characteristics. (Adapted from Han et al., 2014; Mehrian-Shai et al., 2007; Patil et al., 2016.

5.1.2 Suppression of IGFBP-2 signalling activity

Although all the previous publications highlight IGFBP-2s role in promoting IGF-I induced stimulation of angiogenic signalling pathways such as Akt, IGFBP-2 has the

potential of suppressing IGF-I signalling via by sequestering IGF molecules and inhibiting their transport to their receptors (Kiepe et al., 2002). Regarding *in vitro* experiments, this could be important as a set concentration is added to cell growth media for *in vitro* culture, and potentially disrupt the overall affect our added IGFBP-2 may have on signalling.

Heparin is a common component added to media to facilitate the transport of growth factors in the media. However, IGFBP-2 has two functional heparin binding domains. Blockage of these sites may also prohibit HBD-driven signalling activation.

Another problem that may suppress the activity of IGFBP-2 is the presence of additional growth factors in the media such as VEGF, FGF and PDGF. These growth factors are potent stimulators of angiogenesis alone and therefore may competitively down-regulate IGFBP-2s potential to drive angiogenic signalling. As mentioned previously, IGFBP-2 has been reported to modulate VEGF activity (Azar et al., 2011). IGFBP-2s interaction with αVβ3 may also regulate FGF activity *in vitro* (Rusnati et al., 1997).

Therefore, these growth factors may distract IGFBP-2s role to activate angiogenic signalling in HUVECs, resulting in down-regulation of the binding protein's true effect. Optimisation steps have been carried out in this chapter to eliminate any interference caused by these additional media components.

5.1.3 IGFBP-2 and endothelial cells

With the majority of IGFBP-2s potential role in angiogenesis being interrogated in endothelial cells, there are very limited numbers of publications that report how IGFBP-2 may modulate signalling within endothelial cells, specifically vascular endothelial cells. Investigating IGFBP-2 stimulated mechanisms which drive endothelial cell angiogenic-like characteristics may develop our understanding of how IGFBP-2 can be used therapeutically to promote endothelial remodelling during arteriogenesis or angiogenesis.

IGFBP-2 has been previously shown to enhance HUVEC tube formation via inducing VEGF signalling and in turn Akt activation (Das et al., 2013). Upregulation of IGFBP-2s integrin interaction with α5β1, via IGFBP-2 over-expression in HUVECs has shown potential in promoting adhesion of HUVECs to endothelial progenitor cells (Feng et al., 2015). Migration of HUVECs is incrementally elevated as concentrations of circulating IGFBP-2 rise, stimulated via activation of the IGF-IR (Png et al., 2012). A further study using a highly anti-proliferative agent caused the suppression of

angiogenic-like characteristics via suppression of Akt activation, which correlated with a reduction in IGFBP-2 levels in HUVECs (Bhutia et al., 2016).

Although it is clear IGFBP-2 activates Akt phosphorylation in HUVECs, no studies have referenced the role of IGFBP-2s HBDs or IGFBP-2 stimulated activation of other angiogenic signalling pathways in HUVECs. eNOS signalling occurs downstream of Akt but is a key molecule involved in regulation of the vascular environment by modulating the generation of nitric oxide. As mentioned in the introduction (Chapter 1), NO presents protective roles to prevent the onset of cardiovascular disease by maintaining contractility of the vessel wall, preventing high blood pressure, platelet aggregation and vascular tone (Naseem, 2005). These are key variables which need to be maintained following the formation of new blood vessels, therefore if IGFBP-2 presents an angiogenic role, its involvement in the regulation of eNOS is important.

5.1.4 Summary

IGFBP-2s interaction with angiogenic signalling molecules is determined by cell type and interaction type via its domains. However, the limited research carried out in HUVECs suggests IGFBP-2 stimulated Akt phosphorylation may lead modulation of endothelial functions. To determine which angiogenic-like mechanisms IGFBP-2 specifically activates in HUVECs, we will be exploring the effect of IGFBP-2 on all the signalling pathways it has currently been associated with.

5.2 Experimental Objectives

In this chapter, we aim to understand the effects of IGFBP-2 on pro-angiogenic signalling pathways in endothelial cells *in vitro*. Endothelial cells are the primary cells which induce the angiogenic signalling cascades *in vivo* and provide the structural framework for the formation of a new vessel. Investigation of the angiogenic signalling mechanisms activated by IGFBP-2 was carried using the objectives below:

- Investigate the cellular effects of IGFBP-2 in HUVECs on angiogenic signalling pathways.
- Identify the variables that may affect the function of IGFBP-2 on angiogenic signalling

5.3 Materials and Methods

5.3.1 Cell Culture

Standard cell culture protocol was carried out using the method stated Chapter 3.1. HUVECs were cultured using the protocol in Chapter 3.1.1 .The following cells were grown specifically for the experiments in this chapter.

C2C12 myoblasts

C2C12 myoblasts (original source: Professor Michelle Peckham), were grown in DMEM (Invitrogen, 61965-026) supplemented with 10% FBS and 1% AAS. To enable differentiation into myotubes, cells were washed in PBS (Invitrogen 14190250) and incubated in differentiation media (DMEM containing 5% FBS and 1% AAS). Cells were serum-starved overnight in DMEM + 1% AAS prior to lysing.

HepG2 Cells

HEPG2 refers to human liver carcinoma cells (purchased from Public Health England Culture Collections), were cultured in Minimum Essential Medium Eagle (MEME) (Sigma-Aldrich M5650) with 10% FBS, 1% AAS and 2mM L-Glutamine (Life Technologies, 25030081). Prior to lysing, the cells were incubated in serum-free medium (MEME + 1% AAS + 2mM L-Glutamine) overnight.

INS832/13 Pancreatic Cells

INS832/13 cells sourced from a rat cell line (kindly gifted by Professor Christopher Newgard) were cultured in RPMI media (Table 5.1). Cells were serum-starved in a low glucose salt solution (Table 5.1) prior to being lysed.

Solution	Contents
RPMI media (Sigma-Aldrich R8758)	10% FBS, 1% AAS, 10mM HEPES (Life Technologies, 15630056), 1mM sodium pyruvate (Life Technologies, 11360070) and 0.05mM 2-mercaptoethanol (Sigma-Aldrich M6250)
Low Glucose Salt Solution pH 7.2	144mM NaCl (Fisher Scientific, S/3160/63), 1.16mM $MgSO_4$ (Fisher Scientific, M65), 4.7mM KCl (Fisher Scientific, P/4280/60), 2.5mM $CaCl_2$ (Fisher Scientific, C77), 1.2mM KH_2PO_4 (Fisher Scientific P285), 25.5mM $NaHCO_3$ (Fisher, Scientific, S/4920/60), 20mM HEPES and 0.2% bovine serum albumin (BSA) (Cell Signalling, 9998)

Table 5.1 Solutions used to culture Ins832/13 pancreatic cells
Table highlighting the components and concentrations of components required for the media to culture of Ins823/13 pancreatic cells.

Human Saphenous Vein Endothelial Cell (HSaVEC) lysates

HSaVECs (a kind gift from Dr Karen Porter) were derived from patients without diabetes undergoing coronary artery bypass graft surgery at Leeds Teaching Hospitals NHS Trust. Lysates had been stored at -80ºC in NuPage LDS sample buffer (4x) (Life Technologies, NP007) and NuPage sample reducing agent (10x) (NP0009). Previously determined protein concentrations of the samples were used for immunoblotting.

Mouse Pulmonary Endothelial Cell (PEC) lysates

PECs (a kind gift from Dr Hema Viswambharan) were cultured from wild-type C57BL6/J mice. Lysates were sonicated and purified by centrifugation at 13,000 rpm for 15 mins at 4ºC.

5.3.2 Immunoblotting

Cell lysing and immunoblotting was carried out according to the protocols noted in Chapter 3.2/3.3.

5.3.3 Treatment of HUVECs with additional stimulants

HUVECs were serum-starved for 2 hours in serum-free endothelial cell growth medium (M199) (M199 medium (Sigma-Aldrich, M4530) (supplemented with 1%

AAS, ECGS (Sigma-Aldrich E2759), 10mM Hepes, 1mM Sodium Pyruvate and 2500U Heparin) before being stimulated with other proteins. Basal control wells were replaced with fresh serum-free media at the time of the stimulation. In some experimental studies, the stimulant was pipetted directly into the well of the serum-free media which had remained in the plate for 2 hours.

Treatment of HUVECs with recombinant IGFBP-2

Cells were stimulated with recombinant IGFBP-2 (Abcam, ab63223 (reconstituted in sterile-filtered water), IGFBP-2 (R&D Systems, 674-B2-025 (reconstituted in PBS)), diluted in serum-free M199 obtaining final concentrations between the range of 1-1000ng/ml, was added for a minimum stimulation period of 10, 15 or 30 min. For time-dependent changes 200ng/ml IGFBP-2 and incubated for the time points, 15, 30, 45, 60 and 75 min, prepared in serum-free M199 was used as a stimulant.

Treatment of HUVECs with hIGF-1

Cells were stimulated with IGF-1 (R&D Systems, 291-G1 (reconstituted in sterile PBS)), diluted in serum-free M199 for 15 min at concentration of 10-50ng/ml.

Treatment of HUVECs with VEGF-A

$VEGF_{165}A$ (Promocell, C-64423), (reconstituted in H2O)), diluted in serum-free M199 was used for a stimulation period of 10-20 min. The concentration of $VEGF_{165}A$ used was 30ng/ml for all experiments as a positive control.

5.3.4 Data Analysis

GeneTools was used to perform densitometry analysis of the bands on each western blot. Unpaired t-tests were carried out to test data for statistical significance. All error bars represent standard error of the mean (SEM). Some preliminary studies only had n=2 due to time and funding constraints and therefore statistical tests were not carried out on these samples.

5.4 Results

5.4.1 IGFBP-2 from different sources

We initially sourced recombinant human IGFBP-2 from 2 different sources, murine cell (R&D) and insect cell (Abcam) to investigate in vitro angiogenic signalling and activity in future experiments. The functionality of these proteins was tested using IGF ligand blot. Akt signalling was also used to test functionality because IGFBP-2 has already been shown to stimulate Akt activation via its interaction with IGF-IR or via VEGF signalling (Das et al., 2013; Png et al., 2012).

hIGFBP-2 from an insect cell source failed to display IGF-I binding capability using the IGF binding blot, whereas murine sourced hIGFBP-2 bound biotinylated IGF-I (Figure 5.2). However, both IGFBP-2s were able to phosphorylate Akt to the same extent in HUVECs (Figure 5.3).

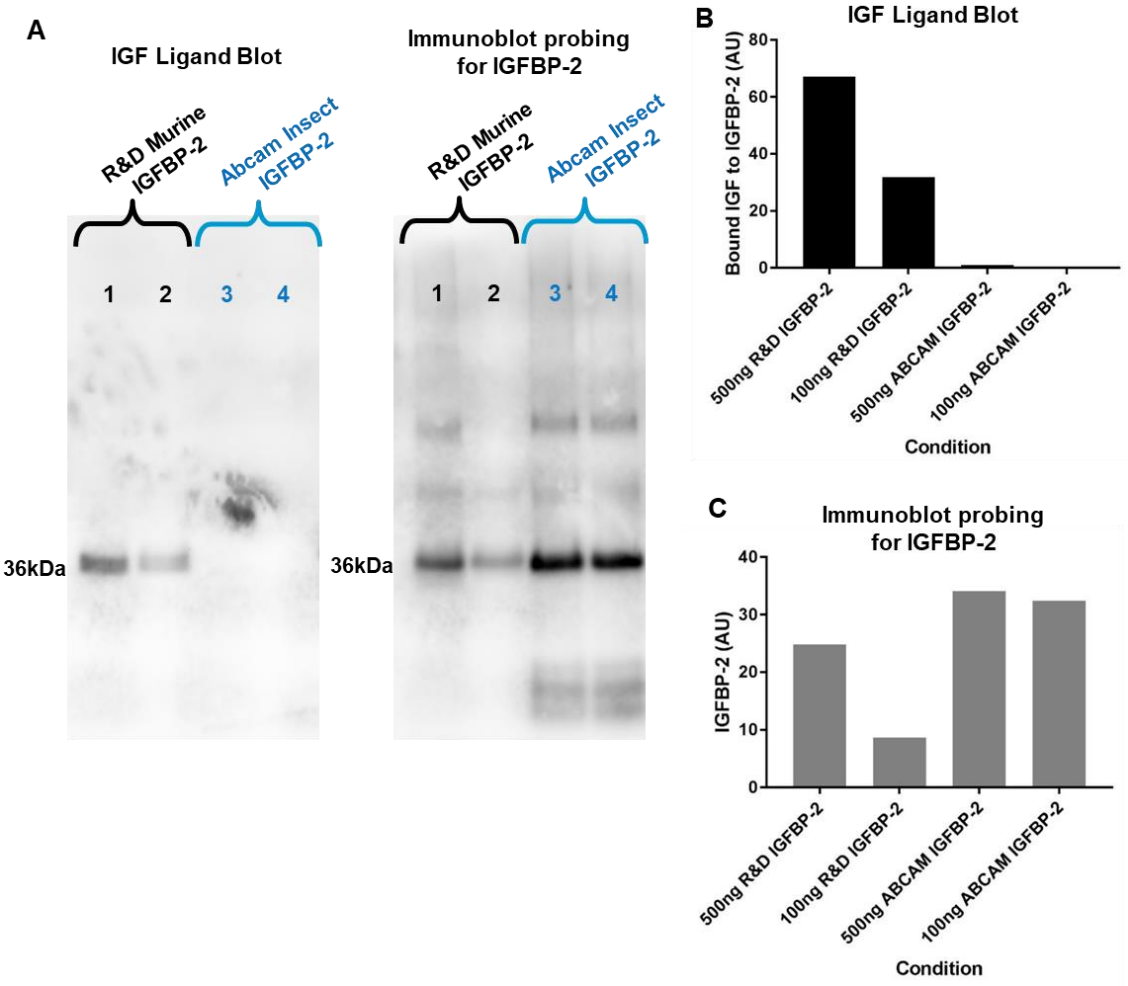

Figure 5.2 IGFBP-2 sourced from Insect cells does not possess IGF binding ability Preliminary study

(A) Non-denatured R&D murine recombinant IGFBP-2 and Abcam insect recombinant IGFBP-2 (100ng and 500ng) were loaded onto a 4-12% Bis Tris gel and transferred onto a membrane. The blot was incubated with blocked with 5% BSA and incubated with biotinylated IGF-I. Streptavidin was used to visualise bound IGF-I. Positive bands appear at functional IGF binding sites (36kDa). The blot was stripped, imaged to confirm no residue remained bound to the blot and probed with a polyclonal goat anti-IGFBP-2 antibody (MW=36kDa) to confirm presence of IGFBP-2. Blot lane 1 = R&D murine IGFBP-2 500ng, lane 2 = R&D murine IGFBP-2 100ng, lane 3 = Abcam insect IGFBP-2 500ng, lane 4 = Abcam insect IGFBP-2 100ng. **(B)** Graphical representation of the densitometry calculated displays the intensity of elevated IGF binding levels in R&D murine IGFBP-2 at 500ng and 100ng compared to Abcam Insect IGFBP-2 using Genetools to measure the blot densitometry in the IGF ligand blot (n=2). **(C)** Densitometry of the bands from the blot probed with polyclonal goat anti-IGFBP-2 antibody were presented graphically to show the levels of IGFBP-2 in each lane (n=2).

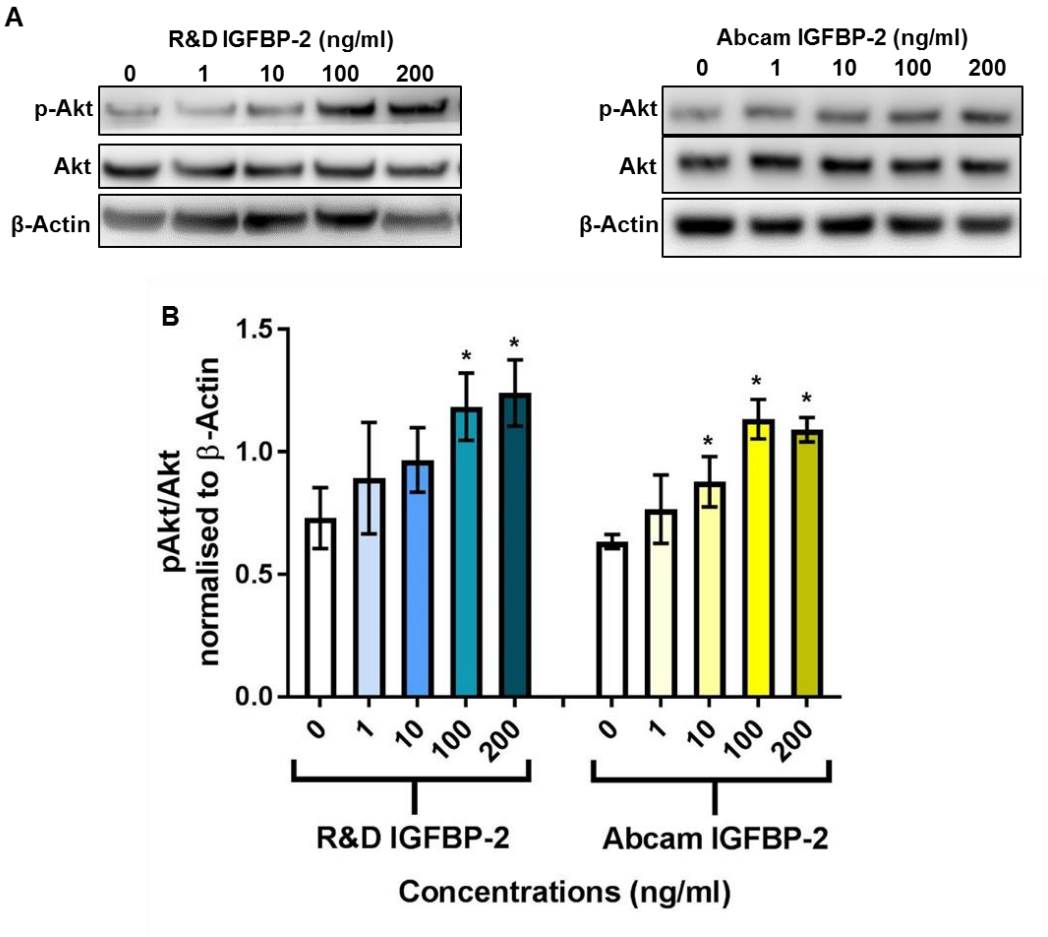

Figure 5.3 IGF-independent interactions are responsible for IGFBP-2 stimulated Akt activation

(A) HUVECs were treated with varying concentrations of R&D murine IGFBP-2 and Abcam insect IGFBP-2 (1-200ng/ml) for 15 minutes. 20µg protein was collected from the stimulated HUVEC lysates and analysed using immunoblotting. The blots were probed for rabbit polyclonal anti-phospho Akt (MW=60kDa) and murine polyclonal anti-Akt (MW=60kDa) and, the loading control, murine monoclonal anti-β-Actin (43kDa). The blots were stripped after incubation with the phospho-antibody and checked for bound residue. Once confirmed that no residue was bound, the blots were probed with the total Akt antibody. **(B)** Densitometry carried out from the blots displayed in 5.3A in a graphical form show both the change in Akt phosphorylation in HUVECs following stimulation with R&D and Abcam IGFBP-2 (1-200ng/ml) (R&D; n=6, *<p=0.01) (Abcam; n=3, *<p=0.05). Error bars represent SEM.

5.4.2 Endogenous IGFBP-2 expression across different cell types

Previous literature has highlighted changes in IGFBP-2 activity between different cell types. The majority of changes in IGFBP-2 activity are influenced by the levels of IGFBP-2 present, as shown by the use of knock out and over-expressing *in vitro* models (Shen et al., 2012). Therefore, a range of available endothelial cells, HUVECs, PECs and HSaVECs were collected to observe how IGFBP-2 levels fluctuated between different tissues. HEPG2, liver carcinoma cells were sourced as a positive control on two fronts; all IGFBPs are predominantly expressed by the liver and IGFBP-2 levels are upregulated in many cancers. C2C12, again serve as a positive control as they have already been reported to endogenously express high levels of IGFBP-2 in response to serum starving (Sharples et al., 2010). INS-Pancreatic cells have been used in many studies regarding insulin resistance. As we know IGFBP-2 protects against insulin resistance, it would be interesting to see how this may affect IGFBP-2 endogenous expression by the cells.

Our results showed that HUVECs endogenously expressed the most IGFBP-2, however other endothelial cells did not replicate this. Endogenous expression of IGFBP-2 in non-endothelial cell types was varied (Figure 5.4).

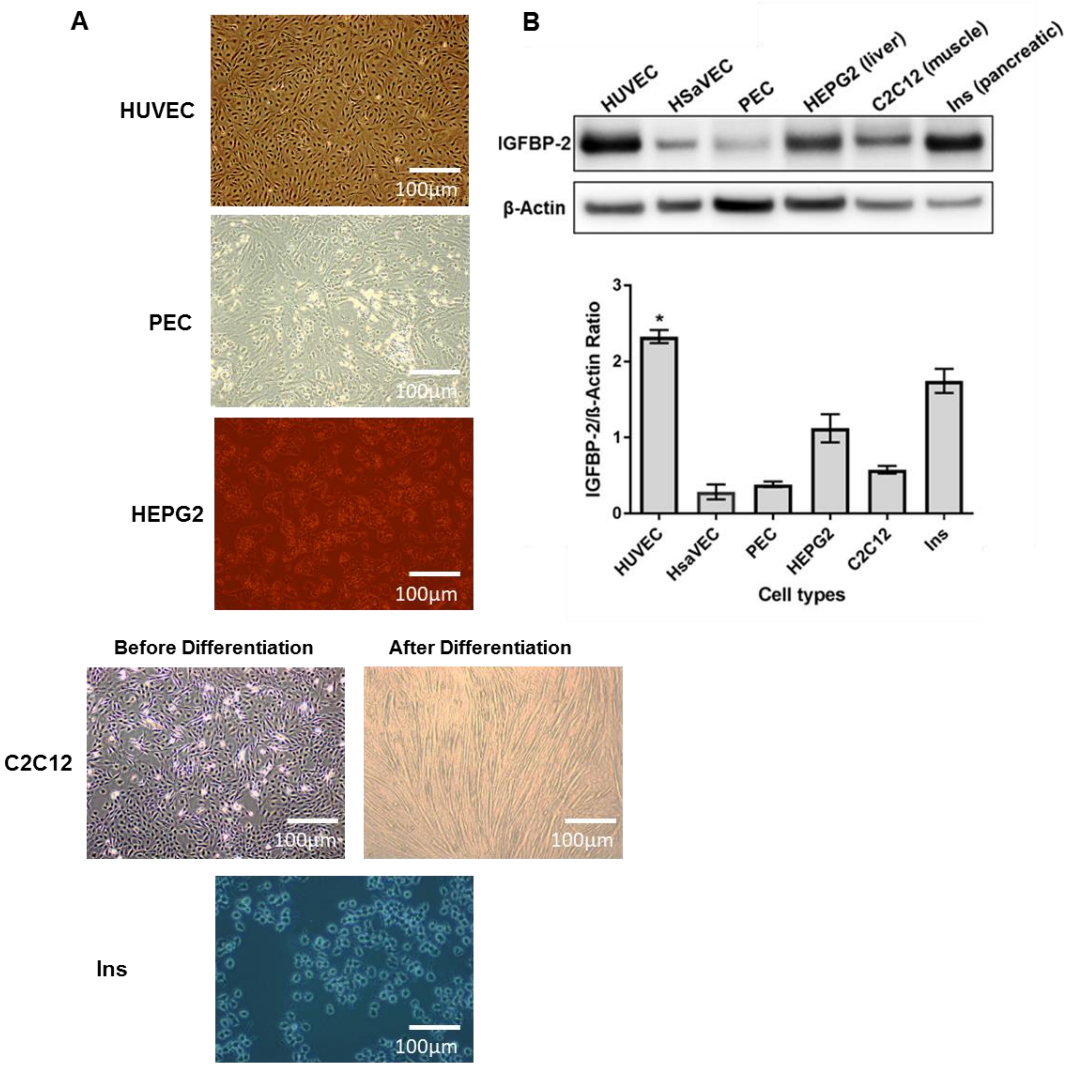

Figure 5.4 Endogenous expression of IGFBP-2 in PEC, HEPG2, C2C12, Ins and HSaVEC cells

(A) Images captured during the culturing of cells at a 40x magnification using an optical zoom microscope. **(B)** Cell lysates were collected from PEC, HEPG2, C2C12, Ins cells and HsaVEC lysates. 40µg protein was added for each sample/cell lysate. The blots were probed for goat polyclonal anti-IGFBP-2 (MW=36kDa) and, the loading control, murine monoclonal anti-β-Actin (43kDa). The blots were stripped after incubation with the IGFBP-2 antibody and checked for bound residue. Once confirmed that no residue was bound, the blots were probed with the loading control. Densitometry was measured using Genetools (n=5, *<p=0.02). Error bars represent SEM.

5.4.3 Serum in media affects IGFBP-2 activity

Very little research has been carried out on HUVECs using IGFBP-2 as a stimulant, especially in regards to *in vitro* angiogenic signalling and activity (Das et al., 2013; Feng et al., 2015; LI et al., 2018). Therefore, we needed to optimise the *in vitro* conditions, which create a HUVEC environment where the angiogenic-like characteristics of IGFBP-2 can be observed.

Media compositions can affect the growth of cells as well as influence the effect of stimulants. As stated in the background (Chapter 5.1) heparin, IGF-I and other growth factors all have ability to affect IGFBP-2 activity. Cells were compared using a high serum media (20%) (M199), which is used universally in our laboratory and a low serum media (2%) (EGM2).

Cells grown in 20% serum following serum starvation displayed a change in morphology, presenting a rigid cell shape and cells floating to the surface (Figure 5.5). Following stimulation with IGFBP-2, Akt and MAPK phosphorylation was more pronounced in HUVECs which didn't retain their endothelial cell phenotypes (Figure 5.6).

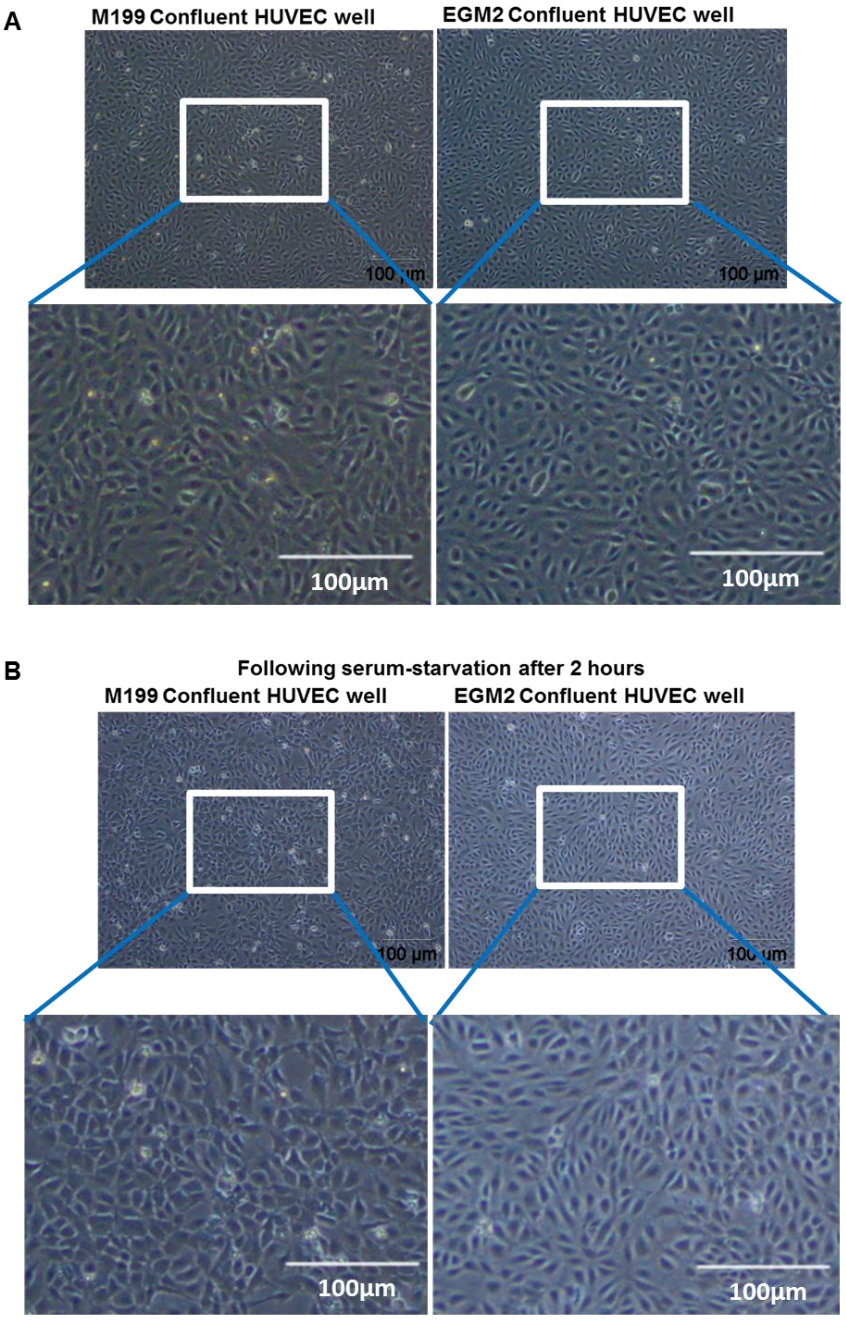

Figure 5.5 Serum-starving influences cell morphology, depending on media used to culture cells - Preliminary study
Images taken at a 40x magnification using an optical zoom microscope of **(A)** HUVECs grown until confluency in M199 media (supplemented with 20% serum) or EGM2 (supplemented with 2% serum) media. **(B)** After changing the media to serum-free media (no serum or endothelial growth factors/supplement) for 2 hours for HUVECs grown in both different mediums. Images were magnified using ImageJ.

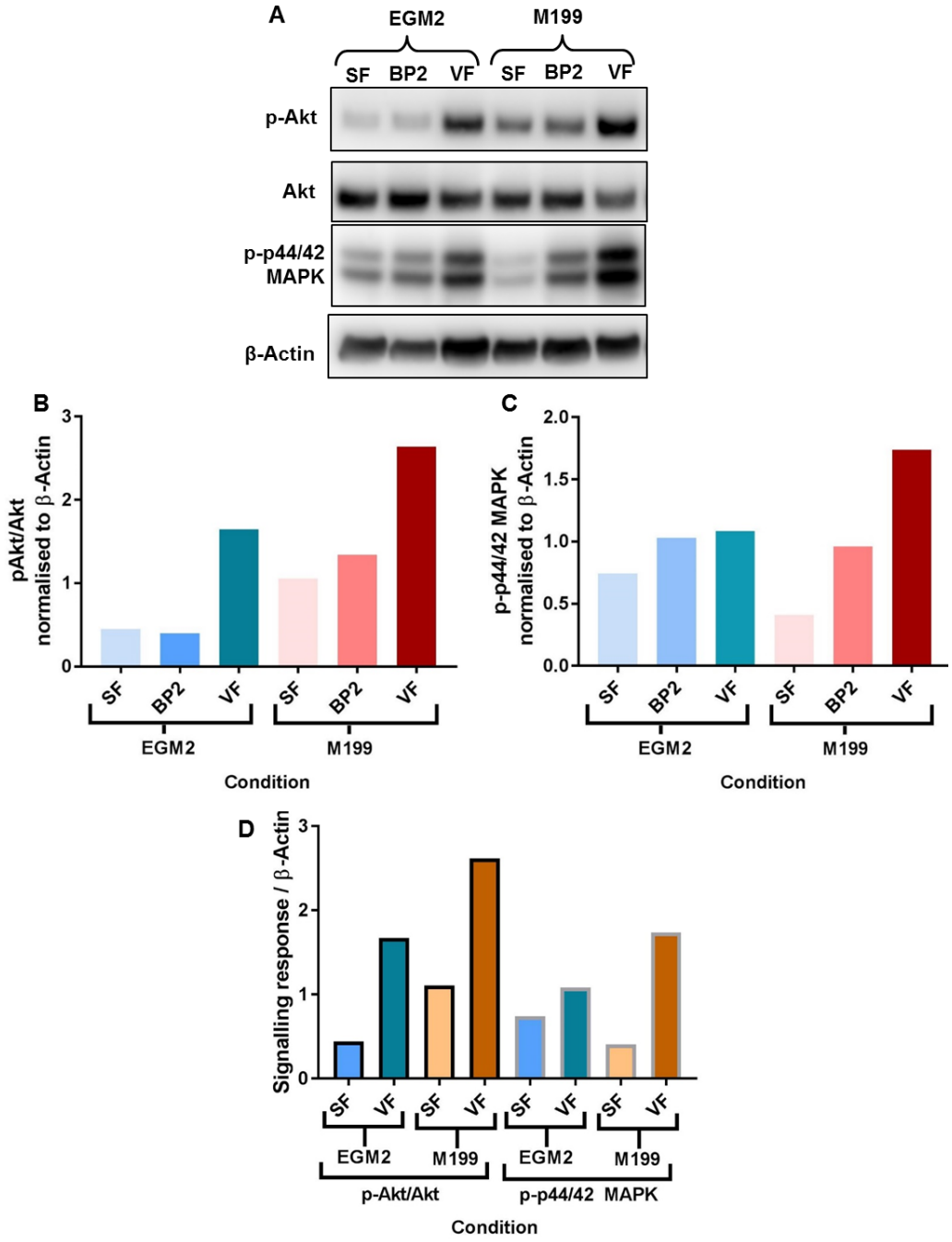

Figure 5.6 Different serum concentrations in cell media influences signalling outputs - Preliminary study

Serum-starved HUVECs grown in either EGM2 (2% serum) or M199 (20% serum) were stimulated with 500ng/ml IGFBP-2 or 30ng/ml VEGF for 20 mins. **(A)** 20µg of protein from the stimulated HUVEC lysates was loaded onto an immunoblot and probed for rabbit polyclonal anti-phospho Akt (MW=60kDa), murine polyclonal anti-Akt (MW=60kDa), rabbit polyclonal anti-phospho-MAPK (MW=44/42kDa) and the loading control, murine monoclonal anti-β-Actin (43kDa). The blots were stripped after each incubation and confirmed that no residue was bound before the next antibody was used. Lane 1-3 = HUVECs grown in EGM2 media, lane 4-6 = HUVECs grown in M199 media. Lane 2 and 5 were stimulated with 500ng/ml IGFBP-2, Lane 3 and 6 stimulated with 30ng/ml VEGF. **(B)** Graphical representation of the densitometry of pAkt/Akt, normalised to β-Actin (n=2). **(C)** Graphical representation of the densitometry of pMAPK normalised to β-Actin (n=2). **(D)** Graphical representation comparing the densitometry of pAkt/Akt and p-MAPK, normalised to β-Actin in non-stimulated (SF) and VEGF-stimulated samples in both mediums (n=2).

5.4.4 Heparin affects IGFBP-2 signalling activity

Heparin is added to most cell growth media to help the delivery of growth factors. The effect of heparin in the media and its possible interference with the HBDs in IGFBP-2 was also verified by observing the changes occurred with Akt and MAPK phosphorylation. Akt phosphorylation and MAPK phosphorylation was blunted in the presence of heparin. (Figure 5.7).

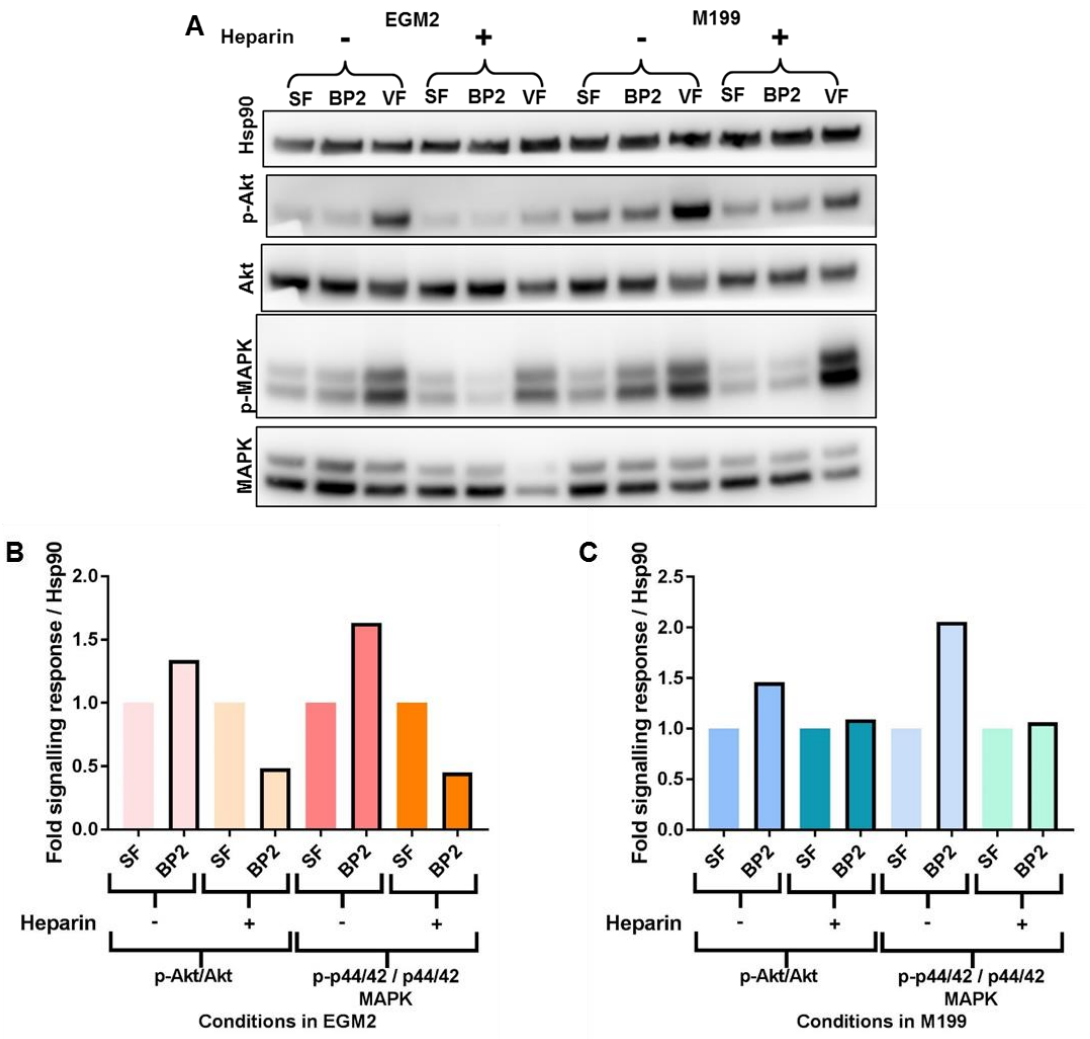

Figure 5.7 Heparin suppresses IGFBP-2 stimulated activity - Preliminary study
(A) Representative images of immunoblots with 20µg of protein from cell lysates of HUVECs grown in EGM2 (2% serum) or M199 (20% serum), in the presence (+) and absence (-) of heparin and stimulated with IGFBP-2 (BP2) (500ng/ml) or VEGF (30ng/ml) for 20 minutes. The blots were probed for rabbit polyclonal anti-phospho Akt (MW=60kDa) and murine polyclonal anti-Akt (MW=60kDa), rabbit polyclonal anti-phospho-MAPK (MW=44/42kDa), murine polyclonal anti-MAPK (MW=44/42kDa) and the loading control, murine monoclonal Hsp90 (MW=90kDa). All these sections were cut separately with phospho-proteins being probed for first, following the total equivalent, with the blots being stripped in between. Between each stripping stage, the blots were imaged to ensure no residue remained **(B)** Densitometry of phospho-Akt and -MAPK changes in HUVECs grown in EGM2, in the presence or absence of heparin, stimulated with or without IGFBP-2 (n=2). **(C)** Densitometry of phospho-Akt and -MAPK changes in HUVECs grown in M199, in the presence or absence of heparin, stimulated with or without IGFBP-2 (n=2).

5.4.5 IGF and ECGS influences cellular expression of IGFBP-2

Endothelial cell growth supplement (ECGS) contains many growth factors such as FGF, PDGF and VEGF, which also may indirectly or directly affect the role IGFBP-2 may play, specifically IGF. IGF-I concentrations may influence IGFBP-2 expression and therefore interfere with the known concentration of IGFBP-2 added to stimulate a response (Clemmons et al., 1992). ECGS and IGF-I in combination and alone increased endogenous expression of IGFBP-2 in HUVECs (Figure 5.8).

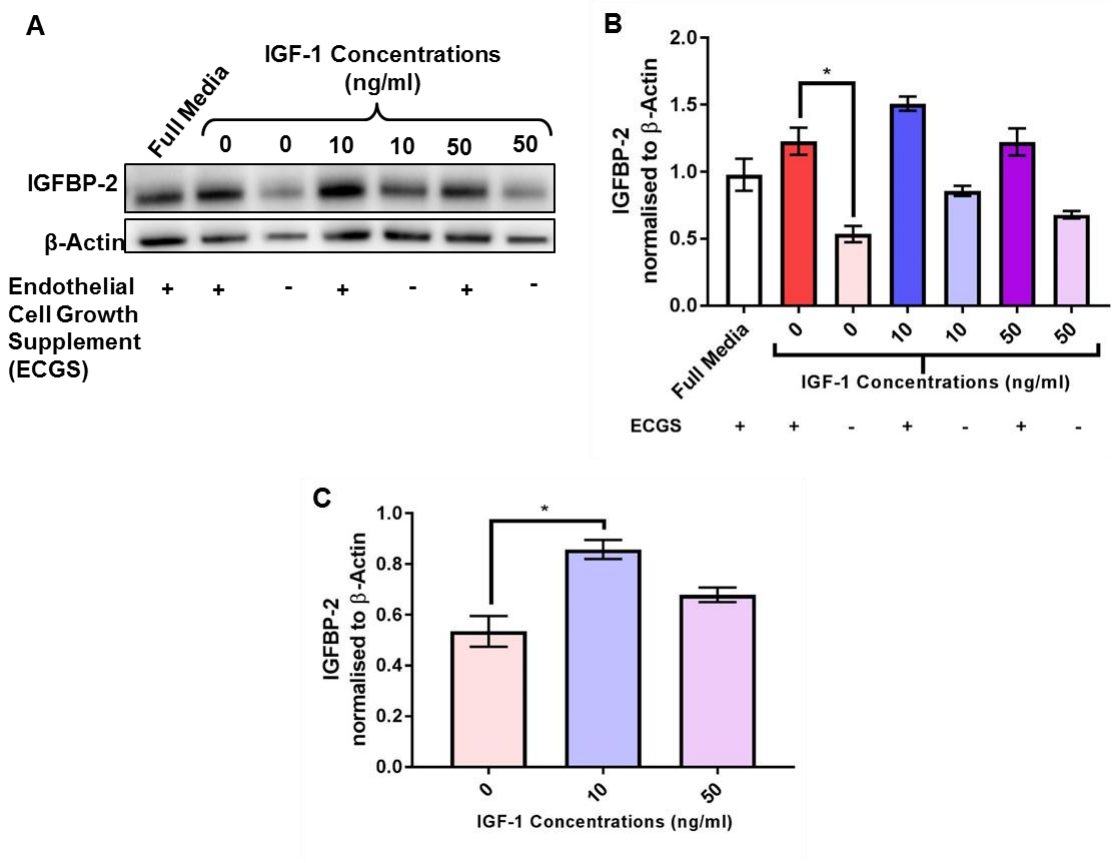

Figure 5.8 IGF-1 and ECGS stimulation significantly enhances cellular IGFBP-2 expression

HUVECs were stimulated with IGF-I (10-50ng/ml) for 10 minutes in the presence (+) and absence (-) of endothelial cell growth supplement (ECGS) following serum starvation or remained in full media (20% serum). **(A)** 20µg protein was loaded from non-stimulated and stimulated cell lysates. Blots were first probed for goat polyclonal anti-IGFBP-2 (MW=36kDa) and the loading control, murine monoclonal al anti-β-Actin (43kDa). Following stripping between antibody probing, the blots were imaged to ensure no residue remained. **(B)** Densitometry of IGFBP-2 levels normalised to β-Actin, comparing full media HUVECs, serum-starved HUVECs, following stimulation with IGF-I for 10 minutes, in the presence or absence of ECGS (n=2, *<p=0.03). Error bars represent SEM. **(C)** Graph comparing IGFBP-2 levels, normalised to β-Actin in the absence of ECGS, following stimulation with IGF-I (10ng/ml and 50ng/ml) (n=2, *<p=0.05). Error bars show SEM.

5.4.6 Cell confluency affects IGFBP-2 stimulated Akt phosphorylation

Cells at different stages of confluency activate different growth and survival signalling pathways, as growth signalling pathways would be activated when populating an area, whereas apoptotic signalling pathways will be triggered during over confluence. We need to ensure the changes in signalling pathways influenced by confluence do not affect the role of IGFBP-2 in *in vitro* angiogenic signalling pathways. IGFBP-2 stimulated Akt phosphorylation is muted at 50% confluence state but the enhancement returns at 100% and over-confluency (Figure 5.9).

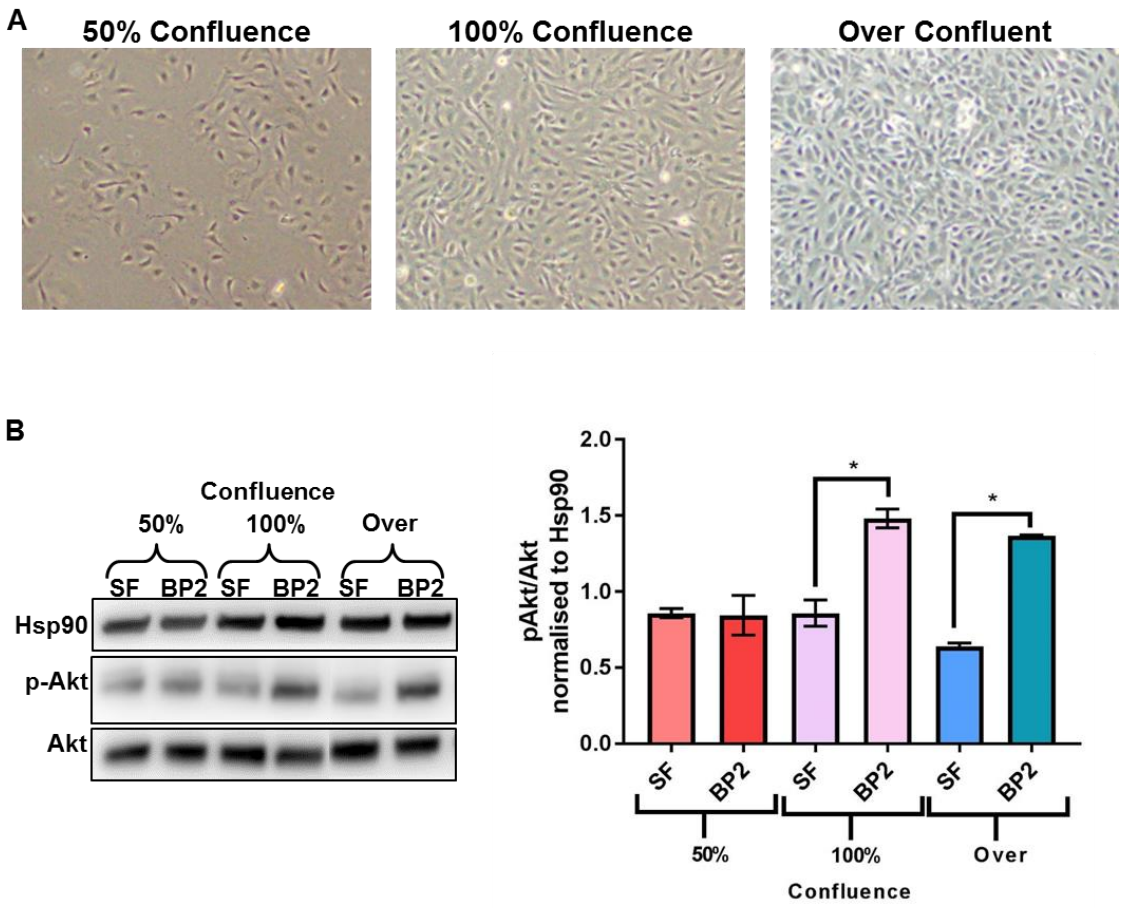

Figure 5.9 Confluence states influences the activity of IGFBP-2
HUVEC were stimulated with IGFBP-2 (500ng/ml) for 20 mins and lysed at 50%, 100% or over-confluent (24 hours after 100% confluency) states. **(A)** Images of HUVECs at the different confluence states before being stimulated with IGFBP-2 (500ng/ml) were taken at a 40x magnification using an optical zoom microscope. **(B)** 20µg of protein was obtained from HUVEC lysates and used for immunoblotting analysis. Blots were probed for rabbit polyclonal anti-phospho-Akt (MW=60kDa), murine polyclonal anti-Akt (MW=60kDa) and the loading control, murine monoclonal Hsp90 (MW=90kDa). Blots were stripped and checked for residue in between probing for phosphor and total levels of Akt. Lane 1 and 2 are HUVECs at 50% confluency, lane 3 and 4 are HUVECs at 100% confluency and lane 5 and 6 are HUVECs at over-confluency. Lane 2, 4 and 6 are stimulated with IGFBP-2 and 1, 3 and 5 are their representative controls. Densitometry of the bands on the blots measured show Akt phosphorylation changes in response to stimulation with IGFBP-2 at different confluence states (50%, 100% and over-confluent) (n=2, *<p=0.03). Error bars represent SEM.

5.4.7 IGFBP-2 stimulated Akt phosphorylation in HUVECs

Having optimised HUVEC culture conditions to ensure they do not interfere with the IGFBP-2 used to stimulate signalling cascades, we can optimise the concentrations and time stimulations required to induce effects on certain angiogenic pathways. Physiological concentrations of IGFBP-2 in healthy humans range from approximately 250ng/ml to 600ng/ml (Lin et al., 2009).

HUVECs stimulated with lower concentrations and concentrations within the human plasma range demonstrated 200ng/ml achieved the maximum level of IGFBP-2 stimulated Akt phosphorylation (Figure 5.10) Time-dependent stimulation showed IGFBP-2 maximal Akt phosphorylation was achieved within 15 mins.

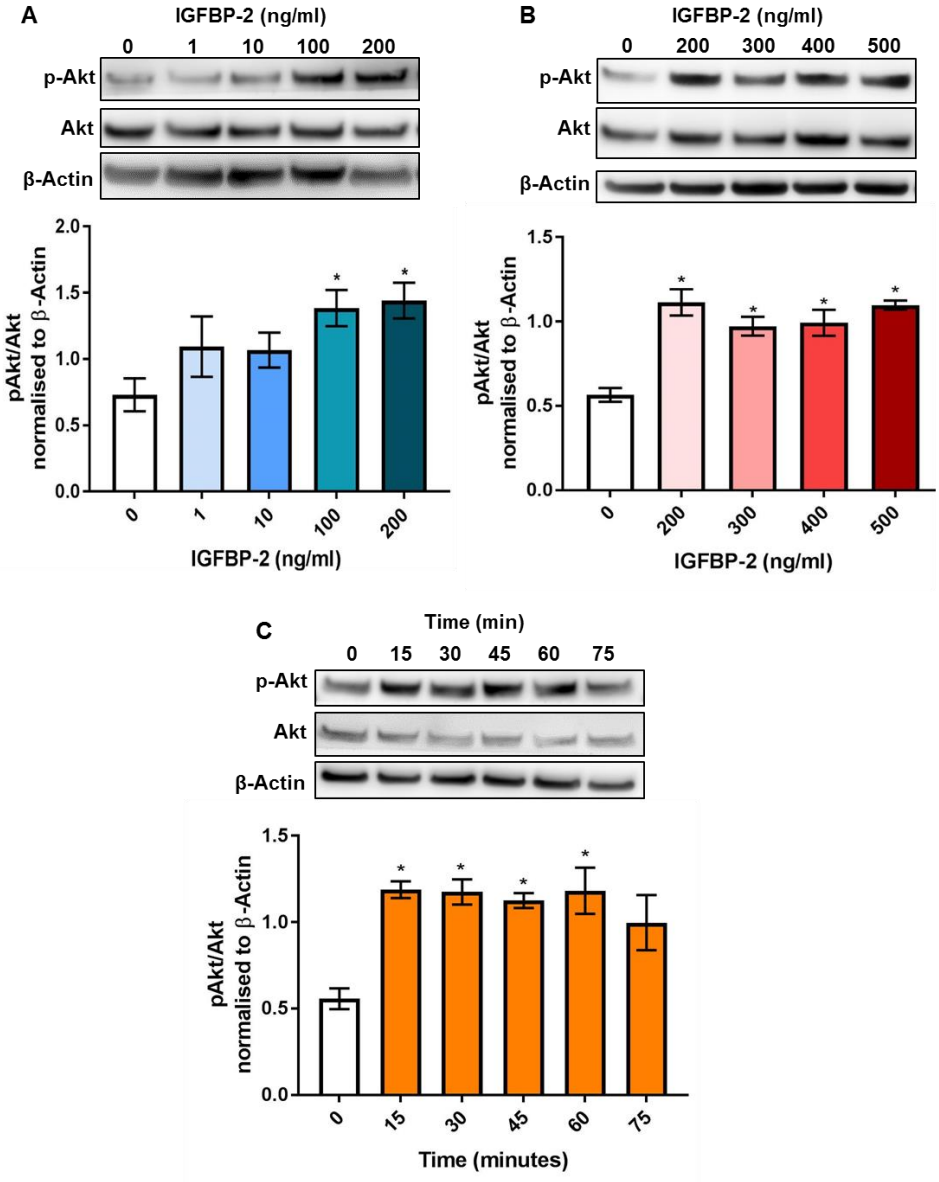

Figure 5.10 IGFBP-2 significantly activates Akt phosphorylation
HUVECs were stimulated with IGFBP-2 (1-500ng/ml) for 15 mins or for 15 mins intervals up to 75 mins. 20µg of protein from cell lysates was loaded onto western blots. The blots were probed for rabbit polyclonal anti-phospho Akt (MW=60kDa) and murine polyclonal anti-Akt (MW=60kDa) and the loading control, murine monoclonal anti-β-Actin (43kDa). Blots were stripped between being probed for phospho and total Akt. **(A)** HUVECs were stimulated with IGFBP-2 (1-200ng/ml) for 15 mins. Densitometry from the blots shows the change in Akt phosphorylation occurred as a result of stimulation with IGFBP-2 of increasing concentrations (n=6, *<p=0.01). **(B)** HUVECs were stimulated with IGFBP-2 (200-500ng/ml) for 15mins. Densitometry of the blots shows the change in Akt phosphorylation vs total levels of Akt in response to stimulation with increasing concentrations of IGFBP-2 (n=5, *<p=0.01). **(C)** HUVECs were stimulated with IGFBP-2 (200ng/ml) for 15-75 mins in 15 min intervals. Densitometry shoes the change in Akt phosphorylation, compared to total Akt levels in response to increasing stimulation times with IGFBP-2 (n=5, *<p=0.01). Error bars represent SEM.

5.4.8 IGFBP-2 stimulated ERK/MAPK phosphorylation in HUVECs

Along with the Akt pathway being the most reported pathway to be influenced by IGFBP-2 via IGF-I, integrin and PTEN interactions, ERK/MAPK activation is also stimulated by IGFBP-2 (Myers et al., 2015; Shen et al., 2012). p44/42 MAPK was activated in response to 500ng/ml IGFBP-2 (10 min stimulation) (Figure 5.11). The incubation time was lowered to 10 mins instead of 15 mins because following optimisation, incubation time at 15 mins did not give us a consistent activation effect.

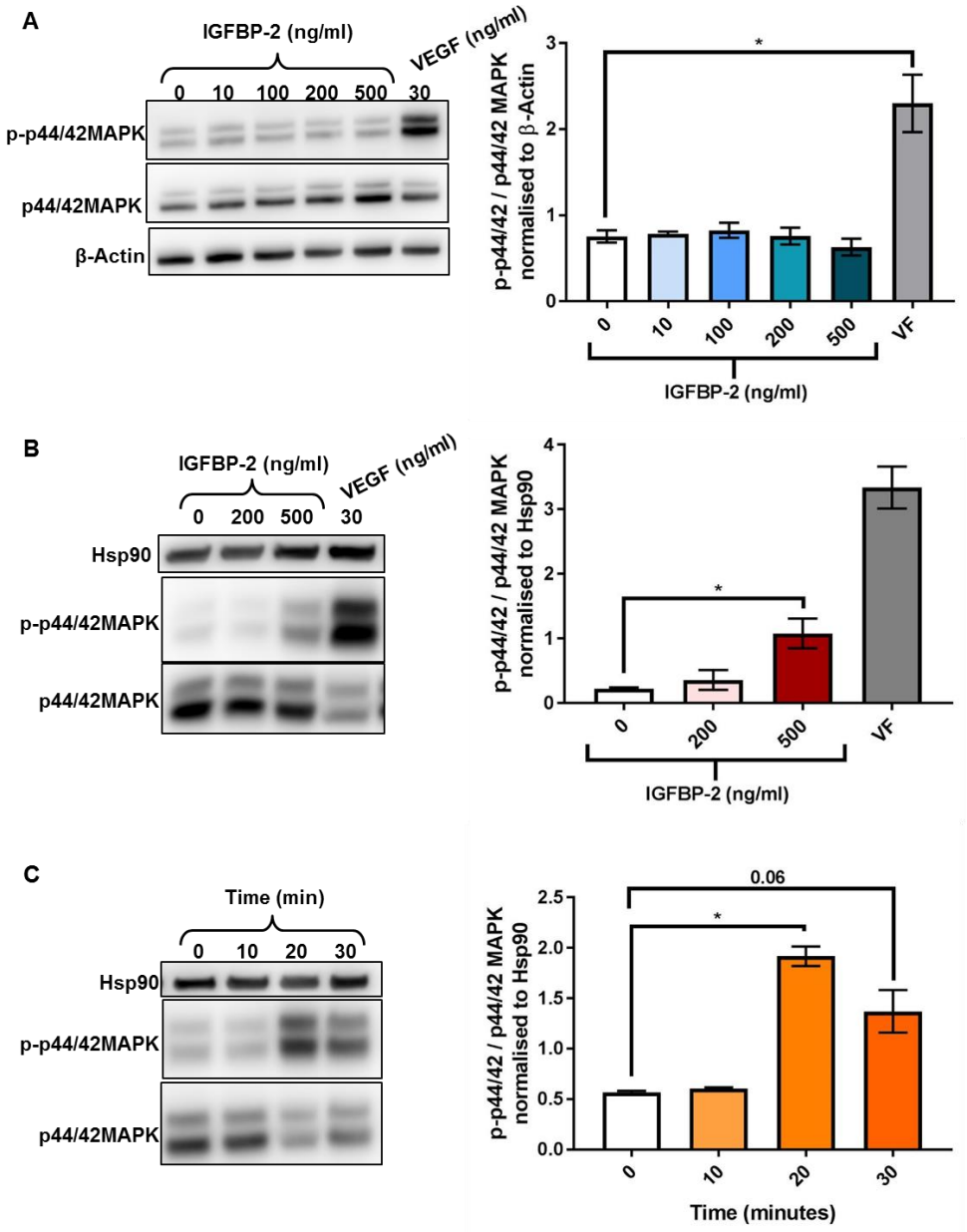

Figure 5.11 IGFBP-2 enhances MAPK activation
Serum-starved HUVECs were stimulated with varying concentrations of IGFBP-2 (10-500ng/ml) for different time periods (10-30mins) or with the positive control (30ng/ml; 10min). 20µg protein cell lysates in blots were probed for rabbit polyclonal anti-phospho-MAPK (MW=44/42kDa), murine polyclonal anti- MAPK (MW=44/42kDa) and the loading control, murine monoclonal anti-β-Actin (43kDa) or murine monoclonal Hsp90 (MW=90kDa). Blots were stripped and checked for bound residue between phospho-, total-MAPK and β-Actin. **(A)** Representative image of the immunoblot with HUVECs stimulated with IGFBP-2 (10-500ng/ml; 10min) or VEGF (30ng/ml; 10min) and probed for phospho-MAPK, total-MAPK and β-Actin. Graph shows change in MAPK phosphorylation compared total MAPK levels and normalised to β-Actin levels in response to stimulation with increasing IGFBP-2 levels (n=3, *<p=0.05). **(B)** Representative image of immunoblot with HUVECs stimulated with IGFBP-2 (200-500ng/ml; 20min) or VEGF (30ng/ml; 10min). Graph shows change in MAPK phosphorylation compared total MAPK levels and normalised Hsp90 levels in response to stimulation with increasing IGFBP-2 levels (n=3, *<p=0.01). **(C)** Representative image of immunoblot with HUVECs stimulated with IGFBP-2 (500ng/ml; 10-30min). Graph shows change in MAPK phosphorylation compared total MAPK levels and normalised Hsp90 levels in response to stimulation with IGFBP-2 (500ng/ml) for 10, 20 or 30mins (n=3, *<p=0.01). Error bars represent SEM.

5.4.9 IGFBP-2 does not stimulate eNOS phosphorylation

IGFBP-2 has rarely been implicated to interact with eNOS until recent years. In HUVECs, down-regulated levels of IGFBP-2 have been associated with a decrease in insulin-stimulated Akt and in turn eNOS (LI et al., 2018). If IGFBP-2 directly modulates endothelial remodelling as hypothesised from Chapter 4, IGFBP-2 may also affect eNOS expression. However, in HUVECs IGFBP-2 did not show any evidence of mediating eNOS phosphorylation (Figure 5.12).

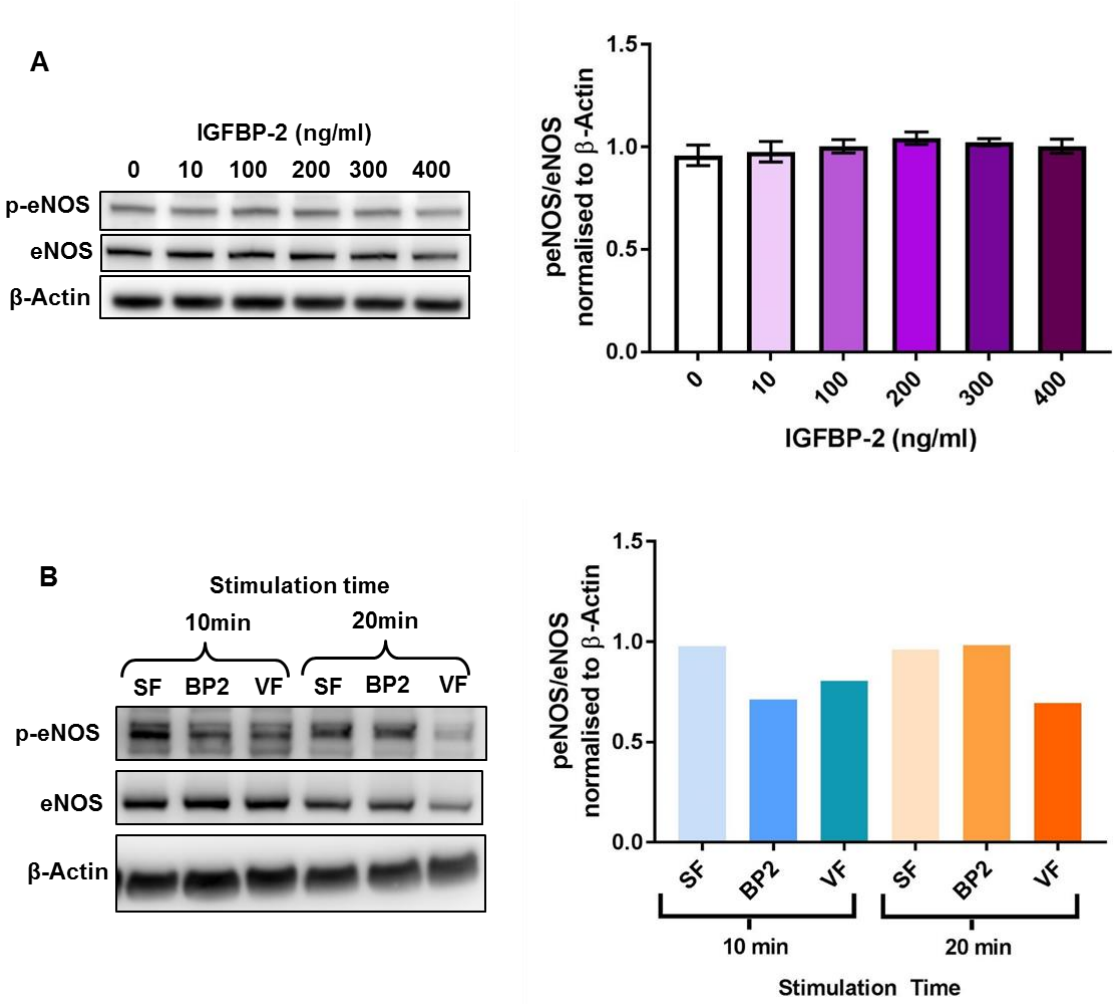

Figure 5.12 IGFBP-2 fails to enhance eNOS phosphorylation
Serum-starved HUVECs were stimulated with varying concentrations of IGFBP-2 (10-400ng/ml) for different time periods (10-20mins) or with the positive control (30ng/ml; 10min). 20µg protein from cell lysate were used on blots which were probed for rabbit polyclonal anti-phospho eNOS (MW=140kDa), rabbit polyclonal anti-eNOS (MW=140kDa) and the loading control murine monoclonal anti-β-Actin (43kDa). Blots were stripped and checked for bound residue between probing for phospho and total levels. **(A)** Representative image of the immunoblot with HUVECs stimulated with IGFBP-2 (10-400ng/ml; 20min). Graph shows change in eNOS phosphorylation compared total eNOS levels and normalised to β-Actin levels in response to stimulation with increasing IGFBP-2 levels (n=4). Error bars show SEM. **(B)** Representative image of immunoblot with HUVECs stimulated with IGFBP-2 (500ng/ml; 10 or 20min) or VEGF (30ng/ml; 10 or 20min). Graph shows change in eNOS phosphorylation compared total eNOS levels and normalised β-Actin levels in response to stimulation with IGFBP-2 levels at different stimulation times (10 or 20min) (n=2).

5.4.10 IGFBP-2 does not activate FAK, GSK3β or PTEN

FAK was investigated due to many published articles linking an association between increased IGFBP-2 concentrations and activation of the FAK pathway (Liu et al., 2017; Yau et al., 2014). However, for the first time we are exploring this link in an endothelial cell (Figure 5.13). The phosphorylation of other potential angiogenic-signalling molecules shown to interact with IGFBP-2 such as GSK3β and PTEN were interrogated to help identify the predominant signalling pathway driving IGFBP-2s influence over angiogenic-like characteristics. In HUVECs, IGFBP-2 failed to activate FAK and GSK3β signalling, or PTEN phosphorylation (Figure 5.13).

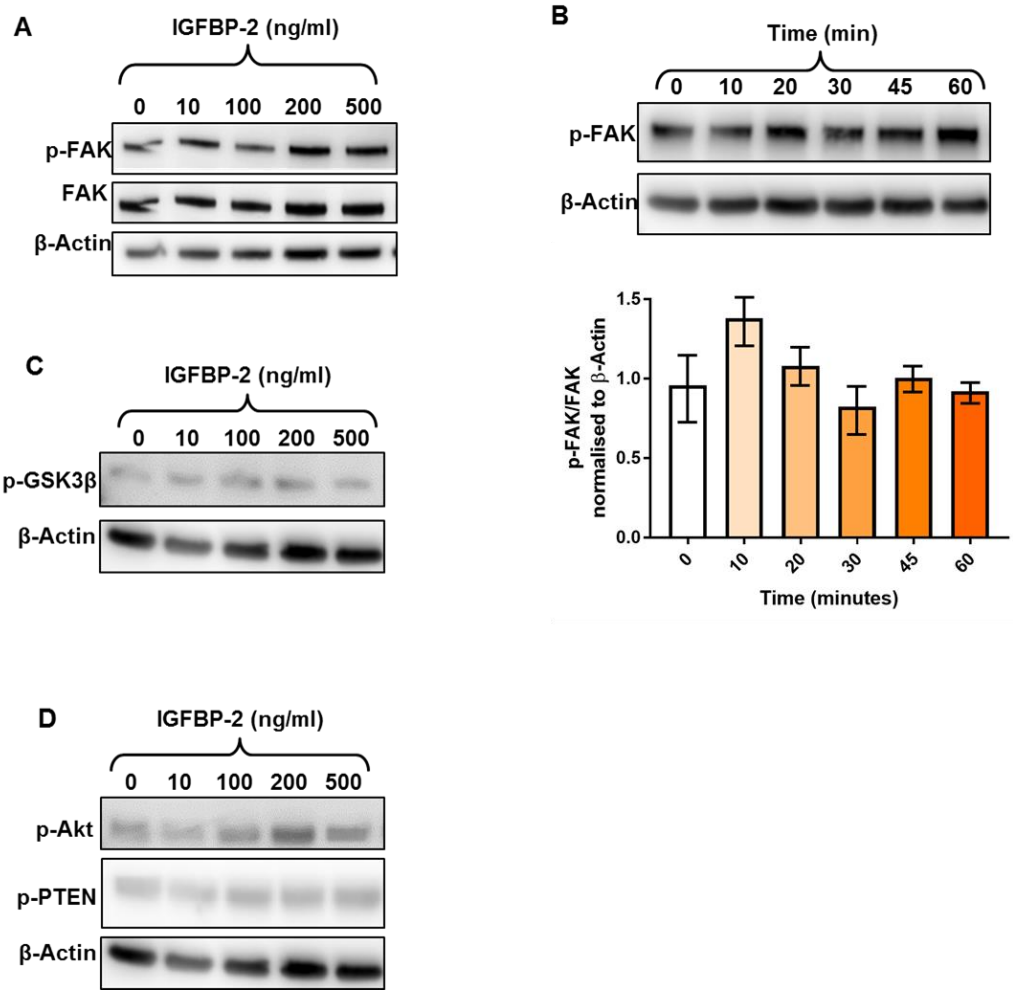

Figure 5.13 IGFBP-2 does not activate other angiogenic signalling molecules
Serum-starved HUVECs were stimulated with varying concentrations of IGFBP-2 (10-500ng/ml) for different time periods (10-60mins). 20µg protein from cell lysate were used on blots which were probed for rabbit polyclonal anti-phospho FAK (MW=125kDa), rabbit polyclonal anti-FAK (MW=125kDa), rabbit polyclonal anti-phospho GSK3β (46kDa), rabbit polyclonal anti-phospho Akt (60kDa), rabbit polyclonal anti-phospho PTEN and the loading control, murine monoclonal anti-β-Actin (43kDa). Blots were stripped and checked for bound residue between probing for phospho, total levels and the loading control. **(A)** Representative image of the immunoblot with HUVECs stimulated with IGFBP-2 (10-500ng/ml; 15min), probing for changes in FAK phosphorylation changes, compared to total FAK levels. **(B)** Representative image of the immunoblot with HUVECs stimulated with IGFBP-2 (500ng/ml; 10-60min). Graph shows change in FAK phosphorylation compared to total FAK levels and normalised to β-Actin levels in response to stimulation with IGFBP-2 for stimulation times at 10 or 15min intervals, up to 60min (n=3). Error bars represent SEM. **(C)** Representative image of the immunoblot with HUVECs stimulated with IGFBP-2 (10-500ng/ml; 15min), probing for changes in GSK3β phosphorylation changes. **(D)** Representative image of the immunoblot with HUVECs stimulated with IGFBP-2 (10-500ng/ml; 15min), probing for changes in PTEN phosphorylation changes, using phosphorylation of Akt as a positive control (as identified previously).

5.5 Discussion

5.5.1 Endothelial cell types endogenously express varying concentrations of IGFBP-2

From earlier studies, changes in IGFBP-2 induced signalling were dependent on levels within different cells. Therefore, it is important to identify which cells endogenously express higher levels of IGFBP-2 as these cells are most likely to be involved in modulating angiogenic-like characteristics. This is confirmed by cells, specifically cancer cells, such as small cell lung cancer cells and breast cancer cell lines, which express elevated levels of IGFBP-2 also display an enhancement in cell growth, survival, proliferation and migration (Hoeflich & Russo, 2015; Yazawa et al., 2009).

Our findings showed HUVECs expressed the largest abundance of endogenously expressed IGFBP-2 compared to all cell types, suggesting they play a more significant role in cell migration and proliferation. We investigated the over-expression of IGFBP-2 on cells that are highly proliferative in their regular phenotype as these are types of cells which will respond to angiogenic signals rapidly.

Bovine aortic endothelial cells have previously been shown to express IGFBP-2 levels, displaying an intense band following northern blotting and RT-PCR (Moser et al., 1992). Interestingly, PECs and HSaVECs produce very small amount of IGFBP-2 in comparison to HUVECs and other non-endothelial cell types. However, this correlates with their growth in *in vitro* culture. 100,000 HUVEC cells are able to reach confluency in approximately 3 days, however PECs and HSaVECs proliferate at a distinctively slower rate as observed in our laboratory.

Strangely, HEPG2 cells also generate significant less IGFBP-2 than HUVECs, even though IGFBP-2 is expressed into circulation from liver cells. C2C12 myoblasts express IGFBP-2 in a small abundance when not put in a state of inflammation due to low serum concentration (Sharples et al., 2010). INS-Pancreatic cells presented a significantly elevated expression of IGFBP-2 in comparison to the C2C12 cells. Many *in vitro* and *in vivo* studies have confirmed IGFBP-2 does play a role in maintaining metabolic homeostasis. As these are insulin producing cells and they have a large presence in modulating metabolism, IGFBP-2 may be expressed by the cell in order to regulate metabolic changes.

These findings validate our use of HUVECs for our exploration of IGFBP-2s angiogenic potential. Their highly proliferative characteristic may be driven by the upregulation of IGFBP-2 we observe. In addition, IGFBP-2 down-regulation or low

IGFBP-2 levels cause negative effects on angiogenic signalling which is opposite to the effect we are aiming to investigate (Gao et al., 2016; Liu et al., 2017).

5.5.2 IGFBP-2 activates Akt signalling independent of IGF binding in HUVECs

Previous *in vitro* studies exploring the effect of IGFBP-2 on HUVECs have all highlighted activation of a potent angiogenic signalling molecule, Akt. The mechanisms reported to drive this activation were through IGF-I signalling or integrin interactions.

We commercially sourced two recombinant IGFBP-2 proteins retrieved from different sources, one from insect cells (Abcam) and one from murine cells (R&D). The use of both recombinant IGFBP-2s have been published, however no citations have been reported on the Abcam product site (Chua et al., 2016; Huynh et al., 2008). Both recombinant proteins were validated using its IGF functional ability to inhibit IGF-stimulated growth responses. However, we failed to display functional binding of biotinylated IGF-I to non-denatured IGF binding sites in the Abcam recombinant IGFBP-2 sourced from insect cells. Immunoblotting using an IGFBP-2 antibody confirmed the protein was recognised as IGFBP-2. The recombinant protein sourced from murine cells displayed IGF binding capacity of the biotinylated IGF-I. From this, we can deduce, post-translational modifications in the IGFBP-2 sourced from insect cell hosts may define its selection of binding to IGF-I. To study this further, we would need to assess for changes in post-translational modifications, such as phosphorylation and glycosylation changes, between the different species hosts of IGFBP-2.

Further investigation into the functionality of these recombinant proteins was carried out on a signalling level. Published data confirmed IGFBP-2 regulates Akt phosphorylation in serum-starved HUVECs to drive survival and migration responses, therefore we used the Akt signalling pathway to determine the effect a non-functional IGF binding IGFBP-2 had on Akt phosphorylation compared to the complete functional protein (Bhutia et al., 2016). Interestingly, both recombinant IGFBP-2s dose-dependently enhanced Akt activation in HUVECs. Thus, suggesting IGFBP-2 induced Akt phosphorylation is via an IGF-independent mechanism. This potential has been highlighted in IGFBP-2 KO mice that were injected with a HBD peptide. The peptide resulted in the upregulation of IGF-I stimulating an enhancement in Akt signalling (Kawai et al., 2011). Therefore, other domains within IGFBP-2 may indirectly influence IGF-I levels without requiring IGF binding potential.

Although the non-binding IGF did not affect Akt signalling, we cannot confirm the other domains are functional and what adverse effect the non-functioning site may have on further angiogenic signalling and assay studies. Therefore, the complete functional recombinant protein sourced from murine cells was used for all further experiments.

Maximum Akt phosphorylation stimulated by IGFBP-2 was achieved using a concentration 200ng/ml in serum-starved HUVECs. Elevated Akt phosphorylation plateaued following stimulation with concentrations above 200ng/ml to 500ng/ml. It is difficult to establish why Akt phosphorylation may plateau, however IGFBP-2 bioavailability and functionality may be dependent on circulating IGF concentrations. Time-dependent stimulation of IGFBP-2 (200ng/ml) highlighted immediate activation of Akt by IGFBP-2 occurred within 15 mins, matching published results (Das et al., 2013). This enhanced response to Akt activation also plateaued with stimulations for increasing periods of time over 15 mins.

Excess IGF-I prevents IGFBP-2 from exerting its inhibitory functionality on the effect of follicle-stimulating hormone, which it would normally exert in low IGF circulating concentrations (Zhou et al., 2013). If IGF-I circulating concentrations are able to affect IGFBP-2s bioactivity, it is possible IGFBP-2 may also rely on the bioavailability of integrins or heparin to exert its actions. Therefore, the plateau effect could be due to a restricted bioavailability of any of these molecules stimulating IGFBP-2-dependent Akt phosphorylation to its maximum possible level or affinity of interaction, as IGFBP-2 may be competing with other IGFBPs.

5.5.3 IGFBP-2 activates MAPK phosphorylation in HUVECs

IGFBP-2 stimulated MAPK activation through ERK and JNK has been associated in many cancer cell lines to enhance cellular migration and proliferation. MAPK signalling induced by IGFBP-2 has never been interrogated in HUVECs. Although most cells stimulated with IGFBP-2 activate MAPK via both ERK and JNK, IGFBP-2 stimulated JNK was shown to be specifically involved in mediating glioma cell migration only. (Han et al., 2014; Mendes et al., 2010). However, angiogenesis involves a combination of cell proliferation and migration, therefore in the initial signalling studies we focused on the activation of ERK1/2 (Wang et al., 2017c).

Stimulation with the lower concentration of IGFBP-2 200ng/ml that can induce Akt phosphorylation activates p44/42 MAPK phosphorylation at a slower rate, therefore longer incubation times were required. A time-dependent stimulation with IGFBP-2 highlighted p44/42 MAPK phosphorylation occurs at 20 mins, compared to the Akt

activation which as been confirmed at 15 mins. These distinct differences between IGFBP-2 stimulated Akt and p44/42 MAPK suggest different interaction mechanisms are responsible for the activation of each pathway.

The activation of the p44/42 MAPK pathway by IGFBP-2 displays distinct differences compared to its Akt activation, suggesting they function through different interactions. The most reported interactions shown to drive IGFBP-2 stimulated MAPK activation is through integrins, specifically the subunits β1 and α5 (Holmes et al., 2012). Whereas IGFBP-2 induced Akt is thought to function via modulation of IGF-I or interactions between HBD1 and RPTPβ. Thus, providing an explanation to the different conditions required to stimulate each pathway.

5.5.4 IGFBP-2 stimulation has no effect on eNOS phosphorylation in HUVECs

eNOS is a highly important regulator of vascular integrity, especial during and after angiogenesis in the formation and maintenance of healthy blood vessels. IGFBP-2 is recently being associated with an increase in NO via activation of Akt in osteoblasts, hepatocellular carcinoma cells and HUVECs, however there is limited information (Hung et al., 2017; LI et al., 2018; Xi et al., 2016).

We have already established IGFBP-2 does activate Akt in serum starved HUVECs, however we have not interrogated downstream activation of targets below Akt in the signalling cascade. IGFBP-2 failed to upregulate eNOS phosphorylation under a variety of different conditions. (LI et al., 2018) observed a reduction of IGFBP-2 to correlate with a reduction in eNOS phosphorylation in an insulin-resistant state. However, with an overnight treatment of IGFBP-2, eNOS activation increased. IGFBP-2s protective properties were discussed in Chapter 4, which suggests that maybe cells need to be in a compromised state before we identify significant changes in angiogenic signalling stimulated by IGFBP-2. From these findings we can deduce, in regular homeostasis, IGFBP-2 does not influence eNOS phosphorylation. Therefore, we need to interrogate which other downstream targets of Akt may be activated via IGFBP-2 stimulation.

5.5.5 IGFBP-2 fails to enhance activation of other associated angiogenic signalling molecules in HUVECs

IGFBP-2 has been reported to modulate the effects of GSK3β and in turn β-catenin, via activation of FAK signalling in breast cancer and glioma cells (Patil et al., 2016; Sehgal et al., 2013). Both, dose- and time-dependent stimulation failed to upregulate

FAK or GSK3β phosphorylation to a significant level in HUVECs. As this mechanism has only been investigated in cancer cells, it may only be limited to highly invasive and proliferative cell lines.

IGFBP-2 has been reported to drive Akt phosphorylation via interactions between its HBD1 in the variable region and RPTPβ (Shen et al., 2012). Active and stable RPTPβ mediates the de-phosphorylation of PTEN. When in de-phosphorylated form, PTEN can undergo degradation, which in turn stimulates Akt stimulation. To determine if PTEN phosphorylation was reduced in response to stimulation with IGFBP-2, serum starved HUVECs were stimulated with different doses of IGFBP-2 (10-500ng/ml). However, as IGFBP-2 shown enhancement of Akt phosphorylation, PTEN phosphorylation levels failed to correlate. Thus suggesting IGFBP-2 stimulated Akt phosphorylation is induced by another interaction independent from RPTPβ and PTEN mediated activation.

5.5.6 Study limitations

As mentioned in the introduction, Chapter 5.1.2, components in the media such as serum and endothelial cell growth supplement contain many additional growth factors and molecules that can inhibit the effect of IGFBP-2. A distinct difference in endothelial cell phenotype was observed when cells were serum starved from 20% serum media (M199), resulting in irregular cell morphology. IGFBP-2 stimulated Akt and p44/42 MAPK phosphorylation was significantly more pronounced in the M199 media with the compromised cells than cells grown in low serum media (EGM2). This finding correlates with IGFBP-2s potential to rescue diseased states to a healthy/regular level, as seen in the case of insulin resistance and osteoblast differentiation (Hedbacker et al., 2010; Xi et al., 2014).

Another limitation which was highlighted due to the ability of IGFBPs to sequester IGF molecules, preventing IGF mediated mechanisms was that heparin in the media could present the same problem regarding blockage of the HBDs (Kiepe et al., 2002). In the presence of heparin, responses were evidently less pronounced in relation to IGFBP-2 stimulated Akt and p44/42 MAPK phosphorylation. This finding suggest heparin binding may play a role in causing the IGFBP-2 stimulated activation of Akt and MAPK. Heparin was removed from all further experiments to ensure it does not interfere with the function of IGFBP-2s HBD.

As mentioned previously in Chapter 5.1.2, growth factors could interfere with the activity of IGFBP-2. VEGF, FGF, PDGF and IGF are all present in the supplement and are extremely potent activators of angiogenesis, therefore any angiogenic-like

stimulation may be induced signalling exerted by these factors. Serum starved HUVECs were stimulated with increasing concentrations of IGF-I, in the presence and absence of ECGS. The supplement alone significantly elevated IGFBP-2 expression levels, however IGF-I at 10ng/ml also caused an increase in IGFBP-2 expression. Thus, increasing the overall bioavailability of IGFBP-2 in circulation. As we only wanted to see the effect of a known concentration of IGFBP-2 we added, all cells were serum-starved before experiments to ensure removal of the growth factors expressed by cells and in the media. The serum starving media contained no serum or added supplements which may adversely increase cellular IGFBP-2 expression.

During growth to confluence, cells activate different signalling pathways to induce proliferation and migration. Cells at different stages of confluency were stimulated with IGFBP-2 (500ng/ml). Surprisingly, at a 50% confluency state, when proliferation and migration signalling pathways would be activated to populate empty areas, stimulation with IGFBP-2 failed to enhance phosphorylation of Akt compared to its basal control. However, at a 100% confluency state or when cells were left 24 hours after 100% confluency (an over-confluent state), proliferation and migration signalling would be down-regulated and contact inhibition begins to take place, resulting in cell death. Contact inhibition results in some cells become senescent and floating to the surface (Sun, 2014). When IGFBP-2 was used as a stimulant in both of these states, an increase in Akt phosphorylation was observed. This supports the rescue theory of IGFBP-2 that when abnormal signals are released by compromised environments such as insulin resistance or reduced osteoblast differentiation, IGFBP-2 aims to restore regular levels (Hedbacker et al., 2010; Xi et al., 2014). In the case of cell confluency, IGFBP-2 may cause an enhancement in Akt phosphorylation to promote the survival of existing cells or growth of new cells to compensate for the cells that are dying (Chen et al., 2013). As cell confluency also influences the effect of IGFBP-2, it is essential cells are used at the same confluency state for each experiment in order to make a fair comparison of true IGFBP-2 stimulated effects.

5.6 Concluding remarks

We have identified IGFBP-2 stimulates Akt and p44/42 MAPK phosphorylation but fails to activate FAK signalling and in turn GSK3β phosphorylation in HUVECs. Activation of both the Akt and MAPK pathways via stimulation with different conditions, such as 200ng/ml IGFBP-2 significantly enhances Akt phosphorylation

but fails to activate p44/42 MAPK at this concentration and Akt phosphorylation takes place within 15 mins. However, IGFBP-2 stimulated phosphorylation of p44/42 MAPK takes a longer period of approximately 20 mins. These differences highlight two different mechanisms via IGFBP-2 may be responsible for activating the Akt and MAPK signalling cascades. The mechanisms responsible for the activation of these pathways will be further investigated using mutant variants of IGFBP-2 possessing non-functional domains. It is clear, MAPK relies on integrin interactions but Akt is possibly driven by IGF-I or HBD interactions. However, our investigation into recombinant IGFBP-2 from different sources and upstream targets suggest other interactions may be responsible for IGFBP-2 stimulated Akt phosphorylation in HUVECs.

A non-functional IGF binding domain did not affect IGFBP-2-stimulated Akt phosphorylation, suggesting IGFBP-2 relies on IGF-independent mechanisms to stimulate Akt. However, stimulation with IGFBP-2 failed to reduce PTEN phosphorylatyion levels, therefore the central HBD interactions do not promote IGFBP-2 stimulated Akt activation in HUVECs. IGFBP-2 failed to induce phosphorylation of a downstream target of Akt that plays a significant role in maintenance of the vascular network, eNOS. Other downstream targets activated by Akt and involved in angiogenesis should be interrogated to determine how the role of IGFBP-2 stimulated Akt activation can be exploited therapeutically.

Chapter 6 - Influence of IGFBP-2 on angiogenic properties of endothelial cells in vitro

6.1 Background

We have established IGFBP-2 is elevated in response to ischemia and enhances perfusion at early stages of recovery following hind limb ischemia in Chapter 4. This was supported by the upregulation of Akt and p44/42 MAPK phosphorylation in HUVECs, in Chapter 5. In published literature, IGFBP-2s angiogenic potential in functional studies using HUVECs remains fairly limited.

Angiogenesis is the formation of new blood vessels from pre-existing vessels. We have hypothesised from findings from Chapter 4, IGFBP-2 may stimulate more arteriogenic type responses rather than angiogenesis. Although both mechanisms are induced by different stimuli, they both involve endothelial adhesion, migration and proliferation. Arteriogenesis uses these mechanisms to induce endothelial remodelling of the pre-existing collaterals.

Once angiogenic signals, such as VEGF, are sensed the pericyte layer which encloses the endothelial monolayer detaches from the vessel wall due to degradation of junctional molecules such as VE-cadherin. This causes vascular hyperpermeability, enabling plasma membranes to install a temporary ECM consisting of plasma proteins such as fibrinogen, collagen, fibronectin and glycosaminoglycans (Rhodes & Simons, 2007). This provides the foundation scaffold which endothelial cells migrate onto to form the vessel endothelial monolayer, once an endothelial cell is transformed into a tip cell to promote sprouting. Although migration is a vital mechanism promoting the migration of the endothelial tip cell onto the temporary ECM during sprouting, the cells are still initially attached to the pre-existing vessel, offering stability to the tip cell via FAK and integrin signalling (Cavalcanti-Adam et al., 2007). IGFBP-2 stimulated angiogenesis has the potential to function through angiogenic signalling as well as interacting with the ECM surface via glycosaminoglycan interactions through its HBD. This summary highlights the roles of endothelial cell adhesion, migration and proliferation in angiogenesis.

6.1.1 Adhesion

In regards to angiogenesis, adhesion is usually presented as a negative effect. This is due to the anchoring mechanisms which down-regulate cell migration and proliferation. However, as described in the angiogenesis mechanism above, integrin signalling has to mediate cell adhesive properties to promote endothelial cell migration along the temporary ECM, driven by the endothelial tip cell and ensure their survival until maturation has been achieved (Figure 6.1). Cell adhesion is also critical for regulating cell morphology by regulating actin organisation and junction formation between adjacent cells (Folkman & Moscona, 1978).

FAK is a tyrosine kinase involved in adhesion signalling to promote cell-ECM adhesion and is regulated via integrin interactions, specifically with the subunit β1 (Schaller et al., 1995). It was confirmed IGFBP-2 cell surface binding to fibronectin was specifically mediated by α5β1, however this ECM binding led to the inactivation of FAK, as well as p44/42 MAPK (Schütt et al., 2004). Thus suggesting integrin signalling determines IGFBP-2s role in cell adhesion, as well as migration. This inactivation of FAK has to be critically regulated as endothelial-specific deletion of FAK disrupted blood vessel development, due to a lack of adhesion (Shen et al., 2005). The majority of research associating IGFBP-2s role within cell adhesion reports it promotes de-adhesion of cells. This has been observed in breast cancer and glioma cells (Beattie et al., 2015; Chua et al., 2016).

Activation of ERK/MAPK signalling is induced by the binding of endothelial cells via α5β1 integrin to a fibronectin coated surface (Sudhakar et al., 2003). This was also observed with IGFBP-2 possibly enhancing interactions between integrin α5, increasing glioma cell adhesion. Activation of this mechanism resulted in activation of the JNK/MAPK pathway (Mendes et al., 2010).

Cell adhesion molecules (CAMs) are glycoproteins on the cell surface which mediate cell-ECM and cell-cell interactions. An association between IGFBP-2 levels and the expression of CAMS such as ICAM-1, ITGAL and CDC42 has been discovered, which correlated with other published data confirming the upregulation of cell adhesion genes such as integrin α5 in response to over-expression of IGFBP-2 (Song et al., 2003; Wang et al., 2003)

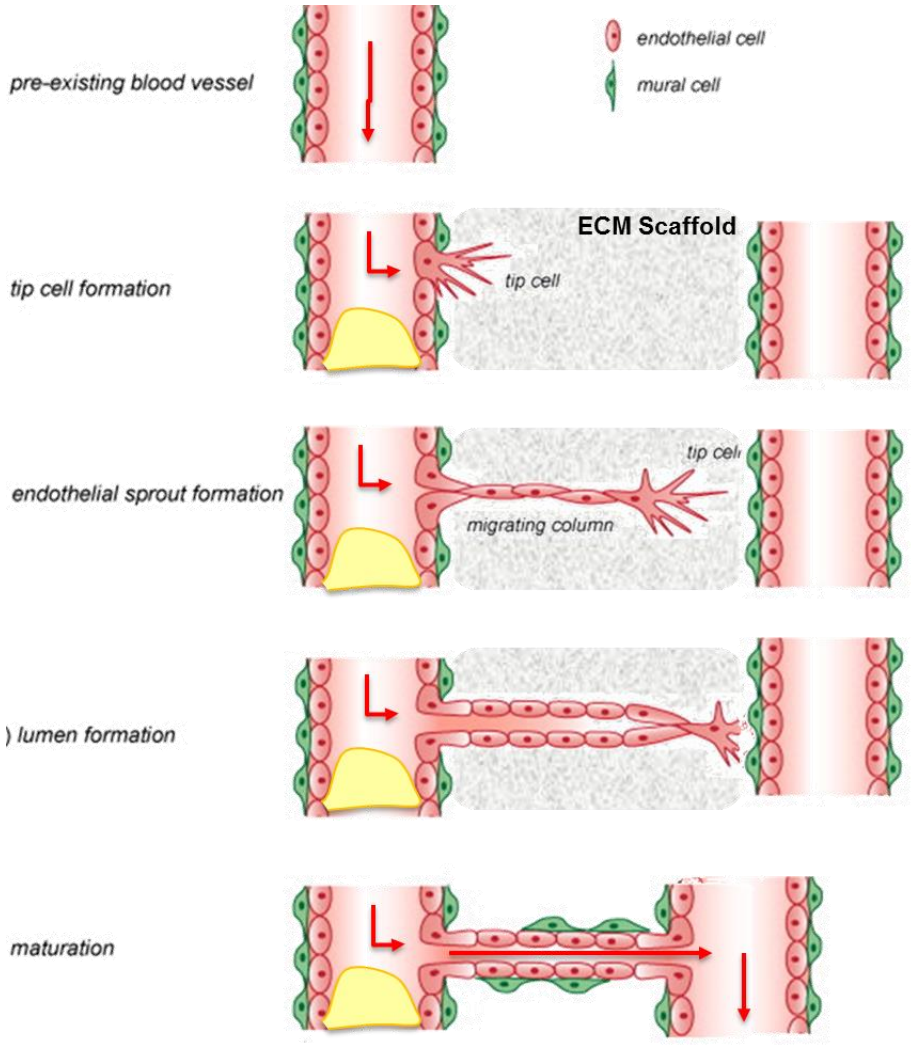

Figure 6.1 Critical cell adhesion stages in angiogenesis
This image represents different stages of angiogenesis from the tip cell formation to maturation of endothelial cells. Thus, highlighting the importance of adhesion to the pre-existing vessel to start the sprouting process and to stabilise the migrating column by adhering to surrounding ECM promoted by focal adhesions. Adapted from Francavilla et al., (2009).

These findings highlight IGFBP-2 does play a role in regulating cell adhesion via its integrin actions, specifically via α5. However, it is unknown what effect IGFBP-2 may have on cell adhesion in driving angiogenic responses to rescue an ischemic environment.

6.1.1.1 Integrins

Integrins are heterodimer transmembrane receptors that facilitate cell adhesion properties between cells and the ECM. They are composed of different combinations of non-covalently bonded α and β subunits.

Once integrins located on the cell surface bind to RGD sites on the ECM, a conformational change takes place resulting in separation of α and β subunits. The separation creates α and β integrin cytoplasmic tails. These tails are recognised by cytoplasmic proteins which once bound increase integrin affinity and also activate integrin-mediated intracellular signalling cascades. (Morse et al., 2014). As integrin affinity increases, more binding to the ECM causes integrins to form focal complexes and eventually focal adhesions, connecting the intracellular actin cytoskeleton to the ECM) (Legate & Fassler, 2009). The maturation of focal complexes into fibrillar adhesions is only apparent when binding of integrin α5β1 to fibronectin occurs (Geiger & Yamada, 2011). Once the actin has connected to the ECM, outside-in signalling activation occurs, leading to the recruitment of signalling components such as FAK, ILK and Src kinases. (Harburger & Calderwood, 2009)

The RGD site in IGFBP-2 has been reported to act via the integrins αVβ3, α1β1 and α5β1 (Hamidouche et al., 2010; Han et al., 2014; Kawai et al., 2011). However, IGFBP-2s interaction with each of these integrins activates different signalling cascades and functionality. Interestingly, interactions between IGFBP-2 and αVβ3 have been reported to negatively modulate IGF-I mediated effects (Miyako et al., 2009). It appears that interaction with this domain may be dependent on IGFBP-2s other domains, as in smooth muscle cells, activation of the HBD induced αVβ3 integrin mediated signalling (Kawai et al., 2011). IGFBP-2 and its interaction with α5 is critical to cell mobility, acting via activation of JNK mediated MAPK phosphorylation (Mendes et al., 2010; Wang et al., 2006). However, its interaction with the subunit β1 also promotes MAPK phosphorylation via activation of ERK (Han et al., 2014).

The integrin mediated role that IGFBP-2 may play in angiogenesis needs to be further interrogated as not only do the integrins modulate adhesion, but also cell migration. The association between IGFBP-2 and αVβ3 has been investigated to a limited extent; however αVβ3 has been identified as a mediator of angiogenesis due to its ability to find to a variety of ECMs and molecules, including fibrin, fibronectin and von Willebrand factor (Bischoff, 1997).

6.1.2 Proliferation and migration

Proliferation and migration of endothelial cells are mechanisms which are critical for angiogenesis, both co-ordinately working together. As stated previously, cell adhesion via integrin binding to the ECM is the initial phase of angiogenesis that causes the stimulation of growth and motility signalling cascades. A VEGF-activated endothelial cell adhered to the pre-existing vessel matures into a tip cell and begins migration mechanisms to drive the endothelial tip cell to the temporary ECM. Stalk cell proliferation then takes place providing stability to the migrating column (Norton & Popel, 2016).

IGFBP-2 upregulated levels were first identified in cancer and further research highlighted a correlation between elevated IGFBP-2 levels and tumour growth, suggesting IGFBP-2 has a role in cancer angiogenesis. Since this discovery, the effect of IGFBP-2 on proliferation and migration angiogenic mechanisms has been researched extensively in cancer and non-cancer cell lines.

In a majority of cancers, IGFBP-2 is highly expressed and correlates with cancer cell angiogenic mechanisms. To truly observe if IGFBP-2 is responsible for the mechanisms that promote the growth and development of tumours, IGFBP-2 is commonly silenced using siRNA. In pancreatic cancer and acute myeloid leukaemia cells, IGFBP-2 played a significant role in cell migration and survival. A knockdown of IGFBP-2 inhibited cell migration and promoted apoptosis, which corresponded with a decrease in Akt phosphorylation induced by increased PTEN levels (Chen et al., 2013; Liu et al., 2017). Cell proliferation and survival was also supressed in breast cancer epithelial cells following silencing of IGFBP-2. However, the suppression was rescued via treatment of an RGD-containing disintegrin, suggesting the RGD domain within IGFBP-2 is responsible for cell proliferation and survival. (Foulstone et al., 2013).

IGFBP-2 stimulated activation of these mechanisms was also observed in non-cancer cell types. In adjuvant arthritis synovial cells, IGFBP-2 enhanced cell proliferation and migration via wound closure, and enhancement of the ERK signalling cascade (Wang et al., 2017a). Human dermal fibroblasts over-expressing IGFBP-2 also displayed enhanced migration, specifically via the α5β1 (Brandt et al., 2015).

IGFBP-2 appears to use a combination of its domains to influence the integrin signalling, Akt, and ERK signalling pathways to drive proliferation and migration mechanisms. Therefore, IGFBP-2 may be using these mechanisms *in vivo* to contribute to the enhancement in perfusion we observed in HLI in Chapter 4.

6.1.3 Summary

It is clear IGFBP-2 plays a regulatory role in cell adhesion, migration and proliferation in many cells types, however IGFBP-2 stimulated activation of the mechanisms has only once been investigated in HUVECs which suggested VEGF was responsible for increases in *in vitro* endothelial cell tube formation (Das et al., 2013). The majority of the angiogenic mechanisms appear to be modulated by integrins, Akt or MAPK signalling pathways. In this chapter we interrogated the effect of IGFBP-2 on each mechanism independent of each other in order to determine how IGFBP-2 may be exploited to achieve growth of healthy vessels via therapeutic angiogenesis in a clinical setting.

6.2 Experimental objectives

In this chapter, we aim to investigate the effects of IGFBP-2 on pro-angiogenic properties in HUVECs *in vitro*. IGFBP-2 has exerted many angiogenic-like characteristics in a variety of cell types, however this has been rarely been examined in endothelial cells. Endothelial cells initiate and drive the angiogenic response via adhesion, migration and proliferation of cells in order to create the base scaffolding for the formation of the remaining vessel. Investigation of the angiogenic mechanisms promoted by IGFBP-2 was carried out using the objectives below:

- Determine what effect stimulation with IGFBP-2 may have on HUVEC adhesion to ECMs.
- Investigate the effect IGFBP-2 may exert on HUVEC motility via migration and proliferation, and migration alone.
- Investigate the effect IGFBP-2 may have on driving mechanisms to promote HUVEC tube formation.

6.3 Materials and Methods

In all assays, recombinant IGFBP-2 commercially bought from R&D Systems, sourced from murine cells and does possess IGF binding capability as confirmed by us was used.

6.3.1 Cell adhesion assay

A cell pellet consisting of HUVECs (after centrifugation at 300xg for 5 mins) was resuspended in either ECGM with 20% FBS (+ve control) or serum-free ECGM (treated and -ve control).

50,000 HUVECs were seeded into each well of a 24-well, 2% gelatin (Sigma, 69391), 100µg/ml Collagen IV (Merckmilipore, CC076) or fibronectin coated plate (Corning, 354411). Positive control wells contained ECGM + 20% FBS; negative control wells contained serum-free ECGM and treated cells contained 200ng/ml or 500ng/ml IGFBP-2 in serum-free ECGM. The plate was incubated for 30 mins in a humidified incubator at a temperature of 37ºC and 5% CO_2. The surface was washed three times with PBS, pH 7.4 to remove non-adherent cells. Images were taken at 5 different points within the well at a 40x magnification. Adhered cells were counted using the cell counter tool in ImageJ.

6.3.2 Scratch wound assay

Wells of a 96-well gridded plate (Essen, 4379) were coated with 0.1%, 1% or 2% gelatin. 40,000 HUVECs were seeded into each coated well with Promocell media (with growth supplement mix and 1% AAS). Cells were pre-treated with 200 or 500ng/ml IGFBP-2 for 20 hours. Cells were then starved with ECGM + 1% FBS (and endothelial cell growth supplement) for 4 hours. 200 or 500ng/ml IGFBP-2 was added to treated wells during the serum-starvation period.

Wound maker 96 (Essen Bioscience) created a uniform scratch across the surface. Wells were washed twice with PBS (containing Ca^{2+} and Mg^{2+}). Conditioned media was made with the basal media (ECGM (2% FBS and ECGS)) and 200 or 500ng/ml IGFBP-2. The positive control contained ECGM with 5% FBS and ECGS. Images were taken at 2 points of the scratch at a 40x magnification before the plate was incubated, and after the 13/16-hour incubation period on the optical zoom microscope. Incucyte images were taken at a 10x magnification. The closure area was measured using the polygon tool to draw around the edge of the empty area in Image J. Time course experiments were placed in the Incucyte imager, placed in an

incubator at optimum cell conditions. Images were retrieved and analysed for wound closure and cell density using IncucyteZoom software Wound Assay tools. The tool is able to locate the original wound gap and measure the closure in wound with over time (Figure 6.2).

Migration only scratch wound assay

Mitomycin C (Sigma, M4287) was prepared to 0.5mg/ml in filtered H_2O. 50,000 HUVECs were seeded in each well. 0.5µg/ml mitomycin C was added to each well, 20 hours prior to making the scratch and was also added to every media change.

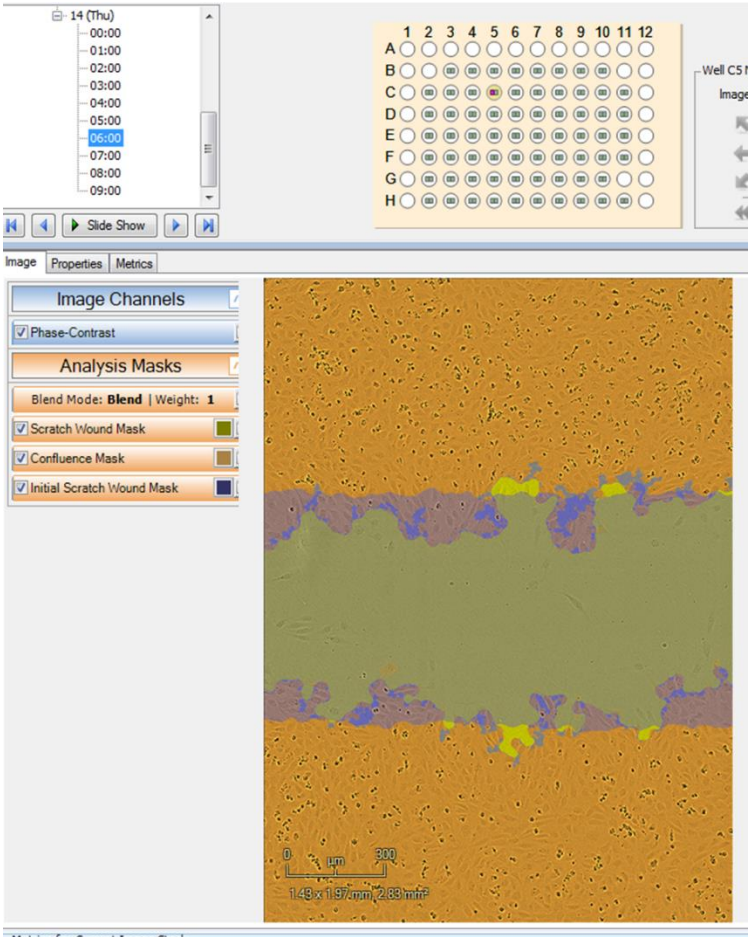

Figure 6.2 Incucyte wound closure review tool
Screenshot of scratch wound assay tool used to measure wound with changes using IncucyteZoom software. The software highlighted the confluent area of cells (orange), the initial scratch (blue) and the change in scratch area over time (yellow). The wound tool calculates the area of the initial scratch (blue region) and subtracts the area of the final scratch (yellow) to provide the change in wound closure value.

6.3.3 Tube formation assay

Thawed Matrigel (Corning, 354230) was set at 37ºC for 30 mins. For certain conditions, equal concentrations of IGFBP-2 to the amount of IGFBP-2 added into the media were also added into the Matrigel before it was set. Cells were trypsinised and washed with PBS, pH 7.4. After centrifuging the cells at 300xg for 5 mins, the pellets were resuspended in ECGM + 1% FBS.

100,000 HUVECs were seeded into each well with conditioned media. The positive control wells consisted of ECGM + 10% FBS, basal wells consisted of ECGM + 1% FBS and the treated well consisted of basal media + 200, 500 or 1000ng/ml IGFBP-2. The plate was incubated for 8 hours. The empty areas created when formed tubes meet at 'nodes' and sprout off again to create a network, are known as meshes (DeCicco-Skinner et al., 2014) (Figure 6.3). The optical microscope was used to capture images at a 40x magnification. The Incucyte was used to capture a time course of tube formation at a 10x magnification. Images were captured at 9 different points in the well.

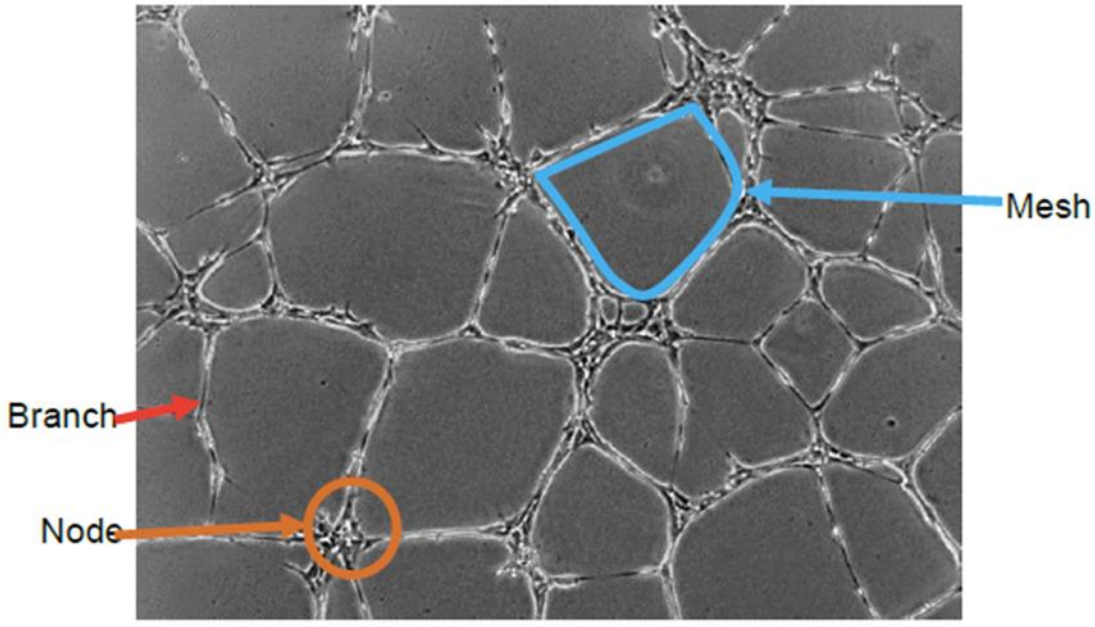

Figure 6.3 Tube formation network
In this image, the mesh that we measure for tube formation assays has been highlighted. Khoo et al., (2011) analysed different methods of quantifying Matrigel tube formation and highlighted the measurement of branches and nodes can also be used for quantification. Our group decided to measure mesh area as we would like to observe the network that if formed. Cells are able to form branches and nodes in the absence of growth factors, however stimulation from growth factors is needed to create a strong network, which is what we are trying to measure.

6.3.4 Data Analysis

ImageJ Cell Counter tool was used to count the number of cells in each image for the cell adhesion assay. ImageJ Area tool was used to measure the area between scratch wounds using the gridded plate. Incucyte Zoom Wound Closure Review Tool was used to measure images taken using the Incucyte for the scratch wound assay. Image J Cell Counter tool was used to count the number of meshes in a pre-determined area. Unpaired t-tests were used to test for significance. Error bars represent SEM.

6.4 Results

6.4.1 Effect of IGFBP-2 on HUVEC adhesion

IGFBP-2 is well known to promote de-adhesion activity in cancer cell lines (Alkharobi et al., 2016; Holmes et al., 2012). In contrast, vascular endothelial cells require strong interactions with the surrounding ECM as they lose stability provided by the pre-existing vessel as they begin to sprout away (Francavilla et al., 2009)

Firstly, incubation times to allow cell adhesion to occur need to be optimised. Integrins are widely known to be responsible for the initial attachment to ECM surfaces. However, once cells have started spreading, they are able to activate other growth and survival pathways which may also include expression of cell adhesion molecules. The optimum time to observe cell adhesion before cells have started spreading was 30 mins. (Figure 6.4).

Extracellular matrices composed of collagen, gelatin and fibronectin were used to interrogate the effect IGFBP-2 has on HUVEC adhesion. These are some of the most well established ECMs present in humans, with collagen being the most abundant in humans (Frantz et al., 2010). Gelatin and fibronectin, also major ECMs in the human body are commonly used as an agent to adhere cells to surfaces in *in vitro* culture. The presence of RGD sites in most ECMs makes it important to identify which one least interfered with IGFBP-2s effect on cell adhesion. All ECMs displayed the same abundance of HUVEC adherence, however the adhesion response in stimulation to IGFBP-2 was highest in fibronectin (Figure 6.5).

As we previously identified in Chapter 5, 200ng/ml IGFBP-2 can stimulate Akt signalling, however 500ng/ml is required to activate p44/42 MAPK. Therefore, we tested stimulation with both of these concentrations. 200ng/ml and 500ng/ml were efficient concentration of IGFBP-2 to enhance HUVEC adhesion to fibronectin (Figure 6.6).

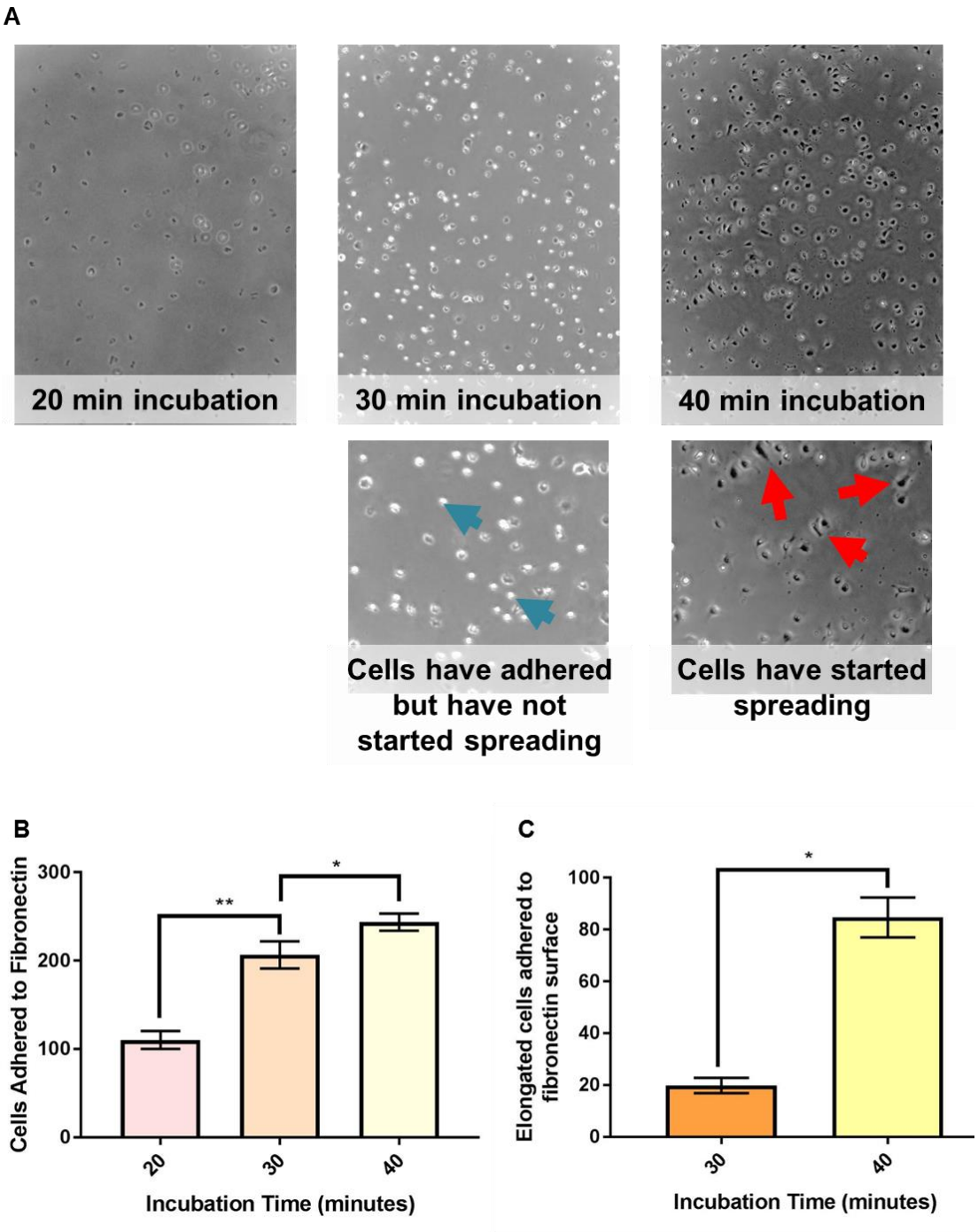

Figure 6.4 HUVEC adhesion incubation time
50,000 HUVECs were placed onto a 100µg/ml fibronectin coated surface, in duplicate, for different time periods, 20, 30 and 40 mins. Non-adhered cells were washed away with 3x washes of room-temperature PBS. **(A)** Representative images at a 40x magnification after non-adhered cells had been removed. Snapshots were magnified using ImageJ for ease of visualisation. Blue arrows highlight adhered cells which have not started spreading. Red arrows highlight adhered cells which have started spreading. **(B)** Number of cells adhered to the fibronectin surface were counted using ImageJ at 5 different points in a well at varying incubation times, 20, 30 and 40 min (*=p<0.01, **p<0.001; n=4). Error bars represent SEM. **(C)** The number of elongated cells, as highlighted by the red arrows in 6.4A, adhered to the fibronectin surface for an incubation time of 30 or 40 mins (*=p<0.01; n=4). Error bars show SEM.

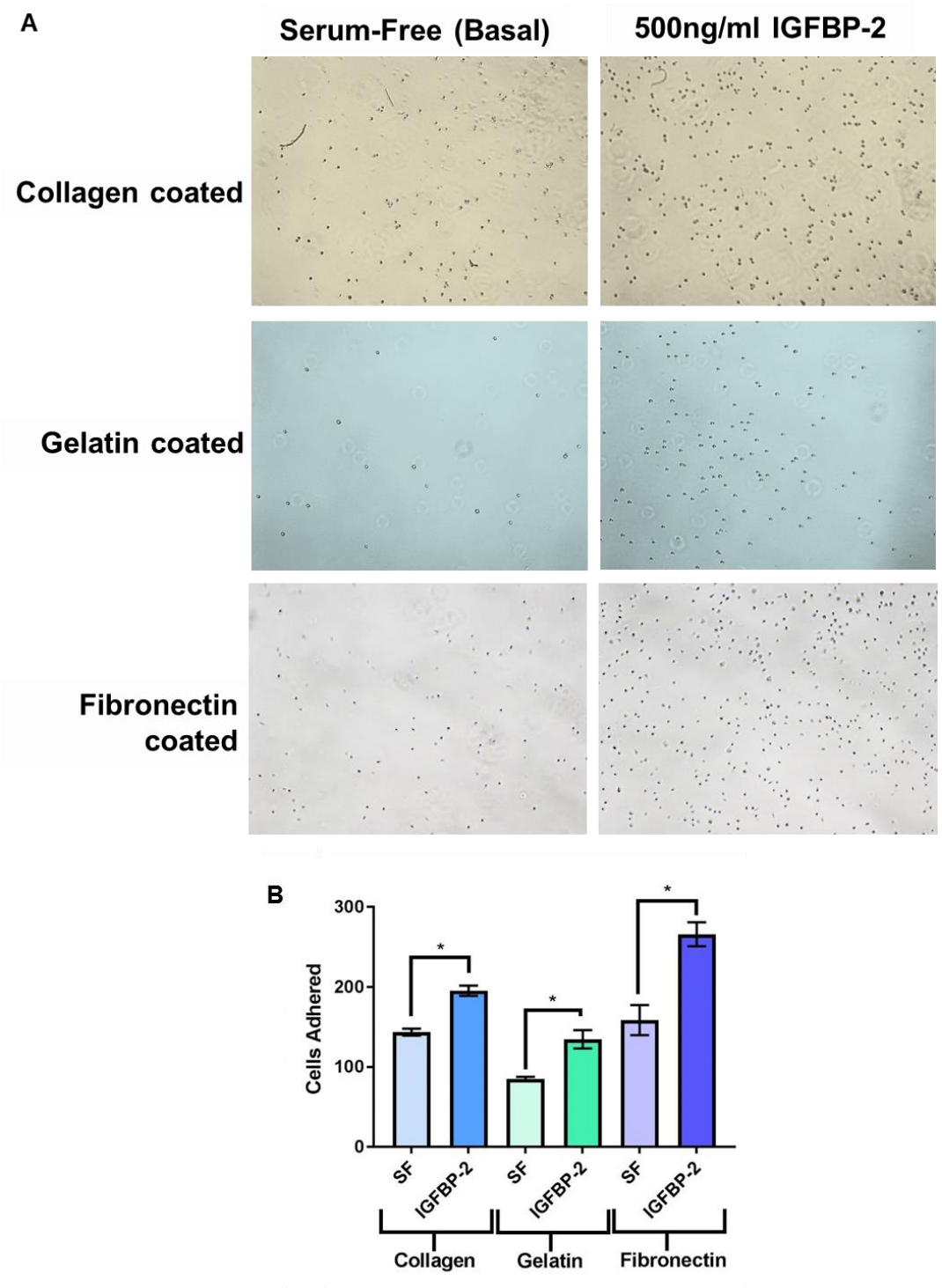

Figure 6.5 Increased number of IGFBP-2 stimulated cells adhere to Fibronectin 50,000 HUVECs were plated onto different ECMs, in duplicate, 100µg/ml collagen, 2% gelatin or 100µg/ml fibronectin for 30 min. Surfaces were washed 3 times to remove non-adhered cells. **(A)** Representative images at a 40x magnification using an optical microscope, of cells adhered in the absence (serum-free) and presence of IGFBP-2 (200ng/ml; 30min) across different ECMs. **(B)** Cells were counted using ImageJ at 5 random points in the well of the cells adhered to collage, gelatin or fibronectin, in stimulation to IGFBP-2, with their representative controls (SF, serum free) (*=$p<0.001$; n=4). Error bars represent SEM.

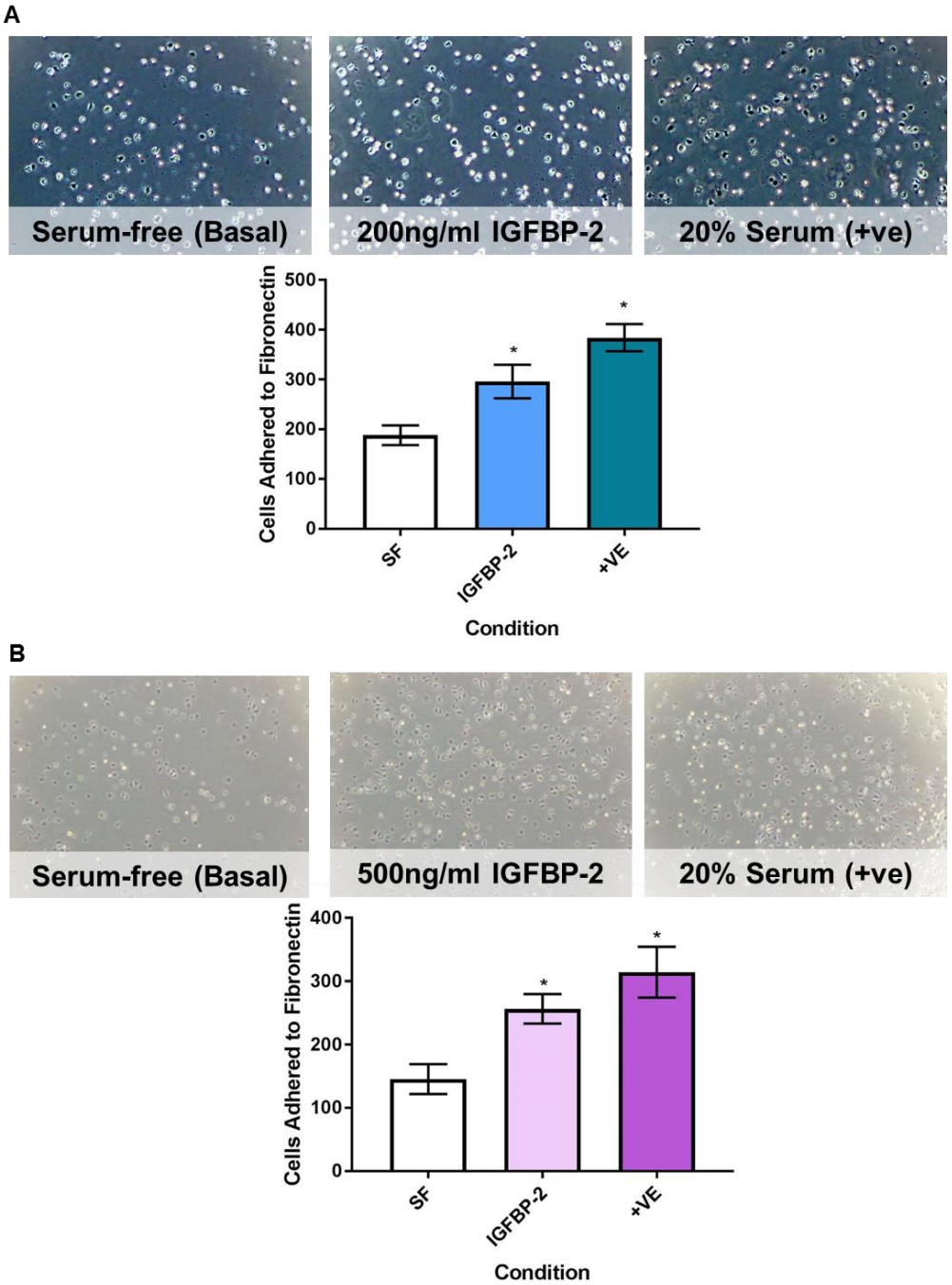

Figure 6.6 HUVEC adhesion is not enhanced following stimulation with increasing IGFBP-2 concentrations

50,000 HUVECs were incubated on a 100µg/ml fibronectin matrix, in duplicate for 30 minutes with varying media conditions, with IGFBP-2 (200/500ng/ml) or 20% serum (+ve). Non-adhered cells were washed off using PBS after the 30 min incubation period. Cells were counted using the cell counter tool on Image J at 5 random spots in the well. **(A)** Representative images, taken at a 40x magnification, using an optical microscope of HUVECs following stimulation with IGFBP-2 (200ng/ml; 30min) or the positive control (20% serum; 30min) on a fibronectin coated surface. Graph compares adhered HUVECs counted, following stimulation with IGFBP-2 and positive control (+ve) (*=$p<0.0001$, n=5). **(B)** Representative images of HUVECs following stimulation with IGFBP-2 (500ng/ml; 30min) or the positive control (20% serum; 30min). Cells were counted using ImageJ at 5 random spots. The graph compares HUVECs adhered, following IGFBP-2 (500ng/ml) stimulation and positive control (20% serum) stimulation to a fibronectin-coated surface (*=$p<0.0001$, n=3). Error bars represent SEM.

6.4.2 IGFBP-2-stimulated HUVEC wound closure

In vitro wound closure is a representation of cell migration and proliferation that can be altered depending on stimulants. Not only are migration and proliferation key mechanisms that promote angiogenesis, but also the majority of current research regarding IGFBP-2s angiogenic-like actions is their potential in enhancing these two mechanisms (Brandt et al., 2015; Liu et al., 2017)

Our laboratory had previously optimised a HUVEC scratch wound assay protocol, creating a uniform scratch across all wells using the wound maker. 2% gelatin was originally optimised to be used to coat the plastic surface to aid HUVEC adherence in the previous protocol. However, gelatin contains a high abundance of RGD sites which may compete with IGFBP-2s action (Xing et al., 2015). Therefore, lower concentrations of gelatin were tested to not affect cell wound closure. The use of 0.1% gelatin to coat the surface instead of 2% had no significant effect on the wound closure outcome (Figure 6.6 A). Using Incucyte Zoom, we recorded the change in wound width every 4 hours to determine the optimum end time to measure a significant difference in wound closure between the negative and positive controls. The earliest time to see a significant difference was 12 hours. (Figure 6.6 B).

The effect of stimulations with different concentrations of IGFBP-2 (optimised in Chapter 5 with Akt and MAPK signalling) was examined using the optical microscope to image gridded areas of the well. Wound closure was only observed in response to 500ng/ml IGFBP-2 and not 200ng/ml (Figure 6.7).

Mitomycin C, a well-known anti-proliferative agent was used to block all proliferation activity, resulting in scratch wound closure occurring due to migration only. A time course was carried out using the Incucyte Zoom to identify the optimum time to observe a significant change between negative and positive controls and the effect IGFBP-2 may have on this wound closure response. IGFBP-2 significantly enhanced migration only wound closure in HUVECs (Figure 6.8).

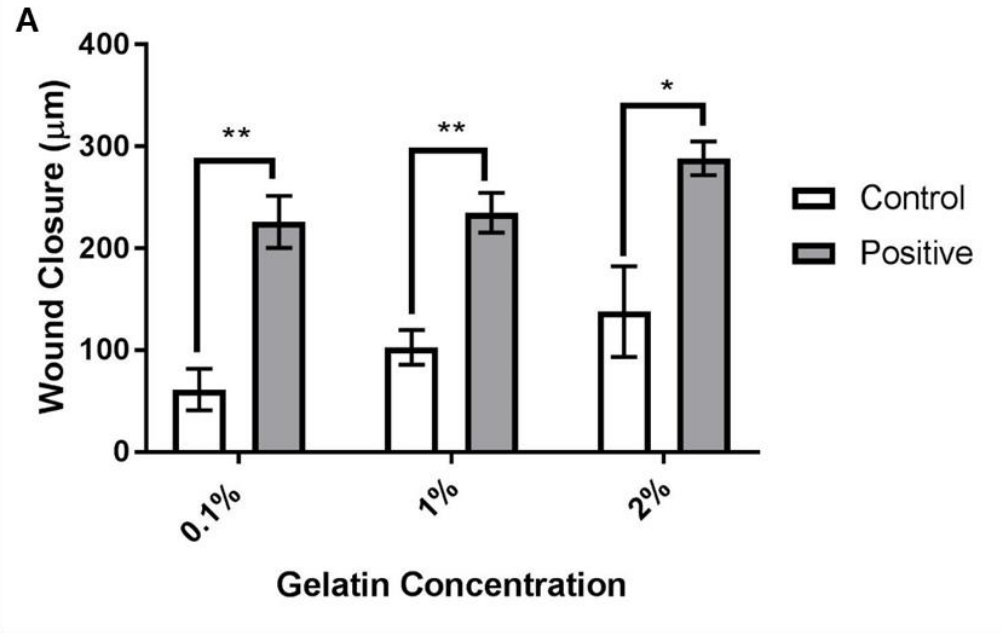

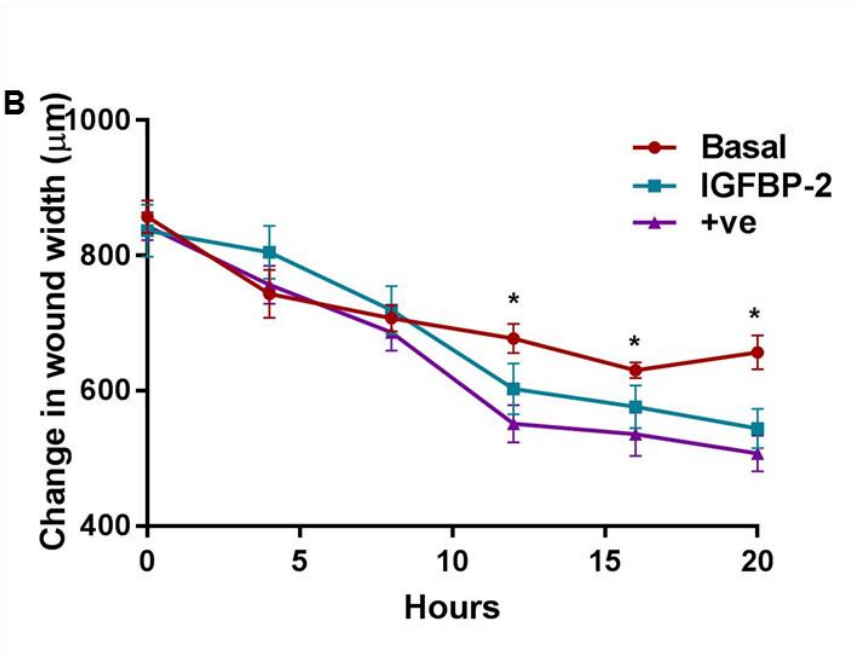

Figure 6.7 Gelatin concentration and incubation time affect wound closure readouts

40,000 HUVECs were plated into each well of a 96 plate in triplicate and the monolayer was scratched on different gelatin concentrations (0.1%, 1% or 2%) and stimulated with or without 5% serum (positive control), or with IGFBP-2 (500ng/ml). Wound closure was measured after 15 hours from before and after images, or at 5-hour intervals up to 20 hours using the IncucyteZoom. **(A)** This graph compares wound closure of the scratched monolayer of HUVECs stimulated with the positive control, compared to the non-stimulated vehicle on different gelatin concentrations (0.1, 1 or 2%) (**=p<0.0001, *=p<0.001; n=3). **(B)** Scratched monolayer of HUVECs was either non-stimulated or stimulated with IGFBP-2 (500ng/ml) or positive control (5% serum). Change in wound width was recorded over 20 hours using the IncucyteZoom (*=p<0.02; n=3). Error bars represent SEM.

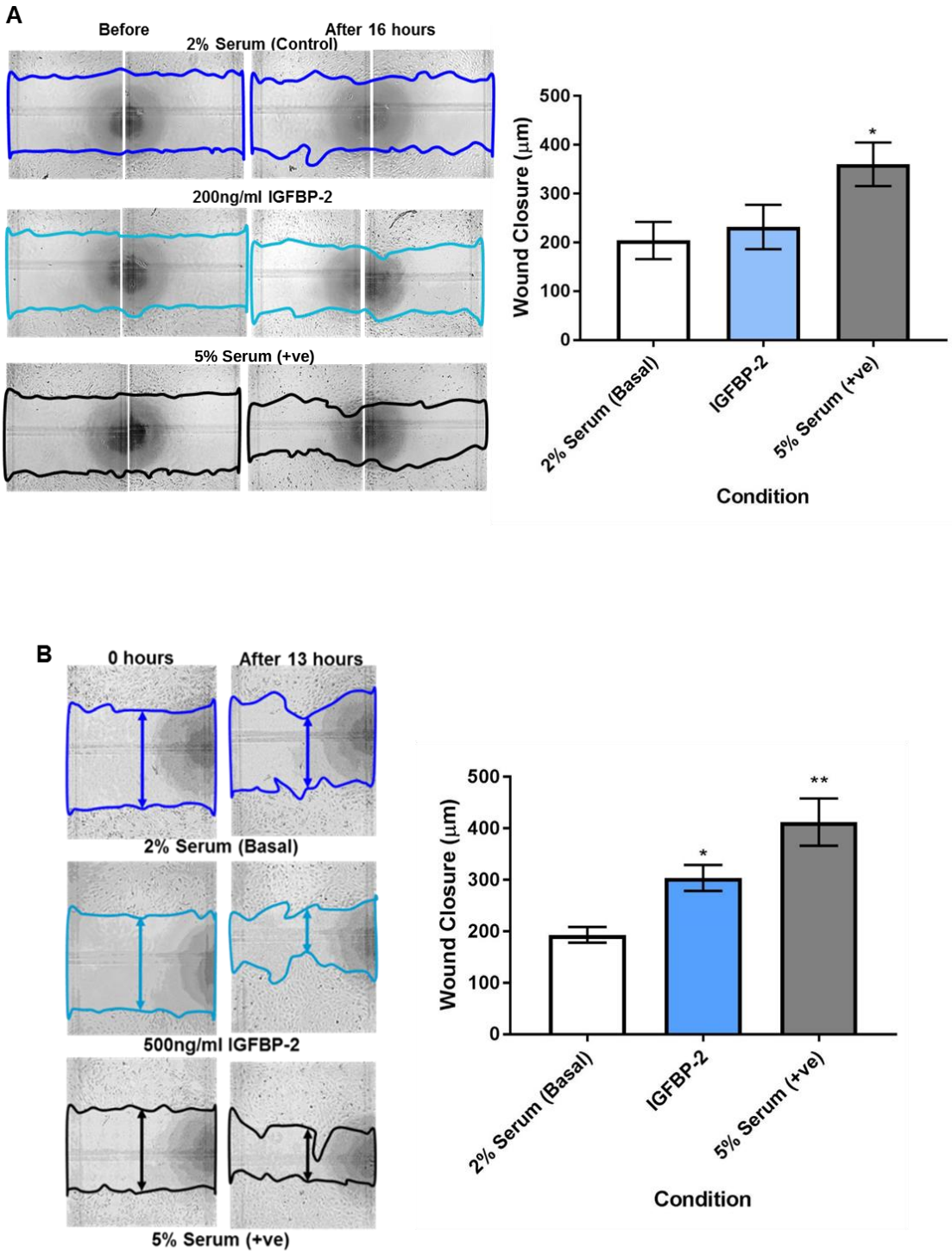

Figure 6.8 500ng/ml IGFBP-2 enhances HUVEC wound closure

40,000 HUVECs were plated into each well of a 96 plate in triplicate. Monolayer was scratched on 0.1% gelatin and stimulated with IGFBP-2 (200 or 500ng/ml) or positive control (5% serum) for 13 or 16 hours. Images were captured at a 40x magnification. Change in wound closure was measured using the polygon tool in Image J. **(A)** Representative images of the width of a well of HUVEC monolayer stimulated with 200ng/ml IGFBP-2 or positive control, following the scratch and after a 16-hour incubation period. Graph compares wound closure over 16 hours in response to stimulation with IGFBP-2 (200ng/ml) or positive control (5% serum) (*=$p<0.02$; n=2). **(B)** Representative images of initial and after (13-hour incubation) of scratched HUVEC monolayer, stimulated with IGFBP-2 (500ng/ml) or positive control (5% serum). Graph compares wound closure over 13 hours, in response to no stimulation and stimulation with IGFBP-2 (500ng/ml) and positive control (*=$p<0.01$, **=$p<0.001$; n=4). Error bars represent SEM.

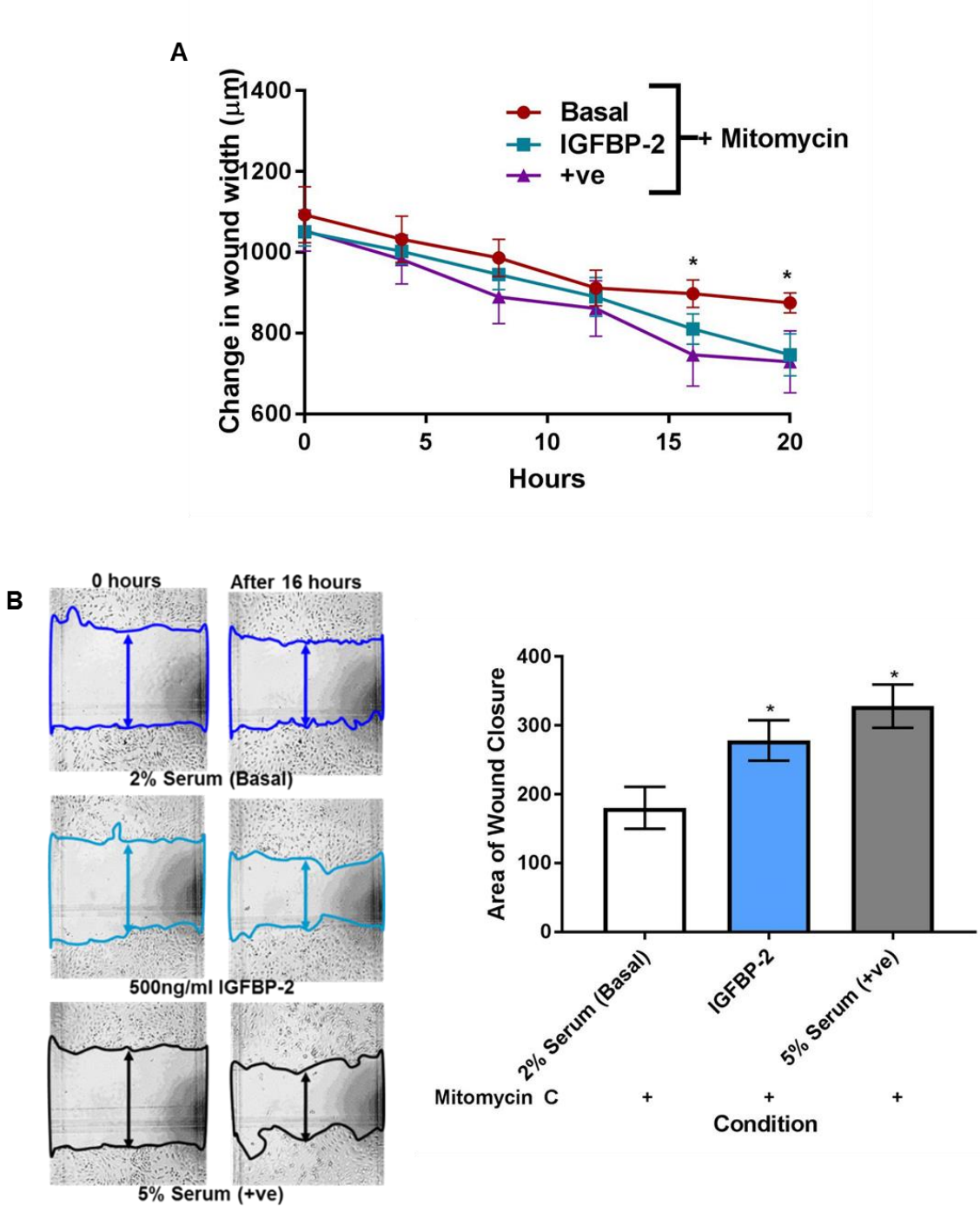

Figure 6.9 The presence of Mitomycin C does not affect IGFBP-2's ability to enhance wound closure

40,000 HUVECs were plated into each well of a 96 plate in triplicate and the monolayer was scratched on 0.1% gelatin and stimulated mitomycin C (0.5µg/ml) and with IGFBP-2 (500ng/ml) or positive control (5% serum) for up to 20 hours. **(A)** Using the IncucyteZoom, change in wound width was measured every 5 hours, up to 20 hours, of HUVECs scratched, in response to stimulation with mitomycin C and IGFBP-2 (500ng/ml) or positive control (*=$p<0.01$; n=5). **(B)** Representative images of initial and after (16-hour incubation) of scratched HUVEC monolayer, in the presence of mitomycin C, stimulated with IGFBP-2 or positive control at a 40x magnification, using an optical microscope. Graphical representation compares HUVEC wound closure area, measured using ImageJ polygon tool, following a scratch, in the presence of mitomycin C, non-stimulated (basal) and following stimulation with IGFBP-2 and the positive control (*=$p<0.001$; n=4). Error bars show SEM.

6.4.3 Effect of IGFBP-2 on HUVEC tube formation

Tube formation is an *in vitro* representation of the formation of an endothelial network that takes place to form the scaffolding during angiogenesis. A combination of adhesion, migration and proliferation is used for endothelial cells to create a mesh-type like structure in Matrigel matrix.

Using the optimised IGFBP-2 concentrations to induce a signalling response in Chapter 5, 200ng/ml IGFBP-2 failed to enhance HUVEC mesh tube formation, however tube formation was significantly enhanced following stimulation with 500ng/ml IGFBP-2 (Figure 6.10). Mesh formation was counted at end point of 8 hours as previous literature stated maximum tube formation occurred at approximately 8 hours (Roberts et al., 2015). Longer periods of time result in breakage of the network, displaying a lack of tube formation.

During the assay, the cells form tubes within the Matrigel in order to have access to the growth factors present in the matrix. Therefore, adding IGFBP-2 into the Matrigel may have an enhanced effect on tube formation, as the cells may not have complete access to IGFBP-2 added to the media alone, however this did not enhance tube formation further. Concentrations of IGFBP-2 outside the regular range did not stimulate tube formation further. (Figure 6.11).

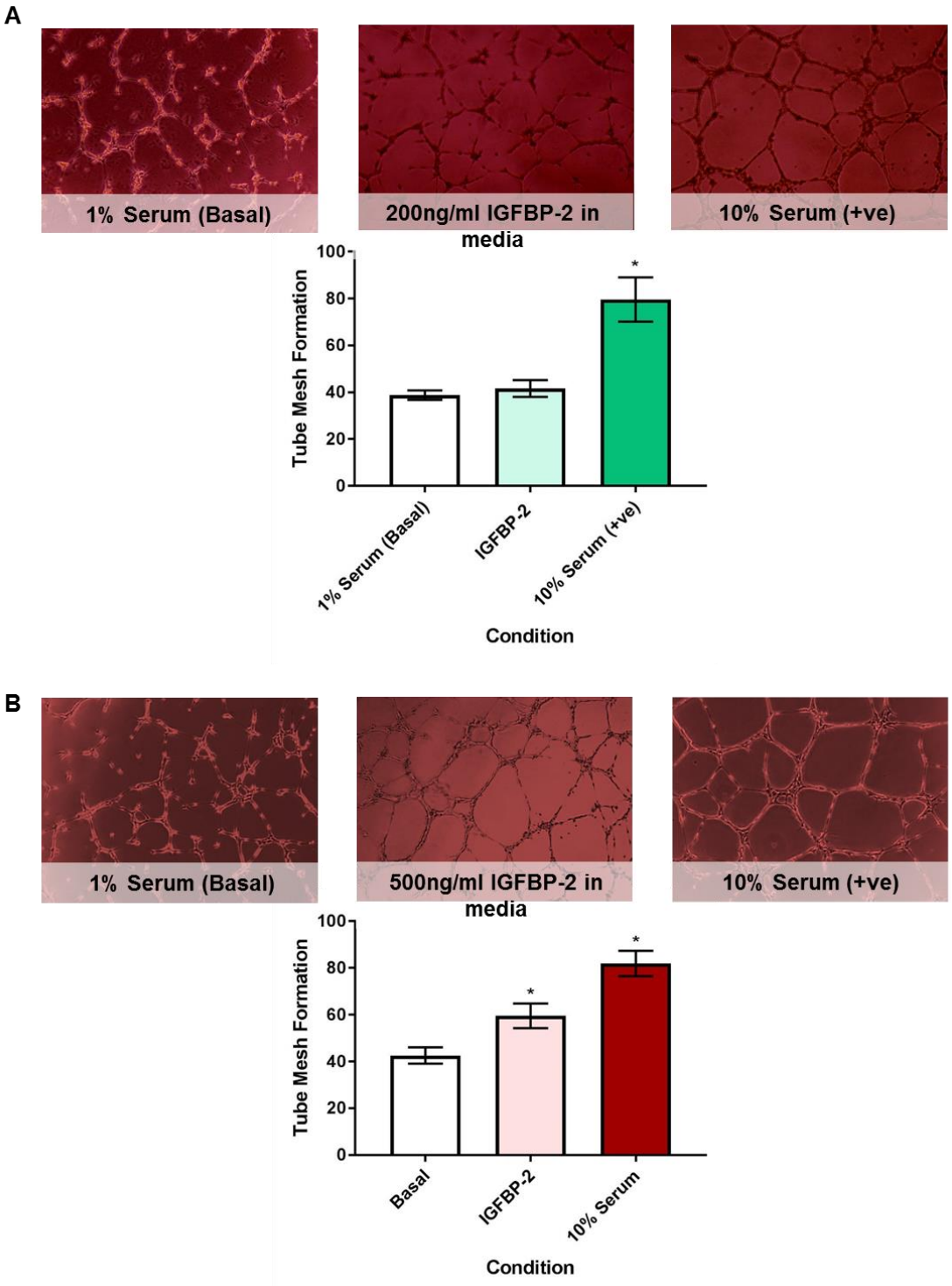

Figure 6.10 500ng/ml IGFBP-2 is required to enhance tube formation
100,000 HUVECs plated onto Matrigel in conditioned media, in duplicate and incubated for an 8-hour period. **(A)** Image (taken at a 40x magnification, using an optical microscope) and graphical representation compares IGFBP-2 (200ng/ml; 8h)-stimulated and positive control (10% serum)-stimulated tube mesh formation, counted using ImageJ tools (*=p<0.01; n=2). **(B)** Representative images captured after 8 hours, at a 40x magnification using an optical microscope. Graph shows HUVEC tube mesh formation non-stimulated and stimulated with IGFBP-2 (500ng/ml; 8h) and positive control (10% serum; 8h) (*=p<0.001; n=5). The number of tube meshes formed were counted using the Cell Counter tool on Image J. All meshes counted had a strong (not broken) tube outline. Error bars represent SEM.

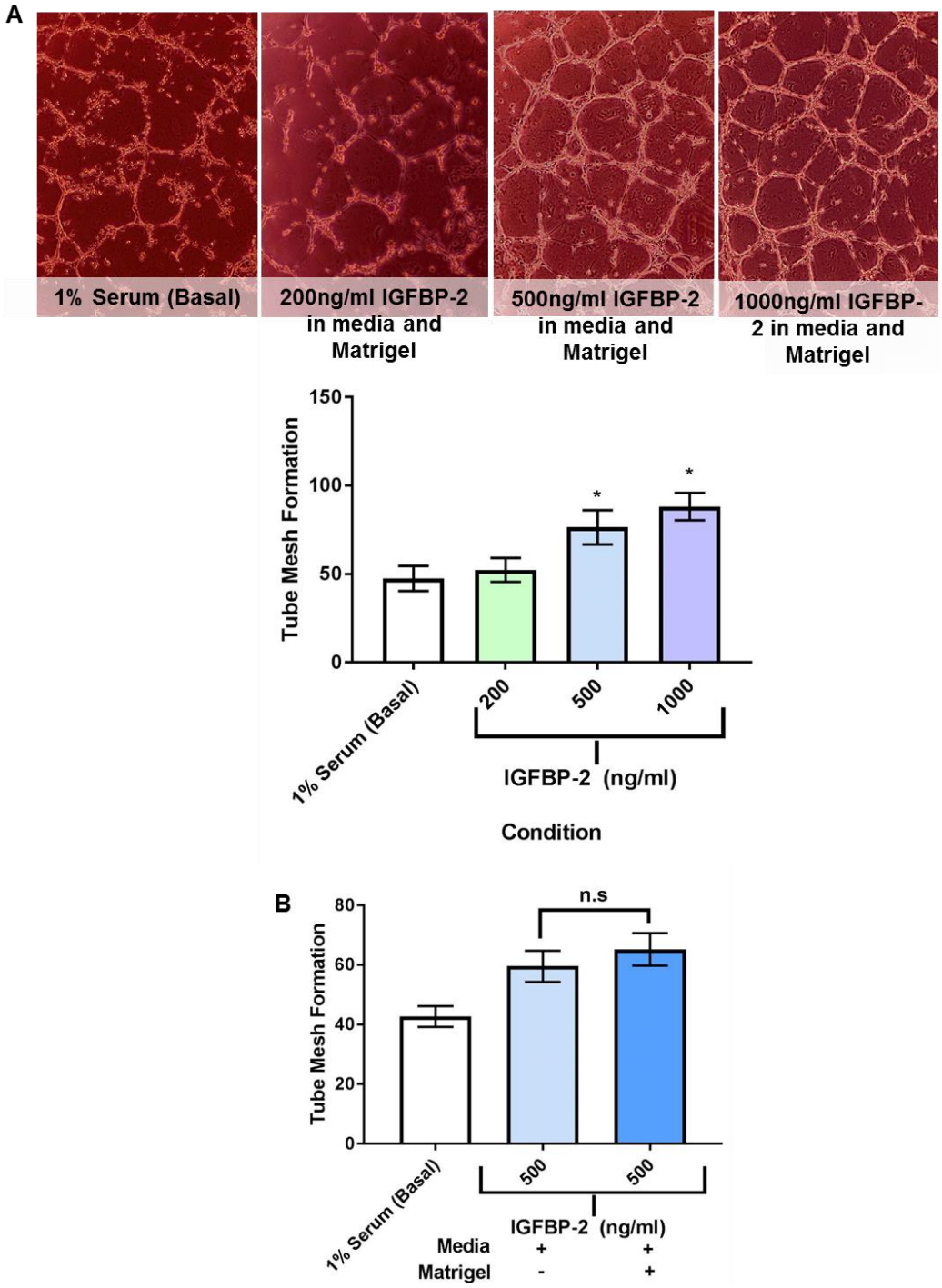

Figure 6.11 Adding IGFBP-2 into the Matrigel failed to enhance tube formation. Varying concentrations of IGFBP-2 (200, 500, 1000ng/ml) were added into the Matrigel before it was set at 37ºC and HUVECs were plated on. The same concenration of IGFBP-2 added to the matrigel was also added into the conditioned media. 100,000 HUVECs plated onto Matrigel in conditioned media and incubated for an 8-hour period. **(A)** Representative images (taken at a 40x magnification, using an optical microscope) of tube formation following no stimulation (basal) and stimulation with IGFBP-2 (200, 500 or 1000ng/ml) in the media and Matrigel. The graph compared the number of tube meshes formed (counted using ImageJ) for each of the conditions (*=p<0.02, n=3). **(B)** HUVEC tube mesh formation was in response to stimuation with IGFBP-2 (500ng/ml) in the media alone and in the Matrigel and media. The number of meshes formed were counted using ImageJ.The graph shows non-stimulated and IGFBP-2 tube mesh formation (n=3; p=not significant). Error bars show SEM.

6.5 Discussion

6.5.1 Stimulation with IGFBP-2 enhances HUVEC adhesion to fibronectin

As previously discussed in the background (Chapter 6.1), adhesion is required; however, adhesion should not inhibit migration or proliferation of cells in angiogenesis.

It was important to optimise the incubation time we were observing cell adhesion at. At 40 mins, some endothelial cells had become elongated due to changes in actin caused by the connection to the ECM. This suggests focal adhesions or fibrillar adhesions may have formed, resulting in possible recruitment of signalling components. It was important we attempted to catch cells at the same stage of adhesion to ensure activation of other signalling cascades did not affect IGFBP-2 activity. An optimum time of 30 mins was used as cells had adhered to the surface, possibly through integrin interactions, however no cells had begun showing a change in morphology.

Initially we hypothesised the RGD domains within the ECM would compete against the RGD domains in IGFBP-2. We cannot be certain the RGD domains in the ECM do not play a role in the adhesion of HUVECs to the surface, however, with the addition of IGFBP-2 for 30mins, the number of cells adhered to the surface significantly increased across collagen IV, gelatin and fibronectin coated surface, compared to their individual controls. Enhancement in HUVEC adhesion with 200ng/ml and 500ng/ml suggests IGFBP-2s integrin interactions will be causing the activation of Akt and MAPK signalling pathways, using the findings from Chapter 5.

This finding of IGFBP-2 enhancing HUVEC adhesion was surprising because IGFBP-2 is known to cause de-adhesion of most cells by preventing integrins on the cell surface binding to RGD sites in the ECM. An explanation for this maybe IGFBP-2 presents a positive feedback mechanism. It has been reported integrin binding to ECM increases the affinity for more integrin and ECM interactions (Morse et al., 2014). Once IGFBP-2 has bound to a cell via its RGD domain, it may cause an increase in affinity for more integrins to become exposed at the cell surface. In glioblastoma, IGFBP-2 has been highlighted to activate the expression of α5 integrins (Wang et al., 2003). Therefore, IGFBP-2 potentially could be increasing the number of integrin/ECM possible interactions, resulting in an enhancement in cell adhesion.

It would be interesting to use live cell imaging and labelling of the integrins to observe if this mechanism explains the IGFBP-2 stimulated enhancement in HUVEC adhesion to fibronectin.

6.5.2 Exogenous IGFBP-2 elevates HUVEC migration and proliferation rates

IGFBP-2 is well known to activate migration and proliferation mechanisms in a range of many cell types, including HUVECs (Png et al., 2012). Interestingly 200ng/ml IGFBP-2 failed to cause a difference in wound closure compared to the basal control, even though we demonstrated 200ng/ml IGFBP-2 was sufficient enough to phosphorylate Akt. IGFBP-2s established effect of enhancing cell migration and proliferation in an array of cell types with angiogenic potential was mimicked in HUVECs using 500ng/ml IGFBP-2 to stimulate mechanisms. However, to confirm this enhancement in HUVEC wound closure is due to IGFBP-2, a knockdown of IGFBP-2 specifically would eliminate the observation. Using the data obtained from Chapter 5 regarding signalling changes, we can hypothesis that IGFBP-2 stimulated migration and proliferation in this assay may be stimulated by MAPK activation, rather than activation of the Akt pathway.

Many publications have looked at the effect of IGFBP-2 on proliferation and migration separately as we cannot speculate how much of an effect IGFBP-2 has on proliferation compared to migration from the combined assay. Previous literature suggests IGFBP-2 stimulated proliferation and migration in some cells may function through activation of different signalling pathways (Chen et al., 2013; Foulstone et al., 2013).

Mitomycin C, a potent anti-proliferative agent slowed down the rates of HUVEC wound closure as a significant difference between the basal and positive control was observed at 16 hours rather than 12. This confirms this assay functions through migration and proliferation activity.

Stimulation with IGFBP-2 (500ng/ml) significantly enhanced HUVEC wound closure via migration alone to a similar extent as the combined proliferation and migration assay. Thus, suggesting IGFBP-2 may predominantly enhance migration of cells, rather than proliferation. This supports the speculation that the observed effect is functioning through MAPK activation. Most current studies regarding IGFBP-2s activation of cell migration has been shown to function via activation of JNK and ERK mediated MAPK signalling (Han et al., 2014; Mendes et al., 2010). However, this theory could be only confirmed by exploring the effect of IGFBP-2 in a HUVEC proliferation assay independent of migration.

6.5.3 Exogenous addition of IGFBP-2 enhances HUVEC tube formation

Mesh formation signifies network formation, whereas if no mesh formation is present, and tubes are present, the endothelial cells have been unable stimulate angiogenic signalling to establish or maintain a strong network-like structure (DeCicco-Skinner et al., 2014).

Similarly, to IGFBP-2-stimulated HUVEC wound closure, there was no change in mesh formation following stimulation with 200ng/ml IGFBP-2 compared to the basal control. However, a significant change in HUVEC mesh formation was observed following stimulation with 500ng/ml IGFBP-2. Again, paired with the results from the signalling data, this suggests HUVEC tube and mesh formation is not initially driven by activation of the Akt pathway.

The tubes formed by endothelial cells are formed within the Matrigel complex. Therefore, we assumed the cells would have easier access to IGFBP-2 that is within the Matrigel and as a result enhance the effect of IGFBP-2 stimulated network formation even further. Unfortunately, adding IGFBP-2 in the Matrigel displayed no additional enhancement in mesh formation compared to the condition without any IGFBP-2 in the media. A possible explanation to the lack of enhancement may be as the matrix solidifies and becomes fibrous, IGFBP-2 may not be able to circulate and therefore is not available to the cells (Frantz et al., 2010).

Over-expression of IGFBP-2 is a common model used to *in vitro* and *in vivo* to investigate the effects of IGFBP-2 on angiogenic-like mechanisms. We added an extra condition using 1000ng/ml IGFBP-2 alongside the optimised 500ng/ml. However, the increase availability of IGFBP-2 did cause further enhancement in mesh formation. A possible explanation to this may be that IGFBP-2 has a regulatory feedback system, as shown with other IGFBPs. IGFBPs have the ability to promote and inhibit activity, however very little has been published regarding IGFBP-2s role of inhibiting IGF stimulated activity. If IGFBP-2 is able to control its activity regardless of how high IGFBP-2 concentrations may be, this mechanism could be a breakthrough for therapeutic angiogenesis to control rate and phenotype of vessels.

This matches the plateau effect we observed with IGFBP-2 stimulated Akt phosphorylation in Chapter 5, as increasing concentrations above the optimum concentration (200ng/ml) maintained Akt at the same level and did not enhance it further. This finding could suggest IGFBP-2 relies on the bioavailability of other molecules such as IGF-I, integrins and RPTPβ to determine its function (Zhou et al., 2013).

6.5.4 Study limitations

It is difficult to replicate cell adhesion that may occur in *in vivo* angiogenesis, as *in vivo* one endothelial cell senses a VEGF signal to initiate the process. The cells used in the assay were not stimulated by angiogenic responses before and therefore this assay is not a true representation of angiogenesis. The scratch wound assay has been widely used to test *in vitro* cell migration and proliferation. Although we used mitomycin C to separate both mechanisms, it is difficult to establish if IGFBP-2 is a more potent regulator of either proliferation or migration. With both the cell adhesion and scratch wound assay we cannot be sure the RGD domains within fibronectin and gelatin are not affecting IGFBP-2-stimulated cell adhesion, proliferation and migration. Even though we used growth factor reduced Matrigel, there are still growth factors present. Therefore, we can't confirm IGFBP-2 is solely responsible for the enhancement in tube formation we observe.

6.6 Concluding remarks

Findings from this chapter demonstrate for the first time IGFBP-2 enhances HUVEC adhesion to fibronectin, HUVEC wound closure via migration and proliferation and migration alone and HUVEC mesh formation. However, the minimum conditions of 200ng/ml IGFBP-2 which stimulated HUVEC adhesion failed to activate HUVEC wound closure or tube formation. This finding suggests that the initial process that drives HUVEC migration and proliferation is not activated by the Akt signalling pathway but instead relies on MAPK signalling. However, these assays take place over hours and therefore we cannot assume the Akt signalling pathway does not play a part in regulating these mechanisms at a later stage.

To identify which signalling pathways do drive this IGFBP-2 stimulated effect in the cell adhesion, scratch wound assay and tube formation assay, we would need to use signalling inhibitors. In further exploration of which IGFBP-2 domain is responsible for this activity, mutant variants of IGFBP-2 with non-functional domains have been described in later Chapters. These *in vitro* angiogenic assays will be repeated in Chapter 8, in order to identify which IGFBP-2 domain is critical for adhesion, migration and proliferation properties. This will help us identify the mechanism we need to exploit to drive healthy vessel growth to rescue ischemic limbs following PAD.

Chapter 7 - Expression and purification of recombinant IGFBP-2

7.1 Background

Previous chapters have all confirmed IGFBP-2 plays a role in activating angiogenic signalling pathways and pro-angiogenic functions in HUVECs *in vitro*, as well as displaying angiogenic potential *in vivo.* The next following chapters describe the generation of an in-house recombinant IGFBP-2 and mutations of this generated protein in order to determine which IGFBP-2 domain is critical for the enhancement in angiogenic mechanisms we see *in vitro.*

In Chapter 5, we struggled to validate IGF binding potential of a commercially available recombinant hIGFBP-2, which claimed to be validated via an IGF functional assay. This led to questioning the functionality of other domains in recombinant IGFBP-2. Using an expression system to generate IGFBP-2, we can validate the functionality and sequence of the protein through every step of the process, confirming it retains its complete activity.

Expressions systems are commonly used in research to generate large volumes of recombinant protein in a short period of time. There are a number of advantages that support its use over commercially sourced proteins which will be discussed in the following subchapters.

This is a technical chapter which covers the optimisation and validation steps which have led to the generation of the wild-type recombinant IGFBP-2 and its mutant variants.

7.1.1 Expression system

Expression systems essentially involve an expression vector in which the DNA coding sequence of a target protein has been inserted into, a multiple cloning site (MCS) and a promoter to drive expression of the target gene. The target gene is introduced to the host cell via the expression vector. The hosts have protein synthesis mechanisms in place to rapidly generate large volumes of the protein. The

recombinant protein is then isolated from the host cell and purified, ready for research use (Figure 7.1) (Rosano & Ceccarelli, 2014).

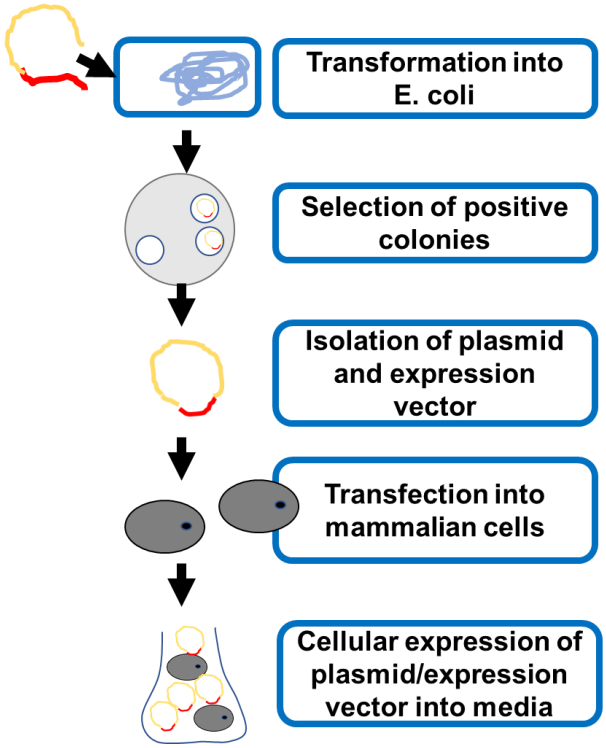

Figure 7.1 Mammalian expression system
A flow diagram showing the process of transformation of the ligated plasmid and expression vector being transformed into E. coli. This results in colonies positive for plasmid/expression vector. Plasmid/expression vector is then isolated and transfected into mammalian cells in DNA form. The cells then express this plasmid/expression vector as a protein into the media which is collected and purified. Adapted from Sigma-Aldrich (2018).

There are several advantages to using an expression system to generate an in-house recombinant protein. The main advantage is producing a large volume of protein in a short amount of time. Expression systems are also more cost efficient compared to commercially sourcing the same volume of recombinant protein. (Terpe, 2006). You can select a specific expression system depending on the protein you want to generate; for example, a mammalian protein may be difficult to synthesise using a eukaryotic expression system, as it is inefficient for retaining the regular protein folding, which in turn can cause overall protein dysfunction (Khow & Suntrarachun, 2012). Commercial recombinant proteins are often produced using the most low-cost method and are only validated using one specific assay, however irregular folding could cause other problems that are not tested for. This is providing an explanation for the non-IGF binding properties of IGFBP-2 sourced from Abcam in Chapter 4, as it was produced using Insect cells.

There are 4 commonly used expression systems; bacterial, yeast, insect and mammalian, however each expression system has its own advantages and disadvantages depending on the type of protein to be generated and therefore should be carefully selected. In regards to the generation of human IGFBP-2, we used a mammalian expression system. This expression system is well-known for retaining normal protein folding and its biological activity, as well as no non-specific post-translation modifications being carried out by the host cell (Khan, 2013). Although the disadvantage with the mammalian expression system is that it is the most expensive expression system to run as the cells require a lot of maintenance and it can take up to a few weeks to obtain protein (Yin et al., 2007). Each expression system has its specialised vector that can ensure generation of the desired protein.

7.1.2 pM-secSUMOstar vector

It is important to use an expression vector that corresponds with your chosen expression system to yield the best yield of protein, hence our choosing of a mammalian expression vector that functions in human Expi293 cells, pM-secretory small ubiquitin-like modifier (SUMO)star vector, generated by Lifesensors. This pM-SUMOstar expression plasmid was chosen over other mammalian vectors, purely because many publications have highlighted its enhanced protein production in comparison to traditional vectors (Panavas et al., 2009; Peroutka III et al., 2011).

SUMO technology enhances protein production via regulating post-translational modifications of proteins and cell processes, such as protein stabilisation and nuclear transport (Malakhov et al., 2004). The SUMOprotease as part of the SUMOstar kit has never shown cleavage activity within the sequence of the target protein, highlighting the specificity of the protease. SUMOprotease recognises the cleavage site produced by the restriction enzyme BsmBI overhang. This overhand is initially used to ligate the amplified protein with the vector. As a result, the sequence of the target protein is not affected and retains its full N terminus. (Lau et al., 2018).

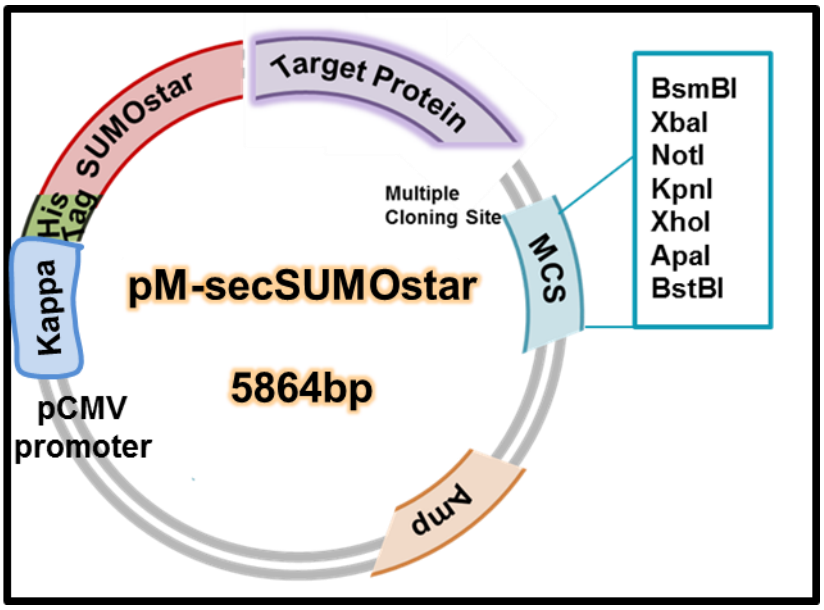

Figure 7.2 Representative image of the pM-secSUMOstar vector
This visualisation highlights the location of the protein and all the other site in the circular pM-secSUMOstar plasmid, such as the multiple cloning site, which consists of sites which are recognised by many restriction enzymes, making it easy to use this vector with a variety of proteins. The histidine tag is also located on the side of the SUMOstar furthest from the protein, so when SUMOprotease cuts between SUMOstar and the target protein, the his-tag will not intervene with following purification steps. Adapted from Lifesensors (2013).

The pM-SUMOstar plasmid drives protein expression via cytomegalovirus (CMV) promoter. Bovine growth hormone (BGH) mediates the inhibition of the promoter activity. All expression vectors possess signal peptides at the end of their N terminus. Signal peptides sometimes affect levels of secretion depending on the protein as they are responsible for signalling proteins for translocation. The SUMOstar plasmid secretes protein via the mouse IgG kappa secretory signal which has been reported to modulate stabilisation of the mammalian protein by ensuring phosphorylation sites and protein folding are not affected through translation (Haryadi et al., 2015; Ho et al., 2013)

After the signalling peptide, a his6 tag is present which is used to enhance purification of the target recombinant protein. Hispur columns have a great affinity for these tags which consist of 6 histidine amino acids and therefore can be used to remove contaminants from the protein before and after cleavage with SUMOprotease (Spriestersbach et al., 2015). Additionally, ampicillin is the bacterial resistance marker used by pM-SUMOstar, ensuring the formation of colonies that only possess

the vector. The presence of all these tags on the pM-SUMOstar vector will aid the successful cloning and expression of IGFBP-2 with its protein folding and phosphorylation sites intact. IGFBP-2 has been reported to have a phosphorylation site present at Ser^{106}, however no further publications have confirmed this (Graham et al., 2007).

7.1.3 IGFBP-2 mutants

In chapter 5 and 6, we discovered IGFBP-2 functions differently to activate Akt and ERK/MAPK signalling pathways and between cell adhesion and migration and proliferation. We hypothesis this difference may be a result of different IGFBP-2 domains affecting the induction of different mechanisms. Most published literature has exposed IGFBP-2 to function through integrin interactions to induce migration of cells via the MAPK signalling pathway (Mendes et al., 2010). The Akt pathway has been referenced to activate critical angiogenic mechanisms including survival (Chen et al., 2013). Therefore, by creating IGFBP-2 mutant variants with a non-functional RGD domain, IGF, heparin binding or NLS sites, we can identify which IGFBP-2 domain is critical to induce the *in vitro* responses we see.

All of the domains in IGFBP-2 have been mutated in previous literature (Demambro et al., 2012; Jones et al., 1993; Xi et al., 2013). We will be using the published mutation sequences to optimise our mutations of IGFBP-2. The published mutation for the HBD1 crosses over the HBD site and NLS signal and therefore presents itself as a combined mutation (Figure 7.3) (Azar et al., 2014). All of these mutations will be inserted in the generated ^{WT}IGFBP-2/pM-SUMOstar plasmid via site-directed mutagenesis to achieve mammalian expression of the mutant proteins.

```
HBD1    QHRQMGKGGKHHLGLEEPKKLRPPPARTPCQQELDQVLERISTMRLP
        ||||||||||||||||||||||||||||||||||||||||||||||||
NLS     QHRQMGKGGKHHLGLEEPKKLRPPPARTPCQQELDQVLERISTMRLP
```

Figure 7.3 Overlap of HBD1 and NLS in IGFBP-2
Sequence highlighting at which section of the sequence the HBD1 and NLS overlap. Adapted from Azar *et* al., (2014) and Demambro *et* al., (2012).

The RGD mutant has been used to confirm the importance of IGFBP-2s interaction with integrin subunit α5 to promote cell migration and motility responses (Brandt et al., 2015). This mutation has been specifically shown to affect migration responses in cancer lines via suppression of JNK phosphorylation, possibly due to a reduction in lamellipodia at the cell surface resulting in a lack of integrin induced signalling via the actin cytoskeleton and ECM (Mendes et al., 2010; Wang et al., 2006). Interestingly, the IGF and HBD1 mutations highlighted a possible crosstalk mechanism occurring between both domains. Both domains had to retain functional activity in order to promote osteoclast differentiation (Demambro et al., 2012). Mutation of the HBD1/NLS site prevented nuclear translocation and suppression to VEGF signalling (Azar et al., 2014). Non-functional HBD2 significantly enhanced differentiation of pre-adipocytes, suggesting it may have importance in regulating IGFBP-2s protective role against obesity (Wheatcroft et al., 2007; Xi et al., 2013). Published literature regarding IGFBP-2 mutants with non-functional domains will be discussed in more detail in the next chapter, Chapter 8.

7.1.4 Summary

Using a mammalian expression system, the pM-SUMOstar expression vector and SUMO technology, we should obtain a high yield of recombinant ^{WT}IGFBP-2 protein with intact protein folding, glycosylation sites and no post-translational modifications carried out by the host cell. Published mutation sequences will be inserted into the ^{WT}IGFBP-2/pM-SUMOstar plasmid via site directed mutagenesis. This chapter includes the optimisation and validation steps to confirm the sequence and functionality of IGFBP-2 and its mutants following the expression, secretion and purification steps.

The generated IGFBP-2 variants will be used to interrogate the key domains which promote angiogenic potential in *in vitro* experiments, which are discussed in Chapter 8.

7.2 Experimental Objectives

This technical chapter outlines each stage of the generation of recombinant ^{WT}IGFBP-2 and its mutants. There are many variables that need to be optimised to ensure the host cell's machinery does not cause any post-translational modification and maintains regular protein folding and function. Purification steps also need to be optimised for each IGFBP-2 variant to maximise the final yield and purification.

The main objectives of this chapter are:

- Generate ^{WT}IGFBP-2 and validate its sequence and functionality
- Generate individual mutations of the RGD, IGF, HBD1/NLS and HBD2 sites
- Validate insertion of the mutation using sequencing and their functionality

7.3 Method

7.3.1 Generation of pM-SUMOstar Wild-Type IGFBP-2

IGFBP-2 cDNA was commercially sourced (BioScience) using the full published IGFBP-2 sequence from NCBI: Homo sapiens insulin-like growth factor binding protein 2, 36kDa, mRNA (cDNA clone MGC: 88661 IMAGE: 6650239), complete cds (GenBank: AAH71967.1). This cDNA provided the foundation plasmid for the production of a ^{WT}IGFBP-2 which could be used in *in vitro* assays.

7.3.1.1 Phusion PCR

PCR was used to exponentially amplify the IGFBP-2 plasmid using primers containing restriction enzyme sites, recognised by the pM-SUMOstar vector (LifeSensors, 7121). Phusion High Fidelity DNA Polymerase PCR protocol provided by New England Biolabs was used, with the addition of Dimethyl sulfoxide (DMSO) to all samples.

WebCutter 2.0 was used to identify restriction enzyme sites which are not present in the complete IGFBP-2 sequence but are also recognised by the pM-SUMOstar vector. BsmBI and XbaI restriction sites were inserted into the IGFBP-2 sequence using the primers in Table 7.1.

Primer Name	**Primer Sequence (5' to 3')**	**Length of Primer (bp)**	**Restriction Enzyme Site**	**Restriction enzyme sequence (5' to 3')**
Forward Primer	CGGCGCGTCTCGAG GTGAGGTGCTGTTCC GCTG	33	BsmBI	CGTCTC
Reverse Primer	GCTGGCTCTAGACTA CTACTGCATCCGCTG GGTGTG	36	XbaI	TCTAGA

Table 7.1 pM-SUMOstar Wild-type IGFBP-2 Primer and Restriction Site
The forward and reverse primer with the restriction site sequence highlighted in yellow on the full primer sequence. These restriction sites represent the restriction sites recognised by the pM-secSUMOstar vector to insert the IGFBP-2 DNA into the vector.

The PCR cycle, with varying annealing temperatures used is shown in table 7.2. All annealing temperatures (63-67°C) provided the correct PCR product.

PCR Stage	Number of Cycles	Time	Temperature
Initial Denaturation	1	30 sec	98°C
Denaturation	35x	10 sec	98°C
Annealing		30 sec	Gradient temperature: Lane 1 & 2 = 63°C Lane 3 & 4 = 65°C Lane 5 & 6 = 67°C
Extension		30sec	72°C
Final Extension	1	10 min	72°C
End	1	∞	4°C

Table 7.2 Phusion PCR cycle
The Phusion PCR cycle, reporting the different annealing temperatures, 63, 65 or 67ºC that were trialled to insert the restriction enzyme sites into the IGFBP-2 sequence.

PCR products were validated using DNA loading buffer (Thermo Scientific R0611), agarose gels, stained with Ethidium Bromide (Sigma, E1510).

7.3.1.2 Restriction Enzyme Digest

PCR products were purified using the QIAquick PCR purification kit prior to and after the digestion. Information provided by New England Biosciences determined the optimum temperatures and the NEBuffer required for 100% activity of the enzymes (Table 7.3). All restriction enzymes were activated for 1 hour and deactivated for 20mins. The IGFBP-2 sequence was cut at both sites, XbaI and BsmBI. pM-SUMOstar vector only possesses the BsmBI restriction site, therefore the vector was not digested by the XbaI enzyme. When BsmBI cuts at this point, it creates the overhang which represents the XbaI site.

Restriction Enzyme	Activation Temperature (°C)	Deactivation Temperature (°C)	Optimum Buffer
^{WT}IGFBP-2/pM-SUMOstar Vector			
XbaI	37	65	Buffer 4
BsmBI	55	80	

Table 7.3 Restriction enzyme ligation conditions
The optimum restriction enzyme activation and deactivation temperatures provided by New England Biosciences, including the most optimum buffer to use for the ligation reaction. As the activation temperatures were different, the lowest activation temperature was initiated first, following the activation for the BsmBI. XbaI was deactivated first, following BsmBI. Buffer 4 provided by New England Biosciences was used to stabilise the reaction.

7.3.1.3 Ligation

Mixture of the pM-SUMOstar vector and the IGFBP-2 insert containing the specific restriction sites recognised by the vector, was incubated with ligase buffer (NEB, B0202S) and T4 ligase (NEB, M0202S) overnight at 4ºC.

7.3.1.4 Transformation

Bacterial growth was carried out in autoclaved lysongeny broth (LB) (Thermo Fisher, BP9723-500). Ampicillin (Sigma, A5354), 100µg/ml, was added to the LB-agar (Thermo Fisher. BP9724-2) to prepare culture plates. 25ml of the LB-agar and ampicillin mixture was added to each bacterial culture plate and was left to set at room temperature for 30 minutes. Invitrogen transformation protocol was carried out using sourced E. coli competent cells (Invitrogen, 18265017). Agar/ampicillin plates coated with the culture were incubated overnight, in an inverted position at 37ºC. All plates were stored at 4ºC following the overnight incubation for long-term storage.

7.3.1.4.1 Transformation PCR for pM-SUMOstar vector colonies

Colonies were picked and suspended in milliQ H_2O. PCR (Table 7.4) was carried out using the colony water, PCR mastermix (Biorad, 1665009EDU), T7 promoter (T7F) primer, Bovine Growth Hormone Terminator (BGH) primer (Table 7.5) and DMSO.

PCR stage	Cycles	Temperature (ºC)	Time
Initial Denaturation	1x	95	7 min
Denaturation Annealing Extension	35x	94 53 72	30 sec 30 sec 1 min 30 sec
Final Extension	1x	53	5 min
End	1x	72	∞

Table 7.4 PCR cycle for pM-SUMOstar Transformation PCR
Optimised temperatures and time periods for different PCR stages. These conditions are standard to identify successful cloning of the pM-SUMOstar vector/IGFBP-2 plasmid.

PCR products were run on 1% agarose gel, stained with ethidium bromide at 100V for 1 hour.

7.3.1.5 Miniprep

Colonies from the re-streaked pM-SUMOstar ampicillin plates were picked and added to antibiotic treated LB and incubated in a shaker at 300rpm, 37ºC overnight. An aliquot of the incubated mixture was stored in 50% glycerol (Sigma, G5516) at -80ºC. The protocol used was “Plasmid DNA Purification using the QIAprep Spin Miniprep Kit and a Microcentrifuge” from the QIAprep Miniprep Handbook.

DNA, along with vector primers (Invitrogen) (Table 7.5) were sent to MRC Protein Phosphorylation and Ubiquitylation Unit (PPU) to determine the sequence matched the original IGFBP-2 sequence, using Chromas Lite (version 2.1.1) and Emboss Needle Pairwise Nucleotide Alignment.

pM-SUMOstar Primers	Sequence 5’ to 3’
T74	TAA TAC GAC TCA CTA TAG GG
BGH	TAG AAG GCA CAG TCG AGG

Table 7.5 Primers recognising the pM-SUMOstar vector
These primers were used to validate the cloning of the pM-SUMOstar vector and the IGFBP-2 DNA by sequencing. These primers specifically recognise the pM-SUMOstar vector.

7.3.1.6 Maxiprep

The glycerol stock was used re-streak LB-agar antibiotic treated plates. Plates were incubated, in an inverted position at 37ºC overnight and then placed in the fridge following the incubation to prevent over growth.

The starting culture was prepared by adding a colony to 200ml LB with ampicillin (100µg/ml) and was then incubated in a shaker at 300rpm at 37ºC for 7/8 hours. Overnight culture was made using an aliquot from the starting culture diluted in LB. The culture was left shaking at 300rpm at 37ºC overnight.

The protocol “Plasmid DNA Purification using QIAGEN Plasmid Maxi Kits” was retrieved from QIAGEN Plasmid Purification Handbook.

7.3.1.7 Transfection

Expi293 expression system kit and protocol (Thermo Fisher Scientific, A14635) was used to transfect the pM-SUMOstar ^{WT}IGFBP-2 into Expi293 cells.

It was critical cell density reached a maximum point of 500,000 cells in each 50ml cell/media suspension mixture. Cells were grown in antibiotic-free and light sensitive media and supplemented with the growth factors by the company.

Protocol for the transfection of Expi293 cells was provided by Thermo Fisher Scientific. Expi293 transfection enhancers were added to transfected cells after 24 hours, as stated in the protocol. The cells were incubated in the ^{WT}IGFBP-2 Expi293 product on an orbital shaker (37ºC, 8% CO_2, 125rpm). Media was collected 7 days after transfection.

7.3.1.8 pM-SUMOstar Protein Purification

Media was collected and spun for 400xg for 10mins at 4ºC. The supernatant was transferred into a fresh tube and the pellet was discarded. The supernatant was centrifuged at 4600xg for 15mins at 4ºC. Protease and phosphatase inhibitors (1:1000) were added to the media before using a bottle top filter to filter sterilise the media. Media not purified immediately was stored at -80ºC.

Two methods were used for the first stage of the purification process:

1) Ammonium sulphate (VWR, IC808229) was mixed with the media collected from the transfection incubated at 4ºC overnight. Tubes were spun at 4600xg at 4ºC for 90 mins. Floating pellets were removed and re-dissolved in PBS, pH 7.4.

2) Media from the transfection was added into a concentrating column (Thermo Scientific, 88532) and left to spin for 2 hours at 4600xg and 4ºC.

Buffer exchange was carried out using Zeba columns (Thermo Scientific, 87773). Samples were added to equilibrated Zeba columns and centrifuged at 1000xg for 2 mins.

Flowthrough from the Zeba was added to capped equilibrated HisPur columns (Thermo Scientific, 89969) and incubated at 4ºC for 30 mins on a tube rotator. The column was then centrifuged at 700xg for 2 mins before 3 washes of equilibration buffer (pH 7.4) (50mM $NaH_2PO_4.2H_2O$ (Sigma, 71505), 300mM NaCl and 10mM Imidazole (Sigma, I5513)). Elution of the sample was carried out with 3 washes with elution buffer (pH 7.4) (50mM $NaH_2PO_4.2H_2O$, 300mM NaCl and 150mM Imidazole).

7.1.3.8.1 Digestion of pM-SUMOstar expression vector

β-mercaptoethanol were added to the pM-SUMOstar ^{WT}IGFBP-2 and was incubated at 30ºC for 60, 30 or 0 mins, followed by an overnight incubation at 4ºC with 1 Unit or variable units from 2.5 to 10 Units of pM-SUMOstar Protease.

7.1.3.8.2 Collection of pure ^{WT}IGFBP-2

The digestion mixture was mixed with equilibration buffer (50mM $NaH_2PO_4.2H_2O$, 300mM NaCl and 10mM Imidazole). The concentration of imidazole was changed to 20mM and 40mM to optimise obtaining a high yield of pure IGFBP-2. 20mM imidazole was the optimum concentration to gain the most available yield of IGFBP-2. The mixture was incubated with a Hispur column for 30 mins at 4ºC. The column was centrifuged at 700xg for 2 mins and the flow through was collected. The column was washed twice with equilibration buffer and centrifuged at 700xg for 2 mins each time. The flow through and washes were all collected in separate falcon tubes. The hispur column was cleaned using elution buffer three times to remove all his-tagged components.

7.3.2 Generation of IGFBP-2 mutants

7.3.2.1 Mutation and primer design

Human IGFBP-2 cDNA sequence, which was retrieved from NCBI (GenBank: AAH71967.1) was used to create primers to introduce the mutations. Primers were made using the primer design tool supplied by Agilent. They recommend a maximum of 7 nucleotide substitutions per primer and to have a minimum of 10 nucleotides identical to the IGFBP-2 sequence before the first mutation and after the last. Primer sequences cannot be more than 46 nucleotides in length.

All primers were produced by Biorad in a solid state form and diluted in DNA/RNA free water to a concentration of 100ng/µl.

7.3.2.1.1 RGD mutation

The integrin binding site in the IGFBP-2 sequence is highlighted below:

atccagggagcccccaccatc**cgggggac**ccgagtgtcatctcttctacaatgagcag

I Q G A P T I **R G D** P E C H L F Y N E Q

The mutated sequence will appear as below:

atccagggagcccccaccatc**t**gggggggaccgagtgtcatctcttctacaatgagcag

I Q G A P T I **R G D** P E C H L F Y N E Q

The change to WGD requires a change from a cytosine to thymine (Jones et al., 1993).

The following primers were used to insert the mutation, as designed by Agilent Primer Tool (Table 7.6, Figure 7.4):

Forward Primer	5′ cccccaccatc**t**gggggggacccc 3′
Reverse Primer	5′ ggggtccccccc**a**gatggtggggg 3′

Table 7.6 RGD mutant site-directed mutagenesis primers
Forward and reverse primers to insert the mutation of cytosine to thymine for the RGD mutant. This table highlights the location of the change.

Primer sequences:

Primer Name	Primer Sequence (5' to 3')
c910t_	5'-cccccaccatctgggggacccc-3'
	5'-ggggtccccccagatggtgggggg-3'

Oligonucleotide information:

Primer Name	Length (nt.)	Tm	Duplex Energy at 68 °C	Energy Cost of Mismatches
c910t_	23	79.89°C	-45.48 kcal/mole	9.14%
	23	79.89°C	-44.98 kcal/mole	9.49%

Figure 7.4 RGD primer output from Aligent primer tool
Output of the most optimum primers which can include the chosen mutation, including primer details such as length (nucleotides) and melting temperature. This output was sourced from the Aligent primer tool which is provided online.

7.3.2.1.2 IGF Binding Domain Mutation

The IGF binding site in the IGFBP-2 sequence is highlighted below:

ccccacccgggctccgagctgcccctgcaggcgctggtcatgggcgagggcacttgtgag

P H P G S **E** **L P L Q A L V** M G E G T C

The mutated sequence will appear as below (Demambro et al., 2012):

ccccacccgggctccgag**gc**g**cc**g**c**g**caggcg**gc**g**c**atgggcgagggcacttgtgag

P H P G S **E** **L P L Q A L V** M G E G T C

There are 8 substitutions present in this mutation.

The mutation was split up into a two-step process with 2 sets of primers (Table 7.7, Figure 7.5).

Primer 1 (A)	Forward	5′ gcctgcaggggc**gc**ctcggagcccgg 3′
	Reverse	5′ ccgggctccgag**gc**gcccctgcaggc 3′
Primer 2 (B)	Forward	5′ cctcgcccatg**g**cc**gc**cgcctgc**gc**gg**c**cgcctcggagc 3′
	Reverse	5′ gctccgaggcg**g**cc**gc**gcaggcg**gc**gg**c**catgggcgagg 3′

Table 7.7 IGF mutant site-directed mutagenesis primers
The forward and reverse primers for each of the two steps required for the IGF mutation. The first mutation was inserted via primer 1. A second site-directed mutagenesis was carried out on the DNA following the first mutation, using the second primer.

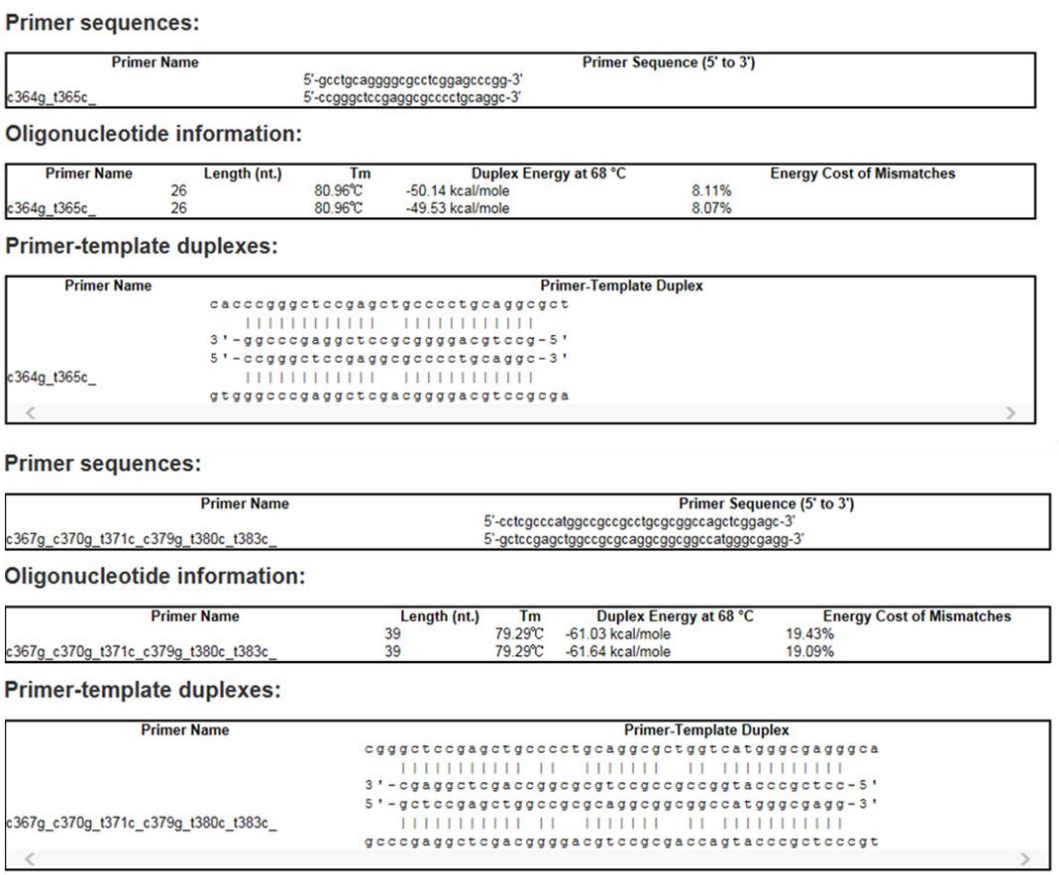

Primer sequences:

Primer Name	Primer Sequence (5' to 3')
	5'-gcctgcaggggcgcctcggagcccgg-3'
c364g_t365c_	5'-ccgggctccgaggcgcccctgcaggc-3'

Oligonucleotide information:

Primer Name	Length (nt.)	Tm	Duplex Energy at 68 °C	Energy Cost of Mismatches
	26	80.96℃	-50.14 kcal/mole	8.11%
c364g_t365c_	26	80.96℃	-49.53 kcal/mole	8.07%

Primer-template duplexes:

Primer Name	Primer-Template Duplex
	cacccgggctccgagctgcccctgcaggcgct
	3'-ggcccgaggctccgcggggacgtccg-5'
	5'-ccgggctccgaggcgcccctgcaggc-3'
c364g_t365c_	gtgggcccgaggctcgacggggacgtccgcga

Primer sequences:

Primer Name	Primer Sequence (5' to 3')
	5'-cctcgcccatggccgccgcctgcgcggccagctcggagc-3'
c367g_c370g_t371c_c379g_t380c_t383c_	5'-gctccgagctggccgcgcaggcggcggccatgggcgagg-3'

Oligonucleotide information:

Primer Name	Length (nt.)	Tm	Duplex Energy at 68 °C	Energy Cost of Mismatches
	39	79.29℃	-61.03 kcal/mole	19.43%
c367g_c370g_t371c_c379g_t380c_t383c_	39	79.29℃	-61.64 kcal/mole	19.09%

Primer-template duplexes:

Primer Name	Primer-Template Duplex
	cgggctccgagctgcccctgcaggcgctggtcatgggcgagggca
	3'-cgaggctcgaccggcgcgtccgccgccggtacccgctcc-5'
	5'-gctccgagctggccgcgcaggcggcggccatgggcgagg-3'
c367g_c370g_t371c_c379g_t380c_t383c_	gcccgaggctcgacggggacgtccgcgaccagtacccgctcccgt

Figure 7.5 IGF mutant Aligent primer tool output

The sequence region of IGFBP-2, plus excess was inputted into the Aligent primer tool with the desired mutations. Due to the size of this mutation, the mutation was split into 2 steps, ensuring there were at least 10 matching nucleotides from the beginning of the first mutation and from the last mutation change. The primers were created according to the output of the tool.

7.3.2.1.3 Heparin Binding Domain 1 and NLS Mutation

The HBD1/NLS binding site in the IGFBP-2 sequence is highlighted below:

cagatgggcaagggtggc**aa**g**ca**t**ca**ccttggcctggaggagccc**aa**g**aa**gctg**cg**accac

cc

Q M G K G G K H H L G L E E P K K L R P P

The mutated sequence will appear as below (Demambro et al., 2012):

cagatgggcaagggtggc**gc**g**gc**t**gc**ccttggcctggaggagccc**gc**g**gc**gctg**gc**accac

cc

Q M G K G G K H H L G L E E P K K L R P P

There are 12 substitutions present in this mutation.

The mutation was split up into a two-step process with two sets of primers (Table 7.8, Figure 7.6).

Primer 1 (A)	F	5′ gcagatgggcaagggtggc**gc**g**gc**t**gc**ccttggcctggaggagcc 3′
	R	5' ggctcctccaggccaagg**gc**a**gc**c**gc**gccacccttgcccatctgc 3′
Primer 2 (B)	F	5' ggcctggaggagccc**gc**g**gc**gctg**gc**accacccccctgccag 3'
	R	5′ ctggcaggggtggt**gc**cagc**gc**c**gc**gggctcctccaggcc 3′

Table 7.8 HBD1/NLS mutant primers
Forward (F) and reverse (R) primer sequences for the two-step mutation process of inserting the HBD1/NLS. The mutation using Primer 1 was carried out first. The DNA, following insertion of mutation from Primer 1, underwent site-directed mutagenesis using Primer 2.

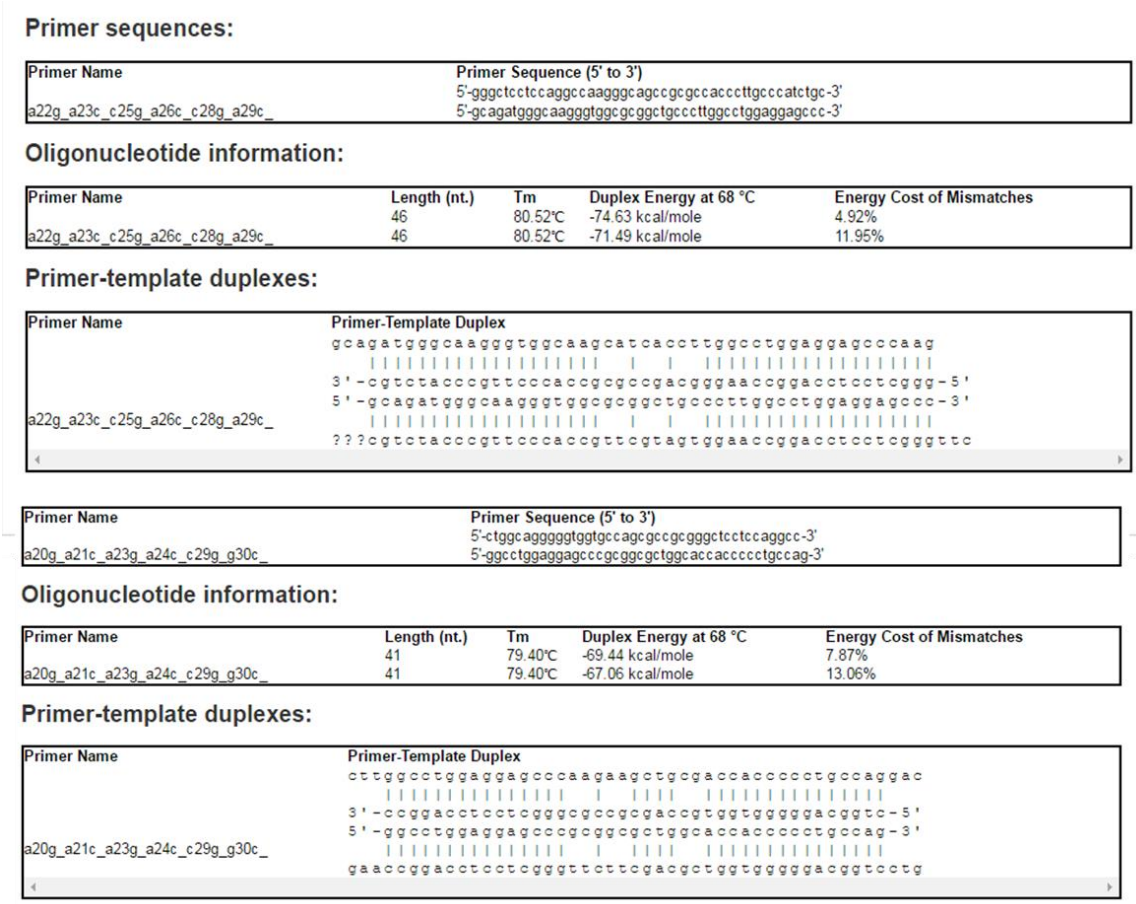

Primer sequences:

Primer Name	Primer Sequence (5' to 3')
	5'-gggctcctccaggccaagggcagccgcgccacccttgcccatctgc-3'
a22g_a23c_c25g_a26c_c28g_a29c_	5'-gcagatgggcaagggtggcgcggctgcccttggcctggaggagccc-3'

Oligonucleotide information:

Primer Name	Length (nt.)	Tm	Duplex Energy at 68 °C	Energy Cost of Mismatches
	46	80.52℃	-74.63 kcal/mole	4.92%
a22g_a23c_c25g_a26c_c28g_a29c_	46	80.52℃	-71.49 kcal/mole	11.95%

Primer-template duplexes:

Primer Name	Primer-Template Duplex
	gcagatgggcaagggtggcaagcatcaccttggcctggaggagcccaag
	3'-cgtctacccgttcccaccgcgccgacgggaaccggacctcctcggg-5'
	5'-gcagatgggcaagggtggcgcggctgcccttggcctggaggagccc-3'
a22g_a23c_c25g_a26c_c28g_a29c_	???cgtctacccgttcccaccgttcgtagtggaaccggacctcctcgggttc

Primer Name	Primer Sequence (5' to 3')
	5'-ctggcaggggtggtgccagcgccgcgggctcctccaggcc-3'
a20g_a21c_a23g_a24c_c29g_g30c_	5'-ggcctggaggagcccgcggcgctggcaccacccctgccag-3'

Oligonucleotide information:

Primer Name	Length (nt.)	Tm	Duplex Energy at 68 °C	Energy Cost of Mismatches
	41	79.40℃	-69.44 kcal/mole	7.87%
a20g_a21c_a23g_a24c_c29g_g30c_	41	79.40℃	-67.06 kcal/mole	13.06%

Primer-template duplexes:

Primer Name	Primer-Template Duplex
	cttggcctggaggagcccaagaagctgcgaccacccccctgccaggac
	3'-ccggacctcctcgggcgccgcgaccgtggtgggggacggtc-5'
	5'-ggcctggaggagcccgcggcgctggcaccacccccctgccag-3'
a20g_a21c_a23g_a24c_c29g_g30c_	gaaccggacctcctcgggttcttcgacgctggtgggggacggtcctg

Figure 7.6 HBD1 mutant primers using Aligent primer tool
The sequence section with HBD1/NLS signal was inputted into the Aligent Primer Tool. The HBD1 mutant also had to be split into 2 primer sets. This output provided the most optimum primers to induce the mutations to create a non-functional HBD/NLS site.

7.3.2.1.4 Heparin Binding Domain 2

The HBD2 binding site in the IGFBP-2 sequence is highlighted below:

aactgtgac**aa**g**ca**tggcctgtacaac**ct**c**aa**acagtgc**aa**gatgtctctgaacgggcag**cg**tgggga
g

The mutated sequence will appear as below (Xi et al., 2013):

aactgtgac**gc**g**gc**tgccctgtacaac**gc**c**gc**acagtgc**gc**gatgtctctgaacgggcag**gc**tgggga
g

The mutation, KHGLYNLKQCKMSLNGQR>AAGLYNAAQCAMSLNGQA was split up into a three-step process with two sets of primers (Table 7.9).

Primer 1 (A)	F	5' cacatccccaactgtgac**gc**g**gc**tggcctgtacaacctcaaa 3'
	R	5' tttgaggttgtacaggcca**gc**c**gc**gtcacagttggggatgtg 3'
Primer 2 (B)	F	5' gctggcctgtacaac**gc**c**gc**acagtgc**gc**gatgtctctgaacgg 3'
	R	5' ccgttcagagacatc**gc**gcactgt**gc**g**gc**gttgtacaggccagc 3'
Primer 3 (C)	F	5' tctgaacgggcag**gc**tggggagtgctgg 3'
	R	5' ccagcactcccca**gc**ctgcccgttcaga 3'

Table 7.9 HBD2 mutant primers
Primer sequences of forward and reverse reactions in the three-step site-directed mutagenesis process to inset the HBD2 mutation into IGFBP-2. The mutation changes have been highlighted in red bold font. These primers were optimised according to the sequence inputted into Aligent primer tool.

7.3.2.2 Site Directed Mutagenesis

100ng ^{WT}IGFBP-2+SUMO template DNA (obtained from the maxiprep before transfection) was added to the PCR reaction supplied by Aligent Quikchange Lightening Site-directed Mutagenesis kit (Aligent, 200523). The PCR components were added as stated plus one set of the forward and reverse primers (125ng each). Chapter 8.3.7 discusses the protocol regarding 2 step mutations. The optimum annealing temperature for all mutants was 68ºC.

7.3.2.3 Ethanol Precipitation

This step further purifies and concentrates the DNA obtained from the site-directed mutagenesis PCR in order to obtain a greater yield of successfully mutated colonies.

Sodium acetate (pH 5.2) and 99% pure ethanol were added to the PCR product and incubated at -80ºC for 1 hour. The mix was centrifuged at 15,000xg for 30 mins at 4ºC, following resuspension of the pellet in 70% ethanol. The ethanol was removed by centrifuging at the same speed for 5 mins and resuspending the pellet in EB buffer, containing tris-HCl and EDTA which helps stabilise DNA. The precipitated DNA was then used for the transformation stage.

7.3.2.4 Transformation

The protocol by Quikchange Lightening kit was used for successful transformation into E. coli cells provided by Aligent in their site-directed mutagenesis kit. Transformed cells were plated on LB-agar plates with added Ampicillin and colonies were left to grow at 37ºC overnight (method in Chapter 7.3.1.4).

Colonies were picked from the centre of the plate and suspended in 50µl DNA/RNA free H_2O. These colonies were re-streaked onto Ampicillin treated LB-Agar plates and incubated overnight at 37ºC.

7.3.2.5 Miniprep

The miniprep protocol was carried out in the same manner as stated in 7.3.1.5 but with the mutated re-streaked colonies. The obtained DNA product was also sent to MRC PPU to identify the insertion of the mutation and to check no further mutations had occurred to disrupt the activity of IGFBP-2. The primers sent to PPU were T74 and BGH (Table 7.5).

Retrieved sequences were checked using Chromas Lite and Emboss Needle Pairwise Nucleotide Alignment.

7.3.2.6 Two-step mutation process

For the mutations that require a 2-step mutation process, once the insertion of the correct mutation from one of the primer sequences had been confirmed, 100ng of DNA collected from the miniprep of the half-mutated sequence was used to undergo site-directed mutagenesis again (Chapter 7.3.2.2), this time using the other primer set. Optimum annealing temperatures remained at 68ºC. Ethanol precipitation, transformation and miniprep protocols were carried out again and the DNA product was sent to MRC PPU with the primers T74 and BGH.

This time the full mutation was be validated via Chromas Lite and Emboss Nucleotide Alignment.

7.3.2.7 Maxiprep and transfection

The same protocols were carried out in an identical manner as stated in chapters 7.3.1.6 and 7.3.1.7.

7.3.2.8 pM-SUMOstar mutant purification

Media was harvested and separated from the cells via the centrifugation and sterilisation steps as mentioned at the beginning of chapter 7.3.1.8. Media was concentrated to a smaller volume using concentrating columns. The remaining purification protocol was carried out as stated in chapter 7.3.1.8.

Digestion of the pM-SUMOstar from the mutant was carried out with only pM-SUMOstar Protease (1 Unit) at 4ºC, overnight. The digested mixture of RGD and IGF domain mutant was mixed with equilibration buffer with 20mM imidazole (50mM $NaH_2PO_4.2H_2O$, 300mM NaCl and 20mM Imidazole pH 7.4) and incubated in a hispur column for 30 mins. The HBD1 mutant was mixed with 10mM imidazole equilibration buffer. The flow through plus 2 further washes with the corresponding equilibration buffer were collected. Elution buffer (50mM $NaH_2PO_4.2H_2O$, 300mM NaCl and 150mM Imidazole, pH 7.4) was used to remove the remaining his-tagged contaminants separately.

7.3.2.9 Mutant validation

Sequence checks, as well as IGF binding blots were used to validate the IGFBP-2 mutant variants. The protocol for IGF binding blot can be found in the General methods Chapter 3.4.

7.3.3 Data analysis

GeneTools was used to perform densitometry analysis of the bands on each western blot. Unpaired t-tests were carried out to test data for statistical significance. All error bars represent standard error of the mean (SEM). Some preliminary studies only had n=2 due to time and funding constraints and therefore statistical tests were not carried out on these samples.

7.4 Optimisation and Validation Results

7.4.1 Optimising phusion PCR of ^{WT}IGFBP-2

Phusion PCR is the process used to insert the primers that contain the restriction enzyme sites recognised by the expression vector pM-SUMOstar.

However, as IGFBP-2 has a high GC content, as well as the primers, PCR has to be optimised to ensure we do not obtain any undesirable mutations that may affect IGFBP-2s full sequence. The standard Phusion High-Fidelity Buffer in the absence of DMSO did not achieve successful PCR product for IGFBP-1 (control) or IGFBP-2. With the addition of DMSO, a clear band was observed for IGFBP-1 with an annealing temperature of 60ºC. However, no clear bands were obtained for IGFBP-2 Phusion PCR. The Phusion GC Buffer was used instead of Phusion High-Fidelity Buffer, as this GC buffer specifically stabilises sequences with a high GC content. Successful Phusion PCR product was obtained with IGFBP-2 at annealing temperatures in between 63-67ºC with Phusion GC Buffer (Figure 7.7).

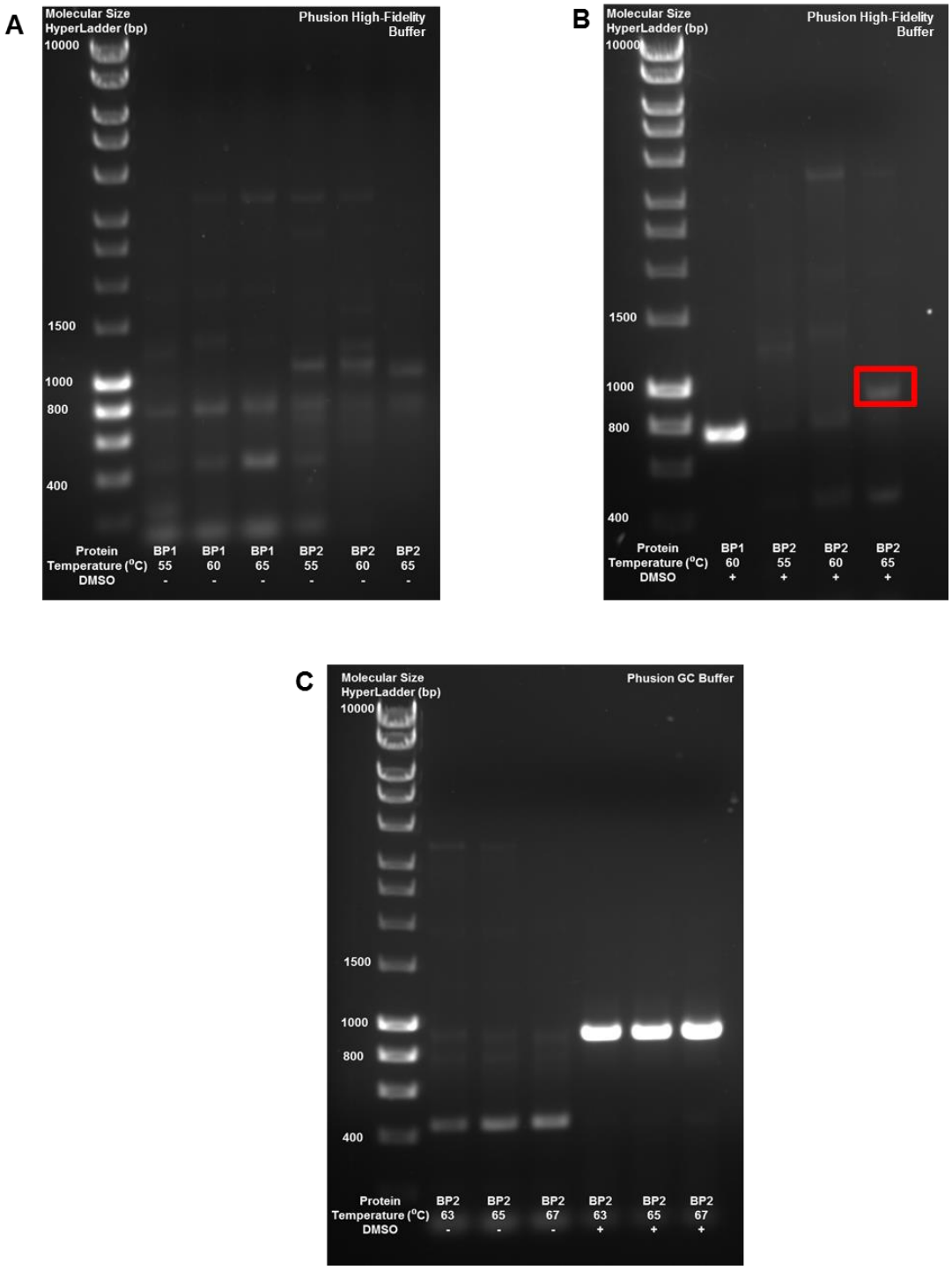

Figure 7.7 Optimising Phusion PCR
Agarose gel (1%) was stained with Ethidium Bromide. It contained Phusion PCR products of IGFBP-1(BP1) and IGFBP-2(BP2) at varying annealing temperatures (63-67ºC). 250ng of DNA was used for each reaction. Positive IGFBP-1 bands should have an approximate MW of 750bp. Positive IGFBP-2 bands should present a MW of approximately 980bp. (**A)** In the absence of DMSO and Phusion High-Fidelity (HF) buffer, with IGFBP-1 (BP1) as a negative control, (**B)** In the presence of DMSO and Phusion HF buffer, BP1 represents a positive control. (**C)** BP2 using Phusion GC buffer (to stabilise high GC rich sequences) in the absence and presence of DMSO.

7.4.2 ^{WT}IGFBP-2/pM-secSUMOstar bacterial transformation PCR gels

Transformation involves the uptake of protein/expression vector DNA into E. coli cells using heat shock. A proportion of the cells will take up the plasmid DNA and rapidly replicate the inserted sequence. Positive colonies that have taken up the plasmid DNA will appear as a band with a molecular weight higher than the empty vector. As DMSO was required to stabilise the DNA in the Phusion PCR, the transformation PCR was successful in the presence of DMSO (Figure 7.8).

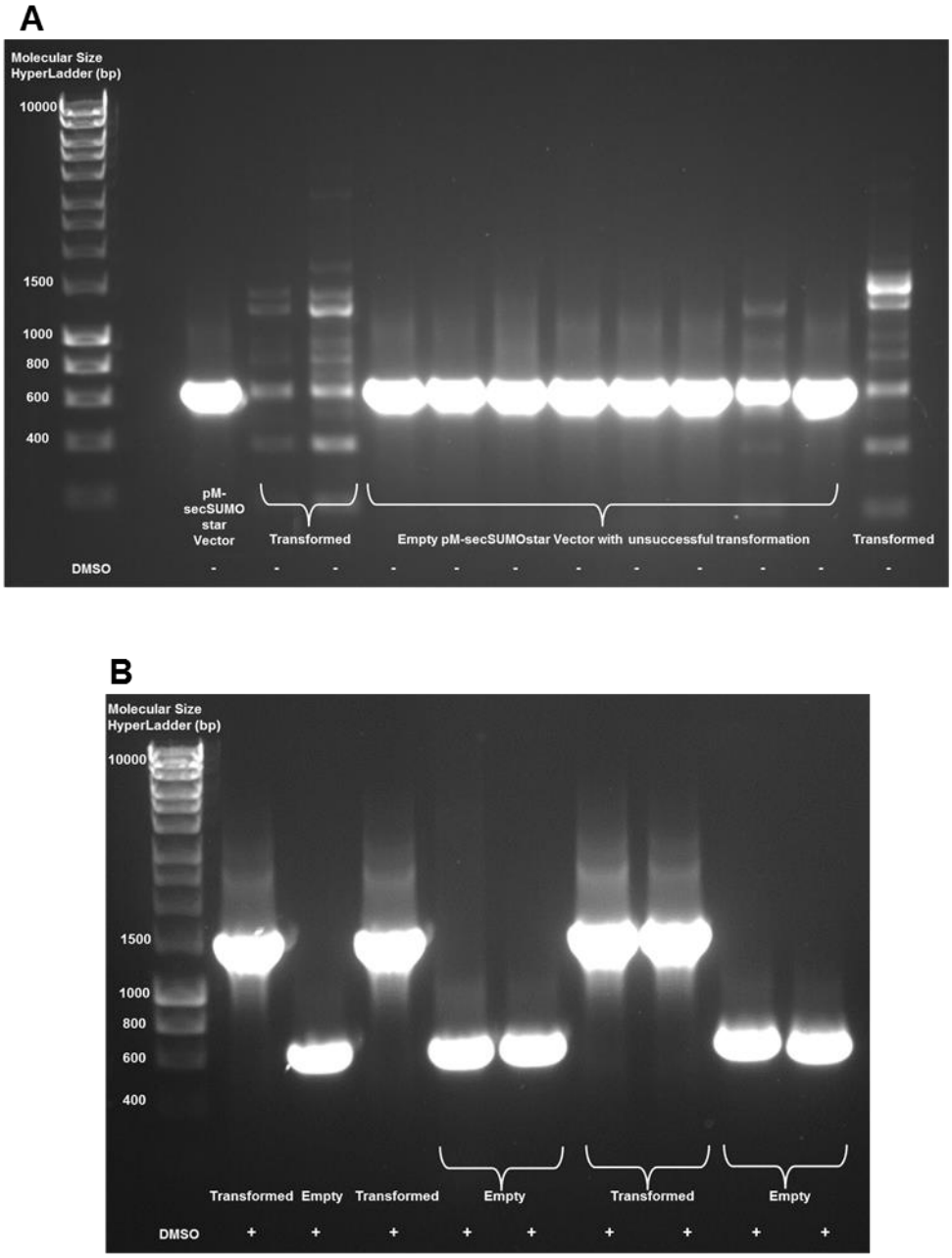

Figure 7.8 Successful transformation of IGFBP-2+pM-SUMOstar vector using E. coli cells confirmed by PCR

Agarose gels (1%) stained with Ethidium Bromide (**A)** in the absence of DMSO, un-transformed bands appear as an identical band to the empty vector (600bp) and transformed bands appear fragmented. **(B)** In the presence of DMSO, all transformed bands appear as one single band at an approximate MW of 1400bp. Empty vectors appear as a lower molecular weighted single band. A 10000bp MW marker was used to identify the molecular weight of the desired transformation. Successful transformation confirms fusion of the IGFBP-2 plasmid into the vector.

7.4.3 Confirmation of complete ^{WT}IGFBP-2 sequence

Miniprep was carried out to isolate the DNA consisting of the pM-SUMOstar/IGFBP-2 sequence from the bacterial cells. The DNA was sent to an external sequencing unit, where a nucleotide sequence of the DNA was provided to us in a written format. The sequence was validated against the original full IGFBP-2 sequence sourced from an NCBI hit of the protein (GenBank: AAH71967.1), confirming no unexpected mutations were present (Figure 7.9 A). A Chromas output file highlighted the peaks of nucleotides that were reported in the DNA was used to support the sequence we had retrieved by the MRC sequencing unit (Figure 7.9 B).

A

```
COLONYBP2       199 TCGGGGTCCCCCCGGATGGTGGGGGCTCCCTGGATCAGCTTCCCGGTGTT  248
                    ||||||||||||||||||||||||||||||||||||||||||||||||||
IGFBP2           82 tcggggtccccccggatggtgggggctccctggatcagcttcccggtgtt  131

COLONYBP2       249 GGGGTTCACACACCAGCACTCCCCACGCTGCCCGTTCAGAGACATCTTGC  298
                    ||||||||||||||||||||||||||||||||||||||||||||||||||
IGFBP2          132 ggggttcacacaccagcactccccacgctgcccgttcagagacatcttgc  181

COLONYBP2       299 ACTGTTTGAGGTTGTACAGGCCATGCTTGTCACAGTTGGGGATGTGCAGG  348
                    ||||||||||||||||||||||||||||||||||||||||||||||||||
IGFBP2          182 actgtttgaggttgtacaggccatgcttgtcacagttggggatgtgcagg  231

COLONYBP2       349 GAGTAGAGGTGCTCCAGAGGGCCCCGCTCATCCGGAAGGCGCATGGTGGA  398
                    ||||||||||||||||||||||||||||||||||||||||||||||||||
IGFBP2          232 gagtagaggtgctccagagggccccgctcatccggaaggcgcatggtgga  281

COLONYBP2       399 GATCCGCTCCAGGACCTGGTCCAGTTCCTGTTGGCAGGGAGTCCTGGCAG  448
                    ||||||||||||||||||||||||||||||||||||||||||||||||||
IGFBP2          282 gatccgctccaggacctggtccagttcctgttggcagggagtcctggcag  331

COLONYBP2       449 GGGGTGGTCGCAGCTTCTTGGGCTCCTCCAGGCCAAGGTGATGCTTGCCA  498
                    ||||||||||||||||||||||||||||||||||||||||||||||||||
IGFBP2          332 ggggtggtcgcagcttcttgggctcctccaggccaaggtgatgcttgcca  381
```

B

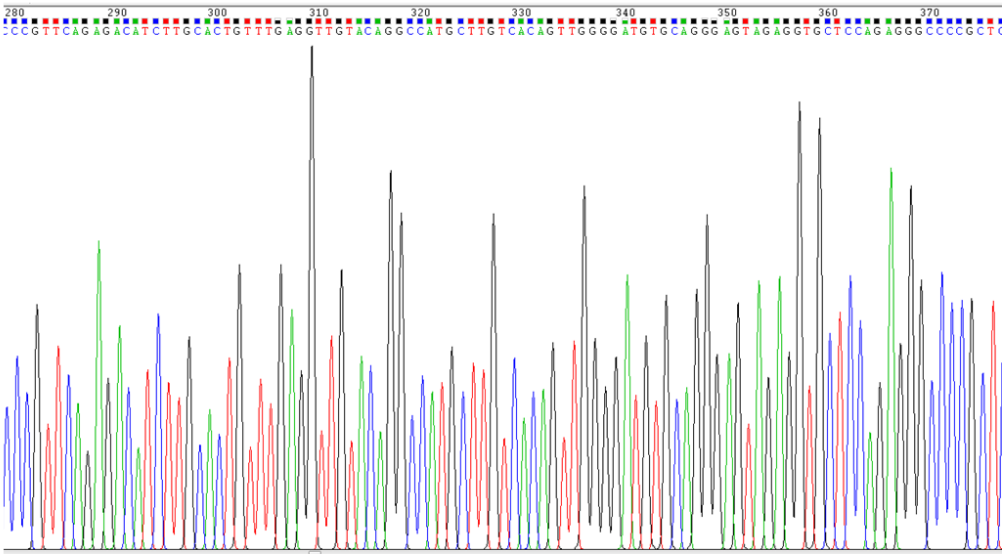

Figure 7.9 Confirmation of correct IGFBP-2 sequence in the plasmid product
Following preparation of vector+IGFBP-2 plasmid DNA using a miniprep kit, the DNA was sent for sequencing to the MRC Sequencing Unit. (**A)** Representative data displaying a section of the alignment between the sequence of miniprep product (retrieved from MRC Protein Phosphorylation and Ubiquitylation Unit, using the primers T7 (Forward) and BGH (Reverse) and the published complete hIGFBP-2 sequence (IGFBP2) using EMBOSS needle sequence alignment tool. (**B)** A representative selection of a chromatogram displaying the nucleotide peaks identified during the DNA sequencing of the ^{WT}IGFBP-2+pM-SUMOstar.

7.4.4 Purification of pure IGFBP-2

Expi293 cells expressed large quantities of the IGFBP-2/pM-SUMOstar following transfection with the IGFBP-2/pM-SUMOstar DNA. To retrieve the ^{WT}IGFBP-2, the protein was precipitated from the cells and purified. The purification process involved using SUMO protease to digest the vector at the cleavage site, resulting in separation of the expression vector, pM-SUMOstar and IGFBP-2. Aliquots taken from the media before cleavage of the pM-secSUMOstar vector.

Unfortunately, initially we only obtained very small amounts of ^{WT}IGFBP-2, which were barely visible on a coomassie, but validated on an immunoblot probing for IGFBP-2 (Figure 7.10).

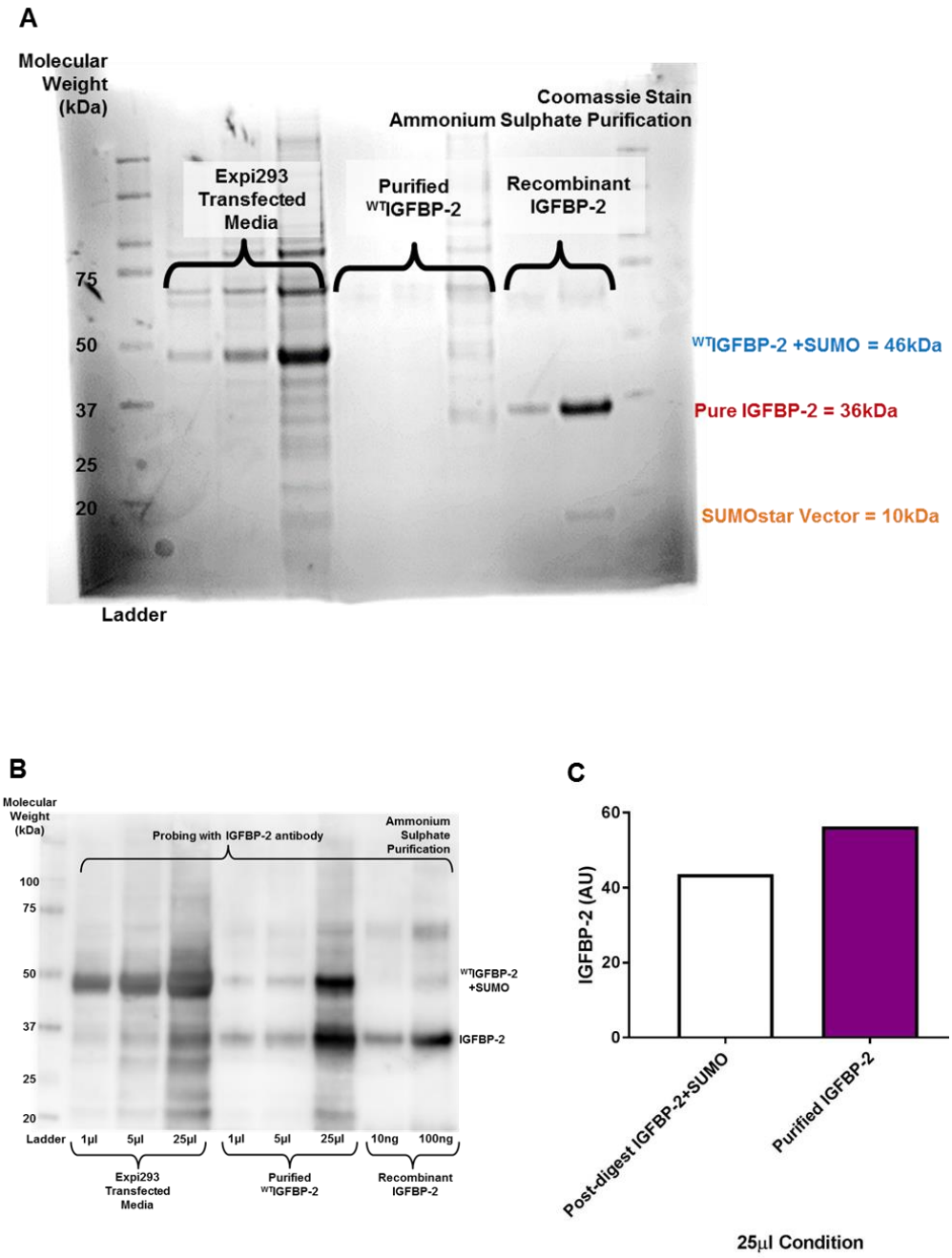

Figure 7.10 Digestion of ^{WT}IGFBP-2+SUMO to produce pure IGFBP-2 using SUMO protease

Purification of transfected Expi293 media, containing the WTIGFBP-2+SUMO was carried out using ammonium sulphate purification. **(A)** Coomassie stain on a 4-12% Bis-Tris gel, with lane 1 showing the molecular weight ladder, 1, 5 or 25µl of transfected media containing WTIGFBP-2+SUMO (MW=50kDa) (lane 2-4) and 1, 5 or 25µl purified WTIGFBP-2 (MW=36kDa) loaded onto the gel (lane 5-7). Recombinant IGFBP-2 (MW=36kDa) (10 and 100ng) was loaded as a positive control (lane 8–9). SUMOstar vector alone has an approximate MW of 10kDa. **(B)** Immunoblot, probed with goat polyclonal anti-IGFBP-2 on a 4-12% Bis-Tris gel, with lane 1 showing the molecular weight ladder, 1, 5 or 25µl of transfected media containing WTIGFBP-2+SUMO (MW=50kDa) (lane 2-4) and 1, 5 or 25µl purified WTIGFBP-2 (MW=36kDa) loaded onto the gel (lane 5-7). Recombinant IGFBP-2 (MW=36kDa) (10 and 100ng) was loaded as a positive control (lane 8–9), highlights presence of IGFBP-2. **(C)** Densitometry analysis compares the two bands in lane 7 from immunoblot 7.10B, 25µl purified WTIGFBP-2, of WTIGFBP-2+SUMO (MW=50kDa) and purified IGFBP-2 (MW=36kDa) (n=2).

7.4.5 Optimising precipitation of ^{WT}IGFBP-2 from Expi293 media

Ammonium sulphate precipitation is a commonly used method of protein purification from cultured cells. However, as established previously, due to the high GC rich content, the sequence of IGFBP-2 is unstable and we could not confirm if ammonium sulphate affected the pure IGFBP-2 yield obtained. Therefore, we used another precipitation method, which involved concentrating the media with the cells using concentrating columns with a 100kDa MW cut off point. This ensured the protein with a total MW of just less than 50kDa was collected and any waste with higher MWs was removed. The difference in yield of pure ^{WT}IGFBP-2 was confirmed by coomassie staining and western blotting probing for IGFBP-2 (Figure 7.11).

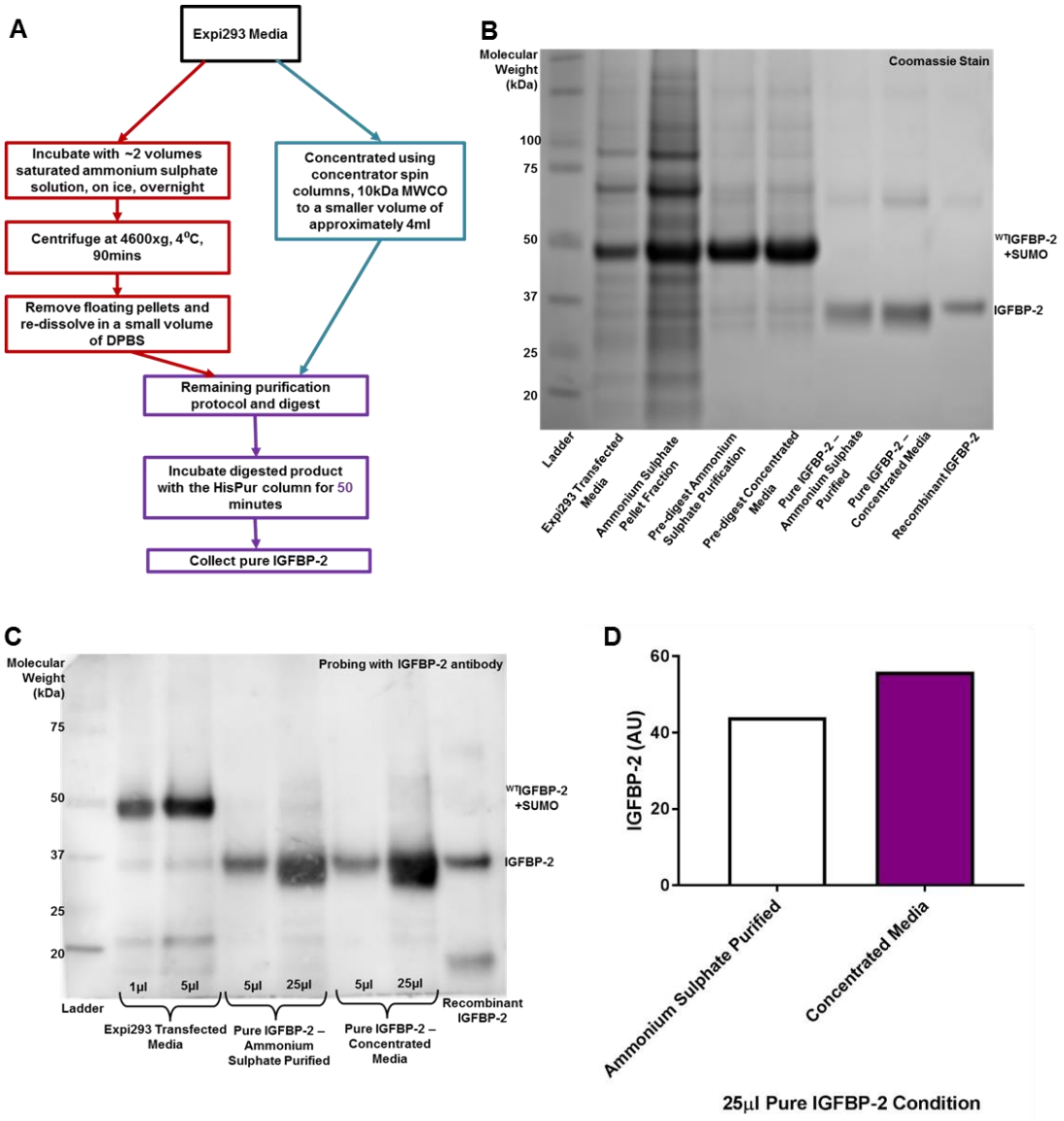

Figure 7.11 Purification method affects the purity of ^{WT}IGFBP-2
(A) Flow diagram depicting the different purification methods tested and the changes made, extending the final incubation stage with the HisPur column so the final constructs possessing the His tag are retained. (**B)** Coomassie stained gel (4-12% Bis-Tris) with products from different stages of the purification process using ammonium sulphate purification and concentrating, pre- and post-digest. 5µl of sample was loaded onto the gel for each condition. Bands for ^{WT}IGFBP-2 + SUMO complex (50kDa) and pure IGFBP-2 (36kDa) can be identified. Recombinant IGFBP-2 (100ng/ml) was used as a positive control. (**C)** Immunoblot probing for goat polyclonal anti-IGFBP-2 with 5µl and 25µl samples of media before purification and the end product after each purification (ammonium sulphate and concentrating) method. Recombinant IGFBP-2 (100ng/ml) was loaded as the positive control. Bands for ^{WT}IGFBP-2 + SUMO complex (50kDa) and pure IGFBP-2 (36kDa) can be identified. (**D)** Graph shows calculated densitometry, from immunoblot 7.11C of comparing the concentration of pure IGFBP-2 obtained in a 25µl sample following ammonium sulphate purification and concentrating of media (n=3).

7.4.6 Removal of contaminants in pure ^{WT}IGFBP-2

Once the cleavage site in the expression vector has been cleaved, the IGFBP-2/pM-SUMOstar complex at approximately 50kDa should not be seen. Only two bands should appear representing the pure IGFBP-2 (36kDa) and the SUMOstar vector at approximately 10kDa. The IGFBP-2 alone is isolated from this broken mixture using hispur columns. The his6 tag on the vector ensures the SUMOstar vector remains bound to the column and therefore the non-bound flow through should contain all of the IGFBP-2 protein. The final elutions of the column should only contain the SUMOstar vector. Coomassie staining of samples taken at different stages of the purification process confirmed we were losing the maximum yield of pure ^{WT}IGFBP-2 in the elutions (Figure 7.12).

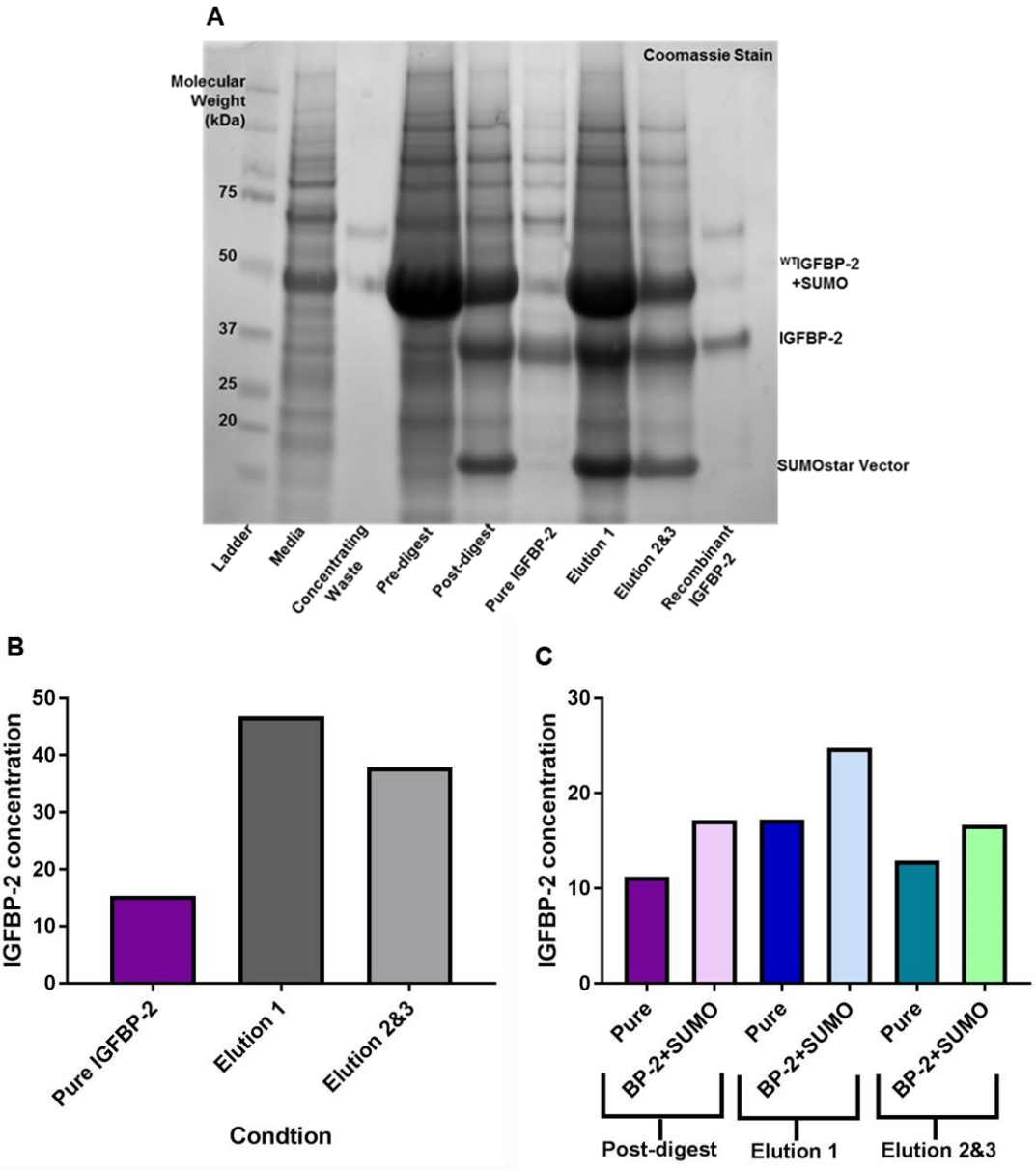

Figure 7.12 Pure non-his tagged IGFBP-2 is eluted in final elution of all his-tagged components

Transfected Expi293 media was purified using the concentration method. Aliquots were taken at each stage of the purification process, including pre-, post-digest and elution outputs, to identify at which stage, the purification process was not taking place successfully. **(A)** Coomassie stain, on a 4-12% Bis-Tris gel, displays the ^{WT}IGFBP-2+SUMO complex (50kDa), pure ^{WT}IGFBP-2 (36kDa), SUMOstar vector (10kDa) and recombinant IGFBP-2 (positive control – lane 9 (36kDa)) bands from 25µl aliquots from the media (lane 2), concentrated waste (lane 3), pre-digest (lane 4), post-digest (lane 5), pure ^{WT}IGFBP-2 (lane 6), 1st elution (lane 7), 2nd and 3rd elution (lane 8). (B) Graph displays the concentration of IGFBP-2 obtained in the pure ^{WT}IGFBP-2 wash and following elution 1 and elution 2&3 containing any remaining residue bound to the column, including ^{WT}IGFBP-2 from densitometry collected from the Coomassie stain 7.12A (n=3). (C) This graph highlights the concentration of pure ^{WT}IGFBP-2 and ^{WT}IGFBP-2+SUMO complex in the post-digest wash and elution washes, which should not contain un-digested ^{WT}IGFBP-2+SUMO complex, using the densitometry collected from the Coomassie stain, 7.12A (n=3).

7.4.7 Increasing ^{WT}IGFBP-2 yield by further washes

Figure 7.10 confirmed pure IGFBP-2 remained adhered to the hispur column in the elution, which should only contain his-tagged components (SUMOstar vector). Extra washes were carried out using equilibration buffer after the flow through had been collected to see if purer IGFBP-2 could be removed off the column. Extra washes with equilibration buffer removed more of the pure ^{WT}IGFBP-2 from the Hispur mixture (Figure 7.13).

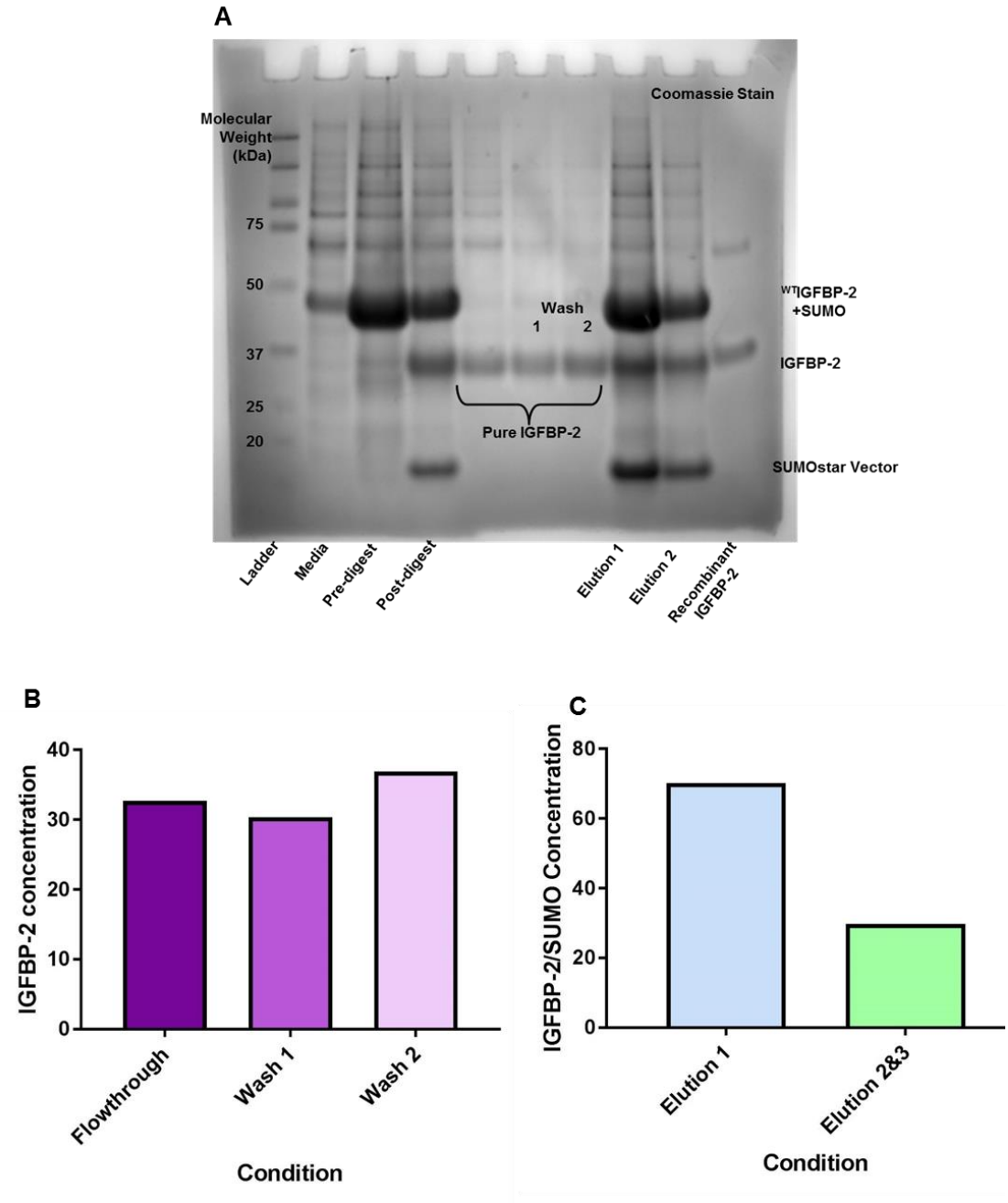

Figure 7.13 Further washes of the His-Pur column releases purer IGFBP-2
Transfected Expi293 media was purified using the concentration method. Aliquots were taken at each stage of the purification process, including pre-, post-digest, pure ^{WT}IGFBP-2, with additional washes and elution outputs, to identify at which stage, the purification process was not taking place successfully. **(A)** Coomassie stain, on a 4-12% Bis-Tris gel, displays the ^{WT}IGFBP-2+SUMO complex (50kDa), pure ^{WT}IGFBP-2 (36kDa), SUMOstar vector (10kDa) and recombinant IGFBP-2 (positive control – lane 10 (36kDa)) bands from 25µl aliquots from the media (lane 2), pre-digest (lane 3), post-digest (lane 4), pure ^{WT}IGFBP-2 (lane 5), pure ^{WT}IGFBP-2 wash 1 (lane 6), pure ^{WT}IGFBP-2 wash 2 (lane 7), 1st elution (lane 8) and elution 2 (lane 9). **(B)** Densitometry from Coomassie stain 7.13A, showing the IGFBP-2 concentration in the pure ^{WT}IGFBP-2 flow-through and wash 1 and wash 2 is displayed in the graph (n=3). **(C)** This graph shows the concentration of un-digested ^{WT}IGFBP-2+SUMO complex which remains in the elution 1 and elution 2&3, post-digest, measured from the densitometry of the bands in the Coomassie stain 7.13A (n=2).

7.4.8 Optimising imidazole concentrations for ^{WT}IGFBP-2 purification

Imidazole is a molecule that is commonly used for protein elution from histidine matrices (Bornhorst & Falke, 2000). It is added to wash buffers (low concentrations) and elution buffers (high concentrations) to act competitively with non-histagged proteins, preventing non-specific binding. As pure IGFBP-2 remained bound to the column, we hypothesised increasing imidazole concentrations in the wash buffer would release a larger yield of pure IGFBP-2 into the flow through. As imidazole possesses a histidine ring, it will have a higher affinity for the column than IGFBP-2, therefore IGFBP-2 is less likely to remain bound. Increasing imidazole concentrations to 20mm removed the majority of ^{WT}IGFBP-2 from the elution (Figure 7.14).

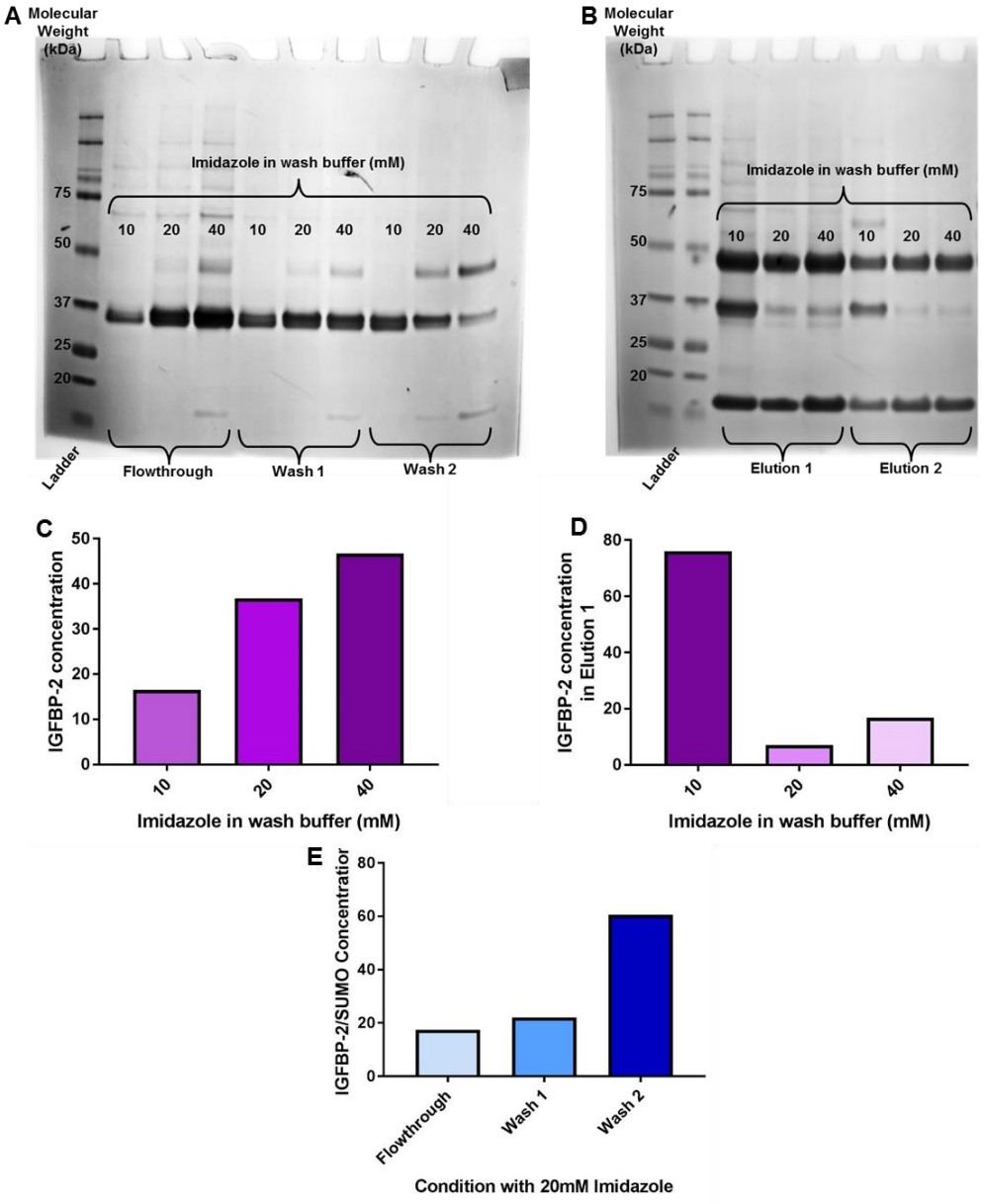

Figure 7.14 Increasing imidazole concentration aids the elution of purer IGFBP-2
The imidazole concentration in the wash buffer was altered from 10mM to 20mM or 40mM. Aliquots were collected from all stages of the purification process. 25µl aliquots were loaded onto a 4-12% Bis-Tris gel. **(A)** Coomassie staining on the gel shows the abundance of pure ^{WT}IGFBP-2 present in the initial flow-through (lane 2-4), wash 1 (lane 5-7), wash 2 (lane 8-10), after changing the imidazole concentration in the wash buffers used throughout the purification process. **(B)** Coomassie staining on the gel shows the abundance of pure ^{WT}IGFBP-2 present in the 1st elution (lane 2-4) and 2nd elution (lane 5-7), after changing the imidazole concentration in the wash buffers used throughout the purification process. **(C)** Densitometry of the bands representing ^{WT}IGFBP-2 (36kDa) in the flow through, from gel 7.14A, show the change in IGFBP-2 concentration obtained in the initial purification, in response to increasing imidazole concentration from 10mM to 20mM or 40mM (n=2). **(D)** Densitometry of the bands representing ^{WT}IGFBP-2 (36kDa) in the elution 1, from gel 7.14B, show the change in IGFBP-2 concentration obtained in the final elution, which should contain all the waste residue, in response to increasing imidazole concentration from 10mM to 20mM or 40mM throughout all purification steps (n=2). **(E)** Densitometry of the bands representing ^{WT}IGFBP-2+SUMO complex (50kDa) in the flow through, 1st wash and 2nd wash with 20mM imidazole, from the gel 7.14A, show the change in ^{WT}IGFBP-2+SUMO complex contamination in the samples which should only contain pure ^{WT}IGFBP-2 (n=2).

7.4.9 Double digest of ^{WT}IGFBP-2/pM-SUMOstar complex

As we have shown in previous figures, a large abundance of IGFBP-2/pM-SUMOstar complex remained undigested by the SUMOprotease, therefore resulting in a lower yield of pure ^{WT}IGFBP-2. To tackle this, we attempted to digest elutions collected from previous purification attempts, which contained the IGFBP-2/pM-SUMOstar complex for the second time. Increasing the concentration of SUMOprotease enhanced the digestion at the cleavage site (Figure 7.15 A and B).

β-Mercaptoethanol is a common substance added to the mixture prior to incubation with SUMOprotease. It compromises the disulphide bonds in the cleavage site beforehand, making it easier for SUMOprotease to function (Bondos & Bicknell, 2003). However, we have previously observed these substances may also be affecting the IGFBP-2 sequence, which could alternatively be inhibiting maximum digestion. Reduced incubation times with β-mercaptoethanol failed to increase the yield of pure ^{WT}IGFBP-2 (Figure 7.15 C and D).

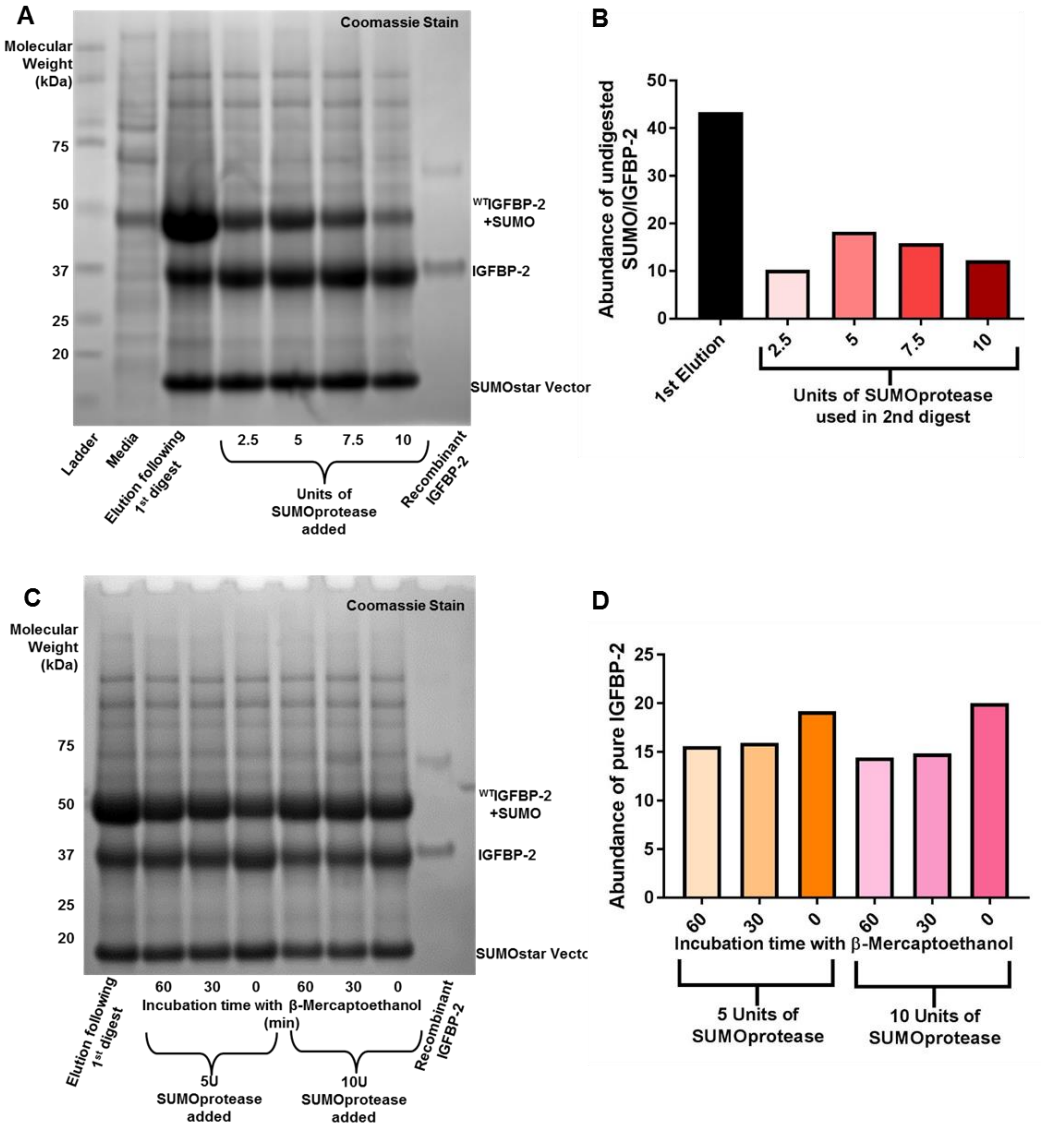

Figure 7.15 Double digest using increasing concentrations of SUMOprotease increases digestion activity

Due to problems with the digestion of the complex, different concentrations of SUMOprotease (2.5, 5, 7.5 or 10 units) were used for a double digest of the un-digested ^{WT}IGFBP-2+SUMO complex. **(A)** 25µl aliquots were taken from different stages of the digest step and loaded on a 4-12% Bis Tris gel and stained with Coomassie blue. Media (lane 2), elution following 1st digest (lane 3), elution following 2nd digest with 2.5 units (lane 4), 5 units (lane 5), 7.5 units (lane 6) and 10 units (lane 7). Recombinant IGFBP-2 (100ng/ml) (36kDa) was loaded (lane 8) as a positive control. ^{WT}IGFBP-2+SUMO complex has a MW of 50kDa and ^{WT}IGFBP-2 has a MW of 36kDa. **(B)** This graph highlights the reduction in un-digested ^{WT}IGFBP-2+SUMO complex following the 2nd digest, in response to incubation with increasing units of SUMOprotease (n=2). **(C)** The elution following the 1st digest was incubated with β-mercaptoethanol for the normal time, 60min or 30min or in absence, following a 2nd digest with 5 or 10 units of SUMOprotease. 25µl aliquots were loaded onto the gel and stained with Coomassie blue. ^{WT}IGFBP-2+SUMO complex has a MW of 50kDa and ^{WT}IGFBP-2 has a MW of 36kDa. **(D)** This graph shows densitometry measuring change in pure IGFBP-2 concentrations, following different incubation periods (30 or 60min) with or without β-mercaptoethanol, followed by a 2nd digest with 5 or 10 units SUMOprotease (n=2).

7.4.10 Validation of functional ^{WT}IGFBP-2

There are many components in the purification process, which may alter the functionality of the ^{WT}IGFBP-2. Using IGF-I ligand blotting, we confirmed ^{WT}IGFBP-2 retained functional IGF-I domains (Figure 7.16).

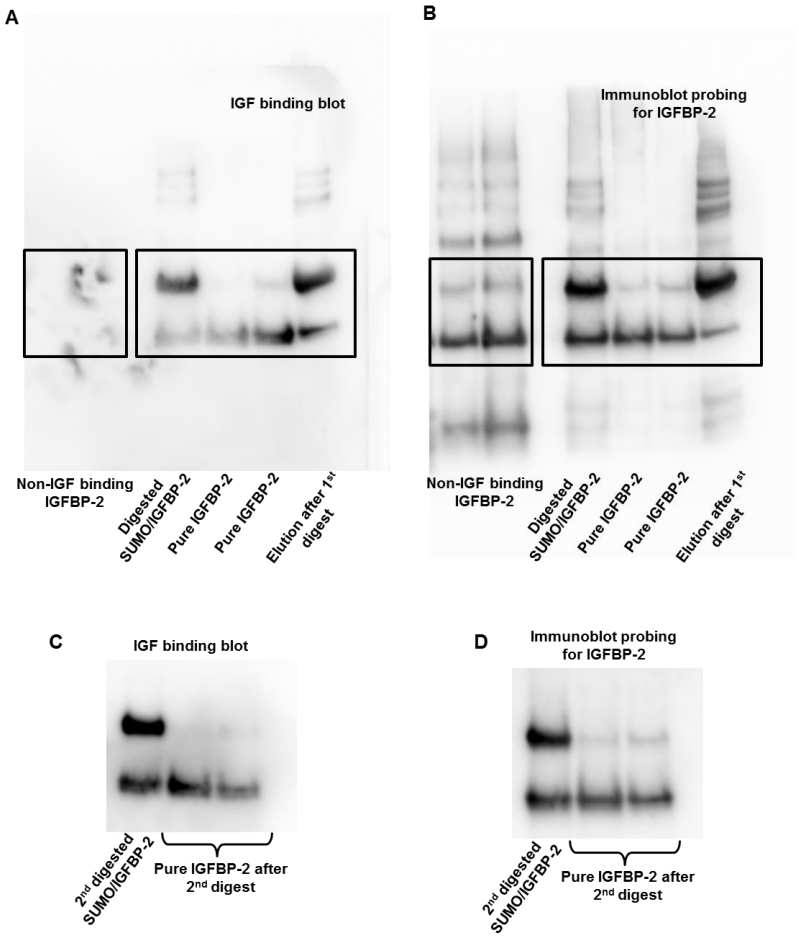

Figure 7.16 ^{WT}IGFBP-2 retains its IGF binding ability through all stages of the purification process

Samples, non-denatured were run using immunoblotting. Membranes were incubated with biotinylated IGF and imaged using streptavidin. Non-IGF binding commercial IGFBP-2 was used as a negative control. 25µl aliquots were taken following the digestion and loaded onto a 4-12% Bis-Tris gel. **(A)** Non-IGF binding IGFBP-2 (50ng/ml (lane 1) and 100ng/ml (lane 2)) was used as the negative control. Digested ^{WT}IGFBP-2+SUMO complex (lane 3), pure ^{WT}IGFBP-2 (lane 4 and 5) and elution following the 1st digest was incubated with the biotinylated IGF-I and visualising the bound IGF-I with streptavidin to confirm IGF-binding functionality in the ^{WT}IGFBP-2+SUMO complex (50kDa) and pure ^{WT}IGFBP-2 (36kDa). **(B)** This blot 7.16A was stripped, checked for residue and probed with goat polyclonal anti-IGFBP-2 (36kDa) showing the presence of IGFBP-2 within the ^{WT}IGFBP-2+SUMO complex (50kDa) and pure ^{WT}IGFBP-2 (36kDa). **(C)** The undigested ^{WT}IGFBP-2+SUMO complex underwent a 2nd digest. The product of the 2nd digest and the pure ^{WT}IGFBP-2 obtained was tested for functional IGF binding domains in the IGFBP-2 containing bands, by incubating the blot with biotinylated IGF-I and streptavidin. **(D)** Blot 7.16D was stripped, checked for residue and probed with goat polyclonal anti-IGFBP-2 (36kDa), showing the presence of IGFBP-2 in the complex (50kDa) following 2nd digest and pure IGFBP-2 (36kDa).

7.4.11 Confirmation of RGD mutant and successful purification

Mutation of the RGD site inhibits all activity mediated via integrin interactions, however IGF and HBD sites will still remain functional. The RGD mutation, C to T was inserted via site-directed mutagenesis. Following transformation, the miniprep DNA product was sent to MRC sequencing unit to confirm the insertion of the correct mutation. Purification was carried out using the optimised steps from Section 7.4.4-7.4.10. Samples taken from different stages of the purification process were run on a Coomassie stained gel to confirm the presence of pure RGD mutant (Figure 7.17).

A

```
RGD MUT     TGCTGGTGTGTGAACCCCAACACCGGGAAGCTGATCCAGGGAGCCCCCAC
            ||||||||||||||||||||||||||||||||||||||||||||||||||
IGFBP2      tgctggtgtgtgaaccccaacaccgggaagctgatccagggagccccCAC

RGD MUT     CATCTGGGGGGGACCCCGAGTGTCATCTCTTCTACAATGAGCAGCAGGAGG
            ||||.||||||||||||||||||||||||||||||||||||||||||||
IGFBP2      catccggggggaccccgagtgtcatctcttctacaatgagcagcaggagg
```

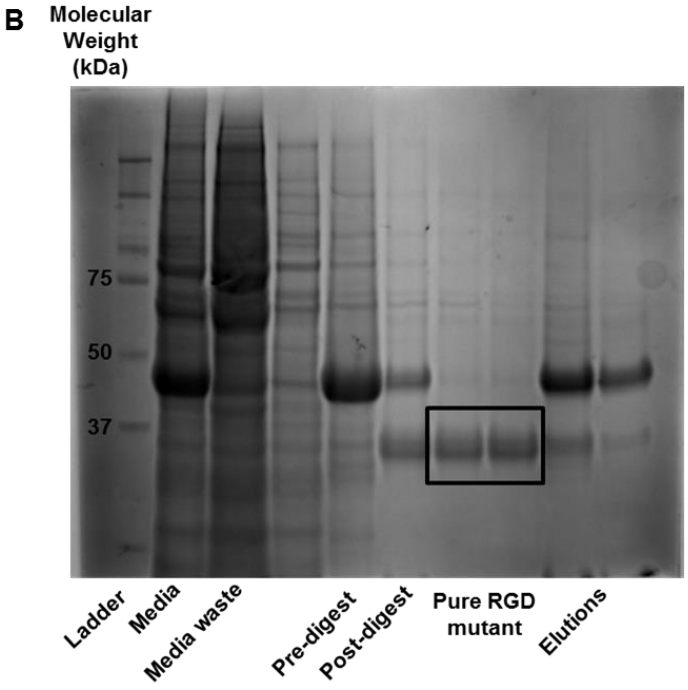

Figure 7.17 Confirmation of RGD mutant
DNA collected from the Miniprep following insertion of the RGD mutation were sent for DNA sequencing. **(A)** Mutant sequence retrieved from MRC PPU was compared with the full IGFBP-2 sequence using Emboss Sequence Alignment Tool highlights the successful change of Cysteine to Thymine. **(B)** End products from each stage of the purification process were visualised using Coomassie staining. 25µl of aliquots taken from each stage were loaded onto a 4-12% Bis-Tris gel, confirming successful digestion and purification of the RGD mutant (outlined, 36kDa) from the ^{RGD}IGFBP-2+SUMO complex (50kDa). Elutions contain the waste and the un-digested ^{RGD}IGFBP-2+SUMO complex (50kDa).

7.4.12 Confirmation of IGF binding mutant and successful purification

The IGF mutation was carried out using a two-step process of site-directed mutagenesis. The first mutation inserted via site-directed mutagenesis was confirmed after retrieving sequencing analysis from MRC sequencing unit (Figure 7.18 A). The mutated DNA was used to undergo another round of site-directed mutagenesis, inserting the remaining mutation. Sequence was clarified after transformation and miniprep (Figure 7.18 B). Purification steps of the IGF mutant following transfection into Expi293 cells were examined using coomassie staining to confirm the retrieval of pure IGF mutant. (Figure 7.18 C).

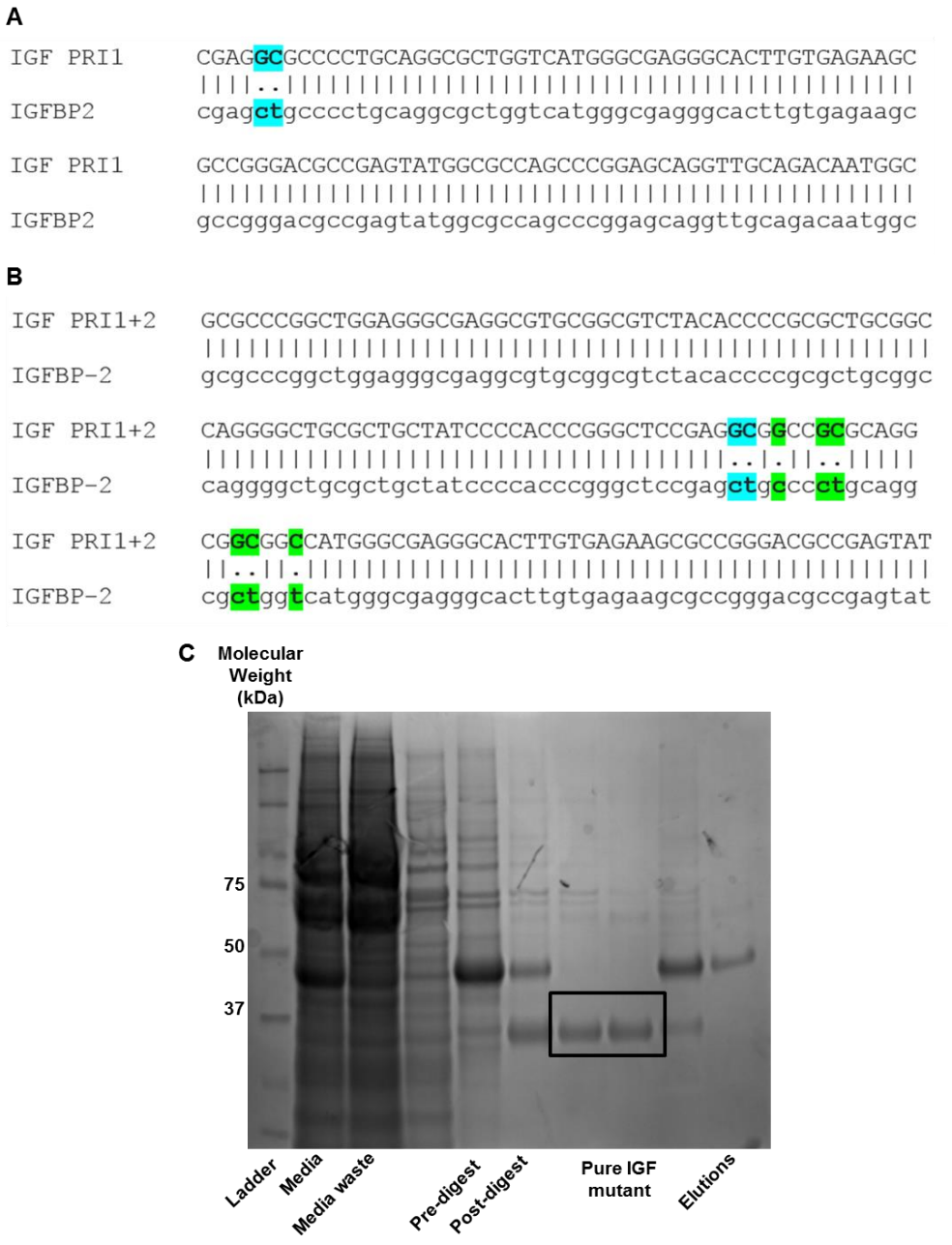

Figure 7.18 Confirmation of IGF mutant
(A) DNA from the Miniprep, following site-directed mutagenesis to insert the IGF binding domain mutation in, was sent to MRC sequencing unit. IGF mutant sequence compared to the full sequence of IGFBP-2 published on NCBI confirms insertion of mutation from primer 1 using EMBOSS Nucleotide Alignment. **(B)** Compared against the full IGFBP-2 sequence, confirmation of the insertion of the remaining nucleotide mutations present using primer 2. **(C)** 25µl samples were loaded onto a 4-12% Bis-Tris gel. Coomassie stain of products from the different purification stages after transfection, post digestion with SUMOprotease (displaying 2 bands, complex (50kDa) and pure IGF mutant (36kDa) and pure IGF mutant (36kDa) was confirmed. Undigested ^{IGF}IGFBP-2+SUMO complex (50kDa) remains in post-digest and in the final elution aliquots.

7.4.13 IGF and RGD mutant binding to IGF-I

IGF-I ligand blots were carried out to validate the functionality of the proteins. Samples from different stages of the purification process were examined for IGF binding potential. The mutant proteins were not denatured before being loaded on to immunoblot gels. Blots were probed with biotinylated IGF-I that bound to recognised IGF-I binding sites and visualised using streptavidin (Figure 7.19). Stripped blots were probed with IGFBP-2 antibody to confirm the mutants were still recognised as IGFBP-2.

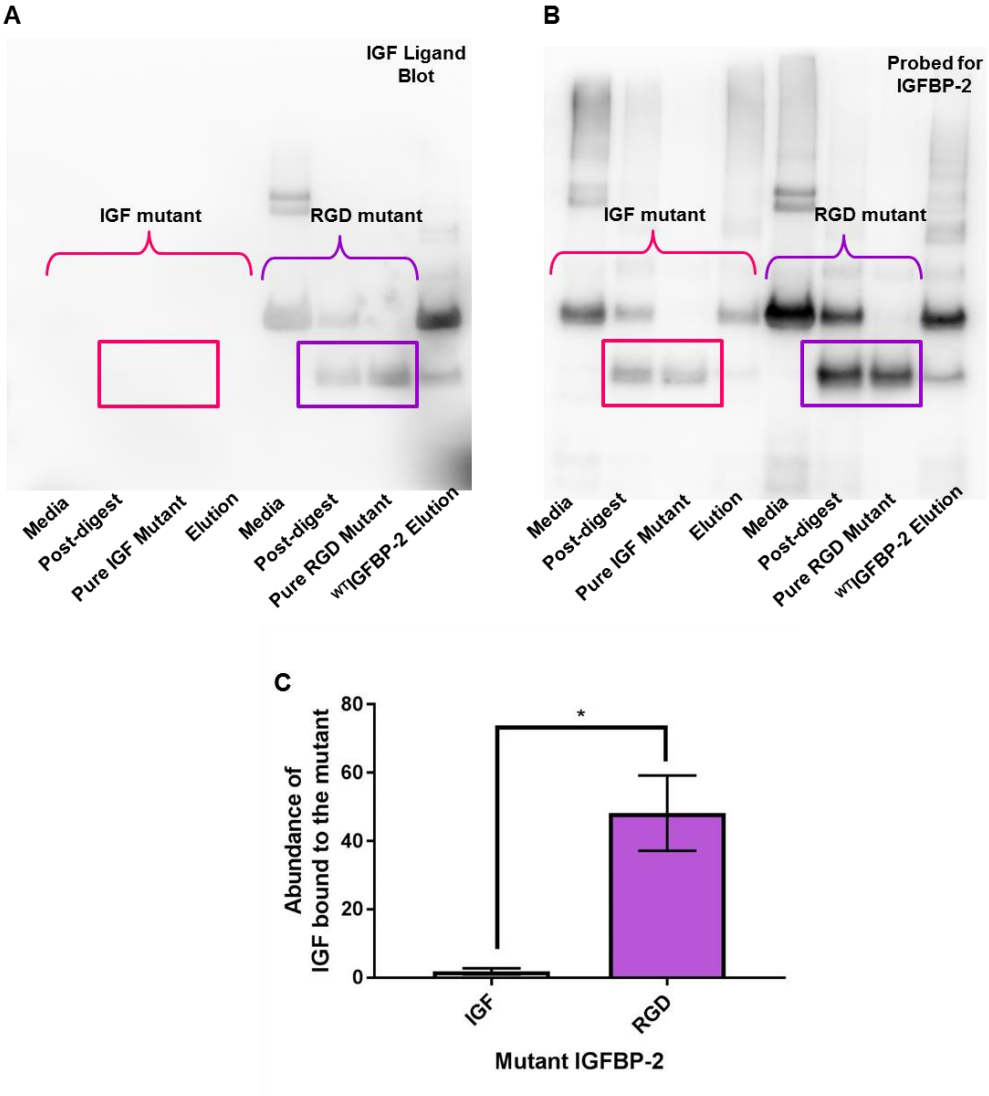

Figure 7.19 IGF mutant fails to bind IGF but RGD retains IGF binding ability
25µl sample loaded onto a 4-12% Bis-Tris gel and the blot was incubated with biotinylated IGF-I and streptavidin. **(A)** IGF binding blot displays the IGF mutant at different stages of the purification process, in the media, post-digest, pure IGF mutant and IGF mutant elution. The RGD mutant was used as a positive control, as it retained full IGF binding ability to biotinylated IGF in the media, post-digest, pure RGD mutant and RGD mutant elution. **(B)** Blots were stripped and then probed with goat polyclonal anti-IGFBP-2. Immunoblotting confirms the presence of the IGF mutants and RGD mutants on the blot by probing for total IGFBP-2 levels. Successful stripping with 2% glycine was confirmed by imaging the blot before probing with IGFBP-2. **(C)** Graphical representation of the densitometry measuring the abundance of biotinylated IGF-I bound to 25µl of the IGF mutant and RGD mutant (*=$p<0.01$, n=3). Error bars represent SEM.

7.4.14 HBD binding mutants

The HBD1/NLS mutant was carried out in two steps, inserting half of the total mutation at a time. After each site-directed mutagenesis step, transformation and miniprep, the DNA was sent for sequencing. The retrieved sequences were compared against the complete IGFBP-2 sequence to validate insertion of the mutation. IGF ligand binding blots were used to validate the IGF binding functionality of the HBD1 mutant at different stages of the purification process. The blot was then stripped and probed for IGFBP-2 to observe the IGFBP-2 antibody still recognised the mutant as IGFBP-2 (Figure 7.20).

Unfortunately, site-directed mutagenesis of the HBD2 mutation into ^{WT}IGFBP-2 was not successful. Positive colonies were not formed following transformation. Further attempts to mutate this site were halted due to time limitations.

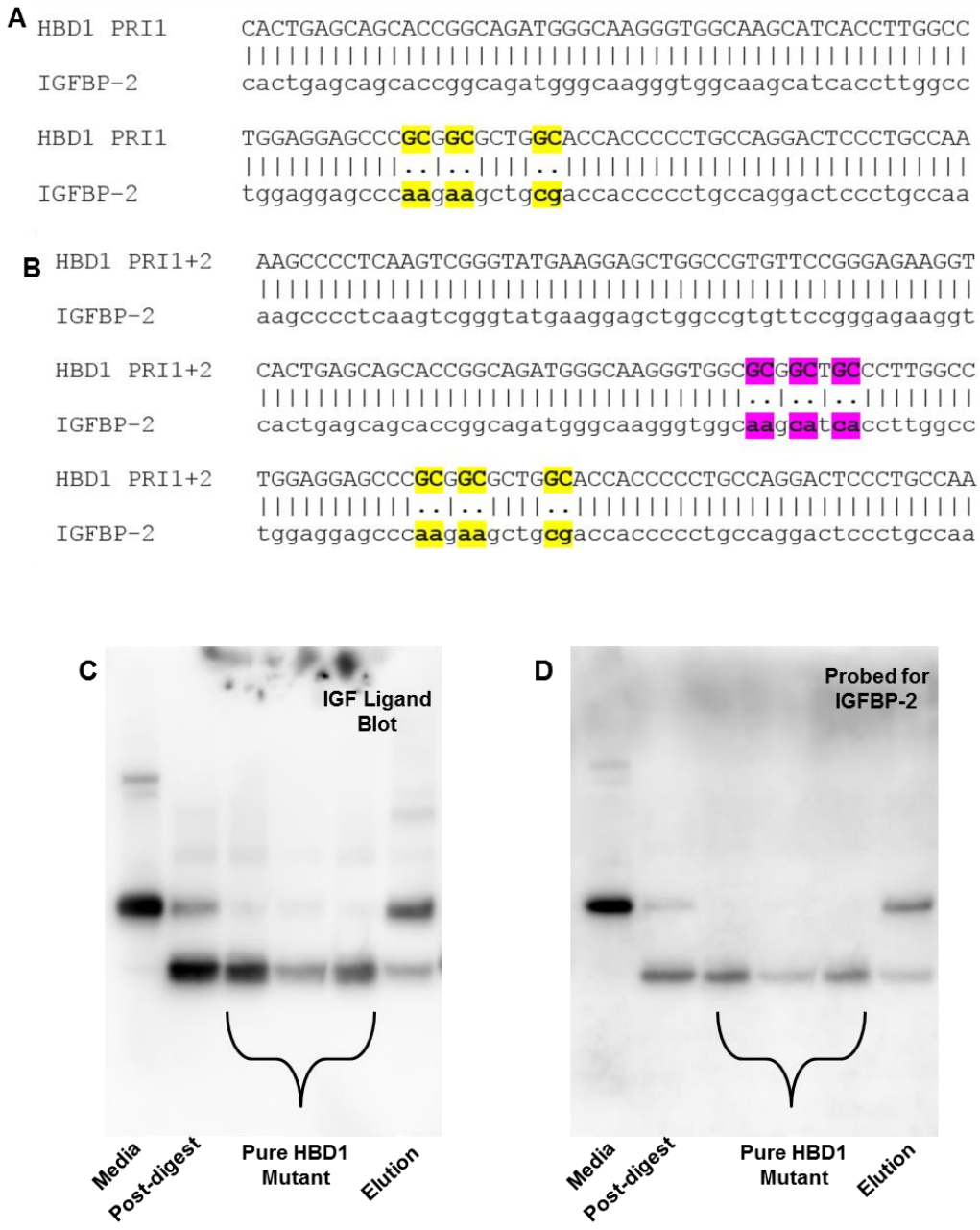

Figure 7.20 Confirmation of the HBD1 mutant
DNA was collected following the Miniprep after site-directed mutagenesis and sent for DNA sequencing. EMBOSS Nucleotide Alignment compares the mutated sequence to complete IGFBP-2 sequence published and confirms successful insertion of the mutation using primer 1 **(A)** and the complete mutation with the addition of primer 2 **(B)**, without affecting the remaining IGFBP-2 sequence. **(C)** 25µl of samples were loaded onto a 4-12% Bis-Tris gel and probed for IGF-binding functionality in the aliquots collected during the purification process of the HBD1 mutant, from the media, post-digest, pure HBD1 mutant and elution. **(D)** The IGF-I binding blot was stripped and probed with goat polyclonal anti-IGFBP-2, confirming the presence of IGFBP-2 in the different steps of the purification process to purify the HBD1 mutant variant. Stripping before probing for IGFBP-2 was carried out using 2% glycine and successful stripping was confirmed by imaging the blot again.

7.4.15 Purification of contaminated HBD1 mutant

Protein purification was carried out using the optimised steps in Chapter 7. However, these steps needed optimising for the HBD mutant as excess HBD1 IGFBP-2/pM-SUMOstar complex was leaking into pure mutant flow through (Figure 7.21). Imidazole concentrations were lowered during the final purification process to optimise the yield of pure HBD1 mutant. Samples from different stages of the purification process were analysed to observe the effect of changing imidazole concentrations (Figure 7.22).

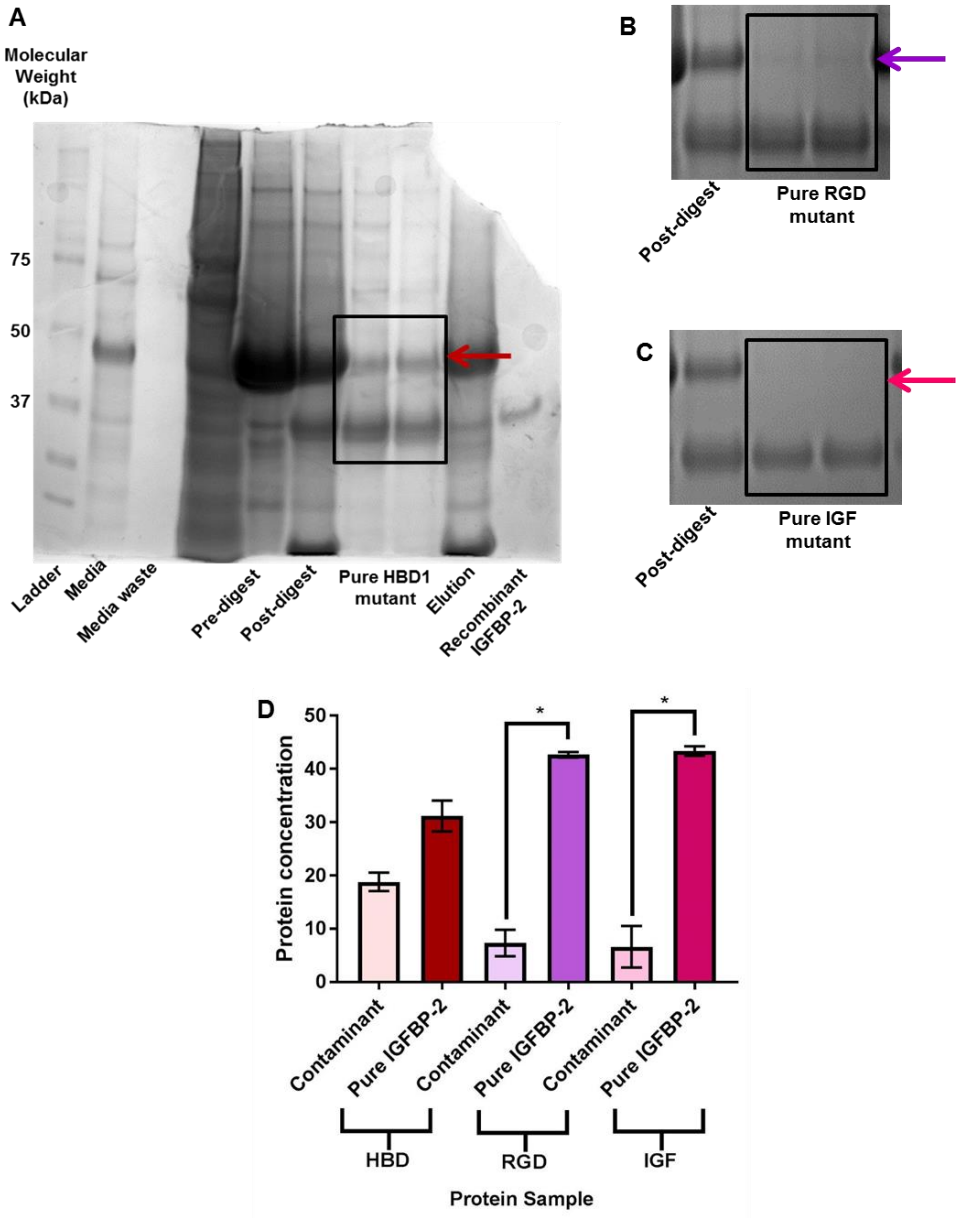

Figure 7.21 Pure HBD1 is contaminated when using the same purification conditions as the IGF and RGD mutant
25µl of sample was loaded onto a 4-12% Bis-Tris gel from different stages of the purification process. **(A)** Coomassie stain visualises the products from different stages of the purification process of the HBD1 mutant. The red arrow depicts contamination of the undigested SUMO/HBD1 mutant complex within the pure HBD1. **(B&C)** Coomassie stains of from the purification of the RGD and IGF mutant depict no contamination from the undigested complex in the pure IGFBP-2 mutant samples. **(D)** Graphical representation of the densitometry of the bands from 7.21A, B and C, measured using Genetools, of the coomassie stained gels highlight the contamination of the SUMO/HBD1 mutant complex in comparison to absence of contamination in the pure RGD and IGF mutant products (*=$p<0.01$, n=3). Error bars show SEM.

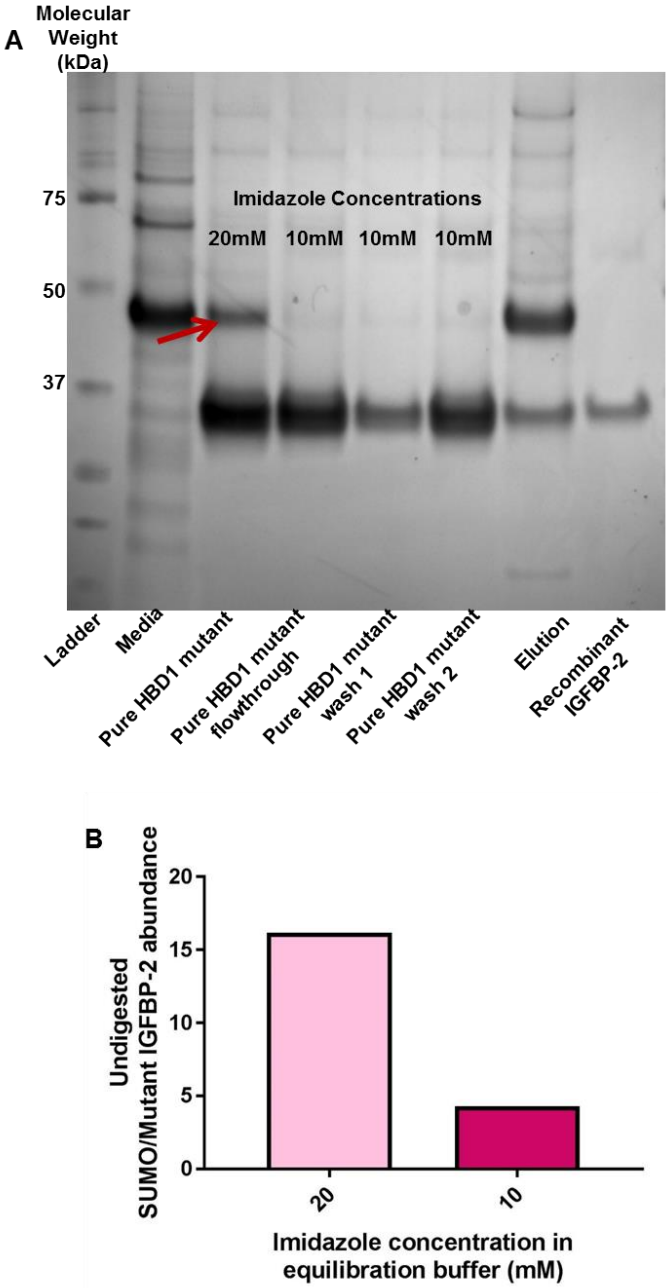

Figure 7.22 Reducing imidazole concentration achieves non-contaminated HBD1 mutant

25µl of sample was loaded onto a 4-12% Bis-Tris gel from each stage of the protein purification process. **(A)** Purification end products, from media, containing the complex (50kDa) (lane 2), pure HBD2 mutant, using 20mM imidazole wash buffer (lane 3), pure HBD1 mutant flow through (lane 4), 1st and 2nd wash (lane 5 and 6), using 10mM imidazole wash buffer, elution (lane 7) and recombinant IGFBP-2 (36kDa) as a positive control. The gel was stained with Coomassie blue. The arrow highlights the contaminant present when using 20mM imidazole for final washes. When reduced to 10mM imidazole, the contaminant is absent in the final flowthrough and all further washes. Undigested complex still appears in the elution. **(B)** Densitometry measured using Genetools, highlights the change in the abundance of undigested SUMO/HBD1 mutant contaminating the sample using 20mM imidazole wash buffer and 10mM wash buffer (n=2).

7.5 Discussion

7.5.1 ^{WT}IGFBP-2, RGD, IGF and HBD1/NLS molecular size and mutant sequences verified against published hIGFBP-2 sequence data

The expected MW of the IGFBP-2 was checked throughout the cloning and expression process, ensuring it was correct before moving forward. The MW was confirmed after Phusion PCR, providing an expected molecular size of 898bp. Once transfected and purified, the ^{WT}IGFBP-2/pM-secSUMOstar plasmid was presented at a 50kDa and purified IGFBP-2 appeared at approximately 36kDa, matching IGFBP-2s published MW. As all the mutations were missense in the three mutants, the MW of the plasmid or pure protein did not differ from ^{WT}IGFBP-2. We can confirm post-translational modifications that may have occurred have not affected the MW or the nucleotide sequence compared to the complete published IGFBP-2 information. However, we would have to carry out further examination into post-translational modifications that may have occurred which could alter the affinity of binding and the full activity of IGFBP-2. Immunoprecipitation and western blotting could be used to identify post-translational modifications which may have occurred during production of these mutants.

The sequences retrieved from MRC Sequencing Unit confirmed that ^{WT}IGFBP-2 displayed complete alignment with the published NCBI sequence of hIGFBP-2 (GenBank: AAH71967.1). Any misread mutations that appeared were verified as mistakes using the chromatogram. This may occur due to two peaks being read very close to each other, which can often misalign the remaining sequence. However, misreading usually takes place at the beginning or end of the sequence. The sequences were also read forwards and in reverse, via the T7 forward primer or the BGH reverse primer (resulting in the sequence being reverse complemented). The forward and reverse sequences were compared for mistakes as a true non-specific mutation would be present in both sequences.

The insertion of the mutations was also verified using pairwise nucleotide alignment. Except for the mutated area, the remaining sequence completely aligned with the published IGFBP-2 sequence.

7.5.2 ^{WT}IGFBP-2, RGD, HBD retained full IGF binding potential except the IGF mutant

The functionality of the proteins produced was tested via IGF ligand blots, which has become a common method of testing IGFBPs (Rosenzweig, 2004). We confirmed all

IGFBP-2 variants except the IGF mutant bound to biotinylated IGF-I throughout the purification stages. This was supported by the confirmation of the full IGF binding sequence being present in the earlier sequences. The mutation at the N terminal IGF binding site eliminated all binding to the biotinylated IGF-I, confirming that both IGF binding sites are involved in the sequestering of IGF molecules.

7.5.3 Ammonium sulphate precipitation reduced the yield of protein obtained

As mentioned previously, ammonium sulphate precipitation is a common salt precipitation process used due to its rapid precipitation of a large yield of protein, condensing it into a small workable volume (Wingfield, 1998). We cannot confirm the salting out process does have negative effects on the IGFBP-2 protein. However, we believe ^{WT}IGFBP-2 was lost when collecting the floating pellets which contained the protein at the end of the technique.

The use of the concentrating columns to reduce the media to a workable volume enhanced the yield of ^{WT}IGFBP-2 slightly compared to the yield obtained with ammonium sulphate precipitation. Concentrating columns would not result in the same purity of the protein as obtained by ammonium sulphate, however the 100kDa cut off point ensures larger molecules present in the media are removed. The remaining components in the protein mixture would be eliminated via the use of the hispur column in a later stage of the purification process which would only bind the ^{WT}IGFBP-2/pM-secSUMOstar complex.

7.5.4 Altering imidazole concentration in equilibration buffer enhances the obtained yield

Imidazole in the purification buffers contributes to the purification of the protein in the end product. Imidazole has a histidine ring, which can bind to the free spaces on the hispur column. However, it is important to note it doesn't compete with the pM-secSUMOstar at low concentrations as the his6 tag has an increased affinity in comparison to imidazole. Initially, the use of 10mM imidazole resulted in ^{WT}IGFBP-2, RGD and IGF mutant protein sticking to the column. This suggests there were still free areas on the hispur column causing non-specific binding. With an increased concentration of 20mM imidazole, we obtained an increased yield of IGFBP-2 with a significantly smaller amount of pure IGFBP-2 remaining in the final elution of everything in the column.

Further washes with the equilibration buffer also increased overall yield of the pure IGFBP-2 obtained as more IGFBP-2 was isolated following every wash. This suggests IGFBP-2 is able to non-specifically bind to the hispur column quite strongly. Increasing the concentration of imidazole to 40mM resulted in the IGFBP-2/pM-secSUMOstar contaminating the pure fraction. It is difficult to identify why all of IGFBP-2 is not eluted in the first flow through. We would need to assess the structure of IGFBP-2 and understand how IGFBP-2 is interacting with the column to optimise this step.

Interestingly, the HBD mutant was the only mutant not to yield pure IGFBP-2 with 20mM imidazole. Some of the undigested HBD/pM-secSUMOstar complex also came through in the initial flow through that should only contain pure HBD mutant. This highlighted the concentration of 20mM imidazole was acting competitively against the binding of the his6 tag of the vector to the column. When reduced to 10mM imidazole, a pure HBD mutant sample was obtained. This may suggest a possible post-translational modification which could have affected the protein folding, however this could only be confirmed via further proteomic studies.

7.5.5 SUMOprotease failed to cleave 100% of the ^{WT}IGFBP-2/SUMO protein

Publications have reported the use of SUMOprotease to promote cleavage is an easy and efficient mechanism to obtain clear separation of the vector and pure protein (Lee et al., 2008). As observed throughout the purification process, a large amount of the complex remains undigested by SUMOprotease. We attempted to carry out a double digest by incubating the initial elution with the undigested complex with SUMOprotease again, however the concentration of SUMOprotease was increased above the recommended units.

Interestingly, the double digest did reduce the concentration of the complex, however the abundance of IGFBP-2 or SUMO vector alone did not increase as much. Also the addition of increased concentrations of the SUMOprotease did not enhance the digestion of the complex. Although the sequence of the end of the vector and the N-terminal of IGFBP-2 were correct, post-translational modifications may have taken place at this region, affecting the cleavage. This can only be confirmed via structural analysis using techniques such as X-ray crystallography or nuclear magnetic resonance (NMR) (Andrec et al., 2007).

β-mercaptoethanol is a compound used to reduce the disulphide bonds between the protein and vector, priming the complex for successful cleavage. However, as

mentioned in the introduction, IGFBP-2 retains 12 conserved cysteine molecules which all form disulphide bonds (Baxter, 2000). The β-mercaptoethanol may also affect these bonds as they are closely located to the cleavage site and as a result affecting the overall cleavage. In the absence of incubation with β-mercaptoethanol, the yield of pure ^{WT}IGFBP-2 slightly increased. Therefore, this incubation step was removed for following generation of the ^{WT}IGFBP-2 and its mutants.

7.5.6 Study limitations

Size exclusion chromatography was attempted to purify the proteins further as a few non-specific bands were noted on coomassie stains. However, we were unable to achieve successful separation of the markers or the protein according to molecular size. Due to time constraints, this could not be optimised further.

Ideally, the mutants would have been validated in more detail than sequencing and IGF ligand blots. The individual mutations of the domains should be clarified to support the sequence data. We also cannot be sure that post-translational modifications have not taken place affecting a part of the protein that has not been verified. Heparin binding assays should have been used to confirm the loss of heparin binding function in the middle domain. Integrin binding potential could be clarified through functional assays.

Structure of the protein should have been assessed to ensure the secondary structure of IGFBP-2 was maintained. Circular dichroism spectra or crystallisation techniques such as X-ray crystallography could have used to determine any changes in protein folding or secondary structure that may have occurred (Greenfield, 2006). Unfortunately, due to funding and time constraints, we were unable to validate this.

The inability to achieve complete cleavage of the ^{WT}IGFBP-2/pM-secSUMOstar suggests a post-translational modification, which may have altered the cleavage site. We cannot be certain of this unless the secondary structure has been analysed. However, this problem has resulted in a lower yield of the protein than expected.

Unfortunately, we were unable to obtain successful transformation of the HBD2 mutant on multiple attempts. Due to time restraints, we were unable to optimise the generation of this mutant further.

7.6 Concluding remarks

This chapter describes experiments carried out to generate, purify and test the function of mutant variants of IGFBP-2, in order to ensure they have maintained their expected functionality.

Except for the inserted mutation, the sequences of ^{WT}IGFBP-2 and its mutant variants completely aligned the published complete sequence of hIGFBP-2 (GenBank: AAH71967.1). The ^{WT}IGFBP-2, RGD and HBD variants all retained full IGF binding potential as confirmed by IGF ligand blotting. The IGF mutant, as expected fail to display IGF binding capabilities.

Obtaining a pure yield of IGFBP-2 was optimised for each individual IGFBP-2 variant by altering concentrations of imidazole in the buffer. The HBD mutant was the only mutant which resulted in a weaker interaction with the column, and therefore required a lower concentration of imidazole for elution.

Unsuccessful cleavage of the SUMO vector from the pure protein remains a problem unsolved. Double digesting did reduce the amount, however other methods of exploring the structure of the cleavage region should be interrogated further.

Although the recombinant protein and the mutants were verified through sequence checks and IGF binding potential, more validation is required to confirm the RGD and HBD mutations are functional. Due to the issues during the purification of the protein, it is essential we use structural analysis techniques such as X-ray crystallography to confirm no post-translational modifications have altered the structure. The biological functionality of these variants will be tested in the series of experiments described in the next chapter, to observe if they mimic the responses of commercially sourced recombinant IGFBP-2 in *in vitro* angiogenic signalling and the assays (Chapter 5 and 6).

Chapter 8 - Influence of mutant IGFBP-2 variants on *in vitro* angiogenic signalling and properties in endothelial cells

8.1 Background

In the previous Chapters, 4, 5 and 6, we have shown through *in vivo* and *in vitro* means that IGFBP-2 does display potential in angiogenesis and promotes angiogenic mechanisms in endothelial cells. However, many publications have highlighted certain IGFBP-2 domains (e.g. RGD site and HBDs) determine IGFBP-2s activity (Mendes et al., 2010; Ross & Gericke, 2009). Some publications have created peptides of the domains to enhance angiogenic responses driven by those domains in particular (Xi et al., 2014). Therefore, identification of the key interaction involved will enable to exploit this interaction alone therapeutically, providing a more specific modulation of the therapeutic angiogenesis treatment to PAD.

In Chapter 7, we validated the insertion of the mutations of the RGD, HBD/NLS and IGF domains into IGFBP-2 and confirmed, as expected, all except the IGF mutant retained complete IGF binding potential. In this chapter, these validated mutant variants will be used to determine which domains are responsible for the effect of IGFBP-2 in signalling (Chapter 5) and fundamental assays (Chapter 6) (Figure 8.1). As an additional experiment, we have also observed the effect IGFBP-2 and its mutants may have on vascular permeability compared to the endothelial cell hyperpermeable responses exerted by VEGF (Kumar et al., 2009). The importance of maintaining vascular permeability will be discussed below in Section 8.1.4.

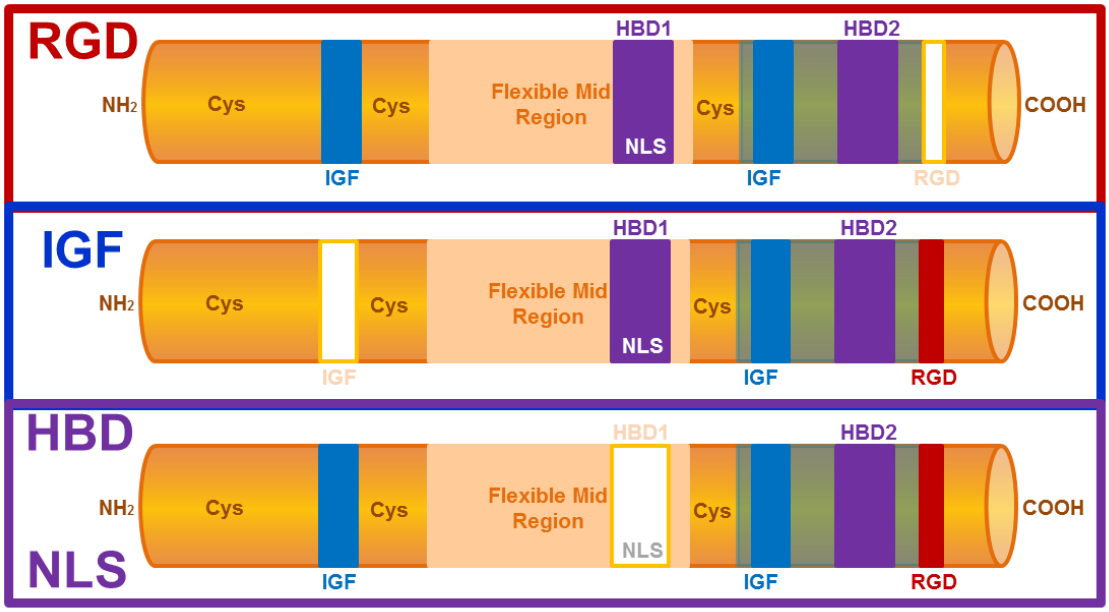

Figure 8.1 Location of IGFBP-2 mutations
Representative visualisation of IGFBP-2 structure with the location of the mutations for each mutant variant mutated in a white colour. IGFBP-2's RGD mutation is at the C terminal end of the protein. The IGF mutant is located on the N-terminus. The HBD1/NLS mutation is located within the flexible mid-region. Adapted from (Yau et al., 2015b).

8.1.1 RGD mutant

The majority of publications discussing IGFBP-2 induced cell migration have reported integrin interactions, specifically with α5 and β1 are responsible for JNK and ERK mediated activation of the MAPK pathway (Han et al., 2014; Wang et al., 2017c). This proposed mechanism has been verified using IGFBP-2 consisting of a non-functional RGD site. Although, we substituted the arginine (R) site to tryptophan (W) to mutate the integrin site, another common RGD mutation incorporates substitution of aspartic acid (D) with glutamic acid (E).

Over-expression of the RGE mutant in neuroblastoma cells increased integrin-ECM interaction, potently enhancing cell migration, proliferation and invasion (Russo et al., 2005). The RGE mutant also presented the same survival activity in hematopoietic stem cells as the ^{WT}IGFBP-2 (Huynh et al., 2011). Therefore, this suggests the RGD domain may not be responsible for IGFBP-2-stimulated promotion of these mechanisms. Contrastingly, GK Wang et al., (2006), highlighted the RGE mutant failed to induce glioma cell motility due to a reduced abundance of lamellipodia presented by cells. This was validated by the non-functional RGD disrupting the activation of the ERK/MAPK, and Akt/PI3K signalling pathways (Holmes et al., 2012).

The effect of the RGD mutant could vary between different cell types and therefore may display a different phenotype in vascular endothelial cells.

8.1.2 IGF binding mutant

Creating a non-functional IGF binding domain within IGFBP-2 has proven to be the most interesting mutant. All IGFBP's were first established to primarily function through IGFs, however IGFBP-2 has multiple IGF-independent domains which may have more influence over enhancing angiogenic mechanisms. The majority of publications discussing IGFBP-2s potential in angiogenesis refer more to IGF-independent mechanisms rather than IGF-dependent mechanisms, suggesting IGF driven activity is not as prominent via this binding protein.

IGF binding activity of IGFBP-2 plays an essential role in differentiation of osteoclasts. IGF-independent domains are unable to compensate for the lack of differentiation displayed by the non-IGF binding domain, to the level of differentiation induced by fully functional IGFBP-2. Interestingly, the IGF mutant supresses PTEN activity, similarly to ^{WT}IGFBP-2, suggesting IGF-independent domains modulate PTEN activation. It has been highlighted there may be interplay between the IGF binding domain and the other domains. A functional IGF domain requires a functional HBD in addition to elevate osteoclast differentiation, to a level induced by ^{WT}IGFBP-2, via activation of the PI3K/Akt pathway (Demambro et al., 2012).

This finding was supported by further published research. The non-IGF binding IGFBP-2 reduced the phosphorylation activity of RPTPβ, however a variant with the HBD1 site mutated with a functional IGF binding site had no effect on the phosphatase capabilities of RPTPβ. ^{WT}IGFBP-2 enhances RPTPβ phosphorylation and therefore highlighting both a functional IGF and HBD are required to replicate the ^{WT}IGFBP-2 induced effect (Shen et al., 2012).

8.1.3 HBD1/NLS mutant

Shen et al., (2012), confirmed the HBD1 IGFBP-2 mutant can interact via RPTPβ, whereas the HBD2 present on the C terminal cannot, highlighting both HBDs have significantly different roles. Non-functional HBD1's failure to activate RPTPβ has been established to also contribute to downstream PTEN levels. HBD1's suppression of PTEN is an essential modulator of osteoclast formation and differentiation, through regulation of Akt phosphorylation (Demambro et al., 2012).

Although less potent than HBD2, this central HBD1 and NLS domain has been shown to also suppress preadipocyte differentiation and proliferation by generating mutants of both of these regions (Xi et al., 2013).

Mutation of the HBD and NLS in the variable region also failed to induce migration and invasion of WT-SHEP cells, whereas ^{WT}IGFBP-2 enhanced these activities (Azar et al., 2014).

Mutation of the NLS sequence prevents nuclear translocation of IGFBP-2 via importin α (Azar et al., 2014; Chelsky et al., 1989). Therefore, as hypothesised, if IGFBP-2 activates VEGF via its NLS, and IGFBP-2 stimulated angiogenesis functions through VEGF activation, the NLS mutant would abolish all IGFBP-2s angiogenic potential. From current published literature, it is clear this central region encapsulating the HBD1 and NLS interactions is vital for differentiation and motility of essential cell types.

8.1.4 VE-cadherin in vascular permeability

Permeability is a crucial component of successful angiogenesis as weak blood vessels will be unable to withstand the pressure and cause leakages within the circulatory system. As observed in many *in vitro* studies and clinical phase trials using VEGF as an angiogenic stimulus results in an excessive leakiness due to the induction of a hyperpermeable state (Ved et al., 2017). Vascular permeability is determined by adheren junctions. These junctions mediate cell-cell adhesion through transmembrane proteins called cadherins. VE-cadherin is the most prominent cadherin that regulates adhesion between endothelial cells and therefore is key during angiogenesis. VEGF creates a hyperpermeable state by disrupting the function of VE-cadherin, resulting in poor adhesion between endothelial cells (Gavard & Gutkind, 2006).

As IGFBP-2 has been reported to promote angiogenesis by increasing expression of VEGF, it is crucial we are able to show that IGFBP-2 does not cause hyperpermeability as a potential therapeutic (Das et al., 2013). However, it is important IGFBP-2 can maintain permeability at a regular level. IGFBP-2 has recently been shown to enhance adhesion between endothelial progenitor cells to HUVECs via its RGD domain, displaying the opposite effect to VEGF (Feng et al., 2015). However, we need to investigate the effect IGFBP-2 and its mutants may have on VE-cadherin.

8.1.5 Summary

The individual domains we have mutated within IGFBP-2 have been reported to effect cell differentiation, migration, proliferation and permeability, possibly in combination with each other via integrin activation, PI3K/Akt, MAPK, nuclear transport or RPTPβ activation. The mutants will help us identify which domain is critical to promoting *in vitro* endothelial cell adhesion, migration, proliferation and vascular permeability. Identification of the predominant mechanism IGFBP-2 functions through to enhance angiogenic properties will enable the creation of a more specific and targeting therapeutic angiogenesis treatment to direct the angiogenic responses to treat ischemia.

8.2 Aim and Hypothesis

In this chapter, we have two main aims. Firstly, to determine the effect the IGFBP-2 mutants (RGD, IGF and HBD1/NLS) may have on pro-angiogenic signalling and pro-angiogenic *in vitro* angiogenic assays investigated in HUVECs in Chapter 5 and 6. Inhibitors were also used to identify the pathways responsible for IGFBP-2s enhancement in por-angiogenic functional assays. Secondly, to determine the effect IGFBP-2 may have on vascular permeability using *in vitro* methods to assess changes in endothelial cell barrier function and cell-cell junctions.

The chapter objectives we aim to target are:

- Investigate the effect of IGFBP-2 variants on angiogenic signalling pathways in HUVECs.
- Determine the angiogenic potential of IGFBP-2 and its mutant variants using *in vitro* angiogenic assays in HUVECs.
- Confirm the signalling pathways responsible for the enhancement in angiogenic mechanisms we see, using signalling inhibitors
- Investigate the effect of IGFBP-2 and its mutant variants on vascular permeability.

8.3 Method

8.3.1 Angiogenic Signalling and Assays

The HUVEC culture and immunoblotting methods used for signalling have been stated in the General Methods (Chapter 3.1-3.3). Cell adhesion, scratch wound and tube formation protocols were used from Chapter 6.

HUVECs were serum-starved for 2 hours before stimulation for signalling pathways only (Chapter 5.3.3). They were stimulated with 500ng/ml ^{WT}IGFBP-2 of 500ng/ml IGFBP-2 mutant (H = HBD1/NLS, I = IGF, R =RGD) for all signalling and angiogenic assays.

In the tube forming assay, fluorescein-5-isotheiocyanate (fitC) (EMD Milipore, 1.24546) was diluted into a sodium chloride solution (0.145M in 100ml). 2.5µg/ml was added to the media prior to the incubation to stain cells.

8.3.2 Use of Akt and MAPK inhibitors

Inhibitors were used in functional tube forming assays to confirm which pathway was responsible.

8.3.2.1 Signalling

Confluent HUVECs were incubated with 10µM Akt inhibitor (Calbiochem, MK-2206) for 30 mins. 500ng/ml ^{WT}IGFBP-2 or mutants were added to cells for 10 mins. Cells were cultured, lysed and collected for immunoblotting using the protocol in Chapter 3.1, 3.2 and 3.3)

8.3.2.2 Assays

Akt (10µM) or (10µM) p38MAPK (Calbiochem, SB 203580) competitive inhibitors were added to conditioned media at the beginning of scratch wound and tube formation assays with 500ng/ml ^{WT}IGFBP-2 or mutants.

8.3.3 Cytodex bead assay

Adapted from Nakatsu et al., (2007). HUVECs were grown in EGM-2 (Lonza, CC-26-6) (+ ECGM-2 BulletKit (Lonza, CC-3162). HUVECs were incubated with cytodex-3 beads (Amersham, 17-0485-01) in a 37ºC/5% CO_2 incubator and agitated every 20 mins for 4 hours. Cells were left to adhere to the beads overnight.

Beads were washed with EGM-2 media twice to remove any non-adhered cells. The adhered cells and beads were resuspended in filter sterilised 2mg/ml fibrinogen (Sigma-Aldrich, F8630) (diluted in PBS, pH 7.4), 0.15 Units/ml aprotinin (Sigma, Aldrich, A-1153), 5ng/ml VEGF and 5ng/ml FGF solution. The mixture (300µl in total volume) was pipetted into wells of an 8-well glass bottom treated IBIDI plate and store in a cell culture incubator. Beads were incubated in conditioned media with the basal control being 2% serum media, 500ng/ml ^{WT}IGFBP-2 and 500ng/ml RGD mutant. After 24 hours, cells were imaged at a 10x magnification using an optical microscope.

8.3.4 Cytodex bead assay immunofluorescent staining

Cells were fixed using 4% paraformaldehyde (PFA) (Sigma-Aldrich, 30525-89-4) for 20 mins at room temperature and then washed 3 times with PBS, pH 7.4, for 1 min each time. 1ml 0.5% triton X-100 (v/v) (Sigma-Aldrich, T9284) was added to the well for 10 mins at room temperature to permeabilise the cell membranes. The cells were washed with 3x PBS pH 7.4, followed by a final incubation with fresh PBS, pH 7.4, for 30 mins. Cells were blocked with 1% BSA/PBS solution for 30 min. After washing the blocking solution with 3 washes of PBS, pH 7.4, cells were incubated with 1% rhodamine phallodin (Thermo Fisher, R415) (diluted in PBS (1:100)) for 1 hour at room temperature. Cells were washed 3 times again and kept in PBS, pH 7.4, ready for imaging. Images were taken using a Zeiss LSM700 confocal microscope. Z stack images were captured at a 20x magnification using the red laser.

8.3.5 Cell Barrier Quality

This experiment was carried out the University of Nottingham in Professor David Bates laboratory, under the supervision of Dr Andrew Benest.

Electric Cell-substrate Impedance Sensing (ECIS) was used to quantify the barrier formed by endothelial cell monolayer. HUVECs were seeded onto electrode array plates (8W10E PET, Applied Biophysics) until 100% confluence was reached in 10% fetal calf serum (FCS) supplemented media (C-22220, Promocell) with the addition of endothelial cell growth media supplement pack (C-39220, Promocell). IGFBP-2 (500ng/ml), the mutants (500ng/ml) or VEGF (30ng/ml) were added to condition the basal media (5% serum). Arrays were placed on array holder and ECIS software was used to collect readings. Readings were taken every 60 seconds at 4000Hz. Resistance data against the endothelial cell barrier was collected by the ECIS software.

8.3.6 Vascular permeability Immunofluorescent staining

This experiment was carried out the University of Nottingham in Professor David Bates laboratory, under the supervision of Dr Andrew Benest.

HUVECs were plated onto IBIDI treated 8 well glass bottom plates in 10% FCS supplemented media plus endothelial cell growth factor supplement and incubated until a 100% confluent state had been obtained. Cell media was changed and supplemented with IGFBP-2 (500ng/ml), the mutants (500ng/ml) or VEGF (Promocell, C-64423) (30ng/ml) for 48 hours. The cell monolayer was washed with PBS, pH 7.4, following fixation of cells using 2% PFA for 30 mins. Surface was washed again with PBS, pH 7.4, followed by a wash with 0.5% PBLEC (PBS (pH 6.8) with the addition of 1M $MgCl_2$, 1M $CaCl_2$, 1M $MnCl_2$, 10% Triton X-100). 1% BSA (A7906, Sigma Aldrich)/PBLEC was used as a blocking agent for 1 hour at room temperature. The primary antibody VE-Cadherin (ab7047, Abcam) (1:200 dilution in 1% BSA/PBLEC) was incubated in the plates overnight at 4ºC. Following 3 washes with 0.5% PBLEC, incubation with the Alexa Fluor 488 donkey anti-mouse IgG (A21202, Thermo Fisher) (1:500 dilution in 1% BSA/PBLEC) was carried out at room temperature for 2 hours. Phalloidin 680 (21839, Thermo Fisher) (1:500 dilution) and DAPI (62248, Thermo Fisher) (1:1000 dilution) was also added at the same conjugate incubation stage. Cells were washed with 0.5% PBLEC and imaged using confocal microscopy (Zeiss, LSM 880). Green, blue and red filters were used to capture single images at a 10x and 20x magnification.

8.3.7 Data analysis

GeneTools was used to perform densitometry analysis of the bands on each western blot. ImageJ Cell Counter tool was used to count the number of cells in each image for the cell adhesion assay. ImageJ Area tool was used to measure the area between scratch wounds using the gridded plate. Incucyte Zoom Wound Closure Review Tool was used to measure images taken using the Incucyte for the scratch wound assay. Image J Cell Counter tool was used to count the number of meshes in a pre-determined area. Image J Cell counter was used to count sprouts in the angiogenic bead assay. Unpaired t-tests were used to test for significance. Error bars represent SEM.

8.4 Results

8.4.1 Mutant stimulated Akt and p44/42 MAPK phosphorylation

We have shown in Chapter 5, complete functional IGFBP-2 significantly enhanced Akt and MAPK phosphorylation. ^{WT}IGFBP-2 and the HBD and IGF mutants significantly enhanced Akt phosphorylation compared to the basal control. However, the RGD mutant prevented phosphorylation of Akt, back to the basal level of (Figure 8.2 A).

^{WT}IGFBP-2 significantly elevated p44/42 MAPK phosphorylation compared to the serum free control, replicating the effect of commercially sourced IGFBP-2 in Chapter 5. However, the HBD, IGF and RGD mutant failed to display a significant enhancement in p44/42 MAPK phosphorylation compared to the vehicle control (Figure 8.2 B).

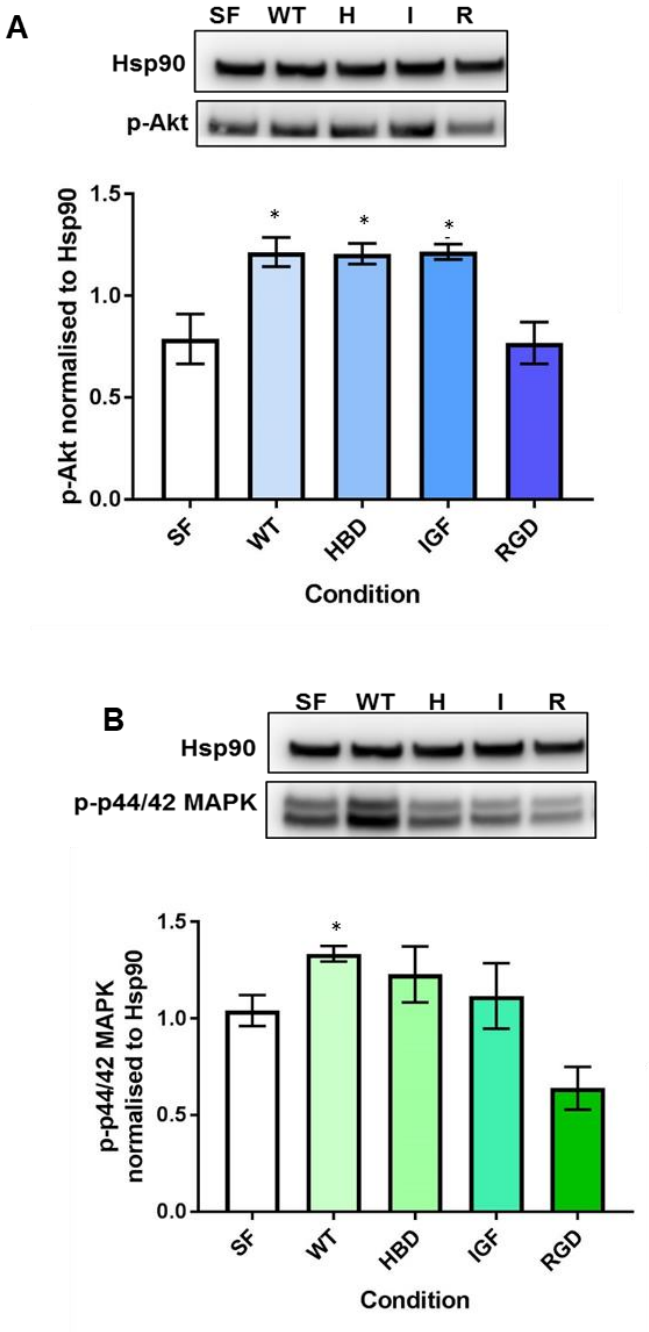

Figure 8.2 RGD mutant failed to phosphorylate Akt or MAPK
20µg of protein in HUVECs was loaded onto a 4-12% Bis-Tris gel and the blots were probed for the relevant genes. HUVECs were stimulated with ^{WT}IGFBP-2, HBD, IGF or RGD mutants (500ng/ml; 20min). Densitometry of the blots was measured using Genetools. **(A)** The blots were probed with rabbit polyclonal anti-phospho Akt (MW=60kDa) and the loading control, murine monoclonal Hsp90 (MW=90kDa) to observe the change in Akt phosphorylation, in response to stimulation with ^{WT}IGFBP-2, HBD, IGF or RGD mutants in HUVECs (*=p<0.01 vs serum-free (SF) control, n=3). **(B)** The blots were probed with rabbit polyclonal anti-phospho p44/42 MAPK (MW=42/44kDa) and the loading control, murine monoclonal Hsp90 (MW=90kDa) to observe the change in MAPK phosphorylation, in response to stimulation with ^{WT}IGFBP-2, HBD, IGF or RGD mutants in HUVECs (*=p<0.05 vs serum-free (SF) control, n=3). Error bars represent SEM.

8.4.2 Effect of the RGD mutant on Akt and p44/42 MAPK activation

Following the results from Figure 8.10, the RGD mutant failed to phosphorylate Akt and MAPK. To confirm this was a true finding we replicated the Akt phosphorylation, normalising against total Akt levels (Figure 8.3 A). Dose-dependent response stimulation of the RGD mutant did not replicate the commercial IGFBP-2 dose-dependent enhancement of Akt phosphorylation shown in Chapter 5 (Figure 8.3 B). The RGD mutant failed to up-regulate the phosphorylation of MAPK compared to the enhancement displayed following stimulation with ^{WT}IGFBP-2 and commercial recombinant IGFBP-2 (Figure 8.3 C).

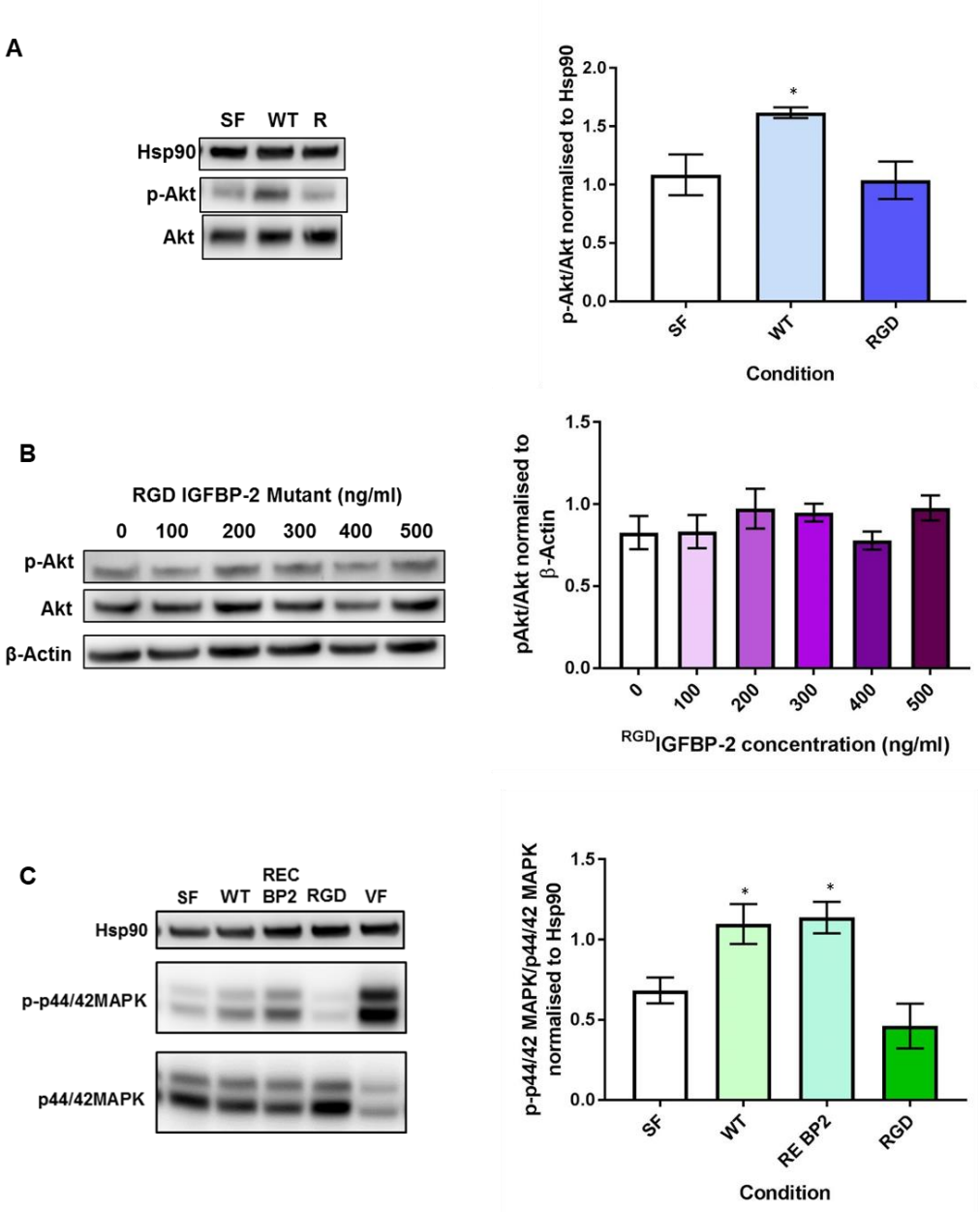

Figure 8.3 RGD domain is critical for Akt and p44/42 MAPK phosphorylation
20µg of protein from HUVEC cell lysates was loaded for each condition onto the gel and probed for the gene of interest. Western blots were stripped following probing for phospho variations of the gene with 2% glycine before being probed for total levels. Successful stripping was confirmed by imaging the blot after stripping to ensure no residue remained on the blot. Densitometry was carried out using Genetools. **(A)** HUVECs were stimulated with ^{WT}IGFBP-2 and RGD mutant (500ng/ml; 20min). The blots were probed for rabbit polyclonal anti-phospho Akt (MW=60kDa), murine polyclonal anti-Akt (MW=60kDa) the loading control, murine monoclonal Hsp90 (MW=90kDa) (*p<0.001, n=3). **(B)** Change in Akt phosphorylation, compared to total levels and normalised to murine monoclonal anti-β-Actin (43kDa) was observed in response to a dose dependent stimulation of the RGD mutant (100-500ng/ml; 20min) on HUVECs (n=3). **(C)** Serum-starved HUVECs were stimulated with ^{WT}IGFBP-2 (500ng/ml; 20min), commercially sourced recombinant IGFBP-2 (RE BP2) (500ng/ml; 20min), the RGD mutant (500ng/ml; 20min) or VEGF (30ng/ml; 15min). Blots were probed for MAPK phosphorylation changes, rabbit polyclonal anti-phospho-MAPK (MW=44/42kDa), murine polyclonal anti- MAPK (MW=44/42kDa) and the loading control, murine monoclonal Hsp90 (MW=90kDa) (*=p<0.01 vs serum-free (SF) control, n=3). Error bars represent SEM.

8.4.3 Effect of mutants on eNOS and FAK phosphorylation

As mentioned in Chapter 5, published literature has highlighted IGFBP-2 may phosphorylate eNOS via stimulation of the Akt pathway in HUVECs (LI et al., 2018). IGFBP-2 has also been shown to stimulate FAK phosphorylation via integrin interactions (Patil et al., 2016). However, we failed to replicate elevated eNOS and FAK phosphorylation stimulated by completely functional IGFBP-2 in HUVECs.

HUVECs stimulated with ^{WT}IGFBP-2, the HBD-, IGF- and RGD-mutants did not cause any further phosphorylation of eNOS or FAK (Figure 8.4).

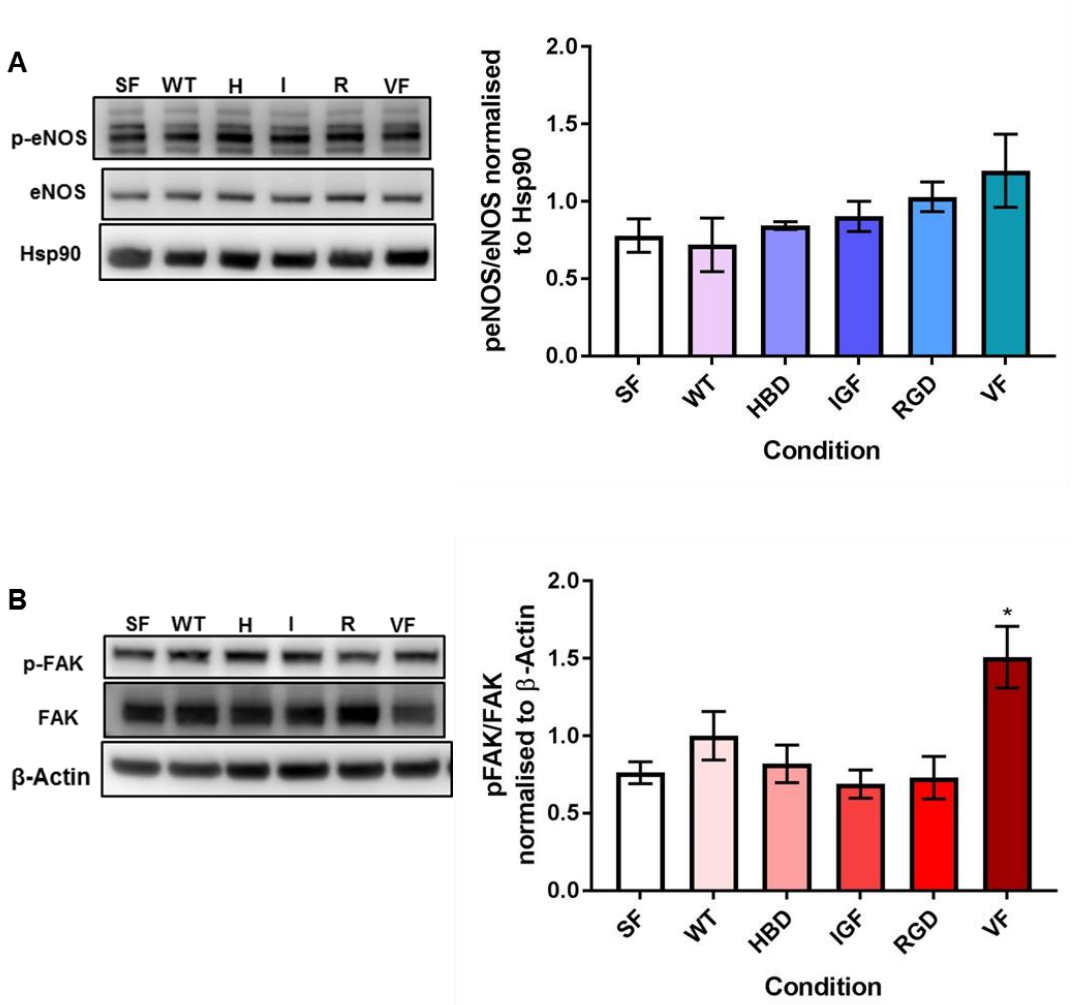

Figure 8.4 ^{WT}IGFBP-2 nor the mutants phosphorylated eNOS or FAK
Serum-starved HUVECs were stimulated with ^{WT}IGFBP-2 (500ng/ml; 15min) or its mutant variants, HBD, IGF and RGD (500ng/ml; 15min) or VEGF (30ng/ml; 15min). 20µg protein was loaded onto a 4-12% Bis-Tris gel. Blots were cut according to the molecular weight of the gene of interest. Blots probed for phospho levels were stripped with 2% glycine, confirmed by imaging for residue and then probed for total levels. **(A)** Blots were probed for rabbit polyclonal anti-phospho eNOS (MW=140kDa) and rabbit polyclonal anti-eNOS (MW=140kDa) and the loading control, murine monoclonal Hsp90 (MW=90kD). Change in eNOS phosphorylation vs total levels, normalised to Hsp90, was measured, in response to stimulation with ^{WT}IGFBP-2, the mutant variants and VEGF (n=3). **(B)** Immunoblot was probed for rabbit polyclonal anti-phospho-FAK (MW=125kDa), rabbit polyclonal anti-FAK (MW=125kDa) and the loading control, murine monoclonal anti-β-Actin (43kDa). Change in FAK phosphorylation vs total levels, normalised to β-Actin was measured, in response to stimulation with ^{WT}IGFBP-2, the mutant variants and VEGF (*=p<0.001, n=3). Error bars represent SEM.

8.4.4 Mutant stimulated HUVEC adhesion to fibronectin

We previously showed in Chapter 6, IGFBP-2 enhanced HUVEC adhesion to fibronectin, which also supports published literature that IGFBP-2 is able to promote adhesion via integrins (Feng et al., 2015). Most adhesion responses are stimulated through integrin interactions. However, HBD1 is also known to interact with the ECM via activation of RPTPβ. Therefore, to determine the domain in IGFBP-2 responsible for this effect the HUVEC cell adhesion assay was replicated using the mutants. The RGD mutant was the only IGFBP-2 mutant which failed to enhance HUVEC adhesion to fibronectin (Figure 8.5).

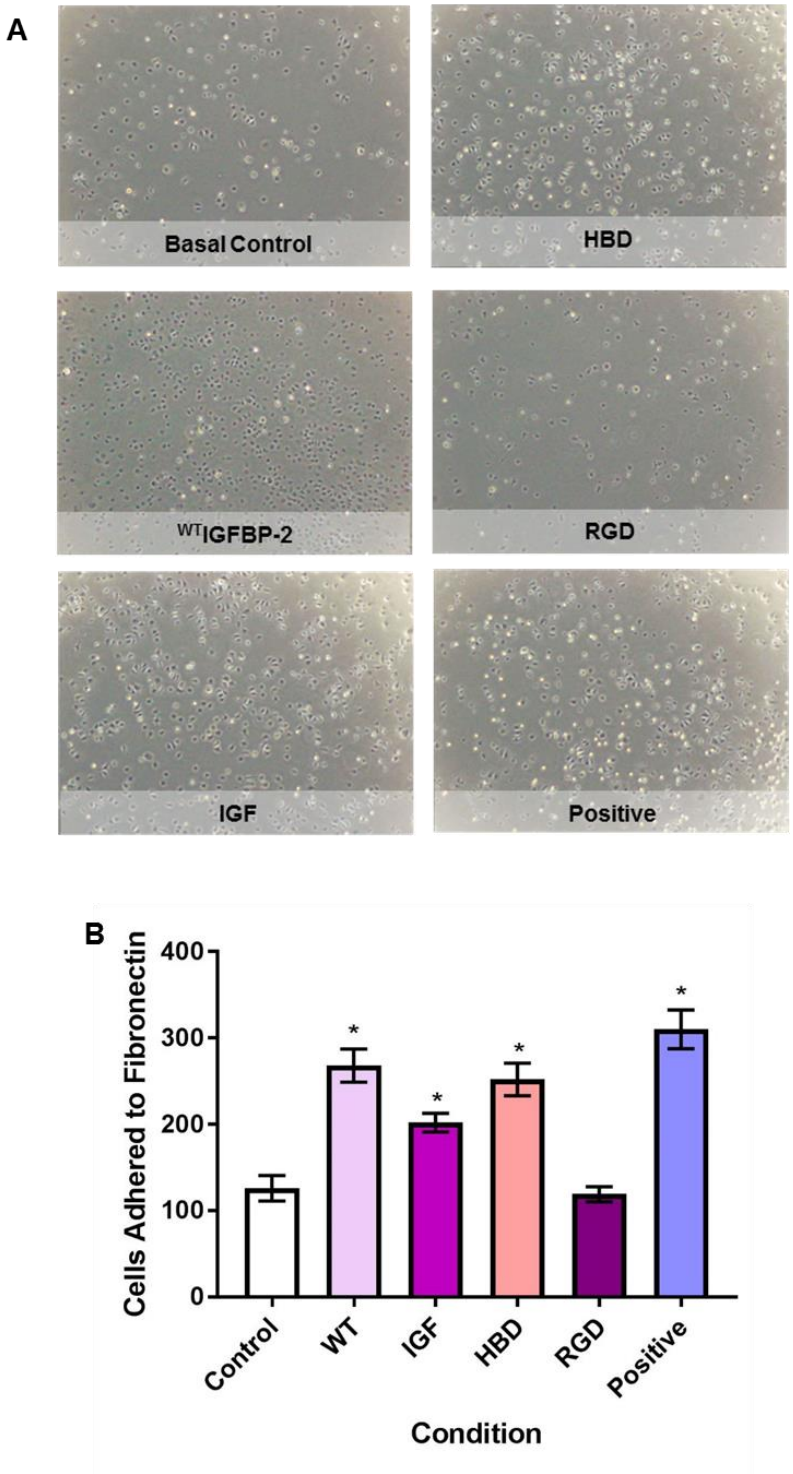

Figure 8.5 RGD mutant affected HUVEC cell adhesion to fibronectin
50,000 HUVECs were plated onto a fibronectin coated plate and incubated to adhere for 30 minutes in a 37ºC/5% CO_2 incubator. After 30 minutes, non-adhered cells were washed off using PBS. Remaining cells were imaged at 5 different points in the well od of the cell. **(A)** Representative Images taken at a 40x magnification using an optical microscope of cells that adhered to fibronectin after 30min in conditioned media with ^{WT}IGFBP-2, IGF, HBD or RGD mutants (500ng/ml) or a positive control of 20% serum + ECGS. **(B)** The cells counted at 5 different points were averaged per well. Graph representation shows the change in HUVECs adhered to the fibronectin matrix in response to stimuli with ^{WT}IGFBP-2 (500ng/ml), IGF mutant (500ng/ml), HBD mutant (500ng/ml), RGD mutant (500ng/ml) or positive control (20% serum + ECGS) (*=p<0.01 vs basal control, n=5). Error bars represent SEM.

8.4.5 Mutant stimulated HUVEC wound closure

IGFBP-2 enhances migration and proliferation, as shown in many published articles and by the findings in Chapter 6, however a clear mechanism responsible for promoting this activity has not yet been established. Integrin, VEGF, RPTPβ and IGF-I interactions have all been reported to be responsible for driving migration and proliferation. However, using these mutants, we will be able to establish which domain, and therefore, identifying the interaction that is critical for this activity. After 13 hours, the RGD mutant failed to enhance HUVEC wound closure to the level achieved by ^{WT}IGFBP-2 and the IGF and HBD mutants (Figure 8.6).

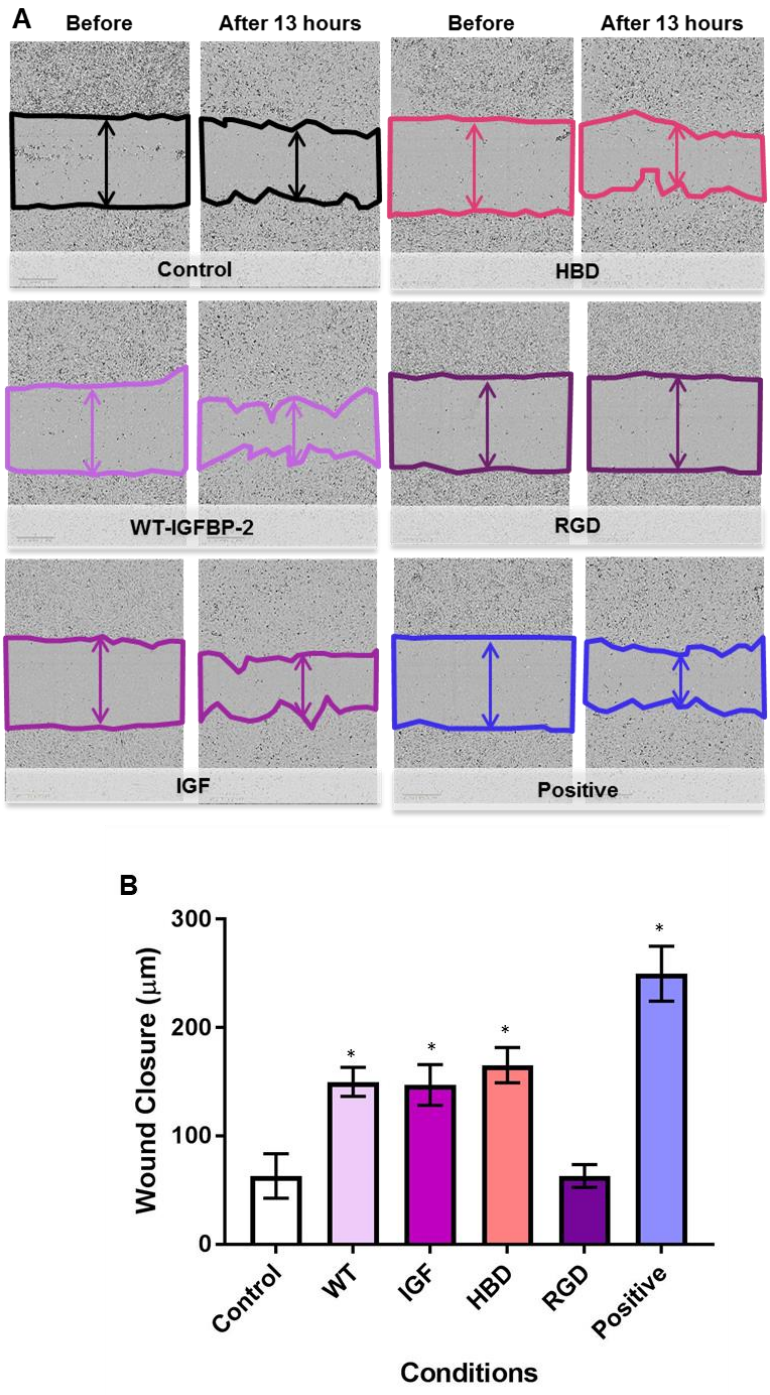

Figure 8.6 RGD mutant fails to enhance HUVEC wound closure
Cells were left to reach confluency in a 96 well plate in triplicate. Conditioned media containing ^{WT}IGFBP-2 (500ng/ml), IGF mutant (500ng/ml), HBD mutant (500ng/ml), RGD mutant (500ng/ml) or positive control (10% serum) were added to the cells prior to serum-starving. The images, before and after a 13-hour incubation, were taken using an optical microscope at a 40x magnification. ImageJ polygon tool was used to measure the change in wound area from the before and after images. **(A)** Representative Images taken using the Incucyte at a 10x magnification of when a scratch was first made and the closure after 13 hours in conditioned media with control (2% serum), ^{WT}IGFBP-2, IGF, HBD or RGD mutant (500ng/ml) and the positive control (5% serum). **(B)** Graphical presentation highlighting the change in wound closure in response to stimulation with ^{WT}IGFBP-2 (500ng/ml), IGF mutant (500ng/ml), HBD mutant (500ng/ml), RGD mutant (500ng/ml) or positive control (10% serum) (*=$p<0.05$ vs basal control, n=3). Error bars show SEM.

8.4.6 Mutant stimulated HUVEC tube formation

Tube formation assays are used commonly as an *in vitro* representation of endothelial cell movement in angiogenesis. We previously supported Das et al., (2013) findings that IGFBP-2 promotes endothelial tube formation. Similarly, to wound closure, tube formation uses a combination of adhesion, migration and proliferation.

The RGD mutant failed in to enhance HUVEC mesh formation to match the level of enhancement achieved following stimulation with ^{WT}IGFBP-2 and the HBD and IGF mutants (Figure 8.7). Observations at regular intervals over the tube formation period displayed RGD struggled to form a clear mesh-like type structure (Figure 8.8).

In order to identify a clear mechanism of how IGFBP-2 could promote angiogenic-like properties, it is essential we determine which signalling pathways the enhancement in tube formation is due to. Therefore, Akt and p38 MAPK inhibitors were used inhibit tube formation stimulated by either of these pathways. The Akt pathway is a requirement for IGFBP-2 induced tube formation (Figure 8.9), however inhibiting p38 MAPK did not diminish IGFBP-2 stimulated mesh tube formation (Figure 8.10).

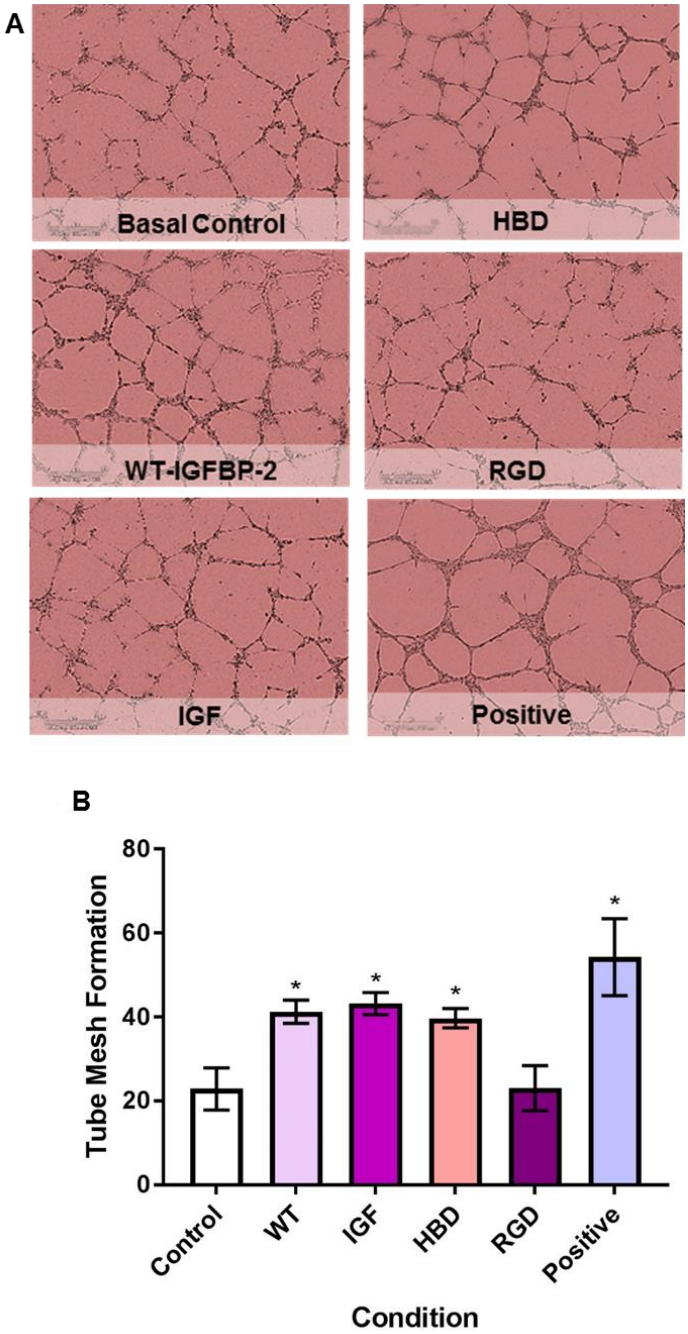

Figure 8.7 RGD mutant did not enhance HUVEC mesh formation
100,000 HUVECs were plated onto set Matrigel in conditioned media (stimulated with IGFBP-2, mutants, or VEGF, in duplicate and incubated for 8 hours in a 37ºC/5% CO_2 incubator. Images were taken using an optical microscope at a 40x magnification after the incubation period. **(A)** Representative Images of HUVECs in a tube formation assay taken after 8 hours of incubation with conditioned media containing basal control (1% serum) ^{WT}IGFBP-2 (500ng/ml), IGF mutant (500ng/ml), HBD mutant (500ng/ml) or RGD mutant (500ng/ml) and positive control (10% serum). **(B)** ImageJ Cell Counter Tool was used to count the number of meshes measured in 5 different points of the well. The measurements were averaged according to each well. Graphical representation of the meshes counted in 5 different areas of the well for each non-stimulated and stimulated well, showing the effect of ^{WT}IGFBP-2 (500ng/ml), IGF mutant (500ng/ml), HBD mutant (500ng/ml) or RGD mutant (500ng/ml) and positive control (10% serum) compared to basal levels (1% serum) (*=$p<0.05$ vs basal control, n=4). Error bars show SEM.

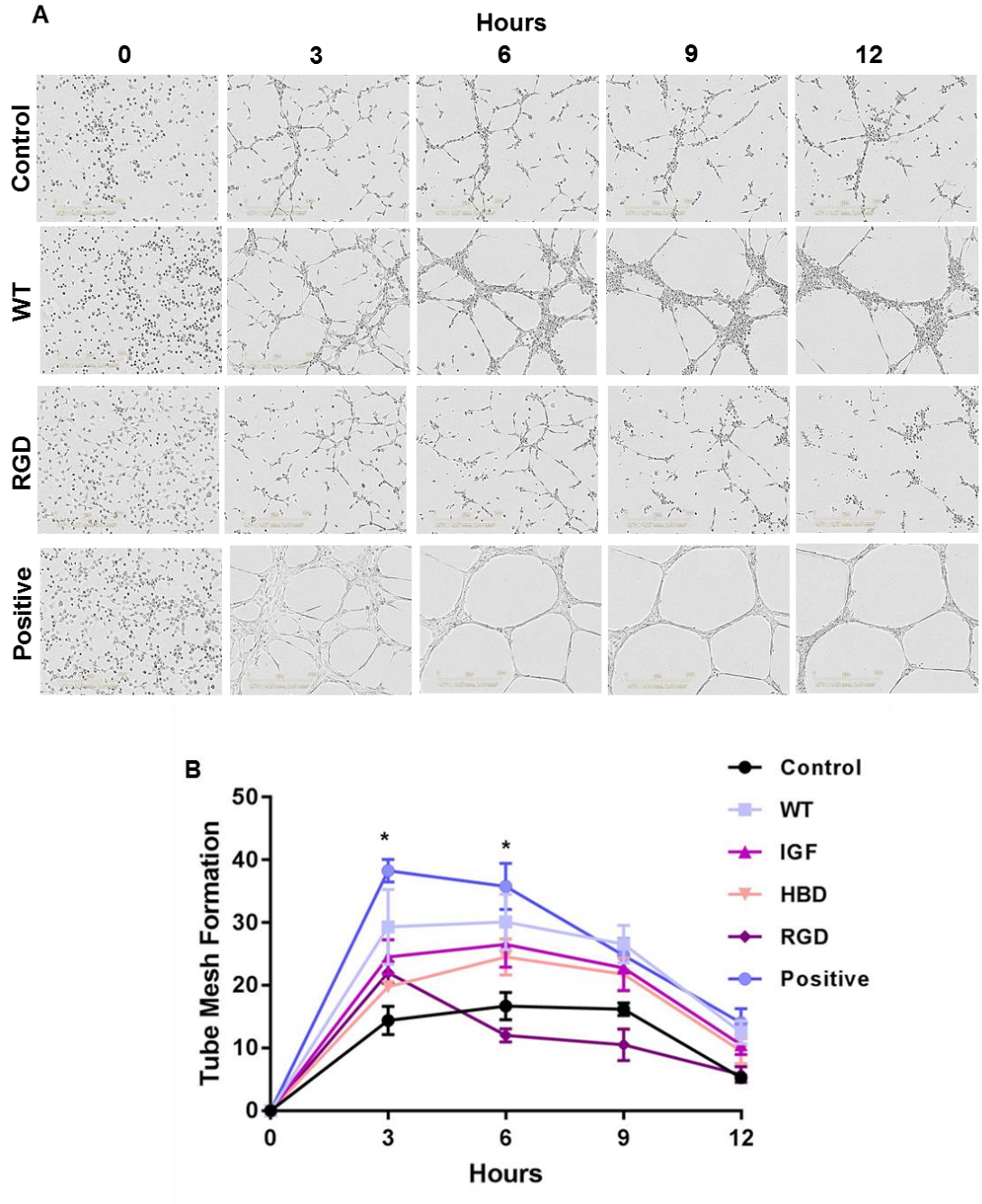

Figure 8.8 Mesh tube formation over time decreases
100,000 HUVECs were plated onto a set Matrigel matrix, in duplicate, in conditioned media. Cells were immediately incubated in a 37ºC/5% CO_2 incubator, which was connected to the Incucyte. Images were taken every 3 hours at a 10x magnification. **(A)** Representative Images taken on the Incucyte, of the basal control wells (1% serum), ^{WT}IGFBP-2 (500ng/ml), RGD mutant (500ng/ml) and positive control (10% serum), every 3 hours for 12 hours. **(B)** Change in wound closure was measured using the Incucyte Zoom software. Graphical representation of tube mesh formation changes over 12 hours in conditioned media with the control, ^{WT}IGFBP-2 (500ng/ml), IGF, HBD or RGD mutants (500ng/m) and positive control (10% serum) (*=$p<0.05$, n=4). Error bars represent SEM.

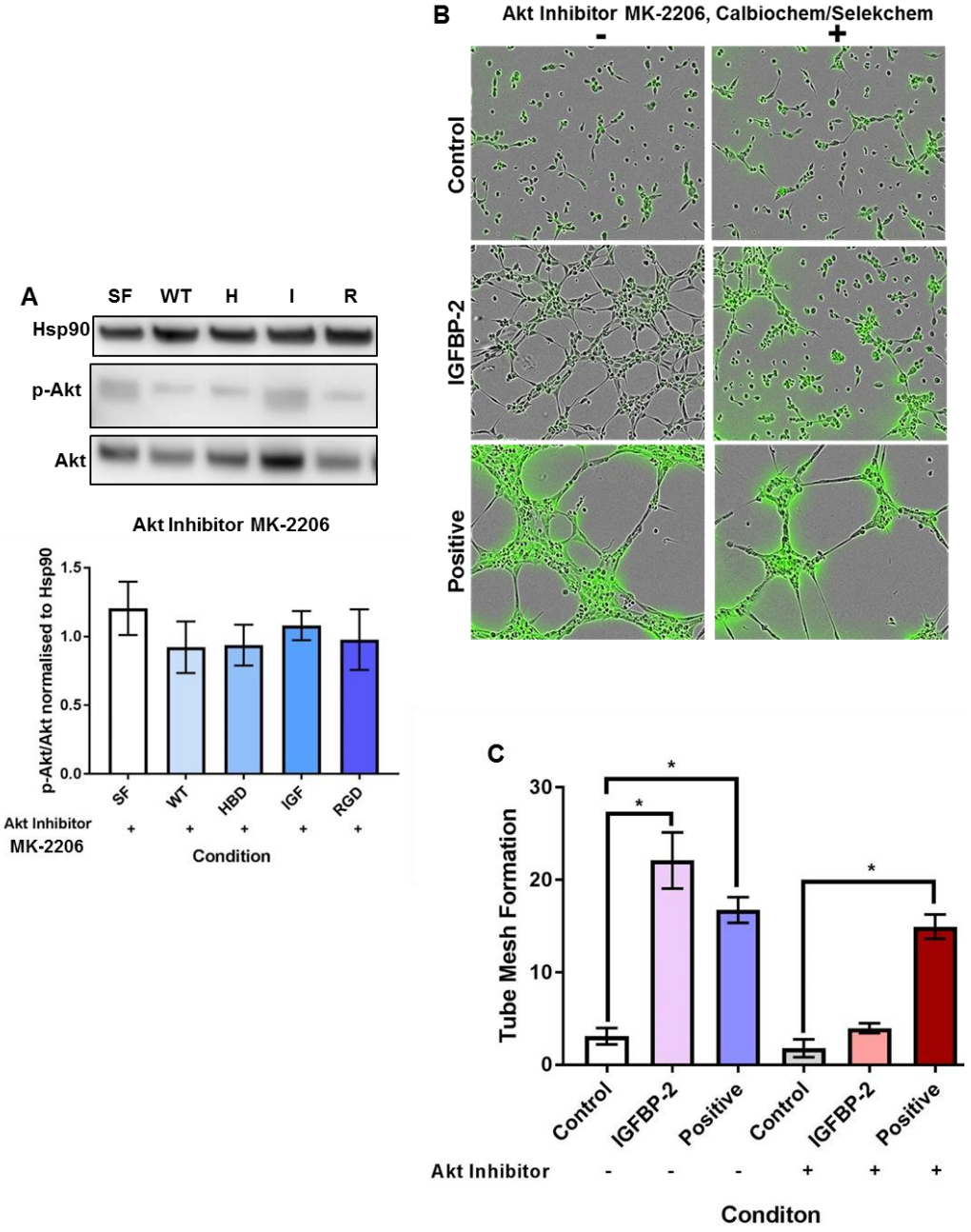

Figure 8.9 Akt inhibitor suppresses ^{WT}IGFBP-2 stimulated mesh formation
100,000 HUVECs were plated onto set Matrigel, in duplicate, in conditioned media. FitC stain was also added to the media. Images of the tube forming were taken using the Incucyte after an 8-hour incubation at 37ºC/5% CO_2. Inhibitors were added in before the incubation. **(A)** Signalling studies carried out on HUVECs stimulated with Akt inhibitor (MK-2206) probing for rabbit polyclonal anti-phospho Akt (MW=60kDa) and murine polyclonal anti-Akt (MW=60kDa), normalised to murine monoclonal anti-Hsp90 (MW=90kDa). Blots were stripped and checked for remaining residue before probing for phospho and total levels of Akt. **(B & C)** Akt inhibitor was added to conditioned media with basal control (1% serum), 500ng/ml ^{WT}IGFBP-2 and positive control (10% serum) at the beginning of 8-hour incubation. **(B)** Representative images taken on the Incucyte using fitC staining at a 10x magnification of mesh formation in conditioned media with control, ^{WT}IGFBP-2 and positive control, in the presence and absence of the Akt inhibitor. **(C)** Graphical representation highlighting the change in tube mesh formation, in response to stimulation with IGFBP-2 (500ng/ml) and positive control (10% serum) in the absence and presence of the Akt inhibitor (MK-2206) (*=p<0.01, n=4). Error bars show SEM.

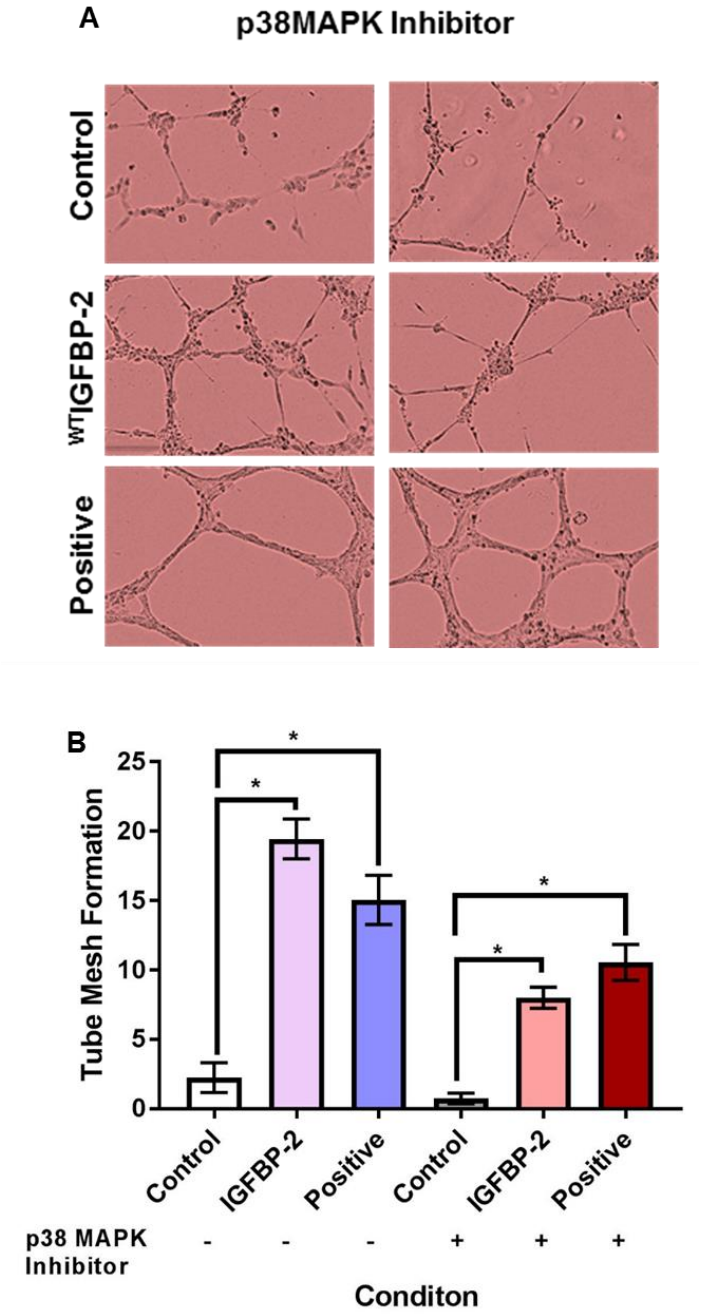

Figure 8.10 p38 MAPK inhibitor lowered ^{WT}IGFBP-2 stimulated mesh tube formation

100,000 HUVECs were plated onto set Matrigel, in duplicate, in conditioned media stimulated with IGFBP-2 (500ng/ml) or positive control (10% serum), in the absence or presence of the inhibitor p38 MAPK. Images were taken at 5 different points in a well after an 8-hour incubation at 37ºC/5% CO_2. **(A)** Representative images were taken at a 40x magnification using the optical microscope after an 8-hour incubation in the absence and presence of p38 MAPK inhibitor in conditioned media (with IGFBP-2 (500ng/ml) or positive control (10% serum)) with basal control (1% serum). **(B)** The number of meshes were counted using ImageJ and averaged per well. Graphical representation highlights differences in tube mesh formation in the absence and presence of p38 MAPK inhibitor, following stimulation with ^{WT}IGFBP-2 (500ng/ml) or the positive control (10% serum) and the basal control (1% serum) (*=$p<0.05$, n=3). Error bars represent SEM.

8.4.7 IGFBP-2 mutant effects on angiogenic bead sprouting assay

This assay represents the sprouting that occurs in the initial process of angiogenesis. It involves coating of a polystyrene ball with endothelial cells in a fibrinogen matrix (Nakatsu et al., 2007). These endothelial cells use a combination of adhesion, migration and proliferation to form a network around the bead. Once the network around the bead is formed, endothelial cells begin sprouting off the network as they migrate into the environment. Sprouting is a different angiogenic process compared to tube formation as sprouting is the initial stage, whereas tube formation takes place during the migration of endothelial cells, and therefore may rely on the activation of different signalling pathways. ^{WT}IGFBP-2 and the RGD mutant both significantly increased the number of sprouts formed in comparison to the basal control (Figure 8.11).

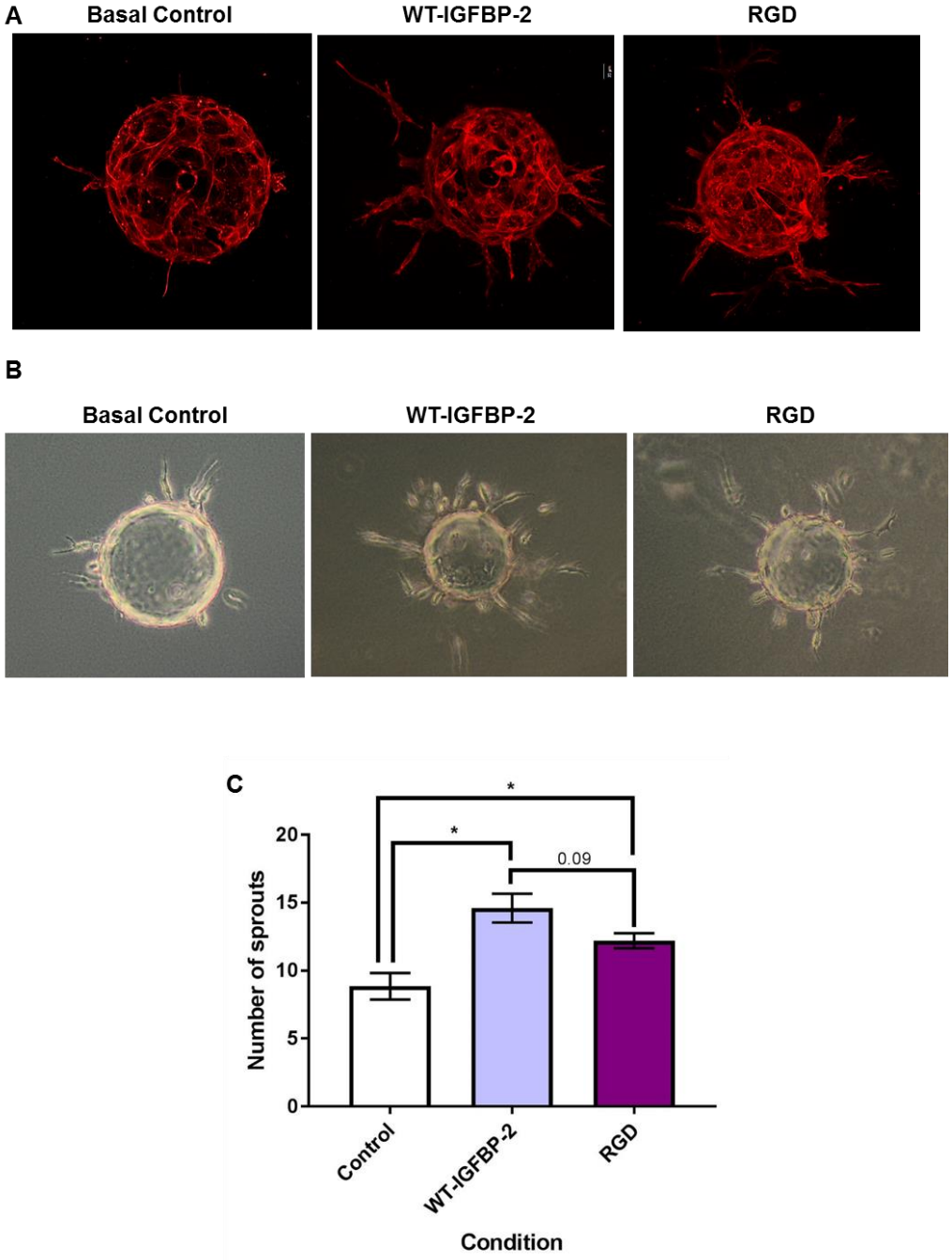

Figure 8.11 ^{WT}IGFBP-2 and RGD mutant enhances HUVEC sprouting
HUVECs were incubated in a mix of beads and left to adhere in a 37ºC/5% CO_2 incubator (in duplicate). Following coating of the bead, conditioned media containing IGFBP-2 (500ng/ml) and other growth factors, FGF (5ng/ml) and VEGF (5ng/ml) were added into the well. The coated beads were incubated for 24 hours. Confocal images were carried out after fixing of the beads following the 24-hour incubation. **(A)** Representative 3D Images taken of HUVEC angiogenic bead sprouting in conditioned media containing basal control (2% serum), ^{WT}IGFBP-2 (500ng/ml) and RGD mutant (500ng/ml), using confocal microscopy after being fixed following 24-hour incubation for sprouting. The stain, rhodamine phalloidin was used to label the actin fibres. The confocal images were taken at a 20x magnification. **(B)** Representative 2D images taken at a 10x magnification using an optical microscope of HUVEC sprouting after 24-hour incubation. **(C)** Graphical representation of the number of sprouts counted from images taken using the optical microscope, highlighting the HUVEC sprouting induced following stimulation with ^{WT}IGFBP-2 (500ng/ml) and the RGD mutant (500ng/ml) (*=p<0.05, ^{WT}IGFBP-2 vs RGD =p=0.09, n=3).

8.4.8 Effect of IGFBP-2 and its mutants on cell permeability

As mentioned, the introduction (Chapter 1.4), cell permeability is essential for achieving healthy angiogenesis. It is well known that VEGF causes hyperpermeability and during angiogenesis induces the formation of leaky blood vessels. Although we have shown in Chapter 4 evidence that IGFBP-2 may not upregulate VEGF to promote angiogenesis, we needed to prove IGFBP-2 does not cause the same hyperpermeable response that VEGF does. These findings would support the use of IGFBP-2 as a viable therapeutic agent in clinical use. Permeability was tested using a system called Electric Cell-substrate Impedance (ECIS), which relies on measuring the resistance required for electrical currents to get through a confluent monolayer of cells. ^{WT}IGFBP-2 did not increase permeability in comparison to VEGF. IGF mutant increased permeability compared to the RGD and HBD mutant and ^{WT}IGFBP-2 (Figure 8.12).

VEGF causes its hyperpermeable response by disrupting VE-Cadherin and compromising vascular integrity (Ourradi et al., 2017). This endothelial cadherin is a molecule that controls cell to cell adhesion via modulating cellular junctions. Under confocal microscopy, normal permeability depicts VE-cadherin outlining the surface of cells. Contrastingly, VEGF causes VE-cadherin to change confirmation, thus causing the opening of gaps. VE-cadherin normal morphology was retained with ^{WT}IGFBP-2 but was disrupted upon stimulation with VEGF-A (Figure 8.13).

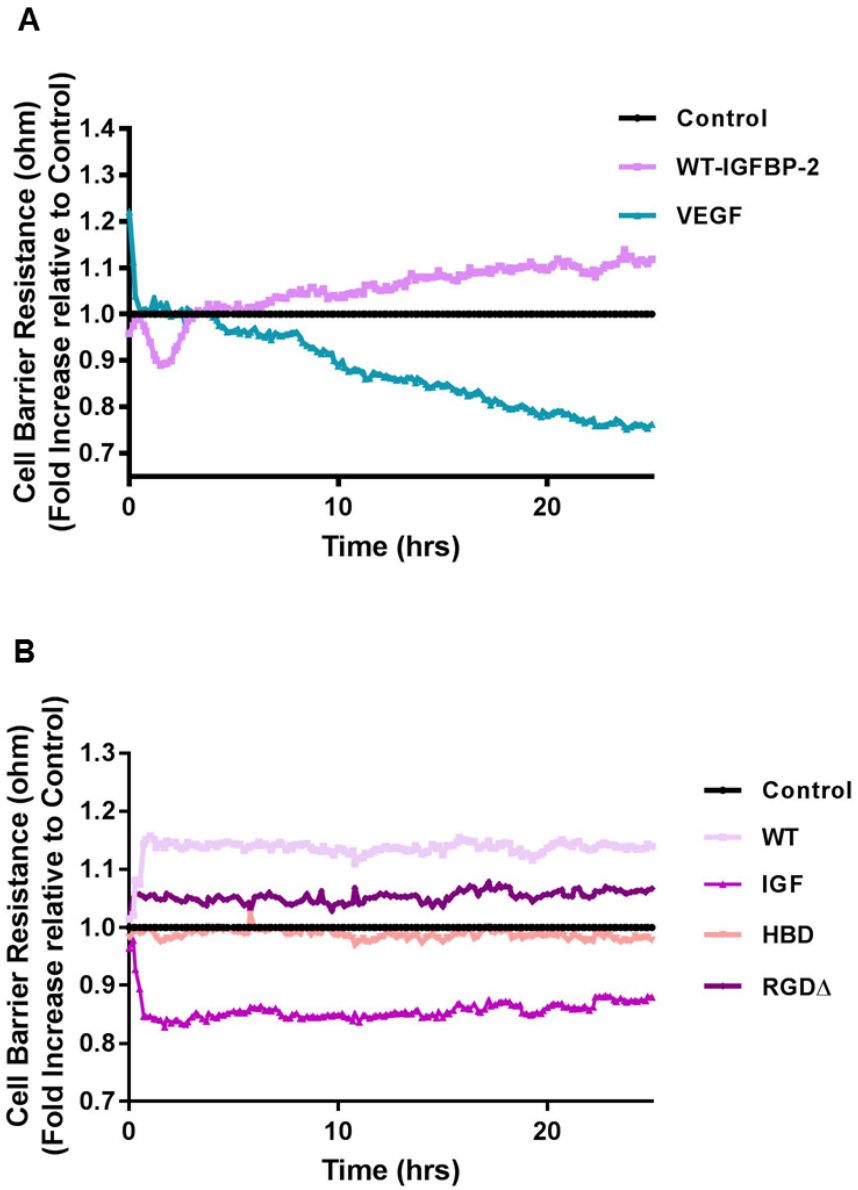

Figure 8.12 ^{WT}IGFBP-2 does not cause hyperpermeability
The ECIS system was used to measure change in resistance required to pass through a confluent HUVEC monolayer. Once a confluent monolayer had been obtained in Ibidi plates, in duplicate, the conditioned media was added, stimulating the HUVECs with ^{WT}IGFBP-2 (500ng/ml), the mutant variants (500ng/ml) of VEGF-A (30ng/ml) . The plate was placed into the ECIS machine which transmitted electrical currents to measure the resistance of the monolayer. The measurements were provided by the ECIS software and compared using Excel. **(A)** Comparison between the fold change in resistance in cells conditioned in basal media (5% serum), either non-stimulated (basal control) or stimulation with the addition of ^{WT}IGFBP-2 (500ng/ml; 25h) or VEGF-A (30ng/ml;'25h) (n=4). **(B)** Graphical representation of the fold change in resistance compared between the mutants, IGF, HBD and RGD and ^{WT}IGFBP-2 (500ng/ml; 25h) and the non-stimulated basal control (n=3).

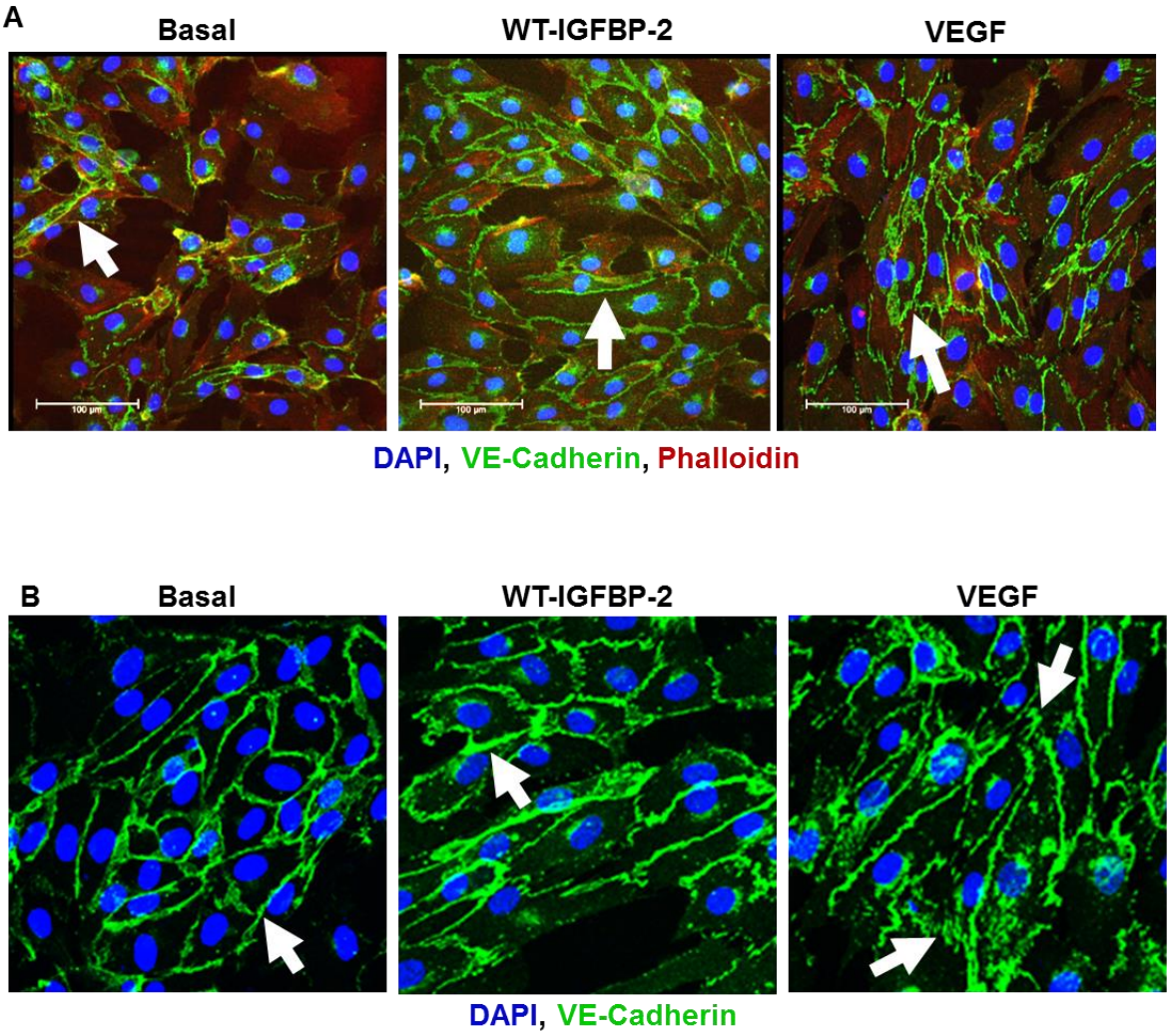

Figure 8.13 ^{WT}IGFBP-2 does not disrupt VE-cadherin
HUVEC confluent monolayers were maintained in conditioned basal media (5% serum), with ^{WT}IGFBP-2 (500ng/ml; 48h) or VEGF-A (30ng/ml; 48h) after running through the ECIS reader. The ECIS did not adversely affect the monolayer (data not shown). Cells were fixed and probed with phalloidin and/or VE-cadherin antibody and their corresponding fluorophores, following with DAPI. White arrows depict changes to VE-cadherin. DAPI highlights the nucleus of the cells in blue, VE-cadherin staining is highlighted in green and Phalloidin staining is highlighted in red. **(A)** Images were captured at a 10x magnification using confocal microscopy. **(B)** Images were captured at a 20x magnification using a confocal microscope, closely showing the jagged appearance of VE-Cadherin, in response to stimulation with VEGF-A.

8.5 Discussion

8.5.1 RGD mutant fails to activate p44/42 MAPK and Akt phosphorylation in HUVECs

We previously found in Chapter 5, IGFBP-2 (500ng/ml; 20mins) does stimulate Akt and p44/42 MAPK phosphorylation in HUVECs. ^{WT}IGFBP2, as well as the HBD1 and IGF mutants significantly enhanced Akt activation. This finding with the mutants contradicts current findings in other cell types highlighting functional HBD or IGF or both in a combination is critical to phosphorylate Akt.

The interaction between IGFBP-2s HBD1 and RPTPβ was critical to the signalling of PTEN and downstream activation of Akt. Stimulation with the HBD peptide alone stimulated Akt phosphorylation in osteoblasts (Kawai et al., 2011). In osteoclasts, the HBD and IGF mutants independently failed to phosphorylate Akt. However, to rescue Akt phosphorylation, both domains were required to be functional (Demambro et al., 2012). It was suggested the mechanism modulating this activity was the enhancement in phosphatase activity due to HBD not mediated RPTPβ, coordinated with inaction of IGF-I and as a result Akt in VSMCs. In HUVECS, we have determined the HBD or IGF mutant relies on other mechanisms to compensate for the loss of activity and still is able to enhance Akt activation to the same level as fully functional IGFBP-2.

Our findings suggest that HUVEC Akt phosphorylation is mediated through integrin interactions. In glioma cells, IGFBP-2 actions of promoting cell migration and proliferation are mediated by integrins recruitment of integrin-linked kinase (ILK) (Holmes et al., 2012). The ILK pathway leads to the activation of downstream targets PI3K and Akt (Kimura et al., 2010). Increased levels of IGFBP-2 correlate with phosphorylated FAK levels; however, the upregulation in FAK does not cause an enhancement in Akt phosphorylation (Lu et al., 2013). Thus, suggesting IGFBP-2s integrin recruitment of ILK is likely to be a more favourable mechanism contributing to IGFBP-2 stimulated Akt phosphorylation via its RGD domain.

Stimulation with ^{WT}IGFBP-2 with the same conditions as optimised in Chapter 5 caused approximately a 1.3 significant fold increase in p44/42 MAPK activation compared to the basal serum-free control. ^{WT}IGFBP-2 also significantly enhanced Akt phosphorylation compared to the basal control. These findings mimic the effects on signalling observed with commercially sourced recombinant IGFBP-2 and display the same biological functionality.

Interestingly, the HBD, IGF and RGD mutants fail to enhance p44/42 MAPK phosphorylation to the same level as ^{WT}IGFBP-2. There has been an indirect association with low IGFBP-2 levels enhance IGF-stimulated ERK/MAPK signalling via inhibiting the suppressive activity of p53 in prostate cancer cells (Grimberg, 2000). This contradicts our initial finding of high IGFBP-2 levels enhances MAPK signalling in HUVECs. No further publications have shown that the HBD1 and IGF domains directly activate MAPK via JNK or ERK. The HBD1 and IGF failure to activate MAPK may be specific to vascular endothelial cells in particular but should be examined further in an array of cell types.

Interactions with α5 and β1 are critical to enhancing JNK and ERK mediated MAPK pathways (Han et al., 2014; Mendes et al., 2010). We support this finding by the suppressive effect the RGD mutant has on p44/42 MAPK signalling compared to ^{WT}IGFBP-2 and the HBD mutant, highlighting the RGD mutant is a requirement for MAPK activation. However, since there is no significant decrease between the IGF and RGD mutant stimulated phosphorylation of MAPK, there may be crosstalk between both of these domains to regulate the activity exerted by IGFBP-2/integrin binding.

8.5.2 ^{WR}IGFBP-2 and the mutants fail to phosphorylate eNOS and FAK

Recent literature has highlighted a link between IGFBP-2 stimulated Akt leading to the phosphorylation of eNOS (LI et al., 2018). ^{WT}IGFBP-2 and the mutants failed to enhance eNOS phosphorylation, confirming the finding from Chapter 5 that IGFBP-2 in HUVECs does not function through the Akt/eNOS pathway. An alternative Akt-stimulated pathway may be responsible for the changes we observe in the angiogenic functional assays.

An association in pancreatic cancer has been established between IGFBP-2 levels and upregulation of phosphorylated FAK (Liu et al., 2017). However, we hypothesised earlier using our current and published findings, IGFBP-2 in HUVECs may function via integrin interactions recruiting ILK instead of FAK. This correlates with our findings that commercially available IGFBP-2 or our in-house generated ^{WT}IGFBP-2 does not up-regulate FAK phosphorylation.

8.5.3 RGD domain of ^{WT}IGFBP-2 is required for enhancement of adhesion

Previously, in Chapter 6 we showed IGFBP-2 enhanced HUVEC adhesion to fibronectin. ^{WT}IGFBP-2, displayed the same functionality as the commercially sourced recombinant IGFBP-2. The HBD and IGF (but to a lesser extent) significantly enhanced HUVEC adhesion to fibronectin compared to the basal control. This was an expected result since they only promote interactions from the surface of the ECM with RPTPβ and IGF-1R, without modulating the cell-ECM adhesion (Lin et al., 2015; Liu et al., 2017).

The RGD mutant fails to enhance HUVEC to adhesion to fibronectin. This contradicts the mechanism stipulated in publications highlighting IGFBP-2s role in promoting de-adhesion (Beattie et al., 2015; Holmes et al., 2012). Their mechanism states activation of IGFBP-2s RGD domain binds cell surface integrins and therefore, prevents the cell surface integrins from attaching to the ECM in cancer cell lines. However, we have observed the opposite effect that a fully functional RGD domain enhances HUVEC adhesion to fibronectin. Supporting our findings, a functional RGD domain with IGFBP-1 was shown to enhance human coronary arterial endothelial cell and HUVEC adhesion to fibronectin, specifically via αVβ3 and α5β1 (Aziz et al., 2018). The mechanism suggested to explain this increase, was that endothelial cells stimulated with IGFBP-1 increased the cellular expression of integrins and as a result, enhances the number of integrin-ECM interactions that can take place causing further cell adhesion. IGFBP-2, as the only other IGFBP to possess an RGD may act in exactly the same way. Cell surface integrins could be visualised in future experiments to interrogate the hypothesis that IGFBP-2 enhances cell adhesion specifically through the RGD domain via a similar mechanism to IGFBP-1.

8.5.4 ^{WT}IGFBP-2 stimulated wound closure and mesh formation is mediated by the RGD domain

As stated previously in Chapter 6, IGFBP-2 stimulated wound closure and tube formation both target proliferation and migration angiogenic mechanisms. ^{WT}IGFBP-2 mimicked the enhanced effect induced by the commercially sourced IGFBP-2 in the scratch wound assay and the tube formation assay, thus confirming it is retained all IGFBP-2 expected functionality. IGF-I is well known to directly influence cell proliferation and migration via activation of the ERK/MAPK or Akt signalling cascade (Choi et al., 2008; Nieto-Estévez et al., 2016). The HBD also has the ability to indirectly influence Akt-mediated migration and proliferation via its interaction with

RPTPβ (Demambro et al., 2012). However, research on the action of these two domains in IGFBP-2 stimulated proliferation and migration is extremely limited. This may be due to reason that both HBD and IGF mutant functioned in the similar manner to the ^{WT}IGFBP-2, significantly enhancing HUVEC wound closure and HUVEC mesh formation.

RGD mutant failed to enhance wound closure and mesh formation to the level of ^{WT}IGFBP-2, highlighting it is the most critical domain to induce cellular migration and proliferation responses. This supports the majority of IGFBP-2 research highlighting Akt and MAPK promotes cell proliferation and migration (Myers et al., 2015). IGFBP-2s interactions with integrin subunits α5 and β1 are critical to mediating MAPK-stimulated cell migration, however IGFBP-2/integrin interactions have not been identified to cause upregulation of Akt phosphorylation (Han et al., 2014; Mendes et al., 2010). Our findings confirm IGFBP-2s interaction with integrins via its RGD domain is essential for cell migration and proliferation in HUVECs.

8.5.5 Akt and p38 MAPK inhibitor suppresses ^{WT}IGFBP-2 induced tube formation

^{WT}IGFBP-2 failed to display its enhancement in HUVEC mesh/tube formation in the presence of an Akt inhibitor, thus confirming IGFBP-2 relies on activation of Akt to drive this elevated effect. This contrasts slightly to our hypothesis as in Chapter 5, 200ng/ml IGFBP-2 was sufficient to activate the maximum response in Akt phosphorylation as this plateaued with increasing IGFBP-2 concentrations. In Chapter 6, 200ng/ml commercially-sourced recombinant IGFBP-2 was not sufficient to induce an enhancement in tube formation, but 500ng/ml IGFBP-2 was. Therefore, we assumed that the pathway would be driven by the MAPK pathway as p44/42 MAPK phosphorylation also did not occur at 200ng/ml. However, our results highlighted that IGFBP-2 stimulated Akt also plays a significant role in enhancing IGFBP-2 induced tube formation.

IGFBP-2 has been established to activate JNK, leading to the activation of p38 MAPK in glioma cells and mesenchymal stem cells (Mendes et al., 2010; Wang et al., 2017c). However, due to time constraints, we focused on establishing activation of p44/42 MAPK as it was reported JNK mediated MAPK activation was responsible for specific cell migration activity (Han et al., 2014). As we have established that Akt plays a significant role, we used a JNK inhibitor to observe if inhibiting p38 MAPK mediated migration activity would also inhibit tube formation. However, although to a lesser extent compared to the effect in the absence of the inhibitor, IGFBP-2 in the

presence of p38 MAPK inhibitor significantly enhanced tube formation in comparison to its basal control. Thus, suggesting that JNK/p38 MAPK may play a moderate role and not a significant role in the enhancement of IGFBP-2 induced HUVEC mesh formation in the tube formation assay.

8.5.6 ^{WT}IGFBP-2 stimulation of HUVEC sprouting is not dependent on a functional RGD domain

In the Introduction (Chapter 1) we discussed how the sprouting by endothelial cells from the pre-existing vessel is the initial process of angiogenesis. This angiogenic bead assay results in endothelial cells forming a mesh-like network around a bead. Once the network is stable, endothelial cells are able to begin migrating to the ECM. As expected, following published data regarding IGFBP-2s upregulation of cell migration and proliferation responses, as well the data from this thesis thus far regarding IGFBP-2s enhancement in cell adhesion, ^{WT}IGFBP-2 significantly increased the number of sprouts grown compared to the basal control. This supports IGFBP-2 is able to maintain a network to stabilise and enhance the migrating of endothelial cells via angiogenic mechanisms *in vitro*.

Unexpectedly, although the RGD mutant has failed to enhance cell adhesion, migration and proliferation in this chapter, there were significantly more sprouts formed when stimulated with the RGD mutant compared to the basal control. This suggests the RGD domain and integrin interactions with IGFBP-2 may not be required and is compensated by the HBD and IGF binding domain at the initial stage of angiogenesis. This opens up the need for further investigation into IGFBP-2s levels and roles at different stages of angiogenesis such as tip cell formation, endothelial sprouting, lumen formation and maturation (Francavilla et al., 2009). It is well-established that other cytokine and growth levels fluctuate during the angiogenesis. Studies have shown IGFBP-2 can interact with HIF-1α to promote angiogenesis, as well as VEGF (Azar et al., 2011; Lin et al., 2015). However, from our findings we can confirm that the RGD domain does not significantly play a role in the sprouting of endothelial cells.

8.5.7 ^{WT}IGFBP-2 does not increase permeability like VEGF$_{165}$a

Vascular permeability is essential to prevent formation of unstable blood vessels which may lead to vessel leakage, but IGFBP-2 has not been investigated in the context of permeability and its possibly interactions with VE-cadherin. As previously

discussed in the background of this chapter, VEGF causes a hyperpermeable state by disrupting VE-cadherin between cell-cell interactions which has led to leaky vessels being formed through therapeutic angiogenesis (Ourradi et al., 2017). Using the ECIS system, we confirmed findings of published literature that VEGF-A causes a hyperpermeable response in a HUVEC monolayer. Contrastingly, our in-house generated ^{WT}IGFBP-2 failed to replicate this effect and maintained the permeability of the endothelial monolayer at a near to basal level. This suggests that IGFBP-2 may not exert its angiogenic effects through activation of VEGF, as reported by Azar et al., (2011) and Das et al., (2013).

Further investigation into which domain may be responsible for maintaining endothelial cell permeability highlighted slight differences between the WT and its mutant variants. ^{WT}IGFBP-2, HBD and RBD all maintained permeability at a similar level, with ^{WT}IGFBP-2 showing a slight reduction in permeability. Surprisingly, stimulation with, the IGF mutant caused immediate increase permeability but maintained it at this lower level for 30 hours. Therefore, it did display a gradual decrease as VEGF does. IGF-I has been shown in enhance the resistance required for currents to pass through an epithelial cell monolayer, therefore reducing the permeability of the monolayer (Lorenzo-Zúñiga et al., 2006). This suggests IGF-I binding is a requirement for maintaining a strong endothelial monolayer too, hence the mutant that could not bind to IGF-I was the only mutant to display an increase in permeability.

Immunofluorescent staining and confocal microscopy on an endothelial monolayer left for 30 hours, alongside the ECIS experiment confirmed IGFBP-2 did not disrupt VE-cadherin as opposed to the “jagged” type effect caused by stimulation with VEGF-A. For the first time we have shown ^{WT}IGFBP-2 maintains VE-cadherin, supporting the data obtained from the ECIS experiment that IGFBP-2 does not increase permeability. Unfortunately, we were not able to carry confocal microscopy with the mutants. It would be interesting to observe the effect of the IGF mutant and compare it to the complete functional IGFBP-2, as this has not previously been investigated.

The findings from this set of experiments suggest IGFBP-2 will not cause the same problem of leakage as VEGF does and therefore is a more viable therapeutic angiogenic treatment option.

8.5.8 Study limitations

Unfortunately, due to time constraints, we were unable to use the Akt and p38 MAPK inhibitors on all functional assays. We also planned to observe the effects of the mutants on p38 MAPK and JNK mediated signalling because IGFBP-2s interactions with integrins α5 or β1 specifically, are known activate these pathways.

Again, due to a limit of time, we were unable to interrogate the effect of the mutants on other permeability assays and *in vivo*. It is extremely important to determine IGFBP-2 in its non-mutated and mutated state does not mimic the effect of VEGF on hyperpermeability.

It is important to note that cells from different passages function differently in relation to angiogenesis. Cells function most efficiently at a low passage and HUVECs beyond passage 6 should not be used for angiogenic assays. We only used HUVECs between passage 2 and 5; however, there was variability in wound closure, mesh formation and the permeability ECIS experiment due to the differences in the HUVEC passage number. For cost-effective reasons, it is not efficient to only use cells at passage 2.

8.6 Concluding remarks

Supporting the previous chapters, ^{WT}IGFBP-2 displays the same biological function as the commercial recombinant IGFBP-2 by enhancing Akt phosphorylation, p44/42 MAPK phosphorylation as well as cell adhesion, scratch wound and tube formation assays.

All mutants except the RGD domain significantly enhanced Akt phosphorylation. However, all the mutants failed to activate p44/42 MAPK phosphorylation. The RGD domain is required for both Akt and MAPK activation.

The HBD and IGF mutant significantly enhanced HUVEC adhesion to fibronectin wound closure and mesh formation to a similar level of that induced by ^{WT}IGFBP-2. The RGD mutant failed to promote cell migration and proliferation, as well as adhesion in all angiogenic functional assays, suggesting these mechanisms function through IGFBP-2s interactions with integrins. ^{WT}IGFBP-2 and the RGD mutant significantly enhanced sprouting and migration of endothelial cells in the angiogenic sprouting bead assay, suggesting integrin interactions may not be involved in the initial sprouting stage of angiogenesis.

Akt inhibitor eliminated the enhanced mesh formation response induced by ^{WT}IGFBP-2. Inhibition of p38 MAPK lowered the elevation of ^{WT}IGFBP-2 induced mesh

formation, compared to the condition without the MAPK inhibitor but was still significant compared to its basal control.

For the first time, we have identified IGFBP-2 does not cause the same negative effects on permeability as VEGF does, causing leaky blood vessels. ^{WT}IGFBP-2 maintained permeability of a HUVEC monolayer at the basal level. However, IGF binding may play a significant role in determining permeability. IGFBP-2 maintained VE-cadherin morphology, whereas VEGF disrupted VE-cadherin, contributing to the hyperpermeability.

In conclusion, the RGD domain is critical to IGFBP-2 stimulated angiogenic mechanisms and IGFBP-2/integrin interactions could be exploited further as a therapeutic. The RGD domain may not be responsible for driving angiogenic mechanisms through all stages of angiogenesis. IGFBP-2 retains vascular integrity in the *in vitro* studies, suggesting that it will not cause formation of leaky blood vessels if used as an angiogenic therapeutic agent.

Chapter 9 – General discussion and conclusion

9.1 Background

IGFBP-2 was presented by our laboratory as a putative angiogenic treatment for ischaemic diseases due to reports of angiogenic-like mechanisms evoked by IGFBP-2 in a variety of cell-types in published literature. Although upregulation of IGFBP-2 has been correlated with tumour growth in cancers, IGFBP-2 has not previously been definitively shown to directly stimulate angiogenesis. Potential molecular mechanisms have been proposed by which IGFBP-2 interacts with cells via its structural domains which could be pertinent to angiogenesis.

IGFBP-2 has domains which can interact with IGF molecules, integrins, RPTPβ, glycosaminoglycans (e.g. heparin), as well as facilitate entry into the nucleus. These interactions have all been investigated to enhance a range of functional effects in a variety of cell types. These include migration of glioma cells through MAPK pathway stimulated by IGFBP-2 interaction with integrins; survival in breast cancer cells or osteoblast differentiation, mediated by the Akt pathway following interaction of IGFBP-2 with the cell surface receptor RPTPβ (Han et al., 2014; Xi et al., 2014).

Although IGFBP-2s interactions with cell surface receptors share certain characteristics, the mechanisms by which IGFBP-2 modulates cellular events and activity is likely to vary from cell to cell type. Therefore, it is important to investigate how IGFBP-2 may alter the function of endothelial cells. As the hypothesis interrogated by this thesis relates to the potential exploitation of IGFBP-2 in a clinical setting, we need to understand how it acts in response to ischemia in an *in vivo* system and determine if it causes any of the adverse effects associated with other pro-angiogenic factors, for example VEGF, in therapeutic angiogenesis. This thesis describes a programme of cellular, molecular and *in vivo* experiments by which we have identified a protective role for IGFBP-2 in ischemia-recovery *in vivo* and determined clear mechanisms critical to IGFBP-2s angiogenic actions, while providing reassurance that IGFBP-2 does not adversely affect vascular endothelial permeability.

9.2 hIGFBP-2 enhances early recovery to ischemia *in vivo*

IGFBP-2 has never previously been investigated *in vivo* in relation to recovery from ischemia, specifically in the setting of PAD. For the first time *in vivo,* we have shown that local IGFBP-2 expression in ischaemic hind limb is elevated after 24 hours following the induction of ischemia to the lower limbs. In the well-established angiogenesis mechanism, HIF-1α activated by an inflammatory response caused by the lack of oxygen is usually responsible for the upregulation of cytokines that are required for vessel formation. However, *in vitro* studies highlighted knockdown of HIF-1α in a breast cancer cell line did not supress basal IGFBP-2 or IGF-stimulated IGFBP-2 expression (Martin & Baxter, 2007). To confirm this, we would have to examine HIF-1α levels in the muscles 24 hours after induced ischemia and demonstrate they do not a show a trend with the upregulation trend of IGFBP-2 we observe in response to ischemia.

The overall recovery response suggests hypoxia was not induced to drive angiogenesis as an increase in perfusion to the limb in WT littermates is observed within 7 days, relieving the hypoxic environment. Over the 28-day recovery period, vessel growth continues to restore perfusion to a maximal level resulting in a plateau in perfusion being achieved by day 21. The clear differences between triggers of angiogenesis and arteriogenesis, suggest this recovery may be due to fluid shear stress influencing the expansion of a pre-existing collateral network rather than the formation of new blood vessels (Heil et al., 2006). However, the particular method of hindlimb ischemia surgery used is by cutting a segment of the artery out. Hence, recovery is more likely to be through a mix of angiogenesis and arteriogenesis, rather than just collateral recruitment. To confirm this, we would have to carry out further analysis on the legs at regular points during recovery, using techniques and tools such as immunohistochemistry and angiography (Cao et al., 2003).

Both the global and endothelial-specific over-expressing hIGFBP-2 mice demonstrated a significant enhancement in recovery at early stages of recovery following ischemia surgery. A study by (Rakue et al., 1998) demonstrated VEGF- and FGF- stimulated hind limb ischemia recovery was as a result of angiogenesis rather than arteriogenesis as the number of vessels formed increased but vessel diameter area remained unchanged.

HGF demonstrated a more potent recovery to HLI by significantly increasing end-point perfusion rates at day 28 compared to its WT littermates (Yamamoto et al., 2009). Therefore, the increase in perfusion on day 7 (in global expressers) and day

14 (in endothelial-specific), may replicate VEGF and FGF's activity to stimulate growth of new collaterals as well as expansion of the pre-existing collaterals. As mentioned previously an angiography would have to confirm collateral vessel changes. The vascularity of the vessels would also need to be verified via histology, as even in clinical trials, VEGF administration caused leaky vessels, resulting in fluid swelling (Isner et al., 1996).

Feedback from clinical trials suggests the method of administration of the growth factor is crucial. Protein delivery failed significantly as a therapeutic therapy in coronary artery disease and therefore gene therapy is commonly trialled (Simons et al., 2002). Gene therapy has its own disadvantages and may result in failure of growth factor delivery. However, PCR data from ischemic muscles has shown hIGFBP-2 in the global over-expresser, as well as mIGFBP-2 is directed to the ischemic soleus and tibialis. These muscles have been reported to be most affected by necrosis during restoration of perfusion (Shireman & Quinones, 2005).

Recently, since VEGF and FGF trials have failed in patients suffering from critical limb ischemia, more research is being driven into the role of these growth factors in diseased mice. Diabetic mice are specifically of interest, due to diabetes significantly increasing the risk of CVD development. Gene therapy of VEGF significantly enhanced perfusion compared to the impaired function in type 2 diabetic mice alone (Li et al., 2007). Most of IGFBP-2s *in vitro* functions have been observed in compromised diseased states, such as cancer and obesity. Therefore, it may be possible we may see a further enhancement in recovery from a mouse which has impaired vascularisation. Clinically, we would be using IGFBP-2 as a therapeutic at a late stage of PAD or CLI, when amputation is the only option, IGFBP-2 would be administered to rescue the dying limb.

It is evident, HLI surgery is not sufficient enough to make any clear assumptions on IGFBP-2s potential role in angiogenesis or arteriogenesis. However, we have observed an initial enhancement that suggests IGFBP-2 has a significant role in recovery *in vivo* and this should be investigated further.

9.3 IGFBP-2 phosphorylates Akt and p44/42 MAPK in HUVEC *in vitro*

Administration of IGFBP-2 to HUVEC significantly enhanced Akt phosphorylation, but higher concentrations were required to induce ERK-mediated MAPK phosphorylation.

Previous studies have reported that IGFBP-2 enhances Akt-, ERK- and JNK-mediated MAPK and FAK signalling cascades via interactions with cell surface tyrosine kinase receptors and its nuclear interactions in a range of cancer, muscle, fat and bone cell lines (Demambro et al., 2012; Holmes et al., 2012; LI et al., 2018; Mendes et al., 2010; Xi et al., 2016). However, we were unable to confirm activation FAK phosphorylation by IGFBP-2 in HUVECs, which was supported by IGFBP-2 having no effect on GSK3β phosphorylation. Although, FAK phosphorylation is induced in lung cancer cells and adipocytes, it has also been shown to be down-regulated in breast cancer cells (Lu et al., 2013; Schütt et al., 2004; Yau et al., 2015c). Therefore, IGFBP-2s RGD domain may function differently in HUVECs and could possibly induce the recruitment of ILK in order to activate the Akt pathway.

Phosphorylation of the downstream target of Akt, eNOS also was not affected by IGFBP-2. Similarly, the critical regulator of Akt signalling, PTEN, was not phosphorylated by IGFBP-2 in HUVECs.

The activation of Akt and MAPK pathways (in addition to other pathways which we have not looked at) are significantly involved in *in vitro* and *in vivo* angiogenesis. Most growth factors, specifically VEGF and FGF are known to mediate their angiogenic effects through Akt and MAPK phosphorylation (Dellinger & Brekken, 2011; Johnson-Farley et al., 2007). FGF has specifically been shown to activate these pathways via IGF-I signalling in neuronal cells. Thus, suggesting IGFBP-2 has the ability to induce the same angiogenic effects exerted by VEGF and FGF *in vivo* and possibly clinically showing promising effects to CLI patients.

Contrasting to VEGF and FGF, IGFBP-2 is able to suppress IGF-I stimulated Akt and ERK even when IGFBP-2 levels are upregulated (Kiepe et al., 2002). Therefore, clinically IGFBP-2 presents more of a regulatory role over angiogenic mechanisms which may promote healthy vessel growth by balancing its angiogneic activity in the ischemic site.

Interestingly, the idea that IGFBP-2 may exert more pronounced angiogenic effects in diseased mice (mentioned in Section 9.2) was supported by IGFBP-2 activating Akt and MAPK phosphorylation more potently when endothelial cells had lost their

morphology and their health had become compromised. IGFBP-2 may be designated to play a recovery role in compromised or diseased states *in vitro* and *in vivo*. This finding was displayed by Aziz et al., (2018) who highlighted cells put into an inflammation state by TNFα or cells stimulated with IGFBP-1 alone failed to present an enhanced effect on cell adhesion. However, when IGFBP-1 was administered to the cells in an inflamed state by TNFα, the cell adhesion response was enhanced. IGFBP-2s role to act as a protector has also been observed *in vivo* in high-fat fed hIGFBP-2 overexpressing mice, preventing pre-adipocyte differentiation and proliferation to protect the onset of obesity (Wheatcroft et al., 2007).

IGFBP-2s role in compromised states clearly needs to be interrogated further to identify which chemokines may regulate the bioactivity and –availability of IGFBP-2 in circulation. However, IGFBP-2 ability to regulate activation of angiogenic mechanisms by the sequestering of IGF-I suggests that it can control activity depending on external stimulants. Therefore, this can be manipulated to enhance and suppress angiogenic activity as required to modulate the formation of a healthy blood vessel network.

9.4 IGFBP-2 enhances angiogenic mechanisms in HUVECs *in vitro*

For the first time, we have demonstrated that IGFBP-2 enhanced HUVEC adhesion to fibronectin. HUVEC wound closure was also enhanced by IGFBP-2. In the presence of an anti-proliferative agent, Mitomycin C, IGFBP-2 enhanced wound closure in a migration-dependent only assay. IGFBP-2 was also responsible for increased mesh formation in a tube formation assay. All these assays are driven by angiogenic-like characteristics which IGFBP-2 has been shown to modulate in a variety of cell types. Previous studies have shown IGFBP-2 has the ability to regulate adhesive properties via integrins in glioma cells, osteoclasts and other cell types, however IGFBP-2 has been mostly associated with de-adhesive effects (Han et al., 2014; Kawai et al., 2011). Migration and proliferation has been driven through Akt and MAPK signalling, as well as integrin interactions (Brandt et al., 2015; Liu et al., 2017; Wang et al., 2017c).

Angiogenesis relies on the activation of migration and proliferation. Reports have also highlighted endothelial adhesion is essential to initiate the sprouting process as an endothelial tip cell forms. VEGF and FGF, as proangiogenic factors have previously

been identified to enhance these mechanisms via angiogenic signalling pathways such as Akt and MAPK (Oommen et al., 2011; Sahni et al., 2004). Interestingly, in both referenced studies, VEGF and FGF both enhance endothelial cell adhesion to the ECM, promoting outside-in and inside-out signalling cascades. This may explain IGFBP-2s ability to enhance HUVEC adhesion to the ECM.

To further determine the signalling mechanisms which promote each mechanism, we need to repeat all functional assays using inhibitors. We have already demonstrated inhibition of the Akt pathway eliminated most mesh formation in the tube formation assay, whereas p38 MAPK inhibition only caused a slight decrease in total mesh formation. This is important in our understanding of target specific IGFBP-2 interactions and exploiting these, depending on the activity we would aim to promote.

9.5 RGD is critical for promoting angiogenic signalling and angiogenic functional properties

As mentioned in the previous chapter, we wanted to determine which interactions and angiogenic signalling pathways promote *in vitro* enhancement of IGFBP-2 stimulated HUVEC adhesion, migration and proliferation. This will enable us to offer a more direct and specific approach to exploiting IGFBP-2s angiogenic potential. We mutated the N terminal IGF binding site, the central heparin binding domain and nuclear localisation signal and the RGD domain in three individual mutant variants.

Mutation of the RGD domain to prevent integrin binding prevented the ability of IGFBP-2 to enhance Akt phosphorylation, whereas all three mutants prevented phosphorylation of ERK/MAPK. The RGD significantly suppressed HUVEC adhesion to fibronectin, wound closure and tube formation. Therefore, the majority of IGFBP-2s angiogenic potential is driven through its interaction with integrins. Published literature highlights IGFBP-2/integrin interactions are critical for the recruitment of ILK to stimulate Akt phosphorylation and JNK or ERK mediated MAPK activation which in turn activate cell migration and proliferation (Han et al., 2014; Hoeflich & Russo, 2015; Holmes et al., 2012). IGFBP-1, the only other IGFBP to possess an RGD domain, has demonstrated enhancement in glucose clearance and insulin sensitivity via IGFBP-1/integrin interactions (Haywood et al., 2017). Therefore, exploiting IGFBP-2s RGD domain may prove beneficial to promoting IGFBP-2 stimulated angiogenesis.

9.6 IGFBP-2 does not affect vascular permeability

Vascular permeability is extremely important in regard to angiogenesis. This is because VEGF failed as a possible therapeutic option due to its negative effect on the endothelium, causing high permeability and in turn resulting in leaky blood vessels (Alfranca, 2009). The leaky vessels resulted in fluid swelling in the lower limbs which was successfully treated in a clinical study with VEGF by Isner et al., (1996), however possible damage caused by the fluid was never interrogated and the limb had was amputated later for gangrene reasons.

There have been reports suggesting IGFBP-2 functions via its NLS to promote VEGF activation by aiding its transport via nuclear importins to its VEGF2R, in order to exert angiogenic-like responses (Azar et al., 2011; Das et al., 2013). Although we previously showed upregulated levels of hIGFBP-2 or mIGFBP-2 following ischemia showed no association with mVEGF levels, it was important we confirmed IGFBP-2 does not cause the same effect to permeability as VEGF.

IGFBP-2 did not affect the endothelial monolayer and retained regular morphology of VE-cadherin, whereas VEGF-A caused a hyperpermeable response and disrupted VE-cadherin junctions. We also discovered IGF binding may be a key regulator of determining IGFBP-2s effect on permeability as the mutant IGF caused increased permeability, whereas ^{WT}IGFBP-2, HBD and RGD mutants sustained a normal permeability level. This supported published evidence demonstrating the role of IGF-I mediating intestinal barrier function (Lorenzo-Zúñiga et al., 2006).

From our findings also plausible to assume IGFBP-2 does not cause upregulated expression of VEGF in HUVECs as we can confirm IGFBP-2 does not mediate the same adverse effects on permeability as VEGF. Therefore, IGFBP-2 presents a safer option to stimulate healthy blood vessel growth via the promotion of angiogenic activity we have seen in the previous chapters and supports its use clinically in cases of CLI or PAD.

9.7 Clinical significance

Upregulation of IGFBP-2 significantly enhances early stages of recovery from ischemia. IGFBP-2s RGD domain is critical to IGFBP-2 stimulated enhancement of phosphorylation of the angiogneic signalling pathways, Akt and MAPK, as well as angiogenic functionality, HUVEC adhesion, wound closure and tube formation. Therefore, IGFBP-2 displays translational angiogenic potential in vascular

endothelial cells, suggesting it may play a significant role in the endothelial remodelling that occurs in arteriogenesis or endothelial migration in angiogenesis. We have also shown it possesses distinct differences between VEGF and FGF's angiogenic effects, specifically VEGF's hyperpermeability response; therefore, functions in an alternative method which may prove to be more beneficial.

IGFBP-2 as a new potential therapeutic agent shows promising potential to produce positive outcomes on preventing amputation, death in CLI and also the onset of other CVD, via its angiogenic effects on vascular endothelial cells. If successful, this could the greatest advance in CVD as it will increase PAD-associated survival rates significantly.

9.8 Future directions

IGFBP-2s specific role in collateral vessel formation needs to be extensively investigated. Its actions via the RGD domain also play a crucial role in mediating IGFBP-2 stimulated angiogenic effects *in vitro*. The mutant RGD domain could also be tested *in vivo* via *in vivo* expression vectors, delivering liver-specific expression of the mutant form of IGFBP-2. It is clear by the outcomes of PAD clinical trials may be dependent on delivery mode, and therefore trialling different therapeutic angiogenic delivery therapies of IGFBP-2 in *in vivo* models may prove beneficial. The safety of using IGFBP-2 via exploitation of its RGD domain would have to be extensively verified via use of *in vivo* models. New directions from this project may include identifying IGFBP-2s angiogenic ability in diseased models.

9.9 Conclusion

Throughout this project, we have demonstrated increasing IGFBP-2 can speed up recovery following ischemia *in vivo,* as IGFBP-2 levels are upregulated following ischemia and IGFBP-2 over-expression cause an enhancement in early recovery stages following HLI. IGFBP-2 mediates angiogenic-like mechanisms in HUVECs such as adhesion, proliferation and migration, which may possibly be mediated through IGFBP-2 induced phosphorylation of Akt or p44/42 MAPK. The RGD domain is critical for all angiogenic-like mechanisms, including the phosphorylation of Akt and MAPK. HBD and IGF are also important to IGFBP-2 stimulated MAPK activation. The RGD domain is not involved in the sprouting of endothelial cells, suggesting different

domains may have different levels of activity at different stages of angiogenesis. Finally, IGFBP-2 maintains vascular permeability and does not cause a hyperpermeable response as does VEGF.

Therefore, IGFBP-2 has promising potential as an acute angiogenic therapeutic treatment, possibly via its RGD domain and IGF domain to drive angiogenic processes and maintain vascular permeability in cases of PAD or critical limb ischemia, in order to restore blood flow to rescue lower limbs from amputation.

Chapter 10 – References

Abbas, A., Imrie, H., Viswambharan, H., Sukumar, P., Rajwani, A., Cubbon, R. M., Gage, M., Smith, J., Galloway, S., Yuldeshava, N., Kahn, M., Xuan, S., Grant, P. J., Channon, K. M., Beech, D. J., Wheatcroft, S. B., & Kearney, M. T. 2011. The Insulin-Like Growth Factor-1 Receptor Is a Negative Regulator of Nitric Oxide Bioavailability and Insulin Sensitivity in the Endothelium. *Diabetes*, 60(8): 2169–2178.

Adamo, M. L., Shao, Z. M., Lanau, F., Chen, J. C., Clemmons, D. R., Roberts, C. T., LeRoith, D., & Fontana, J. A. 1992. Insulin-like growth factor-I (IGF-I) and retinoic acid modulation of IGF-binding proteins (IGFBPs): IGFBP-2, -3, and -4 gene expression and protein secretion in a breast cancer cell line. *Endocrinology*, 131(4): 1858–66.

Aguirre, G. A., De Ita, J. R., de la Garza, R. G., & Castilla-Cortazar, I. 2016. Insulin-like growth factor-1 deficiency and metabolic syndrome. *Journal of translational medicine*, 14: 3.

Akaogi, K., Okabe, Y., Sato, J., Nagashima, Y., Yasumitsu, H., Sugahara, K., & Miyazaki, K. 1996. Specific accumulation of tumor-derived adhesion factor in tumor blood vessels and in capillary tube-like structures of cultured vascular endothelial cells. *Proceedings of the National Academy of Sciences of the United States of America*, 93(16): 8384–9.

Al-Lamee, R., Davies, J., & Malik, I. S. 2016. What is the role of coronary angioplasty and stenting in stable angina? *BMJ (Clinical research ed.)*, 352: i205.

Alfranca, A. 2009. VEGF therapy: A timely retreat. *Cardiovascular Research*, 83(4): 611–612.

Alkharobi, H., Alhodhodi, A., Hawsawi, Y., Alkafaji, H., Devine, D., El-Gendy, R., & Beattie, J. 2016. IGFBP-2 and -3 co-ordinately regulate IGF1 induced matrix

mineralisation of differentiating human dental pulp cells. *Stem Cell Research*, 17(3): 517–522.

American Academy of Family Physicians., J. D., & Santilli, S. M. 1999. *American family physician. American Family Physician* (Vol. 59). American Academy of Family Physicians. Retrieved from https://www.aafp.org/afp/1999/0401/p1899.html

Andrec, M., Snyder, D. A., Zhou, Z., Young, J., Montelione, G. T., & Levy, R. M. 2007. A large data set comparison of protein structures determined by crystallography and NMR: Statistical test for structural differences and the effect of crystal packing. *Proteins: Structure, Function, and Bioinformatics*, 69(3): 449–465.

Antithrombotic Trialists' Collaboration. 2002. Collaborative meta-analysis of randomised trials of antiplatelet therapy for prevention of death, myocardial infarction, and stroke in high risk patients. *BMJ (Clinical research ed.)*, 324(7329): 71–86. Retrieved from http://www.ncbi.nlm.nih.gov/pubmed/11786451

Arai, T., Busby, W., & Clemmons, D. R. 1996. Binding of insulin-like growth factor (IGF) I or II to IGF-binding protein-2 enables it to bind to heparin and extracellular matrix. *Endocrinology*, 137(11): 4571–4575.

Assefa, B., Mahmoud, A. M., Pfeiffer, A. F. H., Birkenfeld, A. L., Spranger, J., & Arafat, A. M. 2017. Insulin-Like Growth Factor (IGF) Binding Protein-2, Independently of IGF-1, Induces GLUT-4 Translocation and Glucose Uptake in 3T3-L1 Adipocytes. *Oxidative Medicine and Cellular Longevity*, 2017: 1–13.

Atkins, R. J., Dimou, J., Paradiso, L., Morokoff, A. P., Kaye, A. H., Drummond, K. J., & Hovens, C. M. 2012. Regulation of glycogen synthase kinase-3 beta (GSK-3β) by the Akt pathway in gliomas. *Journal of Clinical Neuroscience*, 19(11): 1558–1563.

Azar, W. J., Azar, S. H. X., Higgins, S., Hu, J. F., Hoffman, A. R., Newgreen, D. F., Werther, G. a., & Russo, V. C. 2011. IGFBP-2 enhances VEGF gene promoter activity and consequent promotion of angiogenesis by neuroblastoma cells. *Endocrinology*, 152(9): 3332–3342.

Azar, W. J., Zivkovic, S., Werther, G. a, & Russo, V. C. 2014. IGFBP-2 nuclear translocation is mediated by a functional NLS sequence and is essential for its pro-tumorigenic actions in cancer cells. *Oncogene*, 33(5): 578–588.

Aziz, A., Haywood, N. J., Cordell, P. A., Smith, J., Yuldasheva, N. Y., Sengupta, A., Ali, N., Mercer, B. N., Mughal, R. S., Riches, K., Cubbon, R. M., Porter, K. E., Kearney, M. T., & Wheatcroft, S. B. 2018. Insulinlike Growth Factor-Binding Protein-1 Improves Vascular Endothelial Repair in Male Mice in the Setting of Insulin Resistance. *Endocrinology*, 159(2): 696–709.

Bagley, R. G., Weber, W., Rouleau, C., & Teicher, B. A. 2005. Pericytes and Endothelial Precursor Cells: Cellular Interactions and Contributions to Malignancy. *Cancer Research*, 65(21): 9741–9750.

Balaji, S., King, A., Crombleholme, T. M., & Keswani, S. G. 2013. The Role of Endothelial Progenitor Cells in Postnatal Vasculogenesis: Implications for Therapeutic Neovascularization and Wound Healing. *Advances in wound care*, 2(6): 283–295.

Baxter, R. C. 2000. *invited review Insulin-like growth factor (IGF)-binding proteins: interactions with IGFs and intrinsic bioactivities*. *Am J Physiol Endocrinol Metab* (Vol. 278). Retrieved from http://www.ajpendo.orgdownloadedfromwww.physiology.org/journal/ajpendoby$%7BindividualUser.givenNames%7D$%7BindividualUser.surname%7D

Beattie, J., Hawsawi, Y., Alkharobi, H., & El-Gendy, R. 2015. IGFBP-2 and -5: important regulators of normal and neoplastic mammary gland physiology. *Journal of cell communication and signaling*, 9(2): 151–8.

Bentzon, J. F., Otsuka, F., Virmani, R., & Falk, E. 2014. Mechanisms of plaque formation and rupture. *Circulation Research*, 114(12): 1852–1866.

Berry, M., Galinier, M., Delmas, C., Fournier, P., Desmoulin, F., Turkieh, A., Mischak, H., Mullen, W., Barutaut, M., Eurlings, L. W., Van Wijk, S., Brunner-La Rocca, H.-P.,

Caubere, C., Butler, J., Roncalli, J., Evaristi, M. F., Cohen-Solal, A., Seronde, M.-F., Escamilla, R., Ferrières, J., et al. 2015. Proteomics analysis reveals IGFBP2 as a candidate diagnostic biomarker for heart failure. *IJC Metabolic & Endocrine*, 6: 5–12.

Bhutia, S. K., Behera, B., Nandini Das, D., Mukhopadhyay, S., Sinha, N., Panda, P. K., Naik, P. P., Patra, S. K., Mandal, M., Sarkar, S., Menezes, M. E., Talukdar, S., Maiti, T. K., Das, S. K., Sarkar, D., & Fisher, P. B. 2016. Abrus agglutinin is a potent anti-proliferative and anti-Angiogenic agent in human breast cancer. *International Journal of Cancer*, 139(2): 457–466.

Bischoff, J. 1997. Cell adhesion and angiogenesis. *The Journal of clinical investigation*, 100(11 Suppl): S37-9. Retrieved from http://www.ncbi.nlm.nih.gov/pubmed/9413399

Boes, M., Dake, B. L., Booth, B. a, Sandra, a, Bateman, M., Knudtson, K., & Bar, R. S. 2002. Structure-function relationships of insulin-like growth factor binding protein 6 (IGFBP-6) and its chimeras. *Growth Horm IGF Res*, 12(2): 91–98.

Bondos, S. E., & Bicknell, A. 2003. Detection and prevention of protein aggregation before, during, and after purification. *Analytical Biochemistry*, 316(2): 223–231.

Bornhorst, J. A., & Falke, J. J. 2000. Purification of proteins using polyhistidine affinity tags. *Methods in enzymology*, 326: 245–54. Retrieved from http://www.ncbi.nlm.nih.gov/pubmed/11036646

Boucher, J., Tseng, Y.-H., & Kahn, C. R. 2010. Insulin and insulin-like growth factor-1 receptors act as ligand-specific amplitude modulators of a common pathway regulating gene transcription. *The Journal of biological chemistry*, 285(22): 17235–45.

Brandt, K., Grünler, J., Brismar, K., & Wang, J. 2015. Effects of IGFBP-1 and IGFBP-2 and their fragments on migration and IGF-induced proliferation of human dermal fibroblasts. *Growth Hormone and IGF Research*, 25(1): 34–40.

Canto, J. G., & Iskandrian, A. E. 2003. Major Risk Factors for Cardiovascular

Disease. *JAMA*, 290(7): 947.

Cao, R., Bråkenhielm, E., Pawliuk, R., Wariaro, D., Post, M. J., Wahlberg, E., Leboulch, P., & Cao, Y. 2003. Angiogenic synergism, vascular stability and improvement of hind-limb ischemia by a combination of PDGF-BB and FGF-2. *Nature Medicine*, 9(5): 604–613.

Carmeliet, P., Ferreira, V., Breier, G., Pollefeyt, S., Kieckens, L., Gertsenstein, M., Fahrig, M., Vandenhoeck, A., Harpal, K., Eberhardt, C., Declercq, C., Pawling, J., Moons, L., Collen, D., Risau, W., & Nagy, A. 1996. Abnormal blood vessel development and lethality in embryos lacking a single VEGF allele. *Nature*, 380(6573): 435–439.

Carter, S., Li, Z., Lemieux, I., Alméras, N., Tremblay, A., Bergeron, J., Poirier, P., Deshaies, Y., Després, J.-P., & Picard, F. 2014. Circulating IGFBP-2 levels are incrementally linked to correlates of the metabolic syndrome and independently associated with VLDL triglycerides. *Atherosclerosis*, 237(2): 645–51.

Cavalcanti-Adam, E. A., Volberg, T., Micoulet, A., Kessler, H., Geiger, B., & Spatz, J. P. 2007. Cell Spreading and Focal Adhesion Dynamics Are Regulated by Spacing of Integrin Ligands. *Biophysical Journal*, 92(8): 2964–2974.

Chelsky, D., Ralph, R., & Jonak, G. 1989. Sequence requirements for synthetic peptide-mediated translocation to the nucleus. *Molecular and cellular biology*, 9(6): 2487–92. Retrieved from http://www.ncbi.nlm.nih.gov/pubmed/2668735

Chen, X., Zheng, J., Zou, Y., Song, C., Hu, X., & Zhang, C. C. 2013. IGF binding protein 2 is a cell-autonomous factor supporting survival and migration of acute leukemia cells. *Journal of hematology & oncology*, 6(1): 72.

Choi, Y.-S., Cho, H.-Y., Hoyt, K. R., Naegele, J. R., & Obrietan, K. 2008. IGF-1 receptor-mediated ERK/MAPK signaling couples status epilepticus to progenitor cell proliferation in the subgranular layer of the dentate gyrus. *Glia*, 56(7): 791–800.

Chu, H., & Wang, Y. 2012. Therapeutic angiogenesis: controlled delivery of

angiogenic factors. *Therapeutic delivery*, 3(6): 693–714. Retrieved from http://www.ncbi.nlm.nih.gov/pubmed/22838066

Chua, C. Y., Liu, Y., Granberg, K. J., Hu, L., Haapasalo, H., Annala, M. J., Cogdell, D. E., Verploegen, M., Moore, L. M., Fuller, G. N., Nykter, M., Cavenee, W. K., & Zhang, W. 2016. IGFBP2 potentiates nuclear EGFR-STAT3 signaling. *Oncogene*, 35(6): 738–47.

Chung, A. S., & Ferrara, N. 2011. Developmental and Pathological Angiogenesis. *Annual Review of Cell and Developmental Biology*, 27(1): 563–584.

Clauss, M., Gerlach, M., Gerlach, H., Brett, J., Wang, F., Familletti, P. C., Pan, Y. C., Olander, J. V, Connolly, D. T., & Stern, D. 1990. Vascular permeability factor: a tumor-derived polypeptide that induces endothelial cell and monocyte procoagulant activity, and promotes monocyte migration. *The Journal of experimental medicine*, 172(6): 1535–45. Retrieved from http://www.ncbi.nlm.nih.gov/pubmed/2258694

Clemmons, D. R. 2012. Metabolic Actions of Insulin-Like Growth Factor-I in Normal Physiology and Diabetes. *Endocrinology and Metabolism Clinics of North America*, 41(2): 425–443.

Clemmons, D. R., Dehoff, M. L., Busby, W. H., Bayne, M. L., & Cascieri, M. A. 1992. Competition for binding to insulin-like growth factor (IGF) binding protein-2, 3, 4, and 5 by the IGFs and IGF analogs. *Endocrinology*, 131(2): 890–895.

Cohen, P., Peehl, D., & Rosenfeld, R. 1994. The IGF Axis in the Prostate. *Hormone and Metabolic Research*, 26(02): 81–84.

Conover, C. A., Mason, M. A., Bale, L. K., Harrington, S. C., Nyegaard, M., Oxvig, C., & Overgaard, M. T. 2010. Transgenic overexpression of pregnancy-associated plasma protein-A in murine arterial smooth muscle accelerates atherosclerotic lesion development. *American journal of physiology. Heart and circulatory physiology*, 299(2): H284-91.

Corkins, M. R., McQuade, J., Schaffer, B. S., & MacDonald, R. G. 2002. Insulin-like

growth factor binding protein-4 expression is dependent on the carbohydrate in the media in HT-29 cells. *Growth hormone & IGF research : official journal of the Growth Hormone Research Society and the International IGF Research Society*, 12(3): 184–92.

Coverley, J. A., & Baxter, R. C. 1997. Phosphorylation of insulin-like growth factor binding proteins. *Molecular and cellular endocrinology*, 128(1–2): 1–5. Retrieved from http://www.ncbi.nlm.nih.gov/pubmed/9140069

Dai, B., Ruan, B., Wu, J., Wang, J., Shang, R., Sun, W., Li, X., Dou, K., Wang, D., & Li, Y. 2014. Insulin-like growth factor binding protein-1 inhibits cancer cell invasion and is associated with poor prognosis in hepatocellular carcinoma. *International journal of clinical and experimental pathology*, 7(9): 5645–54. Retrieved from http://www.ncbi.nlm.nih.gov/pubmed/25337205

Damon, S. E., Maddison, L., Ware, J. L., & Plymate, S. R. 1998. Overexpression of an Inhibitory Insulin-Like Growth Factor Binding Protein (IGFBP), IGFBP-4, Delays Onset of Prostate Tumor Formation [1]. *Endocrinology*, 139(8): 3456–3464.

Das, S. K., Bhutia, S. K., Azab, B., Kegelman, T. P., Peachy, L., Santhekadur, P. K., Dasgupta, S., Dash, R., Dent, P., Grant, S., Emdad, L., Pellecchia, M., Sarkar, D., & Fisher, P. B. 2013. MDA-9/Syntenin and IGFBP-2 promote angiogenesis in human melanoma. *Cancer Research*, 73(2): 844–854.

de Kort, S. W. K., van Doorn, J., van de Sande, A. G. M., Leunissen, R. W. J., & Hokken-Koelega, A. C. S. 2010. Serum Insulin-Like Growth Factor-Binding Protein-2 Levels and Metabolic and Cardiovascular Risk Factors in Young Adults and Children Born Small for Gestational Age. *The Journal of Clinical Endocrinology & Metabolism*, 95(2): 864–871.

DeCicco-Skinner, K. L., Henry, G. H., Cataisson, C., Tabib, T., Gwilliam, J. C., Watson, N. J., Bullwinkle, E. M., Falkenburg, L., O'Neill, R. C., Morin, A., & Wiest, J. S. 2014. Endothelial cell tube formation assay for the in vitro study of angiogenesis.

Journal of visualized experiments : JoVE, 10(91): e51312.

Deev, R., Plaksa, I., Bozo, I., Mzhavanadze, N., Suchkov, I., Chervyakov, Y., Staroverov, I., Kalinin, R., & Isaev, A. 2018. Results of 5-year follow-up study in patients with peripheral artery disease treated with PL-VEGF165 for intermittent claudication. *Therapeutic Advances in Cardiovascular Disease*, 12(9): 237–246.

Dellinger, M. T., & Brekken, R. A. 2011. Phosphorylation of Akt and ERK1/2 Is Required for VEGF-A/VEGFR2-Induced Proliferation and Migration of Lymphatic Endothelium. (T. Kume, Ed.)*PLoS ONE*, 6(12): e28947.

DeMambro, V. E., Clemmons, D. R., Horton, L. G., Bouxsein, M. L., Wood, T. L., Beamer, W. G., Canalis, E., & Rosen, C. J. 2008. Gender-Specific Changes in Bone Turnover and Skeletal Architecture in *Igfbp - 2* -Null Mice. *Endocrinology*, 149(5): 2051–2061.

Demambro, V. E., Maile, L., Wai, C., Kawai, M., Cascella, T., Rosen, C. J., & Clemmons, D. 2012. Insulin-like growth factor-binding protein-2 is required for osteoclast differentiation. *Journal of Bone and Mineral Research*, 27(2): 390–400.

Deng, Y., wang, L., Ge, lite, duan, da, zhuo, yi, yuan, ting, yan, weiping, huang, peiqi, teng, xiaohua, & lu, ming. 2017. Effects of IGFBP-2 on proliferation and differentiation in neural stem cell line C17.2. *Journal of Neurorestoratology*, Volume 5: 143–153.

Deveza, L., Choi, J., & Yang, F. 2012. Therapeutic Angiogenesis for Treating Cardiovascular Diseases. *Theranostics*, 2(8): 801–814.

Dillon, L. M., & Miller, T. W. 2014. Therapeutic targeting of cancers with loss of PTEN function. *Current drug targets*, 15(1): 65–79. Retrieved from http://www.ncbi.nlm.nih.gov/pubmed/24387334

Duvall, C. L., Taylor, W. R., Weiss, D., & Guldberg, R. E. 2004. Quantitative microcomputed tomography analysis of collateral vessel development after ischemic injury. *American Journal of Physiology-Heart and Circulatory Physiology*, 287(1):

H302–H310.

Eckermann, C. W., Lehle, K., Schmid, S. A., Wheatley, D. N., & Kunz-Schughart, L. A. 2011. Characterization and modulation of fibroblast/endothelial cell co-cultures for the *in vitro* preformation of three-dimensional tubular networks. *Cell Biology International*, 35(11): 1097–1110.

Eltzschig, H. K., & Carmeliet, P. 2011. Hypoxia and inflammation. *The New England journal of medicine*, 364(7): 656–65.

Feng, N., Zhang, Z., Wang, Z., Zheng, H., Qu, F., He, X., & Wang, C. 2015. Insulin-Like Growth Factor Binding Protein-2 Promotes Adhesion of Endothelial Progenitor Cells to Endothelial Cells via Integrin α5β1. *Journal of Molecular Neuroscience*, 57(3): 426–434.

Ferrara, N., Carver-Moore, K., Chen, H., Dowd, M., Lu, L., O'Shea, K. S., Powell-Braxton, L., Hillan, K. J., & Moore, M. W. 1996. Heterozygous embryonic lethality induced by targeted inactivation of the VEGF gene. *Nature*, 380(6573): 439–442.

Ferrara, N., Gerber, H.-P., & LeCouter, J. 2003. The biology of VEGF and its receptors. *Nature Medicine*, 9(6): 669–676.

Fiedler, J., Brill, C., Blum, W. F., & Brenner, R. E. 2006. IGF-I and IGF-II stimulate directed cell migration of bone-marrow-derived human mesenchymal progenitor cells. *Biochemical and Biophysical Research Communications*, 345(3): 1177–1183.

Firth, S. M., & Baxter, R. C. 1999. Characterisation of recombinant glycosylation variants of insulin-like growth factor binding protein-3. *The Journal of endocrinology*, 160(3): 379–87. Retrieved from http://www.ncbi.nlm.nih.gov/pubmed/10076184

Fletcher, L., Isgor, E., Sprague, S., Williams, L. H., Alajajian, B. B., Jimenez, D. F., & Digicaylioglu, M. 2013. Spatial distribution of insulin-like growth factor binding protein-2 following hypoxic-ischemic injury. *BMC neuroscience*, 14: 158.

Folkman, J., & Moscona, A. 1978. Role of cell shape in growth control. *Nature*, 273(5661): 345–9. Retrieved from http://www.ncbi.nlm.nih.gov/pubmed/661946

Forbes, B. E., McCarthy, P., & Norton, R. S. 2012. Insulin-like growth factor binding proteins: a structural perspective. *Frontiers in endocrinology*, 3: 38.

Foulstone, E. J., Zeng, L., Perks, C. M., & Holly, J. M. P. 2013. Insulin-like growth factor binding protein 2 (IGFBP-2) promotes growth and survival of breast epithelial cells: Novel regulation of the estrogen receptor. *Endocrinology*, 154(5).

Fowlkes, J. L., Thrailkill, K. M., George-Nascimento, C., Rosenberg, C. K., & Serra, D. M. 1997. Heparin-binding, highly basic regions within the thyroglobulin type-1 repeat of insulin-like growth factor (IGF)-binding proteins (IGFBPs) -3, -5, and -6 inhibit IGFBP-4 degradation. *Endocrinology*, 138(6): 2280–2285.

Francavilla, C., Maddaluno, L., & Cavallaro, U. 2009. The functional role of cell adhesion molecules in tumor angiogenesis. *Seminars in Cancer Biology*, 19(5): 298–309.

Franklin, S. L., Ferry, R. J., & Cohen, P. 2003. Rapid Insulin-Like Growth Factor (IGF)-Independent Effects of IGF Binding Protein-3 on Endothelial Cell Survival. *The Journal of Clinical Endocrinology & Metabolism*, 88(2): 900–907.

Frantz, C., Stewart, K. M., & Weaver, V. M. 2010. The extracellular matrix at a glance. *Journal of cell science*, 123(Pt 24): 4195–200.

Frystyk, J., Skjaerbaek, C., Vestbo, E., Fisker, S., & Orskov, H. 1999. Circulating levels of free insulin-like growth factors in obese subjects: the impact of type 2 diabetes. *Diabetes/metabolism research and reviews*, 15(5): 314–22. Retrieved from http://www.ncbi.nlm.nih.gov/pubmed/10585616

Gao, S., Sun, Y., Zhang, X., Hu, L., Liu, Y., Chua, C. Y., Phillips, L. M., Ren, H., Fleming, J. B., Wang, H., Chiao, P. J., Hao, J., & Zhang, W. 2016. IGFBP2 Activates the NF-κB Pathway to Drive Epithelial–Mesenchymal Transition and Invasive Character in Pancreatic Ductal Adenocarcinoma. *Cancer Research*, 76(22): 6543–6554.

Gaunt, T. R., Cooper, J. A., Miller, G. J., Day, I. N. M., & O'Dell, S. D. 2001. Positive

associations between single nucleotide polymorphisms in the IGF2 gene region and body mass index in adult males. *Human Molecular Genetics*, 10(14): 1491–1501.

Gavard, J. 2014. Endothelial permeability and VE-cadherin: a wacky comradeship. *Cell adhesion & migration*, 8(2): 158–64.

Gavard, J., & Gutkind, J. S. 2006. VEGF controls endothelial-cell permeability by promoting the β-arrestin-dependent endocytosis of VE-cadherin. *Nature Cell Biology*, 8(11): 1223–1234.

Geiger, B., & Yamada, K. M. 2011. Molecular architecture and function of matrix adhesions. *Cold Spring Harbor perspectives in biology*, 3(5).

George, S. J., & Johnson, J. 2010. Pathogenesis of Atherosclerosis. *Atherosclerosis: Molecular and Cellular Mechanisms* (pp. 5–6).

Gimbrone, M. A., & García-Cardeña, G. 2016. Endothelial Cell Dysfunction and the Pathobiology of Atherosclerosis. *Circulation Research*, 118(4): 620–636.

Giraudo, E., Primo, L., Audero, E., Gerber, H. P., Koolwijk, P., Soker, S., Klagsbrun, M., Ferrara, N., & Bussolino, F. 1998. Tumor necrosis factor-alpha regulates expression of vascular endothelial growth factor receptor-2 and of its co-receptor neuropilin-1 in human vascular endothelial cells. *The Journal of biological chemistry*, 273(34): 22128–35. Retrieved from http://www.ncbi.nlm.nih.gov/pubmed/9705358

Goetz, J. G., Steed, E., Ferreira, R. R., Roth, S., Ramspacher, C., Boselli, F., Charvin, G., Liebling, M., Wyart, C., Schwab, Y., & Vermot, J. 2014. Endothelial Cilia Mediate Low Flow Sensing during Zebrafish Vascular Development. *Cell Reports*, 6(5): 799–808.

Gorenoi, V., Brehm, M. U., Koch, A., & Hagen, A. 2017. Growth factors for angiogenesis in peripheral arterial disease. *Cochrane Database of Systematic Reviews*, 6: CD011741.

Graham, M. E., Kilby, D. M., Firth, S. M., Robinson, P. J., & Baxter, R. C. 2007. The *in Vivo* Phosphorylation and Glycosylation of Human Insulin-like Growth Factor-

binding Protein-5. *Molecular & Cellular Proteomics*, 6(8): 1392–1405.

Granérus, M., Johannisson, A., Ekblom, P., & Engström, W. 2001. Insulin-like growth factors I and II induce cell death in Wilms's tumour cells. *Molecular pathology : MP*, 54(1): 30–5. Retrieved from http://www.ncbi.nlm.nih.gov/pubmed/11212886

Greenfield, N. J. 2006. Using circular dichroism spectra to estimate protein secondary structure. *Nature protocols*, 1(6): 2876–90.

Grimberg, A. 2000. p53 and IGFBP-3: Apoptosis and Cancer Protection. *Molecular Genetics and Metabolism*, 70(2): 85–98.

Grimberg, A., Coleman, C. M., Shi, Z., Burns, T. F., MacLachlan, T. K., Wang, W., & El-Deiry, W. S. 2006. Insulin-like growth factor factor binding protein-2 is a novel mediator of p53 inhibition of insulin-like growth factor signaling. *Cancer biology & therapy*, 5(10): 1408–14. Retrieved from http://www.ncbi.nlm.nih.gov/pubmed/17102589

Gupta, M. B. 2015. The role and regulation of IGFBP-1 phosphorylation in fetal growth restriction. *Journal of cell communication and signaling*, 9(2): 111–23.

Hamidouche, Z., Fromigué, O., Ringe, J., Häupl, T., & Marie, P. J. 2010. Crosstalks between integrin alpha 5 and IGF2/IGFBP2 signalling trigger human bone marrow-derived mesenchymal stromal osteogenic differentiation. *BMC Cell Biology*, 11(1): 44.

Han, S., Li, Z., Master, L. M., Master, Z. W., & Wu, A. 2014. Exogenous IGFBP-2 promotes proliferation, invasion, and chemoresistance to temozolomide in glioma cells via the integrin β1-ERK pathway. *British Journal of Cancer*, 111(7): 1400–1409.

Harburger, D. S., & Calderwood, D. A. 2009. Integrin signalling at a glance. *Journal of cell science*, 122(Pt 2): 159–63.

Harrington, S. C., Simari, R. D., & Conover, C. A. 2007. Genetic Deletion of Pregnancy-Associated Plasma Protein-A Is Associated With Resistance to Atherosclerotic Lesion Development in Apolipoprotein E–Deficient Mice Challenged

With a High-Fat Diet. *Circulation Research*, 100(12): 1696–1702.

Haryadi, R., Ho, S., Kok, Y. J., Pu, H. X., Zheng, L., Pereira, N. A., Li, B., Bi, X., Goh, L.-T., Yang, Y., & Song, Z. 2015. Optimization of heavy chain and light chain signal peptides for high level expression of therapeutic antibodies in CHO cells. *PloS one*, 10(2): e0116878.

Haywood, N. J., Cordell, P. A., Tang, K. Y., Makova, N., Yuldasheva, N. Y., Imrie, H., Viswambharan, H., Bruns, A. F., Cubbon, R. M., Kearney, M. T., & Wheatcroft, S. B. 2017. Insulin-Like Growth Factor Binding Protein 1 Could Improve Glucose Regulation and Insulin Sensitivity Through Its RGD Domain. *Diabetes*, 66(2): 287–299.

Heald, A., Kaushal, K., Siddals, K., Rudenski, A., Anderson, S., & Gibson, J. 2006. Insulin-like Growth Factor Binding Protein-2 (IGFBP-2) is a Marker for the Metabolic Syndrome. *Experimental and Clinical Endocrinology & Diabetes*, 114(07): 371–376.

Heart Outcomes Prevention Evaluation Study Investigators, Yusuf, S., Sleight, P., Pogue, J., Bosch, J., Davies, R., & Dagenais, G. 2000. Effects of an Angiotensin-Converting–Enzyme Inhibitor, Ramipril, on Cardiovascular Events in High-Risk Patients. *New England Journal of Medicine*, 342(3): 145–153.

Hedbacker, K., Birsoy, K., Wysocki, R. W., Asilmaz, E., Ahima, R. S., Farooqi, I. S., & Friedman, J. M. 2010. Antidiabetic Effects of IGFBP2, a Leptin-Regulated Gene. *Cell Metabolism*, 11(1): 11–22.

Heil, M., Eitenmüller, I., Schmitz-Rixen, T., & Schaper, W. 2006. Arteriogenesis versus angiogenesis: similarities and differences. *Journal of cellular and molecular medicine*, 10(1): 45–55.

Ho, S. C. L., Koh, E. Y. C., van Beers, M., Mueller, M., Wan, C., Teo, G., Song, Z., Tong, Y. W., Bardor, M., & Yang, Y. 2013. Control of IgG LC:HC ratio in stably transfected CHO cells and study of the impact on expression, aggregation, glycosylation and conformational stability. *Journal of Biotechnology*, 165(3–4): 157–

166.

Hoang, M. V., Nagy, J. A., & Senger, D. R. 2011. Active Rac1 improves pathologic VEGF neovessel architecture and reduces vascular leak: Mechanistic similarities with angiopoietin-1. *Blood*, 117(5): 1751–1760.

Hoeben, A. N. N., Landuyt, B., Highley, M. S. M., Wildiers, H., Oosterom, A. T. V. a N., Bruijn, E. a D. E., Van Oosterom, A. T., & De Bruijn, E. a. 2004. Vascular endothelial growth factor and angiogenesis. *Pharmacological reviews*, 56(4): 549–580.

Hoeflich, A., David, R., & Hjortebjerg, R. 2018. Current IGFBP-Related Biomarker Research in Cardiovascular Disease—We Need More Structural and Functional Information in Clinical Studies. *Frontiers in Endocrinology*, 9: 388.

Hoeflich, A., & Russo, V. C. 2015. Physiology and pathophysiology of IGFBP-1 and IGFBP-2 – Consensus and dissent on metabolic control and malignant potential. *Best Practice & Research Clinical Endocrinology & Metabolism*, 29(5): 685–700.

Hoeflich, A., Wu, M., Mohan, S., Föll, J., Wanke, R., Froehlich, T., Arnold, G. J., Lahm, H., Kolb, H. J., & Wolf, E. 1999. Overexpression of Insulin-Like Growth Factor-Binding Protein-2 in Transgenic Mice Reduces Postnatal Body Weight Gain. *Endocrinology*, 140(12): 5488–5496.

Holmes, K. M., Annala, M., Chua, C. Y. X., Dunlap, S. M., Liu, Y., Hugen, N., Moore, L. M., Cogdell, D., Hu, L., Nykter, M., Hess, K., Fuller, G. N., & Zhang, W. 2012. Insulin-like growth factor-binding protein 2-driven glioma progression is prevented by blocking a clinically significant integrin, integrin-linked kinase, and NF-κB network. *Proceedings of the National Academy of Sciences of the United States of America*, 109(9): 3475–80.

Hosaka, K., Yang, Y., Nakamura, M., Andersson, P., Yang, X., Zhang, Y., Seki, T., Scherzer, M., Dubey, O., Wang, X., & Cao, Y. 2018. Dual roles of endothelial FGF-2–FGFR1–PDGF-BB and perivascular FGF-2–FGFR2–PDGFRβ signaling pathways

in tumor vascular remodeling. *Cell Discovery*, 4(1): 3.

Htay, T., & Liu, M. W. 2005. Drug-eluting stent: a review and update. *Vascular health and risk management*, 1(4): 263–76. Retrieved from http://www.ncbi.nlm.nih.gov/pubmed/17315599

Hung, C.-S., Huang, C.-Y., Lee, C.-H., Chen, W.-Y., Huang, M.-T., Wei, P.-L., & Chang, Y.-J. 2017. IGFBP2 plays an important role in heat shock protein 27-mediated cancer progression and metastasis. *Oncotarget*, 8(33): 54978–54992.

Huynh, H., Iizuka, S., Kaba, M., Kirak, O., Zheng, J., Lodish, H. F., & Zhang, C. C. 2008. Insulin-Like Growth Factor-Binding Protein 2 Secreted by a Tumorigenic Cell Line Supports Ex Vivo Expansion of Mouse Hematopoietic Stem Cells. *Stem Cells*, 26(6): 1628–1635.

Huynh, H., Zheng, J., Umikawa, M., Zhang, C., Silvany, R., Iizuka, S., Holzenberger, M., Zhang, W., & Zhang, C. C. 2011. IGF binding protein 2 supports the survival and cycling of hematopoietic stem cells. *Blood*, 118(12): 3236–43.

Imrie, H., Abbas, A., Viswambharan, H., Rajwani, A., Cubbon, R. M., Gage, M., Kahn, M., Ezzat, V. A., Duncan, E. R., Grant, P. J., Ajjan, R., Wheatcroft, S. B., & Kearney, M. T. 2009. Vascular Insulin-Like Growth Factor-I Resistance and Diet-Induced Obesity. *Endocrinology*, 150(10): 4575–4582.

Imrie, H., Viswambharan, H., Sukumar, P., Abbas, A., Cubbon, R. M., Yuldasheva, N., Gage, M., Smith, J., Galloway, S., Skromna, A., Rashid, S. T., Futers, T. S., Xuan, S., Gatenby, V. K., Grant, P. J., Channon, K. M., Beech, D. J., Wheatcroft, S. B., & Kearney, M. T. 2012. Novel role of the IGF-1 receptor in endothelial function and repair: studies in endothelium-targeted IGF-1 receptor transgenic mice. *Diabetes*, 61(9): 2359–68.

Isner, J. M., Pieczek, A., Schainfeld, R., Blair, R., Haley, L., Asahara, T., Rosenfield, K., Razvi, S., Walsh, K., & Symes, J. F. 1996. Clinical evidence of angiogenesis after arterial gene transfer of phVEGF165 in patient with ischaemic limb. *Lancet (London,*

England), 348(9024): 370–4.

Iwasawa, E., Ichijo, M., Ishibashi, S., & Yokota, T. 2016. Acute development of collateral circulation and therapeutic prospects in ischemic stroke. *Neural regeneration research*, 11(3): 368–71.

Iyer, S. R., & Annex, B. H. 2017. Therapeutic Angiogenesis for Peripheral Artery Disease. *JACC: Basic to Translational Science*, 2(5): 503–512.

Jiang, Y., Zhang, Q., & Steinle, J. J. 2014. Intravitreal Injection of IGFBP-3 Restores Normal Insulin Signaling in Diabetic Rat Retina. (J. Chen, Ed.)*PLoS ONE*, 9(4): e93788.

Johnson-Farley, N. N., Patel, K., Kim, D., & Cowen, D. S. 2007. Interaction of FGF-2 with IGF-1 and BDNF in stimulating Akt, ERK, and neuronal survival in hippocampal cultures. *Brain Research*, 1154: 40–49.

Johnson, K. E., & Wilgus, T. A. 2014. Vascular Endothelial Growth Factor and Angiogenesis in the Regulation of Cutaneous Wound Repair. *Advances in Wound Care*, 3(10): 647–661.

Jones, J., Gockerman, A., Busby, W., Wright, G., & Clemmons, D. 1993. Insulin-Like Growth Factor Binding Protein 1 Stimulates Cell Migration and Binds to the alpha5beta1 Integrin by Means of its Arg-Gly-Asp Sequence. *Proc Nat Acad Sci*.

Kabir, G., Hossain, M., Faruque, M. O., Hassan, N., Hassan, Z., Nahar, Q., Shefin, S. M., Alauddin, M., & Ali, L. 2010. Association of serum free IGF-1 and IGFBP-1 with insulin sensitivity in impaired glucose tolerance (IGT). *International Journal of Diabetes Mellitus*, 2(3): 144–147.

Kadakia, R., & Josefson, J. 2016. The Relationship of Insulin-Like Growth Factor 2 to Fetal Growth and Adiposity. *Hormone Research in Paediatrics*, 85(2): 75–82.

Kanety, H., Madjar, Y., Dagan, Y., Levi, J., Papa, M. Z., Pariente, C., Goldwasser, B., & Karasik, A. 1993. Serum insulin-like growth factor-binding protein-2 (IGFBP-2) is increased and IGFBP-3 is decreased in patients with prostate cancer: correlation

with serum prostate-specific antigen. *The Journal of Clinical Endocrinology & Metabolism*, 77(1): 229–233.

Kano, M. R., Morishita, Y., Iwata, C., Iwasaka, S., Watabe, T., Ouchi, Y., Miyazono, K., & Miyazawa, K. 2005. VEGF-A and FGF-2 synergistically promote neoangiogenesis through enhancement of endogenous PDGF-B-PDGFR signaling. *Journal of Cell Science*, 118(16): 3759–3768.

Karar, J., & Maity, A. 2011. PI3K/AKT/mTOR Pathway in Angiogenesis. *Frontiers in Molecular Neuroscience*, 4: 51.

Kawai, M., Breggia, A. C., Demambro, V. E., Shen, X., Canalis, E., Bouxsein, M. L., Beamer, W. G., Clemmons, D. R., & Rosen, C. J. 2011. The heparin-binding domain of IGFBP-2 has insulin-like growth factor binding-independent biologic activity in the growing skeleton. *Journal of Biological Chemistry*, 286(16): 14670–14680.

Khan, K. H. 2013. Gene expression in Mammalian cells and its applications. *Advanced pharmaceutical bulletin*, 3(2): 257–63.

Khoo, C. P., Micklem, K., & Watt, S. M. 2011. A comparison of methods for quantifying angiogenesis in the Matrigel assay in vitro. *Tissue engineering. Part C, Methods*, 17(9): 895–906.

Khow, O., & Suntrarachun, S. 2012. Strategies for production of active eukaryotic proteins in bacterial expression system. *Asian Pacific journal of tropical biomedicine*, 2(2): 159–62.

Kiepe, D., Ulinski, T., Powell, D. R., Durham, S. K., Mehls, O., & Tönshoff, B. 2002. Differential effects of insulin-like growth factor binding proteins-1, -2, -3, and -6 on cultured growth plate chondrocytes. *Kidney International*, 62(5): 1591–1600.

Kim, H. S., Nagalla, S. R., Oh, Y., Wilson, E., Roberts, C. T., & Rosenfeld, R. G. 1997. Identification of a family of low-affinity insulin-like growth factor binding proteins (IGFBPs): characterization of connective tissue growth factor as a member of the IGFBP superfamily. *Proceedings of the National Academy of Sciences of the United*

States of America, 94(24): 12981–6. Retrieved from http://www.ncbi.nlm.nih.gov/pubmed/9371786

Kim, S. J., Kim, S. Y., Kwon, C. H., & Kim, Y. K. 2007. Differential effect of FGF and PDGF on cell proliferation and migration in osteoblastic cells. *Growth Factors*, 25(2): 77–86.

Kimura, M., Murakami, T., Kizaka-Kondoh, S., Itoh, M., Yamamoto, K., Hojo, Y., Takano, M., Kario, K., Shimada, K., & Kobayashi, E. 2010. Functional molecular imaging of ILK-mediated Akt/PKB signaling cascades and the associated role of beta-parvin. *Journal of cell science*, 123(Pt 5): 747–55.

Krock, B. L., Skuli, N., & Simon, M. C. 2011. Hypoxia-Induced Angiogenesis: Good and Evil. *Genes & Cancer*, 2(12): 1117–1133.

Kumar, P., Shen, Q., Pivetti, C. D., Lee, E. S., Wu, M. H., & Yuan, S. Y. 2009. Molecular mechanisms of endothelial hyperpermeability: implications in inflammation. *Expert reviews in molecular medicine*, 11: e19.

Lau, Y.-T. K., Baytshtok, V., Howard, T. A., Fiala, B. M., Johnson, J. M., Carter, L. P., Baker, D., Lima, C. D., & Bahl, C. D. 2018. Discovery and engineering of enhanced SUMO protease enzymes. *The Journal of biological chemistry*, 293(34): 13224–13233.

Lee, C.-D., Sun, H.-C., Hu, S.-M., Chiu, C.-F., Homhuan, A., Liang, S.-M., Leng, C.-H., & Wang, T.-F. 2008. An improved SUMO fusion protein system for effective production of native proteins. *Protein science : a publication of the Protein Society*, 17(7): 1241–8.

Lee, J. C., Chow, N. H., Wang, S. T., & Huang, S. M. 2000. Prognostic value of vascular endothelial growth factor expression in colorectal cancer patients. *European journal of cancer (Oxford, England : 1990)*, 36(6): 748–53. Retrieved from http://www.ncbi.nlm.nih.gov/pubmed/10762747

Legate, K. R., & Fassler, R. 2009. Mechanisms that regulate adaptor binding to -

integrin cytoplasmic tails. *Journal of Cell Science*, 122(2): 187–198.

Li, Y., Hazarika, S., Xie, D., Pippen, A. M., Kontos, C. D., & Annex, B. H. 2007. In Mice With Type 2 Diabetes, a Vascular Endothelial Growth Factor (VEGF)-Activating Transcription Factor Modulates VEGF Signaling and Induces Therapeutic Angiogenesis After Hindlimb Ischemia. *Diabetes*, 56(3): 656–665.

LI, Z., LV, Y., GUO, W., & WANG, G. 2018. IGFBP-2 Ameliorates Vascular Insulin Resistance and Contributes to Cardiometabolism. *Diabetes*, 67(Supplement 1): 2193–PUB.

Limbourg, A., Korff, T., Napp, L. C., Schaper, W., Drexler, H., & Limbourg, F. P. 2009. Evaluation of postnatal arteriogenesis and angiogenesis in a mouse model of hind-limb ischemia. *Nature protocols*, 4(12): 1737–46.

Lin, C.-S., Ho, H.-C., Gholami, S., Chen, K.-C., Jad, A., & Lue, T. F. 2001. Gene Expression Profiling of an Arteriogenic Impotence Model. *Biochemical and Biophysical Research Communications*, 285(2): 565–569.

Lin, K. W., Liao, A., & Qutub, A. A. 2015. Simulation Predicts IGFBP2-HIF1α Interaction Drives Glioblastoma Growth. (V. Cristini, Ed.)*PLOS Computational Biology*, 11(4): e1004169.

Lin, Y., Jiang, T., Zhou, K., Xu, L., Chen, B., Li, G., Qiu, X., Jiang, T., Zhang, W., & Song, S. W. 2009. Plasma IGFBP-2 levels predict clinical outcomes of patients with high-grade gliomas. *Neuro-oncology*, 11(5): 468–476.

Liotta, F., Annunziato, F., Castellani, S., Boddi, M., Alterini, B., Castellini, G., Mazzanti, B., Cosmi, L., Acquafresca, M., Bartalesi, F., Dilaghi, B., Dorigo, W., Graziani, G., Bartolozzi, B., Bellandi, G., Carli, G., Bartoloni, A., Fargion, A., Fassio, F., Fontanari, P., et al. 2018. Therapeutic Efficacy of Autologous Non-Mobilized Enriched Circulating Endothelial Progenitors in Patients With Critical Limb Ischemia — The SCELTA Trial —. *Circulation Journal*, 82(6): 1688–1698.

Liu, H., Li, L., Chen, H., Kong, R., Pan, S., Hu, J., Wang, Y., Li, Y., & Sun, B. 2017.

Silencing IGFBP-2 decreases pancreatic cancer metastasis and enhances chemotherapeutic sensitivity. Retrieved from www.impactjournals.com/oncotarget

Livingston, E. H., & Lynm, C. 2012. Stents to Treat Coronary Artery Blockages. *JAMA*, 308(17): 1824.

Lloyd-Jones, D. M., Nam, B.-H., D'Agostino, Sr, R. B., Levy, D., Murabito, J. M., Wang, T. J., Wilson, P. W. F., & O'Donnell, C. J. 2004. Parental Cardiovascular Disease as a Risk Factor for Cardiovascular Disease in Middle-aged Adults. *JAMA*, 291(18): 2204.

Lopez-Lopez, C., LeRoith, D., & Torres-Aleman, I. 2004. Insulin-like growth factor I is required for vessel remodeling in the adult brain. *Proceedings of the National Academy of Sciences*, 101(26): 9833–9838.

Lorenzo-Zúñiga, V., Rodríguez-Ortigosa, C. M., Bartolí, R., Martínez-Chantar, M.-L., Martínez-Peralta, L., Pardo, A., Ojanguren, I., Quiroga, J., Planas, R., & Prieto, J. 2006. Insulin-like growth factor I improves intestinal barrier function in cirrhotic rats. *Gut*, 55(9): 1306–12.

Lozano, I., Capin, E., de la Hera, J. M., Llosa, J. C., Carro, A., & López-Palop, R. 2015. Diffuse Coronary Artery Disease Not Amenable to Revascularization: Long-term Prognosis. *Revista Española de Cardiología (English Edition)*, 68(7): 631–633.

Lu, H., Wang, L., Gao, W., Meng, J., Dai, B., Wu, S., Minna, J., Roth, J. A., Hofstetter, W. L., Swisher, S. G., & Fang, B. 2013. IGFBP2/FAK Pathway Is Causally Associated with Dasatinib Resistance in Non-Small Cell Lung Cancer Cells. *Molecular Cancer Therapeutics*, 12(12): 2864–2873.

Madaric, J., Valachovicova, M., Paulis, L., Pribojova, J., Mateova, R., Sebekova, K., Postulkova, L., Madaricova, T., Bucova, M., Mistrik, M., & Vulev, I. 2017. Improvement in asymmetric dimethylarginine and oxidative stress in patients with limb salvage after autologous mononuclear stem cell application for critical limb ischemia. *Stem cell research & therapy*, 8(1): 165.

Makarevich, P. I., & Parfyonova, Y. V. 2017. Therapeutic Angiogenesis: Foundations and Practical Application. *Physiologic and Pathologic Angiogenesis - Signaling Mechanisms and Targeted Therapy*. InTech.

Malakhov, M. P., Mattern, M. R., Malakhova, O. A., Drinker, M., Weeks, S. D., & Butt, T. R. 2004. SUMO fusions and SUMO-specific protease for efficient expression and purification of proteins. *Journal of Structural and Functional Genomics*, 5(1/2): 75–86.

Marinaro, J. A., Neumann, G. M., Russo, V. C., Leeding, K. S., & Bach, L. A. 2000. O-glycosylation of insulin-like growth factor (IGF) binding protein-6 maintains high IGF-II binding affinity by decreasing binding to glycosaminoglycans and susceptibility to proteolysis. *European Journal of Biochemistry*, 267(17): 5378–5386.

Martha, S., Pantam, N., Thungathurthi, S., Rao, V. L. N., & Devarakonda, K. 2008. Study of insulin resistance in relation to serum IGF-I levels in subjects with different degrees of glucose tolerance. *International journal of diabetes in developing countries*, 28(2): 54–9.

Martin, J. L., & Baxter, R. C. 2007. Expression of Insulin-Like Growth Factor Binding Protein-2 by MCF-7 Breast Cancer Cells Is Regulated through the Phosphatidylinositol 3-Kinase/AKT/Mammalian Target of Rapamycin Pathway. *Endocrinology*, 148(5): 2532–2541.

Marzec, K. A., Baxter, R. C., & Martin, J. L. 2015. Targeting Insulin-Like Growth Factor Binding Protein-3 Signaling in Triple-Negative Breast Cancer. *BioMed research international*, 2015: 638526.

Mehrian-Shai, R., Chen, C. D., Shi, T., Horvath, S., Nelson, S. F., Reichardt, J. K. V., & Sawyers, C. L. 2007. Insulin growth factor-binding protein 2 is a candidate biomarker for PTEN status and PI3K/Akt pathway activation in glioblastoma and prostate cancer. *Proceedings of the National Academy of Sciences*, 104(13): 5563–5568.

Mehta, H. H., Gao, Q., Galet, C., Paharkova, V., Wan, J., Said, J., Sohn, J. J., Lawson, G., Cohen, P., Cobb, L. J., & Lee, K.-W. 2011. IGFBP-3 Is a Metastasis Suppression Gene in Prostate Cancer. *Cancer Research*, 71(15): 5154–5163.

Meier, P., Schirmer, S. H., Lansky, A. J., Timmis, A., Pitt, B., & Seiler, C. 2013. The collateral circulation of the heart. *BMC Medicine*, 11(1): 143.

Mendes, K. N., Wang, G. K., Fuller, G. N., & Zhang, W. 2010. JNK mediates insulin-like growth factor binding protein 2/integrin alpha5-dependent glioma cell migration. *International journal of oncology*, 37(1): 143–53. Retrieved from http://www.ncbi.nlm.nih.gov/pubmed/20514406

Mishra, S., & Murphy, L. J. 2003. Phosphorylation of Insulin-Like Growth Factor (IGF) Binding Protein-3 by Breast Cancer Cell Membranes Enhances IGF-I Binding. *Endocrinology*, 144(9): 4042–4050.

Miyako, K., Cobb, L. J., Francis, M., Huang, A., Peng, B., Pintar, J. E., Ariga, H., & Cohen, P. 2009. PAPA-1 Is a nuclear binding partner of IGFBP-2 and modulates its growth-promoting actions. *Molecular endocrinology (Baltimore, Md.)*, 23(2): 169–75.

Moore, L. M., Holmes, K. M., Smith, S. M., Wu, Y., Tchougounova, E., Uhrbom, L., Sawaya, R., Bruner, J. M., Fuller, G. N., & Zhang, W. 2009. IGFBP2 is a candidate biomarker for Ink4a-Arf status and a therapeutic target for high-grade gliomas. *Proceedings of the National Academy of Sciences of the United States of America*, 106(39): 16675–9.

Morley, R. L., Sharma, A., Horsch, A. D., & Hinchliffe, R. J. 2018. Peripheral artery disease. *BMJ (Clinical research ed.)*, 360: j5842. Retrieved from http://www.ncbi.nlm.nih.gov/pubmed/29419394

Morse, E. M., Brahme, N. N., & Calderwood, D. A. 2014. Integrin Cytoplasmic Tail Interactions. *Biochemistry*, 53(5): 810–820.

Moser, D. R., Lowe, W. L., Dake, B. L., Booth, B. A., Boes, M., Clemmons, D. R., & Bar, R. S. 1992. Endothelial cells express insulin-like growth factor-binding proteins

2 to 6. *Molecular Endocrinology*, 6(11): 1805–1814.

Muhič, M., Vardjan, N., Chowdhury, H. H., Zorec, R., & Kreft, M. 2015. Insulin and Insulin-like Growth Factor 1 (IGF-1) Modulate Cytoplasmic Glucose and Glycogen Levels but Not Glucose Transport across the Membrane in Astrocytes. *The Journal of biological chemistry*, 290(17): 11167–76.

Myers, A. L., Lin, L., Nancarrow, D. J., Wang, Z., Ferrer-Torres, D., Thomas, D. G., Orringer, M. B., Lin, J., Reddy, R. M., Beer, D. G., & Chang, A. C. 2015. IGFBP2 modulates the chemoresistant phenotype in esophageal adenocarcinoma. *Oncotarget*, 6(28): 25897–916.

Nakatsu, M. N., Davis, J., & Hughes, C. C. W. 2007. Optimized fibrin gel bead assay for the study of angiogenesis. *Journal of visualized experiments : JoVE*, (3): 186.

Naseem, K. M. 2005, April. The role of nitric oxide in cardiovascular diseases. *Molecular Aspects of Medicine*.

Nieto-Estévez, V., Defterali, Ç., & Vicario-Abejón, C. 2016. IGF-I: A Key Growth Factor that Regulates Neurogenesis and Synaptogenesis from Embryonic to Adult Stages of the Brain. *Frontiers in neuroscience*, 10: 52.

Niiyama, H., Huang, N. F., Rollins, M. D., & Cooke, J. P. 2009. Murine model of hindlimb ischemia. *Journal of visualized experiments : JoVE*, (23): 12–14.

Norton, K.-A., & Popel, A. S. 2016. Effects of endothelial cell proliferation and migration rates in a computational model of sprouting angiogenesis. *Scientific Reports*, 6(1): 36992.

Novo, S., Coppola, G., & Milio, G. 2004. Critical limb ischemia: definition and natural history. *Current drug targets. Cardiovascular & haematological disorders*, 4(3): 219–25. Retrieved from http://www.ncbi.nlm.nih.gov/pubmed/15379613

Nussbaum, T., Samarin, J., Ehemann, V., Bissinger, M., Ryschich, E., Khamidjanov, A., Yu, X., Gretz, N., Schirmacher, P., & Breuhahn, K. 2008. Autocrine insulin-like growth factor-II stimulation of tumor cell migration is a progression step in human

hepatocarcinogenesis. *Hepatology*, 48(1): 146–156.

Okura, Y., Brink, M., Zahid, A. A., Anwar, A., & Delafontaine, P. 2001. Decreased Expression of Insulin-like Growth Factor-1 and Apoptosis of Vascular Smooth Muscle Cells in Human Atherosclerotic Plaque. *Journal of Molecular and Cellular Cardiology*, 33(10): 1777–1789.

Olin, J. W., & Sealove, B. A. 2010. Peripheral Artery Disease: Current Insight Into the Disease and Its Diagnosis and Management. *Mayo Clinic Proceedings*, 85(7): 678–692.

Oommen, S., Gupta, S. K., & Vlahakis, N. E. 2011. Vascular Endothelial Growth Factor A (VEGF-A) Induces Endothelial and Cancer Cell Migration through Direct Binding to Integrin 9 1: IDENTIFICATION OF A SPECIFIC 9 1 BINDING SITE. *Journal of Biological Chemistry*, 286(2): 1083–1092.

Ourradi, K., Blythe, T., Jarrett, C., Barratt, S. L., Welsh, G. I., & Millar, A. B. 2017. VEGF isoforms have differential effects on permeability of human pulmonary microvascular endothelial cells. *Respiratory research*, 18(1): 116.

Panavas, T., Sanders, C., & Butt, T. R. 2009. SUMO Fusion Technology for Enhanced Protein Production in Prokaryotic and Eukaryotic Expression Systems. *Methods in molecular biology (Clifton, N.J.)* (Vol. 497, pp. 303–317).

Park, S. H., Kim, K. W., & Kim, J. C. 2015. The Role of Insulin-Like Growth Factor Binding Protein 2 (IGFBP2) in the Regulation of Corneal Fibroblast Differentiation. *Investigative Opthalmology & Visual Science*, 56(12): 7293.

Patil, S. S., Gokulnath, P., Bashir, M., Shwetha, S. D., Jaiswal, J., Shastry, A. H., Arimappamagan, A., Santosh, V., & Kondaiah, P. 2016. Insulin-like growth factor binding protein-2 regulates β-catenin signaling pathway in glioma cells and contributes to poor patient prognosis. *Neuro-oncology*, 18(11): 1487–1497.

Patrick, Jr., C. W., & McIntire, L. V. 1995. Shear Stress and Cyclic Strain Modulation of Gene Expression in Vascular Endothelial Cells. *Blood Purification*, 13(3–4): 112–

124.

Pereira, J. J., Meyer, T., Docherty, S. E., Reid, H. H., Marshall, J., Thompson, E. W., Rossjohn, J., & Price, J. T. 2004. Bimolecular interaction of insulin-like growth factor (IGF) binding protein-2 with alphavbeta3 negatively modulates IGF-I-mediated migration and tumor growth. *Cancer research*, 64(3): 977–84. Retrieved from http://www.ncbi.nlm.nih.gov/pubmed/14871828

Perks, C. ., McCaig, C., Clarke, J. ., Clemmons, D. ., & Holly, J. M. . 2002. A non-IGF binding mutant of IGFBP-3 modulates cell function in breast epithelial cells. *Biochemical and Biophysical Research Communications*, 294(5): 988–994.

Peroutka III, R. J., Orcutt, S. J., Strickler, J. E., & Butt, T. R. 2011. SUMO Fusion Technology for Enhanced Protein Expression and Purification in Prokaryotes and Eukaryotes. *Methods in molecular biology (Clifton, N.J.)* (Vol. 705, pp. 15–30).

Planque, N. 2006. Nuclear trafficking of secreted factors and cell-surface receptors: new pathways to regulate cell proliferation and differentiation, and involvement in cancers. *Cell Communication and Signaling*, 4(1): 7.

Png, K. J., Halberg, N., Yoshida, M., & Tavazoie, S. F. 2012. A microRNA regulon that mediates endothelial recruitment and metastasis by cancer cells. *Nature*, 481(7380): 190–194.

Rajwani, A., Ezzat, V., Smith, J., Yuldasheva, N. Y., Duncan, E. R., Gage, M., Cubbon, R. M., Kahn, M. B., Imrie, H., Abbas, A., Viswambharan, H., Aziz, A., Sukumar, P., Vidal-Puig, A., Sethi, J. K., Xuan, S., Shah, A. M., Grant, P. J., Porter, K. E., Kearney, M. T., et al. 2012. Increasing Circulating IGFBP1 Levels Improves Insulin Sensitivity, Promotes Nitric Oxide Production, Lowers Blood Pressure, and Protects Against Atherosclerosis. *Diabetes*, 61(4): 915–924.

Rakue, H., Nakajima, H., Katoh, T., Usui, M., Amemiya, T., Miyagi, M., Hara, T., Tamura, K., Sasame, A., Naito, Y., Nagai, Y., & Ibukiyama, C. 1998. Low-dose basic fibroblast growth factor and vascular endothelial growth factor for angiogenesis in

canine acute hindlimb insufficiency. *Japanese circulation journal*, 62(12): 933–9. Retrieved from http://www.ncbi.nlm.nih.gov/pubmed/9890208

Ramakrishnan, S., Anand, V., & Roy, S. 2014. Vascular Endothelial Growth Factor Signaling in Hypoxia and Inflammation. *Journal of Neuroimmune Pharmacology*, 9(2): 142–160.

Reardon, D. A., Turner, S., Peters, K. B., Desjardins, A., Gururangan, S., Sampson, J. H., McLendon, R. E., Herndon, J. E., Jones, L. W., Kirkpatrick, J. P., Friedman, A. H., Vredenburgh, J. J., Bigner, D. D., & Friedman, H. S. 2011. A review of VEGF/VEGFR-targeted therapeutics for recurrent glioblastoma. *Journal of the National Comprehensive Cancer Network : JNCCN*, 9(4): 414–27. Retrieved from http://www.ncbi.nlm.nih.gov/pubmed/21464146

Reyer, A., Schindler, N., Ohde, D., Walz, C., Kunze, M., Tuchscherer, A., Wirthgen, E., Brenmoehl, J., & Hoeflich, A. 2015. The RGD sequence present in IGFBP-2 is required for reduced glucose clearance after oral glucose administration in female transgenic mice. *American Journal of Physiology-Endocrinology and Metabolism*, 309(4): E409–E417.

Rhodes, J. M., & Simons, M. 2007. The extracellular matrix and blood vessel formation: not just a scaffold. *Journal of Cellular and Molecular Medicine*, 11(2): 176–205.

Ribatti, D., Vacca, A., Nico, B., Roncali, L., & Dammacco, F. 2001. Postnatal vasculogenesis. *Mechanisms of development*, 100(2): 157–63. Retrieved from http://www.ncbi.nlm.nih.gov/pubmed/11165474

Rizzi, A., Benagiano, V., & Ribatti, D. 2017. Angiogenesis versus arteriogenesis. *Rom J Morphol Embryol*, 58(1): 15–19. Retrieved from http://www.rjme.ro/

Roberts, A. C., Gohil, J., Hudson, L., Connolly, K., Warburton, P., Suman, R., O'Toole, P., O'Regan, D. J., Turner, N. A., Riches, K., & Porter, K. E. 2015. Aberrant phenotype in human endothelial cells of diabetic origin: implications for saphenous

vein graft failure? *Journal of diabetes research*, 2015: 409432.

Rosano, G. L., & Ceccarelli, E. A. 2014. Recombinant protein expression in Escherichia coli: advances and challenges. *Frontiers in microbiology*, 5: 172.

Rosenzweig, S. A. 2004. What's new in the IGF-binding proteins?

Ross, A. H., & Gericke, A. 2009. Phosphorylation keeps PTEN phosphatase closed for business. *Proceedings of the National Academy of Sciences of the United States of America*, 106(5): 1297–8.

Roth, G. A., Johnson, C., Abajobir, A., Abd-Allah, F., Abera, S. F., Abyu, G., Ahmed, M., Aksut, B., Alam, T., Alam, K., Alla, F., Alvis-Guzman, N., Amrock, S., Ansari, H., Ärnlöv, J., Asayesh, H., Atey, T. M., Avila-Burgos, L., Awasthi, A., Banerjee, A., et al. 2017. Global, Regional, and National Burden of Cardiovascular Diseases for 10 Causes, 1990 to 2015. *Journal of the American College of Cardiology*, 70(1): 1–25.

Rusnati, M., Tanghetti, E., Dell'Era, P., Gualandris, A., & Presta, M. 1997. alphavbeta3 integrin mediates the cell-adhesive capacity and biological activity of basic fibroblast growth factor (FGF-2) in cultured endothelial cells. *Molecular biology of the cell*, 8(12): 2449–61. Retrieved from http://www.ncbi.nlm.nih.gov/pubmed/9398667

Russo, V. C., Schütt, B. S., Andaloro, E., Ymer, S. I., Hoeflich, A., Ranke, M. B., Bach, L. A., & Werther, G. A. 2005. Insulin-Like Growth Factor Binding Protein-2 Binding to Extracellular Matrix Plays a Critical Role in Neuroblastoma Cell Proliferation, Migration, and Invasion. *Endocrinology*, 146(10): 4445–4455.

Sahni, A., Sahni, S. K., Simpson-Haidaris, P. J., & Francis, C. W. 2004. Fibrinogen binding potentiates FGF-2 but not VEGF induced expression of u-PA, u-PAR, and PAI-1 in endothelial cells. *Journal of Thrombosis and Haemostasis*, 2(9): 1629–1636.

Sainson, R. C. A., & Harris, A. L. 2008. Regulation of angiogenesis by homotypic and heterotypic notch signalling in endothelial cells and pericytes: from basic research to potential therapies. *Angiogenesis*, 11(1): 41–51.

Sampson, U. K. A., Fowkes, F. G. R., McDermott, M. M., Criqui, M. H., Aboyans, V., Norman, P. E., Forouzanfar, M. H., Naghavi, M., Song, Y., Harrell, F. E., Denenberg, J. O., Mensah, G. A., Ezzati, M., & Murray, C. 2014. Global and Regional Burden of Death and Disability From Peripheral Artery Disease. *Global Heart*, 9(1): 145–158.e21.

Santarpia, L., Lippman, S. L., & El-Naggar, A. K. 2012. Targeting the Mitogen-Activated Protein Kinase RAS-RAF Signaling Pathway in Cancer Therapy. *Expert opinion on therapeutic targets*, 16(1): 103.

Schaller, M. D., Otey, C. A., Hildebrand, J. D., & Parsons, J. T. 1995. Focal adhesion kinase and paxillin bind to peptides mimicking beta integrin cytoplasmic domains. *The Journal of cell biology*, 130(5): 1181–7. Retrieved from http://www.ncbi.nlm.nih.gov/pubmed/7657702

Schiaffino, S., & Mammucari, C. 2011. Regulation of skeletal muscle growth by the IGF1-Akt/PKB pathway: insights from genetic models. *Skeletal Muscle*, 1(1): 4.

Schindler, N., Mayer, J., Saenger, S., Gimsa, U., Walz, C., Brenmoehl, J., Ohde, D., Wirthgen, E., Tuchscherer, A., Russo, V. C., Frank, M., Kirschstein, T., Metzger, F., & Hoeflich, A. 2017. Phenotype analysis of male transgenic mice overexpressing mutant IGFBP-2 lacking the Cardin–Weintraub sequence motif: Reduced expression of synaptic markers and myelin basic protein in the brain and a lower degree of anxiety-like behaviour. *Growth Hormone & IGF Research*, 33: 1–8.

Schütt, B. S., Langkamp, M., Rauschnabel, U., Ranke, M. B., & Elmlinger, M. W. 2004. Integrin-mediated action of insulin-like factor binding protein-2 in tumor cells. *Journal of Molecular Endocrinology*, 32(3): 859–868.

Sehgal, P., Kumar, N., Praveen Kumar, V., Patil, S., Bhattacharya, A., Vijaya Kumar, M., Mukherjee, G., & Kondaiah, P. 2013. Regulation of protumorigenic pathways by Insulin like growth factor binding protein2 and its association along with β-catenin in breast cancer lymph node metastasis. *Molecular Cancer*, 12(1): 63.

Senger, D. R., Ledbetter, S. R., Claffey, K. P., Papadopoulos-Sergiou, A., Peruzzi, C. A., & Detmar, M. 1996. Stimulation of endothelial cell migration by vascular permeability factor/vascular endothelial growth factor through cooperative mechanisms involving the alphavbeta3 integrin, osteopontin, and thrombin. *The American journal of pathology*, 149(1): 293–305. Retrieved from http://www.ncbi.nlm.nih.gov/pubmed/8686754

Sharples, A. P., Al-Shanti, N., & Stewart, C. E. 2010. C2 and C2C12 murine skeletal myoblast models of atrophic and hypertrophic potential: Relevance to disease and ageing? *Journal of Cellular Physiology*, 225(1): 240–250.

Shen, T.-L., Park, A. Y.-J., Alcaraz, A., Peng, X., Jang, I., Koni, P., Flavell, R. A., Gu, H., & Guan, J.-L. 2005. Conditional knockout of focal adhesion kinase in endothelial cells reveals its role in angiogenesis and vascular development in late embryogenesis. *The Journal of Cell Biology*, 169(6): 941–952.

Shen, X., Xi, G., Maile, L. A., Wai, C., Rosen, C. J., & Clemmons, D. R. 2012. Insulin-like growth factor (IGF) binding protein 2 functions coordinately with receptor protein tyrosine phosphatase β and the IGF-I receptor to regulate IGF-I-stimulated signaling. *Molecular and cellular biology*, 32(20): 4116–30.

Shen, X., Xi, G., Wai, C., & Clemmons, D. R. 2015. The coordinate cellular response to insulin-like growth factor-I (IGF-I) and insulin-like growth factor-binding protein-2 (IGFBP-2) is regulated through vimentin binding to receptor tyrosine phosphatase β (RPTPβ). *The Journal of biological chemistry*, 290(18): 11578–90.

Shigematsu, S., Yamauchi, K., Nakajima, K., Iijima, S., Aizawa, T., & Hashizume, K. 1999. IGF-1 regulates migration and angiogenesis of human endothelial cells. *Endocrine journal*, 46 Suppl: S59–S62.

Shimamura, M., Nakagami, H., Koriyama, H., & Morishita, R. 2013. Gene Therapy and Cell-Based Therapies for Therapeutic Angiogenesis in Peripheral Artery Disease. *BioMed Research International*, 2013: 1–8.

Shireman, P. K. 2007. The chemokine system in arteriogenesis and hind limb ischemia. *Journal of vascular surgery*, 45 Suppl A(Suppl A): A48-56.

Shireman, P. K., & Quinones, M. P. 2005. Differential Necrosis Despite Similar Perfusion in Mouse Strains after Ischemia1. *Journal of Surgical Research*, 129(2): 242–250.

Sidibé, A., & Imhof, B. A. 2014. VE-cadherin phosphorylation decides: vascular permeability or diapedesis. *Nature Immunology*, 15(3): 215–217.

Sigma-Aldrich 2018. Protein Expression Systems | Sigma-Aldrich. Retrieved September 28, 2018, from https://www.sigmaaldrich.com/technical-documents/articles/biology/protein-expression-systems.html

Sigvant, B., Wiberg-Hedman, K., Bergqvist, D., Rolandsson, O., Andersson, B., Persson, E., & Wahlberg, E. 2007. A population-based study of peripheral arterial disease prevalence with special focus on critical limb ischemia and sex differences. *Journal of Vascular Surgery*, 45(6): 1185–1191.

Simons, M., Annex, B. H., Laham, R. J., Kleiman, N., Henry, T., Dauerman, H., Udelson, J. E., Gervino, E. V, Pike, M., Whitehouse, M. J., Moon, T., & Chronos, N. A. 2002. Pharmacological treatment of coronary artery disease with recombinant fibroblast growth factor-2: double-blind, randomized, controlled clinical trial. *Circulation*, 105(7): 788–93. Retrieved from http://www.ncbi.nlm.nih.gov/pubmed/11854116

Simons, M., & Ware, J. A. 2003. Therapeutic angiogenesis in cardiovascular disease. *Nature Reviews Drug Discovery*, 2(11): 863–872.

Soga, Y., Iida, O., Takahaera, M., Hirano, K., Suzuki, K., Kawasaki, D., Miyashita, Y., Tsuchiya, T., & Tsuchiya, T. 2014. Two-Year Life Expectancy in Patients With Critical Limb Ischemia. *JACC: Cardiovascular Interventions*, 7(12): 1444–1449.

Song, S. W., Fuller, G. N., Khan, A., Kong, S., Shen, W., Taylor, E., Ramdas, L., Lang, F. F., & Zhang, W. 2003. IIp45, an insulin-like growth factor binding protein 2

(IGFBP-2) binding protein, antagonizes IGFBP-2 stimulation of glioma cell invasion. *Proceedings of the National Academy of Sciences of the United States of America*, 100(24): 13970–13975.

Spriestersbach, A., Kubicek, J., Schäfer, F., Block, H., & Maertens, B. 2015. Purification of His-Tagged Proteins. *Methods in enzymology* (Vol. 559, pp. 1–15).

Srinivasan, R., Zabuawala, T., Huang, H., Zhang, J., Gulati, P., Fernandez, S., Karlo, J. C., Landreth, G. E., Leone, G., & Ostrowski, M. C. 2009. Erk1 and Erk2 Regulate Endothelial Cell Proliferation and Migration during Mouse Embryonic Angiogenesis. (R. A. Arkowitz, Ed.)*PLoS ONE*, 4(12): e8283.

Stevens, T., Garcia, J. G. N., Shasby, D. M., Bhattacharya, J., & Malik, A. B. 2000. Mechanisms regulating endothelial cell barrier function. *American Journal of Physiology-Lung Cellular and Molecular Physiology*, 279(3): L419–L422.

Sudhakar, A., Sugimoto, H., Yang, C., Lively, J., Zeisberg, M., & Kalluri, R. 2003. Human tumstatin and human endostatin exhibit distinct antiangiogenic activities mediated by v 3 and 5 1 integrins. *Proceedings of the National Academy of Sciences*, 100(8): 4766–4771.

Sun, P. 2014. Contact inhibition against senescence. *Oncotarget*, 5(17): 7212–3.

Sureshbabu, A., Okajima, H., Yamanaka, D., Tonner, E., Shastri, S., Maycock, J., Szymanowska, M., Shand, J., Takahashi, S.-I., Beattie, J., Allan, G., & Flint, D. 2012. IGFBP5 induces cell adhesion, increases cell survival and inhibits cell migration in MCF-7 human breast cancer cells. *Journal of Cell Science*, 125(7): 1693–1705.

Switkowski, K. M., Jacques, P. F., Must, A., Hivert, M.-F., Fleisch, A., Gillman, M. W., Rifas-Shiman, S., & Oken, E. 2017. Higher Maternal Protein Intake during Pregnancy Is Associated with Lower Cord Blood Concentrations of Insulin-like Growth Factor (IGF)-II, IGF Binding Protein 3, and Insulin, but Not IGF-I, in a Cohort of Women with High Protein Intake. *The Journal of Nutrition*, 147(7): 1392–1400.

Teraa, M., Conte, M. S., Moll, F. L., & Verhaar, M. C. 2016. Critical Limb Ischemia:

Current Trends and Future Directions. *Journal of the American Heart Association*, 5(2).

Terpe, K. 2006. Overview of bacterial expression systems for heterologous protein production: from molecular and biochemical fundamentals to commercial systems. *Applied Microbiology and Biotechnology*, 72(2): 211–222.

Tian, D., Mitchell, I., & Kreeger, P. K. 2016. Quantitative analysis of insulin-like growth factor 2 receptor and insulin-like growth factor binding proteins to identify control mechanisms for insulin-like growth factor 1 receptor phosphorylation. *BMC systems biology*, 10: 15.

Truett, G. E., Heeger, P., Mynatt, R. L., Truett, A. A., Walker, J. A., & Warman, M. L. 2000. Preparation of PCR-quality mouse genomic DNA with hot sodium hydroxide and tris (HotSHOT). *BioTechniques*, 29(1): 52, 54. Retrieved from http://www.ncbi.nlm.nih.gov/pubmed/10907076

Twigg, S. M., & Baxter, R. C. 1998. Insulin-like growth factor (IGF)-binding protein 5 forms an alternative ternary complex with IGFs and the acid-labile subunit. *The Journal of biological chemistry*, 273(11): 6074–9. Retrieved from http://www.ncbi.nlm.nih.gov/pubmed/9497324

Uzoh, C. C., Holly, J. M. P., Biernacka, K. M., Persad, R. A., Bahl, A., Gillatt, D., & Perks, C. M. 2011. Insulin-like growth factor-binding protein-2 promotes prostate cancer cell growth via IGF-dependent or -independent mechanisms and reduces the efficacy of docetaxel. *British journal of cancer*, 104(10): 1587–93.

Vailhé, B., Vittet, D., & Feige, J. J. 2001. In vitro models of vasculogenesis and angiogenesis. *Laboratory investigation; a journal of technical methods and pathology*, 81(4): 439–452.

van Royen, N., Piek, J. J., Buschmann, I., Hoefer, I., Voskuil, M., & Schaper, W. 2001. Stimulation of arteriogenesis; a new concept for the treatment of arterial occlusive disease. *Cardiovascular research*, 49(3): 543–53. Retrieved from

http://www.ncbi.nlm.nih.gov/pubmed/11166267

Ved, N., Hulse, R. P., Bestall, S. M., Donaldson, L. F., Bainbridge, J. W., & Bates, D. O. 2017. Vascular endothelial growth factor-A $_{165}$ b ameliorates outer-retinal barrier and vascular dysfunction in the diabetic retina. *Clinical Science*, 131(12): 1225–1243.

Wang, G. K., Hu, L., Fuller, G. N., & Zhang, W. 2006. An interaction between insulin-like growth factor-binding protein 2 (IGFBP2) and integrin ??5 is essential for IGFBP2-induced cell mobility. *Journal of Biological Chemistry*, 281(20): 14085–14091.

Wang, H., Wang, H., Shen, W., Huang, H., Hu, L., Ramdas, L., Zhou, Y.-H., Liao, W. S.-L., Fuller, G. N., & Zhang, W. 2003. Insulin-like growth factor binding protein 2 enhances glioblastoma invasion by activating invasion-enhancing genes. *Cancer research*, 63(15): 4315–21. Retrieved from http://www.ncbi.nlm.nih.gov/pubmed/12907597

Wang, J., Razuvaev, A., Folkersen, L., Hedin, E., Roy, J., Brismar, K., & Hedin, U. 2012. The expression of IGFs and IGF binding proteins in human carotid atherosclerosis, and the possible role of IGF binding protein-1 in the regulation of smooth muscle cell proliferation. *Atherosclerosis*, 220(1): 102–109.

Wang, X., Li, Y., Chen, L., & Hou, Z. 2017a. *Insulin-like growth factor binding protein 2 regulates cell proliferation and migration in the adjuvant arthritis synovial cells through ERK signaling pathway*. *Int J Clin Exp Pathol* (Vol. 10). Retrieved from www.ijcep.com/

Wang, Y. A., Sun, Y., Palmer, J., Solomides, C., Huang, L.-C., Shyr, Y., Dicker, A. P., & Lu, B. 2017b. IGFBP3 Modulates Lung Tumorigenesis and Cell Growth through IGF1 Signaling. *Molecular Cancer Research*, 15(7): 896–904.

Wang, Y., Liu, Y., Fan, Z., Liu, D., Wang, F., Zhou, Y., & Hare, J. M. 2017c. IGFBP2 enhances adipogenic differentiation potentials of mesenchymal stem cells from Wharton's jelly of the umbilical cord via JNK and Akt signaling pathways.

Warfarin Antiplatelet Vascular Evaluation Trial Investigators, Anand, S., Yusuf, S., Xie, C., Pogue, J., Eikelboom, J., Budaj, A., Sussex, B., Liu, L., Guzman, R., Cina, C., Crowell, R., Keltai, M., & Gosselin, G. 2007. Oral Anticoagulant and Antiplatelet Therapy and Peripheral Arterial Disease. *New England Journal of Medicine*, 357(3): 217–227.

Wheatcroft, S. B., Kearney, M. T., Shah, A. M., Ezzat, V. A., Miell, J. R., Modo, M., Williams, S. C. R., Cawthorn, W. P., Medina-gomez, G., Vidal-Puig, A., Sethi, J. K., & Crossey, P. A. 2007. IGF-Binding Protein-2 Protects Against the Development of Obesity and Insulin Resistance. *Diabetes*, 56(February): 285–294.

Wijnand, J. G. J., Teraa, M., Gremmels, H., van Rhijn-Brouwer, F. C. C., de Borst, G. J., Verhaar, M. C., & SAIL Study Group. 2018. Rationale and design of the SAIL trial for intramuscular injection of allogeneic mesenchymal stromal cells in no-option critical limb ischemia. *Journal of vascular surgery*, 67(2): 656–661.

Wingfield, P. 1998. Protein Precipitation Using Ammonium Sulfate. *Current Protocols in Protein Science* (Vol. Appendix 3, p. A.3F.1-A.3F.8). Hoboken, NJ, USA: John Wiley & Sons, Inc.

Wirtz, V. J., Kaplan, W. A., Kwan, G. F., & Laing, R. O. 2016. Access to Medications for Cardiovascular Diseases in Low- and Middle-Income Countries. *Circulation*, 133(21): 2076–2085.

Wood, A. W., Schlueter, P. J., & Duan, C. 2005. Targeted Knockdown of Insulin-Like Growth Factor Binding Protein-2 Disrupts Cardiovascular Development in Zebrafish Embryos. *Molecular Endocrinology*, 19(4): 1024–1034.

Wood, T. L., Rogler, L. E., Czick, M. E., Schuller, A. G. P., & Pintar, J. E. 2000. Selective Alterations in Organ Sizes in Mice with a Targeted Disruption of the Insulin-Like Growth Factor Binding Protein-2 Gene. *Molecular Endocrinology*, 14(9): 1472–1482.

Xi, G., Rosen, C. J., & Clemmons, D. R. 2016. IGF-I and IGFBP-2 Stimulate AMPK

Activation and Autophagy, Which Are Required for Osteoblast Differentiation. *Endocrinology*, 157(1): 268–281.

Xi, G., Solum, M. a., Wai, C., Maile, L. a., Rosen, C. J., & Clemmons, D. R. 2013. The Heparin-Binding Domains of IGFBP-2 Mediate Its Inhibitory Effect on Preadipocyte Differentiation and Fat Development in Male Mice. *Endocrinology*, 154(11): 4146–4157.

Xi, G., Wai, C., DeMambro, V., Rosen, C. J., & Clemmons, D. R. 2014. IGFBP-2 Directly Stimulates Osteoblast Differentiation. *Journal of Bone and Mineral Research*, 29(11): 2427–2438.

Xing, Q., Yates, K., Vogt, C., Qian, Z., Frost, M. C., & Zhao, F. 2015. Increasing Mechanical Strength of Gelatin Hydrogels by Divalent Metal Ion Removal. *Scientific Reports*, 4(1): 4706.

Yamamoto, Y., Matsuura, T., Narazaki, G., Sugitani, M., Tanaka, K., Maeda, A., Shiota, G., Sato, K., Yoshida, A., & Hisatome, I. 2009. Synergistic effects of autologous cell and hepatocyte growth factor gene therapy for neovascularization in a murine model of hindlimb ischemia. *Am J Physiol Heart Circ Physiol*, 297: 1329–1336.

Yau, S. W., Azar, W. J., Sabin, M. A., Werther, G. A., & Russo, V. C. 2015a. IGFBP-2 - taking the lead in growth, metabolism and cancer. *Journal of cell communication and signaling*, 9(2): 125–42.

Yau, S. W., Azar, W. J., Sabin, M. A., Werther, G. A., & Russo, V. C. 2015b. IGFBP-2 - taking the lead in growth, metabolism and cancer. *Journal of cell communication and signaling*, 9(2): 125–42.

Yau, S. W., Harcourt, B. E., Kao, K.-T., Alexander, E. J., Russo, V. C., Werther, G. A., & Sabin, M. A. 2018. Serum IGFBP-2 levels are associated with reduced insulin sensitivity in obese children. *Clinical Obesity*, 8(3): 184–190.

Yau, S. W., Russo, V. C., Clarke, I. J., Dunshea, F. R., Werther, G. A., & Sabin, M.

A. 2015c. IGFBP-2 inhibits adipogenesis and lipogenesis in human visceral, but not subcutaneous, adipocytes. *International Journal of Obesity*, 39(5): 770–781.

Yau, S. W., Russo, V. C., Clarke, I. J., Dunshea, F. R., Werther, G. a, & Sabin, M. a. 2014. IGFBP-2 inhibits adipogenesis and lipogenesis in human visceral, but not subcutaneous, adipocytes. *International journal of obesity (2005)*, 39(August 2013): 1–12.

Yazawa, T., Sato, H., Shimoyamada, H., Okudela, K., Woo, T., Tajiri, M., Ogura, T., Ogawa, N., Suzuki, T., Mitsui, H., Ishii, J., Miyata, C., Sakaeda, M., Goto, K., Kashiwagi, K., Masuda, M., Takahashi, T., & Kitamura, H. 2009. Neuroendocrine Cancer-Specific Up-Regulating Mechanism of Insulin-Like Growth Factor Binding Protein-2 in Small Cell Lung Cancer. *The American Journal of Pathology*, 175(3): 976–987.

Yi, K. H., & Lauring, J. 2016. Recurrent AKT mutations in human cancers: functional consequences and effects on drug sensitivity. *Oncotarget*, 7(4): 4241–51.

Yin, J., Li, G., Ren, X., & Herrler, G. 2007. Select what you need: A comparative evaluation of the advantages and limitations of frequently used expression systems for foreign genes. *Journal of Biotechnology*, 127(3): 335–347.

Ylä-Herttuala, S., & Baker, A. H. 2017. Cardiovascular Gene Therapy: Past, Present, and Future. *Molecular Therapy*, 25(5): 1095–1106.

Yoshino, Y., Aoyagi, M., Tamaki, M., Duan, L., Morimoto, T., & Ohno, K. 2006. Activation of p38 MAPK and/or JNK contributes to increased levels of VEGF secretion in human malignant glioma cells. *International journal of oncology*, 29(4): 981–7. Retrieved from http://www.ncbi.nlm.nih.gov/pubmed/16964394

Zhang, C., Lu, L., Li, Y., Wang, X., Zhou, J., Liu, Y., Fu, P., Gallicchio, M. A., Bach, L. A., & Duan, C. 2012. IGF binding protein-6 expression in vascular endothelial cells is induced by hypoxia and plays a negative role in tumor angiogenesis. *International Journal of Cancer*, 130(9): 2003–2012.

Zhao, F., Zhang, Y. F., Liu, Y. G., Zhou, J. J., Li, Z. K., Wu, C. G., & Qi, H. W. 2008. Therapeutic Effects of Bone Marrow-Derived Mesenchymal Stem Cells Engraftment on Bleomycin-Induced Lung Injury in Rats. *Transplantation Proceedings*, 40(5): 1700–1705.

Zheng, B., Duan, C., & Clemmons, D. R. 1998. The effect of extracellular matrix proteins on porcine smooth muscle cell insulin-like growth factor (IGF) binding protein-5 synthesis and responsiveness to IGF-I. *The Journal of biological chemistry*, 273(15): 8994–9000.

Zhou, P., Baumgarten, S. C., Wu, Y., Bennett, J., Winston, N., Hirshfeld-Cytron, J., & Stocco, C. 2013. IGF-I signaling is essential for FSH stimulation of AKT and steroidogenic genes in granulosa cells. *Molecular endocrinology (Baltimore, Md.)*, 27(3): 511–23.